JAERI-M
93-018

UCLA-ENG-91-32
UCLA-FNT-53

JOINT REPORT OF JAERI/USDOE COLLABORATIVE PROGRAM ON FUSION NEUTRONICS

— INDUCED RADIOACTIVITY MEASUREMENTS IN FUSION NEUTRON ENVIRONMENT —

February 1993

Yujiro IKEDA, Anil KUMAR[*1], Chikara KONNO, Kazuaki KOSAKO[*2]
Yukio OYAMA, Tomoo NAKAMURA[*3], Hiroshi MAEKAWA
Mahmoud Z. YOUSSEF[*1] and Mohamed A. ABDOU[*1]

日本原子力研究所
Japan Atomic Energy Research Institute

JAERI-Mレポートは，日本原子力研究所が不定期に公刊している研究報告書です。
入手の問合わせは，日本原子力研究所技術情報部情報資料課（〒319-11茨城県那珂郡東海村）あて，お申しこしください。なお，このほかに財団法人原子力弘済会資料センター（〒319-11茨城県那珂郡東海村日本原子力研究所内）で複写による実費頒布をおこなっております。

JAERI-M reports are issued irregularly.
Inquiries about availability of the reports should be addressed to Information Division Department of Technical Information, Japan Atomic Energy Research Institute, Tokai-mura, Naka-gun, Ibaraki-ken 319-11, Japan.

編集兼発行　日本原子力研究所
印　　刷　いばらき印刷㈱

JAERI-M 93-018

Joint Report of JAERI/USDOE Collaborative Program on Fusion Neutronics

- Induced Radioactivity Measurements in Fusion Neutron Environment -

Yujiro IKEDA, Anil KUMAR[*1], Chikara KONNO, Kazuaki KOSAKO[*2]
Yukio OYAMA, Tomoo NAKAMURA[*3], Hiroshi MAEKAWA
Mahmoud Z. YOUSSEF[*1] and Mohamed A. ABDOU[*1]

Department of Reactor Engineering
Tokai Research Establishment
Japan Atomic Energy Research Institute
Tokai-mura, Naka-gun, Ibaraki-ken

(Received January 11, 1993)

The selection of materials and design options for fusion device components depends crucially on the level of radioactivity and decay-heat induced in the components due to D-T neutron irradiation. A series of experiment of induced radioactivity has been carried out in the framework of the JAERI/USDOE collaborative program on fusion neutronics. The experiments aim to characterize induced radioactivities of fusion reactor structural components subjected to D-T neutron environment and to provide experimental data for verifying currently available calculation codes and their associated nuclear data libraries relevant to the activation. The materials subjected were Fe, Ni, Cr, Mn-Cu alloy, Ti, Mo, Zr, Ta, W, Si, Mg, Al, V, Nb, and SS316, which were irradiated in various fusion neutron spectrum fields utilizing experimental configuration through Phase-IIC to Pase-IIIB. The cooling times applied ranged from 10 minutes to 7 days. The data were given as the integrated γ-ray emission rate as well as γ-ray

---

*1 University of California, Los Angeles (UCLA)

*2 Nuclear Data Center (NEDAC)

*3 Japan Synchrotron Radiation Research Institute (JASRI)

spectrum (over 100 keV to 3 MeV) at specific cooling times. Preliminary experimental analyses have been performed using four leading radioactivity codes: DKRICF, REAC*2, RACC and THIDA.

This report summarizes all of experimental results along with the data required for the successive experimental analysis.

Keywords: Induced Radioactivity, D-T Fusion Reactor, Neutron Activation, Structural Materials, Decay γ-ray, Decay Heat, THIDA-2, REAC*2, DKR-ICF, RACC

核融合ニュートロニクスに関する原研と米国エネルギー省との共同実験研究レポート
－核融合中性子環境における誘導放射能測定－

日本原子力研究所東海研究所原子炉工学部
池田裕二郎・Anil KUMAR*1・今野　力・小迫　和明*2
大山　幸夫・中村　知夫*3・前川　洋・Mahmoud Z. YOUSSEF*1
Mohamed A. ABDOU*1

（1993年1月11日受理）

核融合装置の材料及び設計の選択はＤ－Ｔ中性子照射による核融合炉構成要素の誘導放射能及びそれに伴う崩壊熱の生成量に重要な影響を与える。これを受けて，核融合中性子工学に関する原研と米国ＤＯＥとの共同実験計画（日米実験）の一環として誘導放射能実験を行ってきた。この実験の目的はＤ－Ｔ中性子照射による核融合炉構成要素の誘導放射能特性を明かにすると共に計算コード及び放射化に関する核データの妥当性検証のための実験データを測定することである。対象とした材料はFe，Ni，Cr，MnCu合金，Ti，Mo，Zr，Ta，W，Si，Mg，Al，V，Nb及びＳＳ３１６で，これを日米実験の第２段階Ｃから第３段階Ｂにおける実験体系の様々な核融合中性子スペクトル場で30分から10時間照射し，10分から７日の冷却時間をおいて放出ガンマ線を測定した。実験データはそれぞれの冷却時間における100keVから３MeVまでのガンマ線スペクトル並びに１g当りのガンマ線放出率の積分値として与えた。既に，主要な計算コード，ＤＫＲＩＣＦ，ＲＥＡＣ＊２，ＲＡＣＣ及びＴＨＩＤＡ－２を用いた暫定的な実験解析を行った。

本報告書は実験の詳細な記述，これまでに得られた全ての実験データ及び実験解析に必要なデータ並びに予備的な実験解析結果を日米共同レポートとしてまとめたものである。

東海研究所：〒319－11　茨城県那珂郡東海村白方字白根２－４
＊１　カリフォルニア大学ロサンゼルス分校
＊２　原子力データセンター
＊３　高輝度光科学研究センター

Contents

目　　次

List of Tables:

List of Figures:

1. INTRODUCTION

One of the foremost issues in fusion reactor design is neutron induced radioactivity. Reactor safety, biological hazard, reactor maintenance, after-shutdown cooling and waste disposal are among the critical issues impacting the selection of materials for various components from first wall to pressure vessel[1-7].In view of a large number of materials under consideration for leading fusion devices, like ITER, NET, CIT and FER, a series of experimental measurements have been carried out, year 1988 through 1990 so far, at the fusion neutronics source (FNS) facility[8] of JAERI under ongoing USDOE/JAERI collaborative program on fusion neutronics[9-10]. The experiment aimed at characterizing the induced activities in typical D-T fusion neutron environment and providing data for the comprehensive induced activity calculation code and associated nuclear data; activation cross sections and decay data. The experiments have consisted of γ-spectroscopy of material samples irradiated under prototypical fusion environment. Multiple irradiation and cooling times along with different spectral conditions have been implemented. The irradiated materials, during phases IIC through IIIB, include Fe, Ni, Cr, MnCu alloy, Ti, Mo, Zr, Ta, W, Si, Mg, Al, V, Nb, SS316, $YBa_2Cu_3O_7$, $ErBa_2Cu_3O_7$, Sn, Ag, Pb, Zn and In. Most of these measurements have already been analyzed and the results presented in comprehensive publications[11-17]. In addition, results of measurements of very long half life isotopes have also been published[18,19].

This report describes the experimental procedure in detail and summarizes the experimental data to be used for the successive analysis by the currently available calculation code systems. As the number of cases treated in the present series of experiment is so large that we have selected very representative cases in terms of materials, neutron spectrum, irradiation time and cooling time. In addition, results of preliminary experimental analysis by a four leading calculation codes, REAC2, DKRICF, RACC and THIDA are outlined. In the appendix, the papers associated with the present experimental series so far issued are attached.

2. EXPERIMENTS

2.1 Background

The neutron induced radioactivity is defined as the product of neutron reactions, which decays with a specific half-life emitting β-rays and γ-rays. It can be characterized by several parameters, e.g, materials subjected, neutron spectrum, reaction cross section, time length for irradiation and cooling, and associated decay mode. The relation is given as,

$$I_{act} = M \cdot D_i \cdot F_i(t) \int_{E\text{-min}}^{E\text{-max}} \sigma(E)_i \cdot \Phi(E) \cdot dE \ ,$$

where,

I_{act}: Induced radioactivity,
M : material dependent term,
D_i : decay dependent term,
F_i : time dependent term,
$\sigma_i(E)$: reaction cross section,
$\Phi(E)$: neutron spectrum.

In a fusion reactor environment, neutron energy spectrum, $\Phi(E)$, will vary from place to place. Hardest spectrum will be found in close proximity to the burning plasma. As one moves away from the plasma, the spectrum will become softer due to slowing down of 14 MeV D-T neutrons in first wall/blanket/shield and any other surrounding medium. Thus, materials at different locations inside fusion reactor will experience different neutron energy spectra. Production cross-sections, $\sigma(E)$, for radioactive isotopes are functions of neutron energy. (n,n'), (n,p), (n,α), (n,2n), (n,n'p), (n,^{3}He), (n,d), (n,t) reactions are generally endothermic, and, are, thus, provoked by higher energy neutrons. Contrarily, (n,γ) reaction is an exothermic reaction and is, thus, driven by lower energy neutrons. Consequently, the induced radioactivity, I_{act}, is highly integrated products of those independent parameters. In particular, the production cross sections, γ-ray yield, γ-ray half-life data for most of the radioactive isotopes of fusion interest need early validation as all design strategies are critically dependent on it. **Figure 1** shows schematically the function of the integral experiment of induced radioactivity for the fusion applications.

2.2. Strategy of Experiment

Ideally, one needs to have a neutron source that will allow to realize an intense monoenergetic neutron flux, such that one can vary neutron energy from 14 MeV right up to 0.025 eV or lower. Different material samples could then be irradiated under any desired neutron energy spectrum. But, this approach is impossible to realize due to lack of availability of monoenergetic neutron sources over the energy range of interest, on one hand, and huge requirements of expense and effort, even for few monoenergetic sources that one can utilize, on the other. A cruder but more practical approach consists in irradiating material samples in select locations in a simulated fusion reactor environment. One will obtain integral effect of neutron energy spectrum at each location. A number of small material samples can be kept at each location as long as they have minimal impact on neutron energy spectrum in immediate neighborhood. **Figure 2** gives a schematic view of a typical experimental arrangement of sample materials. In fact, this was realized in first experiments done under USDOE/JAERI collaborative program, in coolant channel assembly of phase IIC[11-13].

USDOE/JAERI collaborative and experimental program on fusion neutronics has been designed to simulate reactor-relevant neutron energy spectra in tritium breeding blankets over the years. Two sources of 14 MeV neutrons have been used at fusion neutronics source (FNS) facility[8] of Japan Atomic Energy Research Institute (JAERI). A rotating neutron target (RNT) source (nominal intensity = 3 x 10^{12} n/s) was employed in phases I through IIC. A fixed neutron target with lower nominal intensity (~3 x 10^{11} n/s) has been used in later phases, IIIA through IIIC, where line source was simulated. Induced radioactivity measurements have been conducted during all phases, beginning with phase IIC, as shown in **Figure 2**.

2.3. Measured Items

The major concern in the present study is to measure the γ-ray spectrum of each induced radioactivity, because it gives direct information of radioactivity characteristics in each irradiation environment. The γ-emitting radioactive isotopes span a large range of half lives, going from fraction of a second to million years. Practical considerations oblige us to first focus on half lives comprised between few minutes to few years. Even in this case, number and lengths of irradiation periods has to be so optimized as to obtain adequate and, yet, statistically meaningful data on broad range of half lives within limited availability of neutron source, γ-ray detectors and manpower. It was thought practical to include at the most two irradiations: shorter irradiation of ~30 m was deemed adequate for shorter half lives ranging from few minutes to few hours; an irradiation of 9

to 10 h was generally chosen for half lives ranging from few hours to few years. Radioactive samples were cooled for different times and read-off on 2 to 4 detectors made available.

Another concern of the present experimental study is to extract information on the decay-heat. in a D-T fusion reactor resulted from neutron-induced radioactive isotopes. Bulk of the recommended fusion-reactor materials have low to medium Z (atomic) number. As a result, most of the produced radioactive isotopes de-excite via β-decay (electron/positron emission), electron capture (EC), or isomeric transition (IT). Most often, β-decay and electron capture are also followed by γ–decay. Ideally, one would welcome efforts to do both β- and γ-spectroscopy of emitted radiations from the radioactive isotopes. But, γ-spectroscopy alone is capable of providing wealth of extremely valuable data at this early stage of R&D effort in this area. Subsequently, it would be imperative to extend the effort to studying those radioactive isotopes too that do not give out any γ-rays.

Tables 1 through 4 summarize data on chemical compositions of irradiated samples (**Table 1**), isotopic compositions (**Table 2**), major decay γ-yields of observed radioactive isotopes (**Table 3**), and major nuclear reactions producing these isotopes (**Table 4**).

2.4. SYSTEM CONFIGURATION AND IRRADIATION

1) Phase IIC

Two separate irradiation programs were executed to cover each of the two locations, at 10 and 82 cm from the neutron source respectively (see **Fig. 2**). Two foil packets were irradiated at each location to individually focus on: (i) shorter half life products (less than 1 hour half life), (ii) longer half life products (1 hour to 5 year half life). Each irradiation program consisted of initial half an hour irradiation followed by pulling out of one of the two packets. The γ-spectroscopy of the foils in this packet was to cover primarily shorter half life products. The total irradiation periods were 9 and 10 hours respectively for the locations at 10 and 82 cm, logging average source neutron intensities of 8.75×10^{11} and 1.12×10^{12} n/s. The γ-spectroscopy of each sample was done using four intrinsic germanium detectors and for multiple cooling periods ranging from 20 m to 10 d. Three detectors were relatively calibrated with respect to an absolutely calibrated standard detector, detector #5S.

2) Phase IIIA

The line source simulation was realized by step or continuous mode[20-22]. Detector/assembly are moved by a predetermined spatial step at a time and held at each new position for predetermined time-interval in the step mode. In continuous mode, detector/assembly are constantly moved back and forth at a predetermined speed except very close to the ends. **Figure 3** shows schematic of the experimental configuration for line source simulation. Three different environments were chosen for radioactivity measurements[16,17]: (i) bare line source, (ii) point source inside stationary assembly, (iii) line source driving an annular assembly. The objectives behind this selection are discussed in what follows. It is to be outlined here that all these experiments were conducted in large target room with 80^0 beam line. The nominal source intensity for stationary source is 2 x 10^{11} n/s (for 2 mA beam current), it is an order of magnitude lower than what was available with rotating target neutron source (RNT) in target room#2 during earlier phases. The counting statistics suffers considerably and hence adversely affects accumulation of data on weaker radioactive isotopes.

The degree of achievement of 'ideal' line source simulation attainable through the step and continuous modes is brought out through **Fig. 4**. By 'Ideal' line source, we imply a simulated source that is free from effects of limited speed on any foil activation rate. It is possible only if the moving system attains infinite speed. **Figure 4** shows the ratio of simulated to 'ideal' activation rates as a function of mean axial distance, from the fixed point source, of an irradiated foil. The foil is considered placed at 21.9 cm radial distance from the centerline passing through the target. For continuous mode, the actual temporal profiles of source intensity and deck (or foil) position during 'line source driven assembly' experiment (see Sec. 2.3.3) have been factored in; product half-life is taken to be 10 m. In the actual experiment, an average cycle length of ~ 11 minutes was realized over 54 cycles for a total irradiation period of 9h51m5s. This corresponds to an average speed of movement of 6.1 mm/s. It is to be seen that simulation is close to ideal for a foil located with mean distance of 30 to 40 cm on either side of the stationary target. **Figure 4** also shows the degree of simulation obtainable with stepwise mode for a product of half-life ranging from 10 m to 1 d; actual source intensity and position data realized during 'line source without assembly' experiment (see Sec. 2.3.1) have been factored in. The deviation is much larger for shorter half lives. During this experiment, a spatial step of 10 cm was selected , for a total of 41 irradiations of 13 minutes each and total experiment time of 9h47m; only one spatial cycle was executed. It is to be noted that even for 1 h half life product, the deviation from line source is considerable.

(a) Line Source without Assembly

Three sets of foil packets were irradiated at three initial axial distances of 0, 60 and 100 cm from the target towards its back-side; the corresponding mean distances from the target during

irradiation period are 0, 40 and 100 cm; radial distance from the system axis was 21.9 cm. The foil materials common to the three sets included: Zr, AISI316, Mo, Sn, Ni and Fe. In addition, thinner Nb and Al foils were used for source neutron dosimetry. The set at 100 cm contained additional foils of Co, Ti, V, In, Ta, W, Y, Ag, Pb and Zn. The foils were attached to a stand resting on a movable deck. This deck was moved 10 cm in a step and there was 13 minute irradiation at each step. Only one cycle could be completed during irradiation period of 9h47m. The decay γ spectroscopy was done using three available intrinsic germanium detectors at FNS. Two of these were relative detectors whereas the third one was used as absolute detector with its γ detection efficiency known better than 2 % in the energy range of 100 keV to 3 MeV at a standard sample-detector distance. Generally, more than one cooling time was covered for each foil. The cooling times varied from foil to foil and ranged from 1h50m to 7d22h37m20s. The average source intensity obtained amounts to 1.11×10^9 n/s/cm.

(b) Point Source Driven Assembly

The movable deck was held stationary during the first irradiation with the annular assembly on November 21, that was intended for shorter half life product isotopes; the irradiation lasted half an hour only. The source was all the time located at the center of the stationary assembly. Two sets of foils were irradiated for half an hour at initial axial distances of 0 and 40 cm from the target. The set at 40 cm was kept behind 10 mm thick layers of SS304. The other set was kept just behind 15 mm thick SS304 in the central radial drawer. Each set contained foils of Sn, Zn, Pb, Ag, Ni, Fe and W. In addition, two foils of Nb and one foil of Al were included for source neutron dosimetry. Because of lowering of neutron flux due to line source simulation, on the one hand, and relatively low source neutron strength, on the other hand, it was decided to have irradiation inside stationary assembly. It is clear that this configuration represents only a point source inside annular assembly of phase IIIA. However, this type of neutron energy spectrum was realized for the first time in this collaborative program. only two cooling times per sample were covered. The lowest cooling time was 11m30s for a lead sample, the highest one was 21h21m55s for a nickel sample.

(c) Line Source Driven Assembly

The line source simulation was carried out in continuous mode for 54 cycles during total irradiation time of 9h51m5s. The assembly was initially located such that its farthest end was coincident with the target; thereafter assembly was moved such that this end of the assembly was always within 0 to 2 m of the stationary target. Three sets of foils were irradiated: 2 sets were in the central radial drawer at an initial axial distance of 100 cm from the target and the remaining set was at an initial axial distance of 60 cm from the target. One of the sets in the central drawer was

just behind the 15 mm thick SS304 layers; the second set was inserted just behind first 2" thick Li_2O block. These two locations were chosen so as to provide different neutron energy spectra. The last set was placed behind 10 mm thick SS304 layers. The first two sets had identical sample composition: AISI316, Ti, Ta, Mo, Zr, Fe, Ni and W. The third set contained: Sn, Zn, Pb, Ag, Ni, Fe and Mo. In addition, all the three sets contained source neutron dosimetry foils of Nb (2 each) and Al (1 each). Generally, one cooling time per sample was covered. cooling time varied from sample to sample and ranged from the lowest of 1h37m25s for a AISI316 sample to the highest of 14h33m20s for a lead sample. The source intensity averaged to 9.66 x 10^8 n/s/cm.

3) Phase IIIB

One-inch thick graphite armor layer was added in front of the first wall[22]. The inner cavity had a cross-section of 37.5 cm x 37.5 cm. The line source simulation was carried out in continuous mode for 54 cycles during total irradiation time of 9h51m5s. The source intensity averaged to 9.66 x 10^8 n/s/cm^2. **Figure 5** shows sample locations inside Phase IIIB. The assembly was initially located such that its farthest end was coincident with the target; thereafter assembly was moved such that this end of the assembly was always within 0 to 2 m of the stationary target. Three sets of foils were irradiated: 2 sets were in the central radial drawer at an initial axial distance of 100 cm from the target and the remaining set was at an initial axial distance of 60 cm from the target. One of the sets in the central drawer was just behind the 15 mm thick SS304 layers; the second set was inserted just behind first 2" thick Li_2O block. These two locations were chosen so as to provide different neutron energy spectra. The last set was placed behind 10 mm thick SS304 layers. The first two sets had identical sample composition: AISI316, Ti, Ta, Mo, Zr, Fe, Ni and W. The third set contained: Sn, Zn, Pb, Ag, Ni, Fe and Mo. In addition, all the three sets contained source neutron dosimetry foils of Nb (2 each) and Al (1 each). Generally, one cooling time per sample was covered. cooling time varied from sample to sample and ranged from the lowest of 1h37m25s for a AISI316 sample to the highest of 14h33m20s for a lead sample.

2.5. Gamma-ray Spectroscopy and Data Reduction

After each irradiation, γ-rays emitted from the samples were measured with Ge detectors in conjunction with multi-channel pulse hight analyzers. In order to facilitate the counting of a large number of samples to be treated, four to five detectors were employed. Hereafter, we call the detectors as #1, #3, #4, #5 and #L according to our assignments. The data were recorded in a

VAX-11/780 mini-computer at FNS. The γ pulse-height spectrum for a sample for a each cooling time is processed by a spectrum analysis code BOB75[23] and GENIE system delivered by CANBERRA Inc. to obtain γ-ray energy spectrum. Then background is carefully subtracted. **Figures 6** shows typical background γ count rate spectra for detector #L. **Tables 5** lists background γ count rates for more prominent γ-rays.[24] The radioactivities were identified by their γ-ray energies and relative intensity ratios. **Figure 7** gives a measured γ-ray spectrum for tungsten irradiated for 30 m at 10 cm distance from the RNT in the Phase-IIC system.

The measured γ-ray spectrum is then corrected for detector efficiency (ε_f) and attenuation (μ) of decay γ -rays emitted in a sample. **Figures 8.1** shows absolute γ-ray detection efficiency as a function of γ-ray energy for detectors #5S. The #5S corresponded to the standard sample position for the detector #5, where the absolute efficiency was calibrated. Efficiencies of other detectors were calibrated relative to the detector #5 by using same activities of interest. The relative efficiency curve for the detector #4 is shown in **Fig. 8.2.** Variation of source neutron intensity during irradiation is accounted for to finally obtain decay γ-ray emission rate per gram for a normalizing source neutron intensity of 10^{12} n/s. For simulated line source (step/continuous mode) correction is applied to account for decay during intervening period for step mode and also to account for decay during movement for continuous mode as the speed of movement is not totally uniform over a cycle itself and the speed is quite low, as already described above. The correction factors (S_f) as a function of sample location are shown in **Figs 9.1 to 9.2.** The γ-ray emission rate, E_{act}, is given as,

$$E_{act} = \frac{\lambda \cdot C}{\varepsilon_f \cdot w \cdot \mu \cdot S_f \cdot Y_n \cdot (1-\exp(-\lambda \cdot t_m))} \quad ,$$

where,

λ : decay constant of radioactivity,

C : γ-ray peak counts,

w : sample weight,

t_m: collection time

Y_n: source neutron yield (10^{12}/s for Phase-IIC, 10^{11}/s for Phase-IIIA,B).

2.6 Experimental Error

Regarding error estimation on experimental measurements, it is to be recognized that a number of parameters affect counting statistics. The primary parameters include: neutron flux, half life of

γ-emitter, detector efficiency, cooling time, counting time, activation cross-section and atom density. It is impossible to give a single figure for even one sample material as is amply brought out in **Figs. 10 and 11** that show percent standard deviation on decay rates for different products as a function of half life for nickel and molybdenum samples respectively. The nickel sample was irradiated at 10 cm distance from target for 9 hours in phase IIC. The molybdenum sample was irradiated in 'point source driven assembly' experiment during Phase IIIA. Irradiation (tr), cooling(tcool) and counting (tcount) times are 30 m, 3h18.2m and 10.75 m, respectively. It is to be noted that only most prominent γ-peaks for a given emitter are included (see **Fig. 11**); in addition, 66 h ^{99}Mo peak at 141 keV carries contribution from 6.02 h ^{99m}Tc too. Error varies from 3.0 % for ^{99}Mo(+^{99m}Tc) to 14.4 % for 6.95 h ^{93m}Mo.

3. EXPERIMENTAL RESULTS

3.1. Material-Wise Highlights

Figures 12.1 and **12.2** are plots of decay γ emission rate/s/g versus Z of sample for ~1 day cooling time in phase IIC and III experiments respectively. **Figure 12.3** is derived from **Figures 12.1 and 12.2** for equivalent conditions. Similarly, **Figures 13.1** through **13.3** are plots of decay γ emission rate/s/g for ~1 week cooling time. **Table 6** summarizes spectral conditions and identifiers for the experiments carried out in phases IIC through IIIC. **Tables 7.1 to 7.27** list material-wise important parameters for γ-spectroscopic measurements of samples irradiated in all these experiments.

For some of the irradiated materials, dominant contributors to decay γ emission rates are summarized as follows:

Iron: For cooling times less than 10 h, ^{56}Mn ($T_{1/2}$=2.6 h) dominates. For larger cooling times, ^{54}Mn ($t_{1/2}$=312 d) assumes growing ascendancy. No significant neutron energy spectrum dependence was observed as both these products result from high threshold (n,p) reaction.

Nickel: ^{62m}Co (13.9 m) and ^{57}Ni (36 h) dominate for short cooling times. ^{58}Co (70.8 d), ^{57}Co (271 d), ^{57}Ni, ^{59}Fe (44.6 d) and ^{60}Co (5.3 y) take over at larger cooling times.

Chromium: 320 keV γ line from ^{51}Cr (27.7 d) dominates for long irradiation and cooling times. NaCl and Fe/Mn impurities seem to be present as ^{24}Na (15 h), ^{35m}Cl (32 m) and ^{56}Mn(2.6 h) contribute as much as 3 % to the total decay γ emission rate for cooling time of 1.5 h. For cooling time of 15 h only ^{24}Na contributes- less than 1 % only.

Molybdenum: Major contributors for short cooling times are ^{101}Mo (14.6 m), ^{101}Tc (14.2 m) , ^{97}Nb (1.2 h), ^{98m}Nb (51 m), ^{99}Mo (66 h), ^{99m}Tc (6 h), ^{96}Nb (23.4 h), and ^{93m}Mo (6.9 h). ^{101}Tc results from β^- decay of ^{101}Mo, and ^{99m}Tc is produced by β^- decay of ^{99}Mo. Longer cooling times see dominance of ^{99}Mo, ^{99m}Tc, ^{96}Nb, ^{97}Nb and ^{89}Zr.

Stainless Steel (SS316 & AISI316): It is an alloy of Fe, Ni, Cr, Mn and Mo. ^{56}Mn contributes overwhelmingly at cooling times less than a day. At larger cooling times, ^{99}Mo, ^{99m}Tc, ^{51}Cr, ^{58}Co, ^{57}Ni and ^{54}Mn are leading contributors.

Cobalt: For cooling periods of less than 5 h, ^{56}Mn product of ^{59}Co(n,α)^{56}Mn reaction- made dominating contribution, as much as 95 % for irradiation period of 30m and cooling period of 37 m. The other contributing isotopes include ^{59}Fe (44.6 d), ^{58}Co (70.8 d) and ^{60}Co (5.3 y), the last isotope was noticeable at locations having larger component of softer neutrons.

Tungsten: ^{187}W (23.9 h), ^{186}Ta (10.5 m) and ^{183}Hf (64 m) dominate short cooling times. For larger cooling times, predominant contributor ^{187}W is backed up by ^{183}Ta (5 d) and ^{182}Ta (115

d).

Zirconium: ^{89}Zr (78.4 h), ^{87m}Sr (2.8 h), ^{90m}Y (3.2 h), ^{94}Y (18.7 m), ^{92}Y (3.5 h) and ^{91}Sr (9.5 h) contribute for short cooling times. Larger cooling times bring into focus predominance of ^{89}Zr and ^{90m}Y (3.2 h).

Tantalum: ^{180m}Ta (8 h), ^{180m}Hf (5.5 h) and ^{182}Ta (115 d) dominate γ emission rate.

Lead: ^{203}Pb (52 h) and ^{204m}Pb (67 m) dominate at shorter cooling times. ^{203}Pb dominates at larger cooling times.

Tin: At shorter cooling times, ^{123m}Sn (40 m) dominates. other contributors include ^{117}In (42.3 m), $^{116m1}In$ (54.1 m), ^{117}In (1.93 h), ^{111}In (2.8 d) and ^{117m}Sn (14 d). At larger cooling times, ^{117m}Sn dominates.

Zinc: Annihilation peak at 511 keV dominates at short cooling times. Other significant contributors include ^{63}Zn (38 m), ^{66}Cu (5.1 m), ^{69m}Zn (13.8 h) and ^{65}Ni (2.52 h). At larger cooling times, apart from annihilation peak, leading contributors are ^{69m}Zn, ^{67}Cu (61.9 h), ^{65}Zn (244 d), ^{64}Cu (12.7 h) and ^{65}Ni.

Titanium: At short cooling times, 511 keV annihilation γ -ray from ^{45}Ti (3.1 h) and ^{48}Sc (43.7 h) γ-rays dominate the measured emission rates. At longer cooling times, other contributors include ^{47}Sc (3.42 d) and ^{46}Sc (83.8 d).

Vanadium: At shorter cooling times, ^{51}Ti (5.8 m) dominated the emission rate followed by ^{48}Sc (43.7 h). Also, ^{52}V (3.8 m) was observed. For longer cooling times, ^{48}Sc dominated the scene single handedly.

Aluminum & Magnesium: ^{24}Na (15 h) dominated the decay γ spectra at larger cooling times.

Silver: At short cooling times, a peak at 511-512 KeV dominates. This peak gets large contributions from ^{106}Ag (24 m), ^{106m}Rh (130 m) and ^{106m}Ag (8.5 d). At larger cooling times, a large number of γ lines from ^{106m}Ag dominate the emission rate.

MnCu Alloy: For shorter cooling times, ^{62}Cu (9.73m, 511 keV annihilation γ) and ^{56}Mn (2.6 h) dominated the emission rate. However, their relative contributions varied depending on the hardness of the neutron energy spectrum- ^{62}Cu dominating for harder neutron spectrum. At larger cooling times, ^{54}Mn (312 d) dominates.

$YBa_2Cu_3O_7$: ^{135m}Ba (28.7 h), ^{133m}Ba (38.9 h), ^{139}Ba 82.9 m),$^{135m+g}Xe$ and ^{90m}Y (3.2 h) made large contributions. Other contributors include ^{65}Ni, ^{62}Cu, ^{62m}Co, ^{64}Cu and ^{88}Y. At larger cooling times, ^{88}Y dominated the scene.

3.2. Parametric Dependence

3.2.1.Spectral

Spectrum dependence of γ-ray emission rates is mostly seen only in those materials that have dominating isotopes resulting from (n,γ) reactions. High threshold reactions, e.g, (n,n'), (n,p), (n,n'p), (n,d), (n,2n), are essentially governed by harder part of the spectrum. Comparing the integrated γ-emission rates (between 100 keV to 3 MeV), it is found that for short irradiation time (30m), Fe, AISI316, Al and Co give leading rates in that order. However, the trend changes for ~10h irradiation to: Al, Fe, and AISI316. This is understandable as ^{24}Na (15 h) production rate was unsaturated during 30 m irradiation but almost saturated during ~10 h irradiation.

3.2.2. γ Component of Energy Release Rate

γ component of total energy release rate was obtained from γ emission rate spectrum for each material. Comparison of γ energy release rates at same irradiation and cooling times shows that for short (30m) irradiation time, Fe, AISI316, Al dominate in that order. For larger irradiation and cooling times, the trend is different: for hard spectrum (without blanket), ~10 h irradiation and 15 h cooling time Al domination is meekly followed by Mo and Ti; for softer spectrum (with surrounding blanket) ~10 h irradiation and 15 h cooling time, W, Al, Ta, and Zr contribute in that order.

3.2.3. Total Energy Release Rate

Total energy release rates, directly related to decay-heat, were derived from measured γ emission rates and deduced β emission rates (using known branching ratios and average beta energy release per disintegration). It turns out that β contribution varies widely from material to material and it ranges from 0 to 50%. The lowest beta contribution is observed for Cr followed by Ni. The beta fraction varies both with irradiation and cooling times. V dominance at short irradiation and cooling times under hard spectrum is followed by Zr, AISI316, Co and Fe. At larger irradiation and cooling time , W lead is followed by Fe, Mo, AISI316 and Co. Generally, it is observed that short lived isotopes make dominating contributions towards β energy release at shorter cooling times. This fact underlines the important role of accurate determination of short lived activities in the selection of materials for fusion devices that would be required to be accessed by personnel after relatively short operation time.

3.2.4. Impurity Impact

As stated in individual descriptions for dominant γ-ray contributor, it was found there are lager induced activities due to unexpected impurities in Si and Cr than we expected. Also it should be noted that the ^{24}Na, possible product via ^{27}Al(n,α), ^{24}Mg(n,p) or ^{23}Na(n,γ), was observed in many cases where Al and Na were assumed not to be contained. The most probable explanation for

^{24}Na is given by the contamination of NaCl due to hand touching on the materials unexpectedly even though we paid maximum care not to do. All those evidence of large contribution due to the impurities remind us the importance of consideration for small amount of impurities or unexpected contamination.

3.3. Basis for Data Identification

As reported in **Tables 7.1** through **7.27**, large number of measurements were carried out. However, it is our endeavor to pick and choose what we consider the best quality data for each material. Also, it is aimed to cover as many radioactive products as possible. The data acquired with absolute detector #5S is preferred whenever feasible. 32 cases are listed in **Table 8**. Twenty cases correspond to spectral identifiers A1/A2; 6 cases pertain to B1/B2; 6 cases relate to C1. Fe (2), Ni (3), Cr, Mo (2), SS316, AISI316, MnCu alloy (3), W, Zr, V, Al, Co, Ti, Nb, Sn, Pb, Ta, Ag, Zn, Si, Y, In, Mg, Au, $YBa_2Cu_3O_7$, and $ErBa_2Cu_3O_7$ are included.

3.4. Selected Tabulated Data

Tables 9.1 through 9.32 include γ-emission rates as a function of γ-ray energy for all 32 cases. Decay γ-emission rate expresses total number of decay γ-rays emitted per gram of the irradiated material for a normalized 14 MeV source neutron intensity of 10^{12} n/s. Each table carries a header that includes measurement and detector ID's. Per cent standard deviation on γ-emission rate is provided along with absolute detector efficiency. The standard deviation on γ-emission rate includes errors from all known contributing factors.

4. EXPERIMENTAL ANALYSIS

4.1. Strategy

As shown in **Figure 14**, analysis to obtain decay γ-ray emission rate involves a multi-step procedure. A two or three dimensional transport code is employed to get neutron energy distribution, i.e., neutron flux, at spatial locations of samples. Geometry and material composition of irradiation environment are important inputs for this calculation. Next stage involves computation of decay γ emission spectrum using a radioactivity calculation code. Neutron flux, sample composition, irradiation and cooling (or shutdown) times are required input data for this stage. Decay and activation cross-section libraries form part of the code used. Leading codes used for this purpose include DKRICF[25], REAC[26], RACC[27] and THIDA[28]. In fact, THIDA is a code system that includes neutron flux calculating modules too. However, its central module is ACT4 that calculates induced radioactivity and associated quantities.

Two calculation schemes were followed for analysis. First scheme related to use of externally evaluated neutron flux with four radioactivity codes: DKRICF, REAC, RACC and ACT4. The flux was obtained in a two step process: (1)source neutron energy and angular distribution was obtained by three dimensional MCNP[29] modeling of the rotating neutron target of FNS facility[8], (2)source neutron distribution from MCNP was input to RUFF[30] and DOT4.3[31] code system to compute spatial distribution of neutron flux. 30 group MATXS5 cross-section library of LANL[32] was used for neutron transport. The neutron flux was also obtained by full-fledged MCNP calculation and was found to match the flux via the foregoing approach. As neutron energy group boundaries are different for the radioactivity codes used, flux transformation from one group structure to another was carried out subject to total neutron flux conservation. It is evident that this will add to total numerical error entailed in decay rate computation. However, it should not amount to more than a percent for most of the cases. The second calculation scheme is similar to the one in Ref. 33, wherein THIDA code is employed for whole analysis.

4.2. Neutron Spectral Conditions

The neutron spectrum information is one of the most essential parts in the induced radioactivity production calculations. The adequacy of the spectrum governs the reliability of the calculation results, because reactions for dominant radioactivity production varies location by

location depending on the neutron energy spectrum. The neutron spectra applied in the present calculations are tabulated in **Tables 10.1 and 10.2**. **Figure 15** shows computed neutron energy spectra per unit lethargy as a function of neutron energy in all phases IIC through IIIB.

4.3. Trends

Tables 11.1 to 11.6 summarize results of comparison of integrated, from 100 keV through 3 MeV, decay γ-emission rates per gram normalized to source intensity of 10^{12} n/s. The computed results from REAC-2, DKRICF and THIDA-2 are included. RACC results generally follow same trends as those from DKRICF, though spectral distributions of decay γ-emission rates differ at times. Large deviations in C/E (Computed/Experimental) ratio are observed for Mo, W, MnCu alloy, Cr, Zr, Ta and $YBa_2Cu_3O_7$. **Figures 16.1 to 16.3** show upper and lower bounds of C/E ratios for integrated decay emission rates for the three codes as a function of irradiated material. Though C/E ratios for Fe, Ni, Mo, SS316 and many other materials behave reasonably well, large discrepancies are seen for spectral distributions. **Figures 17.1 to 17.6** typically bring home this aspect. The materials covered include Iron, Nickel, Molybdenum, Stainless Steel (SS316) and Tungsten. The experimental data displayed is of two kinds: energy-group integrated for direct comparison, and γ-ray peak-wise data for detailed break-down. The symbols of tr and tcool respectively stand for irradiation and cooling times.

Table 11.5 provides a typical inter-comparison of computed (C) to measured (E) ratio for different source conditions for iron samples. Quantity being compared here is integrated decay γ emission rate per s per g for a normalizing source strength of 10^{12} n/s. Though there are some changes in C/E values for REAC and DKRICF codes, it is clear that, given rather untested nature of wide body of decay and cross section data of these codes, the change from one spectral environment to another does not bring out any drastic change. Hence, in what follows, we shall generally be presenting results for samples kept inside annular assembly of phase IIIA driven by simulated line source. But, broad conclusions deduced therefrom quite possibly are applicable to other spectral environments too.

Figures 18.1 to 18.5 display C/E for Mo, Zn, AISI316, Sn and Zr for REAC2 code system for line source driven experiments of phase IIIA. **Figure 18.1** for Mo corresponds to bare line source driven experiment for a sample at mean axial location of +100 cm; tr and tcool are 9h47m and 3h18.2m. C/E's for Mo for different products are: (1) ^{99}Mo: 1.25, (2) ^{96}Nb: 3.18, (3) ^{97}Nb: 2.56, (4) ^{97}Zr: 6.64, (5) $^{89m+g}$Zr: 4.07, (6) ^{92m}Nb: 1.02. **Figure 18.5** for Zr corresponds to

'line source driven assembly' experiment wherein a Zr sample was located at position B, i.e., 5 cm inside Li_2O zone in the central drawer; tr, tcool are 9h51m and 3h54.3m respectively. C/E values for different products are: (1) ^{90m}Y: 4.6, (2) ^{87m}Sr: 1.22, (3) ^{91m}Y: 1.82, (4) ^{97}Nb: 0.10, (5) ^{97}Zr: 9.7 x 10^{-2}, (6) $^{89m+g}Zr$. **Figure 18.3** for stainless steel (AISI) represents C/E's for an AISI sample located at position B in 'line source driven assembly' experiment; tcool is 13h13.5m. C/E values are: (1) ^{57}Co: 0.94, (2) ^{51}Cr: 1.18, (3) ^{57}Co: 2.23, (4) ^{54}Mn: 0.58, (5) ^{56}Mn: 1.02, (6) ^{57}Ni: 0.96.

4.3.1. Iron

^{56}Mn dominates for short cooling times, ^{54}Mn takes over at longer cooling times; other contributors include ^{51}Cr and ^{58}Co (nickel impurity). Some samples showed also presence of nickel/aluminum/magnesium impurities. REAC and ACT4 (a component module of THIDA) have, generally, more reliable γ-emission data. RACC cross-section data for $^{56}Fe(n,p)^{56}Mn$ are closest to published experimental ones. Gamma-yield data is generally the lowest for ACT4 even as the activation cross-sections are quite close to others. DKRICF lacks γ-yield data for gamma-rays carrying more than 2.5 MeV. In spite of all these differences, the evaluated and measured reaction rates for ^{56}Mn, ^{54}Mn and ^{51}Cr agree within 15 %, even though, the softer spectrum, at distance of 82 cm from target, tends to raise C/E ratios.

4.3.2. Nickel

^{62m}Co and ^{57}Ni dominate at short cooling times. At longer cooling times, ^{58}Co, ^{57}Co, ^{57}Ni, ^{59}Fe, ^{60}Co dominate. REAC strongly overestimates (by at least a factor of 2) contributions from ^{58}Co and ^{59}Fe. Also ^{57}Co is overestimated by as much as 25 %. C/E for ^{57}Co for DKRICF is in the range of 0.97 to 1.08 for all cases; C/E for ^{58}Co ranges from 0.0.97 to 1.24; C/E for ^{59}Fe is 0.82 for DKRICF as against 2.61 for REAC2; C/E for ^{60}Co is 0.83 as against 1.63 for REAC2.

4.3.3. Molybdenum

For short cooling times, ^{97}Nb, ^{98m}Nb, ^{99}Mo,^{99m}Tc, ^{96}Nb, ^{101}Mo, ^{101}Tc, ^{93m}Mo and ^{91}Mo contribute predominantly. ^{99m}Tc and ^{101}Tc respectively result from β^- decays of ^{99}Mo and ^{101}Mo. Longer cooling times see dominance of ^{99}Mo, ^{99m}Tc, ^{96}Nb, ^{97}Nb and ^{89}Zr. ^{91}Mo contribution is strongly overestimated by REAC. C/E ratios for this isotope are 328 and 307 respectively in 1.5-2 and 2.5-3 MeV ranges respectively. Other products are strongly underestimated by REAC. It is seen from experimental data that ratio of γ-yields for 778 to 569 keV peaks from ^{96}Nb is 3.1 instead of 1.74 (see Ref. 15); it is to be added here that quite possibly the balance of contribution for 778 keV peak pertains to 66 h ^{99}Mo. Respective C/E ratios for different products for REAC2

and DKRICF are: (1)^{93m}Mo: 200/1.11, (2)^{96}Nb: 2.04/3.49, (3)^{99}Mo: 1.08/1.11, (4)$^{89m+g}$Zr: 6/1.35, (5)^{97}Nb: 2.68/2.57, (6)^{95}Nb: 2/2.5, (7)^{95m}Nb: 0.77/0.20, (8)^{92m}Nb: 0.90/0.90, (9)^{95}Zr: 0.87/0.86.

4.3.4. MnCu Alloy

^{56}Mn, ^{62}Cu, ^{52}V, ^{62m}Co and ^{65}Ni are most important contributors for short cooling times. ^{54}Mn dominates larger cooling times. 511 keV γ-ray from ^{62}Cu is overestimated by a factor of more than 3 by REAC2 and DKRICF. C/E ratios are found considerably larger than 1 for ^{56}Mn. In fact, even for other materials, there is a general trend for the codes to predict larger C/E ratios for (n,γ) reactions in presence of softer neutron energy spectrum (at 82 cm from target). REAC gives C/E ratios close to 1 for ^{54}Mn. DKRICF and REAC generally agree between themselves from 0.1 to 2.5 MeV.

4.3.5. Chromium

Dominant contributors are ^{51}Cr and ^{49}Cr. 847 and 1811 keV peaks of ^{56}Mn are also detected-Fe/Mn impurity is expected. Unidentified peaks at 147, 563, 573 and 601 KeV were observed. ^{48}V contribution was absent. However, REAC predicts a large contribution from this isotope; γ-yield data appears acceptable. As a result, C/E (=6.2) is strongly over-predicted in 0.4-1 MeV range. DKRICF has C/E of 2.2 for the same range. REAC yields C/E of 2.63 for ^{49}Cr, whereas DKRICF yields a value of 0.96.

4.3.6. Stainless Steel (SS316 and AISI316)

^{56}Mn contributes overwhelmingly at short cooling times. At larger cooling times, ^{99}Mo, ^{99m}Tc, ^{51}Cr, ^{58}Co, ^{57}Ni, and ^{54}Mn are leading contributors. C/E trends for individual contributors are same as discussed before for Fe, Ni, Cr and Mo.

4.3.7. Vanadium

Short cooling times bring leading contributions from ^{51}Ti, ^{52}V and ^{48}Sc. Larger cooling times bring out total dominance of ^{48}Sc. C/E ratios, from REAC, are 1.01 and 0.86 respectively for ^{51}Ti and ^{52}V at 10 cm location. C/E ratio of 1.5 is found for the same location for ^{48}Sc by the same code. For DKRICF, C/E for ^{48}Sc is ~3.

4.3.8. Zirconium

^{89}Zr, ^{87m}Sr, ^{90m}Y, ^{94}Y, ^{92}Y and ^{91}Sr contribute at short cooling times. Larger cooling times bring out predominance of ^{89}Zr and ^{90m}Y. REAC largely over-predicts C/E (factor of 4 to 5) for

both ^{89}Zr and ^{90m}Y. For ^{91m}Y, C/E is 1.7. However, C/E for ^{87m}Sr is close to 1 for REAC and is just 0.4 for DKRICF. Nevertheless, DKRICF has good agreement with the experimental data otherwise.

4.3.9. Tungsten

^{187}W, ^{186}Ta and ^{183}Hf dominate short cooling time measurements. For larger cooling times, predominant contributor ^{187}W is backed up by ^{183}Ta and ^{182}Ta. One sample indicates the presence of Na/Al/Mg impurity. Tabulated γ-yield data[17] does not match with measured relative ratios for various γ peaks emitted by ^{186}Ta and ^{183}Hf. Further investigation is called for. DKRICF lacks decay data for ^{186}Ta, ^{187}W and ^{181}W. REAC analysis shows ^{179m}W ($t_{1/2}$=6.4 m, 0.03 % 289 keV, 0.19 % 282 keV, 0.22 % 239 keV, 0.32 % 120 keV and 0.61% 102 keV) as making dominant contributions for both short and long cooling times; γ-yield data is 2 to 3 orders higher in decay data library of REAC2. Also, ^{182m}Hf, ^{184}Ta, ^{183}Hf, ^{180m}Hf are strongly overestimated by REAC. γ-yields are found to be grossly overestimated for many products in THIDA.

4.3.10. Tantalum

^{180m}Ta, ^{180m}Hf and ^{182}Ta dominate identifiable contributions to measured data. There are unidentified peaks at 110, 117, 148, 482, 500 and 1001 keV. REAC strongly overestimates in 0.2-0.4 MeV (factor of 5) and 0.4-1.0 MeV (factor of 7) energy ranges.

4.3.11. $YBa_2Cu_3O_7$

^{135m}Ba($t_{1/2}$=28.7 h),^{139}Ba, $^{135m+g}$Xe and ^{90m}Y make largest identifiable contributions at short cooling times. There appears to be ^{87m}Sr peak at 388 keV. Other contributors include ^{65}Ni, ^{62}Cu, ^{62m}Co, ^{64}Cu and ^{88}Y. At larger cooling times, ^{88}Y dominates the scene. REAC lacks decay data for ^{139}Ba, ^{133m}Ba, ^{135m}Ba and $^{135m+g}$Xe. DKRICF lacks decay data for Ba, Xe and Y. C/E ratios for ^{65}Ni, ^{62}Cu and ^{62m}Co deviate considerably from unity even though they are not crucial contributors to overall decay γ-emission rates.

4.3.12. Tin

Figure 18.4 refers to a **Sn** sample located at location C, i.e., at 40 cm axial distance from the mid-point of the assembly in line source driven experiment.; tcool is 3h45.9m. Tin data does have problems with both the codes. In DKRICF, ^{117m}Sn and ^{111}In are largely underestimated. REAC shows total absence of ^{116m1}In ($t_{1/2}$=54.1 m, 417 keV). In addition, ^{117m}Sn and ^{111}In are strongly overestimated.

4.3.13. Zinc

Figure 18.5 refers to a **Zn** sample kept at position C in 'line source driven assembly' experiment and cooled for 5h45.3m. Zinc data has serious problems for both DKRICF and REAC. ^{67}Cu, ^{69m}Zn and ^{64}Cu contributions are practically absent in DKRICF. REAC severely overestimates ^{65}Ni (factor of 1.9), ^{67}Cu (factor of 32) , and ^{69}Zn (absent in experimental data). It largely underestimates ^{69m}Zn (C/E=0.13), ^{65}Zn (C/E=0.62), and ^{64}Cu (C/E=0.78).

4.3.14. Lead

Lead The C/E values for REAC are too high. The reason for this discrepancy lies in overestimation of ^{203}Pb production by a factor of 2.3. The ^{204m}Pb is also strongly overestimated though it does not show up much contribution in our experiments.

4.3.15. Silver

Silver data appear to be acceptable for DKRICF. However, the absence of decay data of ^{106m}Ag severely handicaps REAC results, resulting in abysmally low values of C/E even at rather low cooling times.

4.4. Demonstrative Examples for tungsten

4.4.1 Outline

We present analysis of experimental results for measurements done on tungsten samples kept at 10 cm distance from the rotating neutron target (RNT) of FNS during experiments with coolant channel assembly configuration of phase IIC in 1988. **Figure 1** shows the schematic of the arrangement. Two irradiations of 30m and 9h durations were conducted to cover radioactive products of half lives ranging from 10 m to 1 y. The source neutron intensity averaged 8.75 x 10^{11} n/s during full 9 h irradiation. Two other tungsten samples were irradiated at '82 cm' location. Cooling times ranged from 37.3 m to 2d19 h.

Multitude of neutron induced reactions and range of product half lives can be gauged from **Table 12** which lists measured γ-rays from radioactive products of tungsten, of half life from 10.5 m to 115 d. All tungsten samples were high purity circular discs, each measuring 10 mm diameter x 1 mm thickness; on average, silicon was a major impurity accounting for less than 0.008 %. Each of the irradiated samples had tungsten of natural isotopic composition, i.e., 0.13 % of ^{180}W, 26.3 % of ^{182}W, 14.3 % of ^{183}W, 30.7 % of ^{184}W, and 28.6 % of ^{186}W.

4.4.2 Discussion:

^{187}W, ^{186}Ta and ^{183}Hf dominate short cooling time measurements. For larger cooling times, predominant contributor ^{187}W is backed up by ^{183}Ta and ^{182}Ta. One sample indicates the presence of Na/Al/Mg impurity. **Figure 19** presents integrated γ-energy release rate per g, in units of nW/g, 100 keV through 3 MeV, as a function of cooling time for the tungsten sample irradiated for 9 h at 10 cm location. The normalizing source intensity is 10^{12} n/s. The **figure** shows experimental as well as RACC computed data. It is to be noted that RACC strongly underestimates the energy release rate for all the cooling times. In addition, the functional dependence of the computed and the measured quantities obviously differs. **Figure 20** displays decay γ emission rate/g as a function of cooling time from four radioactivity codes as well as experiment. Though THIDA and REAC results largely over-predict the emission rate at all cooling times, at least they appear to follow the functional characteristic of the measurement. On the other hand, both RACC and DKRICF largely under-predict and follow different functional dependence.

Re-looking carefully at **Figures 19 and 20**, one would suspect that either decay data or activation cross-section data or both, in RACC as well as DKRICF, are suspect. In fact, bulk of the data base for RACC was obtained from that of DKRICF; hence, their apparently similar behaviour is understandable. Investigation of half life and decay gamma spectrum data provided with RACC reveals three major errors: (1) ^{184}Ta half life is 7.519×10^5 s instead of 3.1320×10^4 s, (2) ^{186}Ta half life is 6.301×10^3 s instead of 630 s, (3) decay γ emission data for ^{187}W is mistakenly assigned to ^{186}W, a stable nucleus, and no γ data is assigned to ^{187}W at all. A modified RACC data library was created by rectifying these errors. It is denoted as RACC(m) on **Fig. 21**. C/E for integrated decay γ emission rate is shown as a function of cooling time in **Figure 21**. First cooling time of 37.3 m relates to the tungsten sample irradiated for 30m; the remaining cooling times pertain to full irradiation period of 9h. Large C/E value, e.g., 307, obtained for REAC-2 for cooling time of 37.3 m is to be solely assigned to totally wrong decay γ yields for ^{179m}W ($t_{1/2}$=6.4 m) in REAC-2 data library. In fact, one can notice the discrepancy between the included and the actual values: (i) in 100-200 keV range, 1.45×10^4 % (included) versus 0.94% (actual), (ii) 200-400 keV range, 4.068×10^5 % versus 9.07 %. At longer cooling times, this isotope will make rapidly diminishing contributions in spite of its highly inflated γ yields, and, hence, the C/E's improve for REAC-2. RACC(m) and THIDA stay closest to each other for all the cooling times, but always above 1.

Regarding status of decay data, it is missing altogether for ^{179m}W, ^{183}Hf, ^{184}Ta, ^{185}Ta,

^{186}Ta and ^{187}W in DKRICF. This explains systematically lowest values for DKRICF. Though the decay data is individually presented for all significant decay γ-rays in THIDA decay data library-most transparent and desirable representation- large discrepancies have been observed for two decay γ-rays for ^{187}W, e.g., (1) for 113.8 keV γ, 74.09 % (included) versus 0.074 % (actual), and, (2) for 239 keV γ, 82.98 % versus 0.083 %. The γ-yield spectral data is represented differently in all the four code systems. REAC-2 bins yield data in 21-group structure from 10 KeV upwards. RACC and DKRICF represent equivalent yields for pre-defined set of discrete γ-ray energies; the total number for a nuclide does not exceed 43. For ^{182}Ta, THIDA has γ-yield totalling 0.0 as against 14.9 % in 200-400 keV range; DKRICF and RACC both show 84 % yield as against 31 % in 100-200 keV range. For ^{183}Ta, both DKRICF and RACC have γ-yield of 22 % as against 66.5 % in 200-400 keV range but have large γ-yield of 61 % as against 31.6 % in 100-200 keV range. For ^{184}Ta, RACC shows 63 % as against 112.3 % in 200-400 keV range. For ^{186}Ta, RACC has 0.0 % as against 80.5 % in 200-400 keV range. For ^{179m}W, data is absent in RACC and DKRICF; THIDA shows good agreement with the reference; however, REAC has large disagreement as mentioned above. For ^{187}W, RACC does not show any γ-yield as already mentioned earlier; however, RACC(m) shows good agreement with the standard reference values (marked as '**Table**' on **figure**). For the same nuclide, THIDA shows large discrepancies as already mentioned earlier. In fact, THIDA shows values of 83.2 % as against 0.35 % in 200-400 keV range, and, 82.6 % as against 8.7% in 100-200 keV range. Though not shown, the decay data representation for ^{183}Hf needs improvement both in RACC and DKRICF; 400-1000 keV group shows entire γ-yield of 158 % in these codes as against 93.9 %.

As the inaccurate decay data for one or more nuclides in all the four codes makes it hard to look at the quality of their activation cross-section data, the next step in our analysis has consisted in looking at induced radioactivity producing reaction rates themselves. Then, one does not have to worry about the faulty decay data. **Figure 22** shows C/E for the most prominent reaction products; in fact, these are the products that could be measured experimentally through their signature γ-rays. On average, THIDA cross section data appears to be leading to the best agreement with the measurements. There is a large scatter for all the isotopes. In fact, it is borne out also by comparison of energy-wise cross-section data in different codes with ENDF/B-VI data for ^{182}W(n,p)^{182}Ta, ^{183}W(n,p)^{183}Ta, ^{184}W(n,p)^{184}Ta, ^{184}W(n,α)^{181}Hf, ^{186}W(n,np)^{185}Ta, ^{186}W(n,p)^{186}Ta, ^{186}W(n,α)^{183}Hf and ^{186}W(n,γ)^{187}W reactions. Trend-wise, the ENDF/B-VI data is likely to provide better agreement with the measurements but it seems that still substantial improvements in the cross-section data would be required to obtain closer agreement, say, in the range of 10-15 %, for most of the reactions.

4.4.3. Conclusions:

Integrated and spectral decay γ-emission rates from fusion neutron induced radioactive materials have been measured and computed using four leading radioactivity codes. Large differences between measured and calculated data have been revealed for practically all isotopes. For example, RACC strongly underestimates the energy release rate for all the cooling times. Decay data is discrepant in all the code systems. Also, the representation of decay γ-yield spectral data in RACC, DKRICF and REAC-2 merits improvement so as to enhance its transparence and ability for peak-wise comparison with the experimentally measured data; THIDA is the only code system that has this advantage. Half lives of both ^{184}Ta and ^{186}Ta are entered wrongly in RACC and DKRICF and need immediate correction. In addition, ^{187}W decay γ-yield spectra is erroneously assigned to ^{186}W, a stable nucleus, in RACC. In addition, RACC needs improvement in decay data for ^{182}Ta, ^{183}Ta, ^{184}Ta, ^{186}Ta, and ^{183}Hf. Decay data is absent for both ^{179}W and ^{179m}W. DKRICF has no decay data for ^{179m}W, ^{187}W, ^{186}Ta, ^{184}Ta and ^{185}Ta. THIDA needs improvement in decay data for ^{182}Ta and ^{187}W. ^{179m}W decay data needs immediate improvement in REAC-2.

Activation cross-section data for important nuclides needs substantial improvement. The inter-comparison of cross-section data for ^{182}W(n,p)^{182}Ta, ^{183}W(n,p)^{183}Ta, ^{184}W(n,p)^{184}Ta, ^{184}W(n,α)^{181}Hf, ^{186}W(n,np)^{185}Ta, ^{186}W(n,p)^{186}Ta, ^{186}W(n,α)^{183}Hf and ^{186}W(n,γ)^{187}W shows clearly that ENDF/B-VI data is a significant improvement in so far as it is likely to bring closer agreement between computations and measurements. However, larger modifications in the cross-section data would be required to bring the agreement between computations and measurements in the range of 10-15 %, an eminently desirable goal.

5. SUMMARY AND CONCLUSION

An extensive, experimental effort has been devoted to the induced radioactivity characterization for fusion reactor structural materials in the framework of JAERI/USDOE collaborative program on fusion neutronics. This report summarized all experimental efforts on this subject and is issued as the joint report of the collaboration. The selected data were given in digital form for further testing of calculation code and associated nuclear data relevant to the induced radioactivities. The preliminary experimental analyses with code systems of REAC*2, DKR-ICF, RACC and THIDA-2, were briefly outlined. From the results, it was pointed out that there are severe inadequacies not only in the activation cross sections but also the decay data incorporated. In addition, it revealed that the uncertainty in the primary neutron spectrum calculation should be factored into overall uncertainty in the calculation. The importance of experimental verification has clearly been demonstrated in this work. The authors hope that the present study would provide clear guidancem and encouragement for more serious effort on verification of basic nuclear data as well as codes and associated data libraries through integral measurements of the induced radioactivity. Licensing of fusion reactors will require clear verification and certification of codes and the associated nuclear data.

ACKNOWLEDGEMENTS

Authors wish to acknowledge Messers. J. Kusano, C. Kutukake, S. Tanaka and Y. Abe for operation of the FNS accelerator.

The U.S. contributors were supported by the United States Department of Energy, Office of Fusion Energy, under contract no. DE-FG03-86ER52123.

5. SUMMARY AND CONCLUSION

An extensive, experimental effort has been devoted to the induced radioactivity characterization for fusion reactor structural materials in the framework of JAERI/USDOE collaborative program on fusion neutronics. This report summarized all experimental efforts on this subject and is issued as the joint report of the collaboration. The selected data were given in digital form for further testing of calculation code and associated nuclear data relevant to the induced radioactivities. The preliminary experimental analyses with code systems of REAC*2, DKR-ICF, RACC and THIDA-2, were briefly outlined. From the results, it was pointed out that there are severe inadequacies not only in the activation cross sections but also the decay data incorporated. In addition, it revealed that the uncertainty in the primary neutron spectrum calculation should be factored into overall uncertainty in the calculation. The importance of experimental verification has clearly been demonstrated in this work. The authors hope that the present study would provide clear guidancem and encouragement for more serious effort on verification of basic nuclear data as well as codes and associated data libraries through integral measurements of the induced radioactivity. Licensing of fusion reactors will require clear verification and certification of codes and the associated nuclear data.

ACKNOWLEDGEMENTS

Authors wish to acknowledge Messers. J. Kusano, C. Kutukake, S. Tanaka and Y. Abe for operation of the FNS accelerator.

The U.S. contributors were supported by the United States Department of Energy, Office of Fusion Energy, under contract no. DE-FG03-86ER52123.

REFERENCES

[1] E.E. Bloom et al., "Low Activation Materials for Fusion Applications," *J. of Nuclear Materials*, **122&123**, 17 (1984).

[2] G. Logan, "A Rationale for Fusion Economics Based on Inherent Safety," *J. of Fusion Energy*, **4**, 245 (1985).

[3] T. Noda et al., "Materials Selection for Reduced Activation of Fusion Reactors," *J. of Nuclear Materials*, **155-157**, 581 (1988).

[4] E.T. Cheng, "Radioactivity Aspects of Fusion Reactors," Fusion Engineering and Design, **8-10** (1989).

[5] M. Zucchetti, "Impurity Concentration Limits and Activation in Fusion Reactor Structural Materials," *Fusion Technology*, **19**, 294 (1991).

[6] L.R. Greenwood and D.L. Bowers, "Production of Long-lived Activities in Fusion Materials," J. of Nuclear Materials, 155-157, 585(1988).

[7] R.W. Conn et al., "Lower Activation Materials and Magnetic Fusion Reactors," *Nuclear Technology/Fusion*, **5**, 291(1984).

[8] T. NAKAMURA, H. MAEKAWA, Y. IKEDA, Y. OYAMA AND J. KUSANO, "Present Status of the Fusion Neutronics Source (FNS)," Proc. 4th Symp. on Accelerator Sci. and Technol., RIKEN, Saitama, November 24th - 26th, 1982, pp155-156.

[9] T. Nakamura and M. A. Abdou, "Summary of Recent Results from the JAERI/U.S. Fusion Neutronics Phase-I Experiments," *Fusion Technology* , **10**, 541 - 548 (1986).

[10] H. Maekawa and M. A. Abdou, "Overview of the Latest Experiments under the JAERI/USDOE Collaborative Program on Fusion Neutronics, " Fusion Design and Engineering, 18, 275-280 (1991).

[11] A.Kumar, M.A. Abdou, Y. Ikeda, C. Konno, "Radioactivity and Nuclear Heating Measurements for Fusion Applications," Fusion Technology 1990, pp 872-876, Eds. B.E. Keen, M. Huguet, R. Hemsworth, Elsevier Science Publishers B.V., 1991.

[12] Y. Ikeda, C. Konno, T. Nakamura, A. Kumar, M.A. Abdou, "Experiment on Induced Activities and Decay-Heat in Simulated D-T Neutron Fields: JAERI/USDOE Collaborative Program on Fusion Neutronics," *Fusion Technology*, **19** , 1961-1966 (1991).

[13] A. Kumar, M. A. Abdou, Y. Ikeda, T. Nakamura, "Analysis of Induced Activities Measurements Related to Decay-Heat in Phase IIC Experimental Assembly: USDOE/JAERI Collaborative Program on Fusion Neutronics Experiments," *Fusion Technology*, **19** (1991)1909-1918.

[14] A. Kumar, M.Z. Youssef, Y. Ikeda and C. Konno, "Experiments and Analysis for Measurements of Decay-Heat Related Induced Activities in Simulated Line Source Driven D-T Neutron Fields of Phase IIIA: USDOE/JAERI Collaborative Program on Fusion Neutronics," *Fusion Technology*, **19** (1991)1859-1866.

[15] A. Kumar, "Measurement and Analysis of Decay Radioactivity Data on Tungsten," UCLA memo dated February 19,1991, distributed internationally on March 21, 1991.

[16] Y. Ikeda, C. Konno, Y. Oyama, T. Nakamura, A. Kumar, M.Z. Youssef, and M.A. Abdou, "Experimental Verification of the Current Data and Methods for Induced Radioactivity and Decay Heat Calculation in D-T Fusion Reactors," *Fusion Engineering and Design* , **18** (1991)387-395 .

[17] A. Kumar, M.A. Abdou, and J.-P. Schneeberger, "Integral Fusion Neutronics Experiments and Analysis," pp. , Proceedings of ANS Topical Meeting on New Horizons in Radiation Protection and Shielding, held at Pasco, Washington, 26-30 April, 1992.

[18] Y. Ikeda, A. Kumar, and C. Konno, "Measurements of Long-lived Activation Cross Sections by 14 MeV Neutrons at FNS," presented at Int. Conf. on Nuclear Data for Science and Technology, May 1991, Jülich, Germany; see also same title and authors, p.172, Proc. of International Workshop on Fusion Neutronics, June 7, 1991, Karlsruhe, JAERI-memo 03-305 (September 1991).

[19] A. Kumar, M.A. Abdou, M.Z. Youssef, Y. Ikeda, C. Konno, Y. Oyama, K. Kosako, F. Maekawa, and H. Maekawa, "Measurements of Decay Radioactivity of Long-lived Isotopes," *Fusion Technology*, **21**, 2180 (1992).

[20] T. Nakamura, Y. Oyama, Y. Ikeda, C. Konno, H. Maekawa, K. Kosako, M.Z. Youssef, and M.A. Abdou, "A Line D-T Neutron Source Facility for Annular Blanket Experiment: Phase III of the JAERI/USDOE Collaborative Program on Fusion Neutronics," *Fusion Technology*, **19**, 1873 (1991).

[21] Y. Oyama, C. Konno, Y. Ikeda, H. Maekawa, K. Kosako, T. Nakamura, A. Kumar, M.Z. Youssef, and M.A. Abdou, "Annular Blanket Experiment Using a Line D-T Neutron Source: Phase IIIA of the JAERI/USDOE Collaborative Program on Fusion Neutronics," *Fusion Technology*, **19**, 1879 (1991).

[22] Y. Oyama, C. Konno, Y. Ikeda, H. Maekawa, F. Maekawa, K. Kosako, T. Nakamura, A. Kumar, M.Z. Youssef, and M.A. Abdou, "Phase III Experimental Results of JAERI/USDOE Collaborative Program on Fusion Neutronics," *Fusion Engineering and Design*, **18**, 203 (1991).

[23] H. Baba, "Gamma-ray Spectrum Analysis Code for Ge(Li) Detectors, " RSIC code package PSR-84 (1978); also, JAERI-M 7017, Japan Atomic Energy Research Institute (1977).

[24] E. BROWNE AND R. B. FIRESTONE: V. S. SHIRLEY, Editor, "Table of Radioactive Isotopes" A Wiley-Interscience Publication, John Wiley & Sons (1986).

[25] D.L. Henderson and O. Yasar, "A Radioactivity and Dose Rate Calculation Code Package, " Vol. 1 and 2, RSIC computer code collection, CCC-323 (April 1987).

[26] F.M. Mann, "REAC*2: Users Manual and Code Description, " WHC-EP-0282, Westinghouse Hanford Company (1989).

[27] J. Jung, "Theory and Use of the Radioactivity Code RACC," ANL/FPP/TM-122, Argonne National Laboratory (1979).

[28] Y. Seki et al., "THIDA-2: An Advanced Code System for Calculation of Transmutation, Activation, Decay Heat and Dose Rate, " RSIC computer code collection, CCC-410 (April 1987).

[29] J.F. Briesmeister, editor, "MCNP- An General Monte Carlo Code for Neutron and Photon Transport: Version 3A," report no. LA-7396-M, Rev. 2 (Sep. 1988), along with MCNP3B newsletter dated July 18, 1988, Los Alamos National Laboratory.

[30] L.P. Ku and J. Kolibal, "RUFF- A Ray Tracing Program to Generate Uncollided Flux and First Collision Moments for DOT 4, A User's Manual, EAD-R-16, Plasma Physics Laboratory, Princeton University (1980).

[31] W.A. Rhoades and R.L. Childs, "DOT-IV Version 4.3: One and Two Dimensional Transport Code Collection", RSIC computer code collection CCC-429 (May 1984).

[32] R.E. MacFarlane, "TRANSX-CTR: A Guide for Interfacing MATXS Cross-Section Libraries to Nuclear Transport Codes for Fusion Systems Analysis," Los Alamos National Laboratory, Report LA-9863-MS (Feb. 1984).

[33] Y. Ikeda et al., "Measurements of Induced Activity in Type 316 Stainless Steel by Irradiation in D-T Neutron Fields," *Fusion Technology*, **8**, 1466 (1985).

Table 1 *Chemical Composition of Primary Impurities in the Samples Used in Induced Activity Irradiations*

Sample Material	Chemical Composition by Maximum Weight %
Iron (Fe)	99.92 Fe, 0.059 Mn, 0.02 C
Nickel (Ni)	99.97 Ni, 0.016 C
Chromium (Cr)	99.0 Cr, 0.43 Fe, 0.10 Al, 0.05 Si
Molybdenum (Mo)	99.93 Mo, 0.03 W, 0.01 Fe
Stainless steel SS316	66.22 Fe, 17.75 Cr, 11.60 Ni, 2.08 Mo, 1.33 Mn, 0.42 Si, 0.19 Co, 0.34 Cu, 0.06 V
Stainless steel AISI316	68.6 Fe, 16.5 Cr, 11.30 Ni, 2.12 Mo, 1.46 Mn
Copper (Cu)	99.999 Cu, 0.0002 Ag
Mn-Cu alloy (MnCu)	79.78 Mn, 19.66 Cu, 0.46 Ni, 0.07 Fe
Tungsten (W)	99.97 W, 0.008 Si
Zirconium (Zr)	99.76 Zr, 0.10 Fe, 0.09 Si, 0.03 Ti
Vanadium (V)	99.82 V, 0.044 Si, 0.03 Ta, 0.03 O, 0.013 Mo, 0.01 Zr, 0.01 Fe, 0.01 Al, 0.01 Hf
Aluminum (Al)	99.97 Al, 0.006 Mg
Cobalt (Co)	99.95 Co, 0.04 Ni
Titanium (Ti)-^{RE}	99.79 Ti, 0.12 O, 0.06 Fe, 0.02 C
Titanium (Ti)-^{GF}	99.6 Ti, 0.13 O, 0.03 Al, 0.03 Cr, 0.03 Mn, 0.03 Ni, 0.03 V, 0.02 Fe
Niobium (Nb)	99.91 Nb, 0.018 Ta, 0.01 Zr
Tin (Sn)	99.87 Sn, 0.02 Cu, 0.02 Sb, 0.02 Pb, 0.01 Fe, 0.01 Ni, 0.01 Co, 0.01 S, 0.01 As, 0.01 Bi
Lead (Pb)	99.95 Pb, 0.023 Bi, 0.016 Sn, 0.005 Ag, 0.005 Cu, 0.001 Ti
Tantalum (Ta)	99.98 Ta, 0.007 Fe
Silver (Ag)	99.95 Ag, 0.043 Cu, 0.003 Fe, 0.003 Zn, 0.0006 Pb
Zinc (Zn)	99.95 Zn, 0.038 Pb, 0.006 Cu, 0.004 Cd, 0.002 Sn, 0.0004 Ag
Yttrium (Y)	99.9 Y, 0.06 Ta, 0.005 Gd, 0.002 Eu
Indium (In)	99.99 In, 0.003 Cu
Magnesium (Mg)	99.78 Mg, 0.10 Al, 0.07 Zr, 0.02 Mn, 0.01 Si

RE It was supplied by Reactor Experiments/ **GF** It was supplied by Goodfellow Metals

Table 2 *Isotopic Composition of Leading Elemental Components of Irradiated Samples*

Element	% Isotopic Composition
Mg	78.99 ^{24}Mg, 10.00 ^{25}Mg, 11.01 ^{26}Mg
Al	100 ^{27}Al
Si	92.23 ^{28}Si, 4.67 ^{29}Si, 3.10 ^{30}Si
Ti	8.2 ^{46}Ti, 7.4 ^{47}Ti, ^{48} Ti, 5.4 ^{49}Ti, 5.2 ^{50}Ti
V	0.25 ^{50}V, 99.75 ^{51}V
Cr	4.35 ^{50}Cr, 83.79 ^{51}Cr, 9.50 ^{53}Cr, 2.36 ^{54}Cr
Mn	100 ^{55}Mn
Fe	5.8 ^{54}Fe, 91.8 ^{56}Fe, 2.15 ^{57}Fe, 0.29 ^{58}Fe
Co	100 ^{59}Co
Ni	68.3 ^{58}Ni, 26.1 ^{60}Ni, 1.13 ^{61}Ni, 3.59 ^{62}Ni, 0.91 ^{64}Ni
Cu	69.2 ^{63}Cu, 30.8 ^{65}Cu
Zn	48.6 ^{64}Zn, 27.9 ^{66}Zn, 18.8 ^{68}Zn
Y	100 ^{89}Y
Zr	51.5 ^{90}Zr, 11.2 ^{91}Zr, 17.1 ^{92}Zr, 17.4 ^{94}Zr, 2.8 ^{96}Zr
Nb	100 ^{93}Nb
Mo	14.8 ^{92}Mo, 9.3 ^{94}Mo, 15.9 ^{95}Mo, 16.7 ^{96}Mo, 9.6 ^{97}Mo, 24.1 ^{98}Mo, 9.6 ^{100}Mo
Ag	51.83 ^{107}Ag, 48.17 ^{109}Ag
In	4.3 ^{113}In, 95.7 ^{115}In
Sn	1.01 ^{112}Sn, 0.67 ^{114}Sn, 0.38 ^{115}Sn, 14.8 ^{116}Sn, 7.75 ^{117}Sn, 24.3 ^{118}Sn, 8.6 ^{119}Sn, 32.4 ^{120}Sn, 4.56 ^{122}Sn, 5.64 ^{124}Sn
Ba	0.106 ^{130}Ba, 0.101 ^{132}Ba, 2.42 ^{134}Ba, 6.59 ^{135}Ba, 7.85 ^{136}Ba, 11.2 ^{137}Ba, 71.7 ^{138}Ba
Er	0.14 ^{162}Er, 1.56 ^{164}Er, 33.4 ^{166}Er, 22.9 ^{167}Er, 27.1 ^{168}Er, 14.9 ^{170}Er
Ta	0.0123 ^{180}Ta, 99.987 ^{181}Ta
W	0.13 ^{180}W, 26.3 ^{182}W, 14.3 ^{183}W, 30.7 ^{184}W, 28.6 ^{186}W
Au	100 ^{197}Au
Pb	24.1 ^{206}Pb, 22.1 ^{207}Pb, 52.3 ^{208}Pb
Bi	100 ^{209}Bi

Table 3 *Decay γ yields for Prominent γ-rays Emitted by Major Radioactive Products*

Material	Product	Half Life	Decay γ-yield as a function of Energy (keV)
Fe	^{53}Fe	8.5m	42% 378
	^{56}Mn	2.58h	98.87% 847, 0.040% 1038, 0.099% 1238, 27.19% 1811, 14.34% 2113, 0.99% 2523, 0.019% 2598, 0.65% 2658, 0.31% 2960, 0.17% 3370
	^{51}Cr	27.7d	10.2% 320
	^{59}Fe	44.6d	1.02% 143, 3.08% 192, 0.27% 335, 0.018% 1382, 43.7% 1292, 0.06% 1482
	^{54}Mn	312.2d	100% 835
Ni	^{62m}Co	13.9m	1.8% 778, 1.3% 875, 1.3% 1129, 68.1% 1164, 97.9% 1173, 6.8% 1719, 18.6% 2004, 6.5% 2105
	^{65}Ni	2.52h	4.7% 366, 15.1% 1116, 23.5% 1482, 0.49% 1623, 0.39% 1725
	^{57}Ni	36h	12.88% 127, 77.6% 1378, 7.06% 1757, 14.7% 1919
	^{59}Fe	44.6d	1.02% 143, 3.08% 192, 56.5% 1099, 43.2% 1292
	^{58}Co	70.8d	100% 811, 0.74% 864, 0.54% 1674
	^{57}Co	271d	85.6% 122, 11.13% 137, 0.16% 692
	^{60}Co	5.27y	100% 1173, 100% 1332
Cr	^{49}Cr	41.9m	54.2% 91, 30.9% 153, 0.051% 1362, 0.012% 1424, 0.010% 1508, 0.029% 1515, 0.020% 1571
	^{48}V	15.97d	7.76% 944, 100% 984, 97.5% 1312, 2.41% 2240
	^{51}Cr	27.7d	10.2% 320
Mo	^{101}Tc	14.2m	2.86% 127, 1.69% 184, 88% 307, 1.02% 531, 6.0% 545
	^{101}Mo	14.6m	18.8% 192, 2.86% 196, 1.60% 409, 1.47% 500, 11.8% 506, 22% 591, 7.2% 696, 3.4% 713, 3.4% 877, 4.15% 934, 15.06% 1013, 3.97% 1161, 4.61% 1251, 6.5% 1533, 1.69% 1674, 0.98% 1760, 6.9% 2032
	^{91}Mo	15.5m	0.22% 1582, 0.32% 1634, 0.11% 2632
	^{98m}Nb	51.3m	1.35% 173, 9.51% 335, 9.13% 714, 73.6% 723, 93.2% 787, 7.81% 792, 2.4% 824, 10.8% 834, 2.05% 996, 18.0% 1169, 8.85% 1701

Table 3 continued

	^{97}Nb	72m		98.34% 658, 1.08% 1025, 0.16% 1269, 0.12% 1516
	^{99m}Tc	6.01h		87.2% 141
	^{93m}Mo	6.85h	56.7%	263, 99.7% 685, 99.0% 1477
	^{97}Zr	16.9h		2.27% 355, 5.1% 508, 92.8% 743, 2.6% 1148
	^{96}Nb	23.4h		28.5% 460, 56.8% 569, 96.9% 778, 48.5% 1091, 19.8% 1200
	^{99}Mo	66.0h		90.7% 141, 6.07% 181, 1.16% 366, 12.14% 739, 4.35% 778
	^{89}Zr	78.4h		99.01% 909, 0.07% 1621, 0.10% 1657, 0.76% 1713, 0.13% 1745
	^{95m}Nb	87h		2.34% 204, 24.9% 236
	^{92m}Nb	10.15d		1.73% 913, 99.0% 935, 0.90% 1847
	^{95}Nb	34.97d		99.79% 766
	^{95}Zr	64.02d		44.1% 724, 54.5% 757
	^{88}Zr	83.4d		97.3% 393
Cu	^{62}Cu	9.74m		94.8% 511, 0.36% 1173
	^{62m}Co	13.9m		68.1% 1164, 97.9% 1173
	^{62}Co	1.5m		83.8% 1173, 14.7% 2302
	^{65}Ni*(im)	2.52h		14.8% 1116, 23.5% 1482
	^{64}Cu	12.7h		38.5% 511, 0.48% 1346
	^{60}Co	5.27y		99.90% 1173, 99.98% 1333
Mn	^{52}V	3.75m		100% 1434
	^{56}Mn	2.58h		98.87% 847, 0.040% 1038, 0.099% 1238, 27.19% 1811, 14.34% 2113, 0.99% 2523, 0.019% 2598, 0.65% 2658, 0.31% 2960, 0.17% 3370
	^{54}Mn	312.2d		100% 835
W	^{186}Ta	10.5m		23% 122, 59% 198, 49.9% 215, 8.0% 274, 14.1% 308, 14.8% 418, 33.0% 615, 46% 738
	^{185}Ta	49.5m		47.6% 175
	^{183}Hf	64m		27% 459, 65% 784
	^{184}Ta	8.7h		24.3% 111, 5.0% 161, 13.2% 215, 6.4% 227, 3.6% 243, 49.0% 253, 23.5% 318, 12.8% 384, 73.9% 414, 10.9% 461, 13.2% 537, 15.0% 792, 11.0% 895, 15.3% 903, 32.6% 921, 2.32% 1110, 5.1% 1174
	^{187}W	23.9h		8.56% 134, 21.1% 480, 4.92% 552, 6.07% 618, 1.05% 625, 26.4% 686, 0.288% 745, 3.98% 773, 0.325% 865, 0.137% 879
	^{183}Ta	5.1d		6.5% 99, 11.3% 108, 16.5% 162, 37% 246, 3.8% 292, 7.3% 312, 11.36% 354

Table 3 continued

	^{181}Hf	42.4d	80.6% 482
	^{182}Ta	115d	34.7% 1121, 16.5% 1189, 27.5% 1221, 11.63% 1231
Zr	^{94}Y	18.7m	2.02% 382, 4.9% 551, 56% 919, 6.0% 1139, 2.46% 1671
	^{91m}Y	49.7m	94.9% 556
	^{97}Nb	72m	98.34% 658
	^{87m}Sr	2.80h	82.3% 388
	^{90m}Y	3.19h	96.6% 203, 91% 480
	^{92}Y	3.54h	2.34% 449, 2.40% 561, 13.9% 935, 4.8% 1405
	^{91}Sr	9.52h	61.5% 556, 11.3% 653, 23.6% 750, 33% 1024
	^{97}Zr	16.9h	92.8% 743
	$^{89m+g}$Zr	78.4h	99.01% 909, 0.07% 1621, 0.099% 1657, 0.76% 1713, 0.13% 1745
	^{95}Zr	64d	44.1% 724, 54.5% 757
V	^{52}V	3.75m	100% 1434
	^{51}Ti	5.76m	93.0% 320, 1.18% 609, 6.9% 929
	^{48}Sc	43.7h	7.47% 175, 100% 984, 97.5% 1038, 2.38% 1213, 100% 1312
Al	^{27}Mg	9.46m	73% 844, 29.1% 1014
	^{24}Na	14.66h	100% 1369, 99.944% 2754, 0.051% 3866
Co	^{56}Mn	2.58h	98.87% 847, 0.040% 1038, 0.099% 1238, 27.19% 1811, 14.34% 2113, 0.99% 2523, 0.019% 2598, 0.65% 2658, 0.31% 2960, 0.17% 3370
	^{59}Fe	44.6d	1.02% 143, 3.08% 192, 0.27% 335, 0.018% 1382, 43.7% 1292, 0.06% 1482
	^{58}Co	70.8d	100% 811, 0.74% 864, 0.54% 1674
	^{60}Co	5.27y	100% 1173, 100% 1332
Ti	^{51}Ti	5.8m	93% 320, 1.18% 609, 6.9% 929
	^{45}Ti	3.08h	0.15% 720
	^{44}Sc	3.93h	99.9% 1157
	^{48}Sc	43.7h	7.47% 175, 100% 984, 97.5% 1038, 2.38% 1213, 100% 1312
	^{47}Sc	3.34d	68% 159
	^{46}Sc	83.8d	99.98% 889, 99.99% 1121
Nb	^{90m}Y	3.19h	96.6% 202, 91% 479
	^{92m}Nb	10.15d	1.73% 913, 99.0% 935, 0.90% 1847
Sn	^{125m}Sn	9.5m	97% 332
	^{123m}Sn	40.1m	85.6% 160

Table 3 continued

	^{117}In	43.8m	87% 159, 99.7% 553
	^{116m}In	54.2m	29.2% 417, 56.2% 1097, 84.4% 1294, 10% 1508, 15.6% 2112
	^{116}In	2.18s	36.6% 162
	^{117m}In	1.942h	15.9% 159, 19.1% 315
	^{111}In	2.81d	90.24% 171, 94.00% 245
	^{117m}Sn	13.61d	88.5% 159
Pb	^{204m}Pb	67.2m	89% 375, 99% 899, 94% 912
	^{204}Pb	52.06h	80.1% 279, 3.44% 401, 0.70% 681
Ta	^{180m}H f	5.52h	17% 93, 81.7% 215, 94.4% 332, 85% 443, 12.8% 501
	^{180m}Ta	8.15h	5% 93, 0.74% 103
	^{182}Ta	115d	34.7% 1121, 16.5% 1189, 27.5% 1221, 11.63% 1231
Ag	^{106}Ag	24m	16.7% 512, 0.135% 616, 0.309% 622, 0.195% 873, 0.163% 1050
	^{106m}Rh	2.17h	6.50% 222, 2.07% 229, 1.18% 328, 3.52% 391, 11.97% 406, 13.53% 430, 24.9% 451, 87% 511, 3.05% 601, 20.6% 616, 2.78% 646, 2.43% 680, 4.68% 703, 29.4% 717, 19.8% 748, 5.77% 793, 13.2% 804, 7.57% 808, 13.86% 825, 3.7% 848, 2.00% 1020, 30.8% 1046, 0.63% 1122, 11.1% 1128, 10.8% 1199, 8.0% 1223, 2.85% 1349, 17.4% 1528, 0.61% 1566, 6.8% 1573, 2.50% 1723, 2.12% 1839
	^{106m}Ag	8.46d	6.70% 222, 2.13% 229, 1.15% 328, 3.89% 391, 13.2% 406, 13.1% 430, 27.6% 451, 88% 512, 1.61% 601, 21.7% 616, 1.47% 646, 2.69% 680, 4.45% 703, 29% 717, 20.4% 748, 5.3% 793, 12.5% 804, 4% 808, 15.3% 825, 4.4% 848, 1.06% 1020, 29.9% 1046, 1.23% 1052, 0.57% 1122, 11.7% 1128, 11.9% 1199, 7.3% 1223, 1.51% 1349, 19.2% 1528, 0.48% 1566, 6.6% 1573, 1.32% 1723, 1.93% 1839
Zn	^{63}Zn	38.1m	185.6% 511, 8.4% 670, 6.6% 962, 0.76% 1412
	^{65}Ni	2.52h	14.8% 1116, 23.5% 1482
	^{64}Cu	12.7h	35.8% 511, 0.48% 1346
	^{69m}Zn	13.8h	94.8% 439
	^{67}Cu	2.58d	48.6% 185
	^{65}Zn	244.1d	2.92% 511, 50.75% 1116
Si	^{29}Al	6.56m	91.3% 1273, 3.51% 2028, 5.2% 2426

Table 3 continued

	^{27}Mg	9.46m	0.79% 171, 73% 844, 29.1% 1014
	$^{34m}Cl^{*}$(im)	32.23m	40.5% 146, 14.11% 1176, 42.9% 2128, 12.31% 3303
Y	^{90m}Y	3.19h	96.6% 202, 91% 479
	^{86}Rb	18.66d	8.78% 1077
	^{88}Y	106.61d	92.7% 898, 99.35% 1836, 0.666% 2734
In	^{112m}In	20.9m	12.8% 156
	^{112}In	14.4m	0.669% 607, 2.8% 617
	^{116m}In	54.2m	29.2% 417, 56.2% 1097, 84.4% 1294, 10% 1508, 15.6% 2112
	^{116}In	2.18s	36.6% 162
	^{113m}In	1.658h	64.2% 392
	^{112}Ag	3.14h	43% 617, 5.4% 1388, 2.8% 1614, 1.08% 2507
	^{115m}In	4.486h	45.8% 336
	^{115}Cd	2.228d	1.94% 261, 50.1% 336, 8.03% 492, 27.5% 528
	^{114m}In	49.5d	15.4% 190, 4.4% 558, 4.3% 725
	^{114}In	1.198m	0.14% 1300
Mg	^{24}Na	14.66h	100% 1369, 99.944% 2754
Au	$^{196m2}Au$	9.7h	1.2% 138, 47.2% 148, 7.0% 168, 0.42% 175, 34.4% 188, 1.29% 264, 4.0% 285, 2.66% 316
	^{198}Au	2.694d	95.50% 412, 0.802% 676, 0.159% 1088
	^{196}Au	6.183d	0.050% 326, 22.9% 333, 87% 356, 7.2% 426, 0.389% 521, 0.0061% 688, 0.0443% 758, 0.149% 1091
Ba	^{135}Cs	53m	99.7% 780, 96% 846
	^{139}Ba	1.41h	22% 166
	$^{129m+g}Ba$	2.2h	14.3% 129, 100% 182, 35.6% 202, 19.8% 214, 13.1% 221, 21.3% 392, 25.0% 420, 13.8% 460, 10.6% 546, 14.2% 597, 12.6% 679, 18.9% 893, 6.8% 1000, 8.5% 1035, 17% 1045, 6.8% 1209, 6.2% 1221, 48.5%1459, 10.4% 1624
	^{135}Xe	9.1h	90% 250, 2.90% 608
	^{135m}Ba	1.196d	15.6% 268
	^{133m}Ba	1.621d	17.5% 276
Er	^{166}Ho	1.117d	0.93% 1379

Table 4 Reactions Leading to Radioactive Products from Various Samples

Sample-material	Half-life	Product	Prominent γ-ray energy (keV)	Reaction
Fe	8.5 m	^{53}Fe	378	(n,2n)
	2.6 h	^{56}Mn	847	(n,n'p), (n,d), (n,p)
	27.7 d	^{51}Cr	320	(n,α)
	44.6 d	^{59}Fe	1099	(n,γ)
	312.2 d	^{54}Mn	835	(n,p)
Cr	3.76 m	^{52}V	1434	(n,p)
	5.8 m	^{51}Ti	320	(n,α)
	41.9 m	^{49}V	91/153	(n,2n)
	15.97 d	^{48}V	984	(n,t)
	27.7 d	^{51}Cr	320	(n,γ), (n,2n)
Ni	10.5 m	^{60m}Co	58.6	(n,p)
	13.9 m	^{62}Co	1173	(n,p)
	1.65 h	^{61}Co	67	(n,n'p), (n,d)
	2.52 h	^{65}Ni	1482	(n,γ)
	9.2 h	^{58m}Co	25	(n,p)
	36 h	^{57}Ni	1373	(n,2n)
	44.6 d	^{59}Fe	1099	(n,α)
	70.8 d	^{58}Co	811	(n,p)
	271 d	^{57}Co	122	(n,n'p), (n,d)
	5.27 y	^{60}Co	1332	(n,p)
SS316	3.76 m	^{52}V	1434	Mn(n,α); Cr(n,p)
	5.8 m	^{51}Ti	320	Cr(n,α)
	8.5 m	^{53}Fe	378	Fe(n,2n)
	10.5 m	^{60m}Co	58.6	Ni(n,p)
	13.9 m	^{62}Co	1173	Ni(n,p)
	14.6 m	^{101}Mo	192	Mo(n,γ)
	15.5 m	^{91}Mo	1634	Mo(n,2n)
	41.9 m	^{49}V	91/153	Cr(n,2n)
	51.5 m	^{98m}Nb	787	Mo(n,α),(n,p)
	72 m	^{97}Nb	658	Mo(n,p), (n,n'p),(n,d)
	1.65 h	^{61}Co	67	Ni(n,n'p), (n,α)
	2.52 h	^{65}Ni	1482	Ni(n,γ)
	2.58 h	^{56}Mn	847	Fe(n,p);Mn(n,γ)
	16.9 h	^{97}Zr	743	Mo(n,α)
	23.4 h	^{96}Nb	569/778	Mo(n,p),(n,n'p)
	36 h	^{57}Ni	1373	Ni(n,2n)
	78.4 h	^{89}Zr	909	Mo(n,α)

Table 4 continued

	10.14 d	^{92m}Nb	935	Mo(n,p)
	15.97 d	^{48}V	984	Cr(n,t)
	27.7 d	^{51}Cr	320	Fe(n,α);Cr(n,2n)
	44.6 d	^{59}Fe	1099	Ni(n,α)
	70.8 d	^{58}Co	811	Ni(n,p)
	271 d	^{57}Co	122	Ni(n,n'p),(n,d)
	312.2 d	^{54}Mn	835	Fe(n,p); Mn(n,2n)
	5.27 y	^{60}Co	1332	Ni(n,p)
Ti	5.8 m	^{51}Ti	320	(n,γ)
	3.1 h	^{45}Ti	720	(n,2n)
	3.9 h	^{44}Sc	1157	(n,t)
	43.7 h	^{48}Sc	984	(n,p)
	3.42 d	^{47}Sc	159	(n,p)
	4.54 d	^{47}Ca	1297	(n,α)
	83.8 d	^{46}Sc	889/1121	(n,p)
V	3.75 m	^{52}V	1434	(n,γ)
	5.8 m	^{51}Ti	320	(n,p)
	43.7 h	^{48}Sc	984	(n,α)
	3.42 d	^{47}Sc	159	(n,α)
Nb	6.3 m	^{94m}Nb	871	(n,γ)
	10.1 d	^{92m}Nb	934	(n,2n)
W	10.5 m	^{186}Ta	198	(n,p)
	49.5 m	^{185}Ta	178	(n,n'p), (n,d)
	64 m	^{183}Hf	784	(n,α)
	23.9 h	^{187}W	480	(n,γ)
	5 d	^{183}Ta	246	(n,p)
	115 d	^{182}Ta	1121	(n,p)
	121 d	^{181}W	136	(n,g)
Mo	14.6 m	^{101}Mo	192	(n,γ)
	15.5 m	^{91}Mo	1634	(n,2n)
	51.5 m	^{98m}Nb	787	(n,t),(n,p)
	72 m	^{97}Nb	658	(n,p),(n,n'p),(n,d)
	6.95 h	^{93m}Mo	685	(n,γ)
	16.9 h	^{97}Zr	743	(n,α)
	23.4 h	^{96}Nb	569/778	(n,p),(n,n'p),(n,d)
	66.0 h	^{99}Mo	141/739	(n,γ),(n,2n)
	78.4 h	^{89}Zr	909	(n,α)
	87 h	^{95m}Nb	204	(n,p)
	10.14 d	^{92m}Nb	935	(n,p)
	35 d	^{95}Nb	766	(n,p),(n,n'p),(n,d)
	64 d	^{95}Zr	724/757	(n,p)

Table 4 continued

	83.4 d	^{88}Zr	394	(n,n'α)
Co	10.4 m	^{60m}Co	58.6	(n,γ)
	2.58 h	^{56}Mn	847	(n,α)
	9.2 h	^{58m}Co	25	(n,2n)
	44.6 d	^{59}Fe	1099	(n,p)
	70.8 d	^{58}Co	811	(n,2n)
	5.28 y	^{60}Co	1332	(n,γ)
MnCu	3.76 m	^{52}V	1434	Mn(n,α)
	5.14 m	^{66}Cu	1039	Cu(n,γ)
	9.8 m	^{62}Cu	511	Cu(n,2n)
	10.4 m	^{60m}Co	58.6	Cu(n,α)
	13.9 m	^{62}Co	1173	Cu(n,α)
	1.65 h	^{61}Co	86	Cu(n,n'α)
	2.52 h	^{65}Ni	1482	Cu(n,p)
	2.58 h	^{56}Mn	847	Mn(n,γ)
	12.9 h	^{64}Cu	1346	Cu(n,γ),(n,2n)
	312 d	^{54}Mn	835	Mn(n,2n)
	5.28 y	^{60}Co	1332	Cu(n,α)
Si	2.24 m	^{28}Al	1779	(n,p)
	6.56 m	^{29}Al	1273	(n,α)
	9.46 m	^{27}Mg	844	(n,α)
Al	2.24 m	^{28}Al	1779	(n,γ)
	9.46 m	^{27}Mg	844	(n,p)
	15 h	^{24}Na	1369	(n,α)
Zr	4.18 m	^{89m}Zr	588	(n,2n)
	7.43 m	^{93}Sr	590	(n,α)
	18.7 m	^{94}Y	919	(n,p)
	49.7 m	^{91m}Y	556	(n,p)
	2.81 h	^{87m}Sr	388	(n,α)
	3.19 h	^{90m}Y	480	(n,n'p)
	3.54 h	^{92}Y	935	(n,p)
	9.48 h	^{91}Sr	1024	(n,α)
	78.4 h	$^{89m+g}$Zr	909	(n,2n)
	64 d	^{95}Zr	757	(n,2n)
In	48.6 m	^{111m}Cd	245	(n,t)
	54.1 m	^{116m}In	417	(n,γ)
	99.5 m	^{113m}In	392	(n,n')
	3.14 h	^{112}Ag	617	(n,α)
	4.49 h	^{115m}In	336	(n,n')
	53.4 h	^{115}Cd	336	(n,p)

Table 4 continued

	49.5 d	^{114m}In	725	(n,2n)
	252 d	^{110m}Ag	658	(n,α)
Ta	5.5 h	^{180m}Hf	332	(n,p)
	6.7 d	^{177}Lu	208	(n,α)
	25.1 d	^{179m2}Hf	453	(n,2n)
	42.4 d	^{181}Hf	482	(n,p)
	115 d	^{182}Ta	1121	(n,γ)
	161 d	^{177m}Lu	105	(n,α)
Y	2.8 h	^{87m}Sr	388	(n,t)
	3.2 h	^{90m}Y	480	(n,γ)
	18.8 d	^{86}Rb	1077	(n,α)
	106.6 d	^{88}Y	898/1836	(n,2n)
Zn	5.1 m	^{66}Cu	1039	(n,p),(n,n'p),(n,d)
	38.1 m	^{63}Zn	670	(n,2n),(n,γ)
	38.1 m	^{63}Zn	670	(n,2n)
	2.52 h	^{65}Ni	1482	(n,α)
	13.8 h	^{69m}Zn	439	(n,2n)
	61.9 h	^{67}Cu	185	(n,p),(n,d),(n,n'p)
	244 d	^{65}Zn	1116	(n,2n),(n,γ)
Sn	9.5 m	^{125m}Sn	332	(n,γ)
	18 m	^{119m}In	1065	(n,p),(n,d),(n,n'p)
	35 m	^{111}Sn	1152	(n,2n)
	40.1 m	^{123m}Sn	160	(n,γ),(n,2n)
	48.6 m	^{111m}Cd	245	(n,α)
	54.1 m	^{116m1}In	417	(n,p)
	2.4 h	^{117}Cd	273	(n,α)
	3.4 h	^{117m}Cd	1066	(n,α)
	4.5 h	^{115m}In	336	(n,p),(n,d),(n,n'p)
	53.4 h	^{115}Cd	336	(n,α)
	9.63 d	^{125}Sn	1066	(n,γ)
	14 d	^{123}Sn	1089	(n,2n)
	44.8 d	^{115m}Cd	934	(n,α)
	453 d	^{109}Cd	88	(n,α)
Pb	3.05 m	^{208}Tl	2615	(n,p)
	3.6 m	^{206m}Tl	216	(n,p),(n,d),(n,t)
	66.9 m	^{204m}Pb	899/912	(n,n')
	3.62 h	^{202m}Pb	961/422	(n,3n)
	52.02 h	^{203}Pb	279	(n,2n)
	12.23 d	^{202}Tl	440	(n,t)
	46.76 d	^{203}Hg	279	(n,α)

Table4 continued

Ag	2.4 m	^{108}Ag	633	(n,γ), (n,2n)
	4.34 m	^{104m}Rh	51	(n,p)
	24 m	^{106}Ag	512	(n,2n)
	130 m	^{106m}Rh	512/717	(n,α)
	13.43 h	^{109}Pd	88	(n,p)
	8.5 d	^{106m}Ag	512/717	(n,2n)
	252 d	^{110m}Ag	707/658	(n,γ)
	127 y	^{108m}Ag	434/723	(n,2n)
Au	9.7 h	^{196m}Au	188	(n,2n)
	2.7 d	^{198}Au	412	(n,γ)
	6.2 d	^{196}Au	356	(n,2n)
Mg	15 h	^{24}Na	1369	(n,p)
$YBa_2Cu_3O_7$	5.14 m	^{66}Cu	1039	Cu(n,γ)
	9.8 m	^{62}Cu	511	Cu(n,2n)
	10.4 m	^{60m}Co	58.6	Cu(n,α)
	13.9 m	^{62}Co	1173	Cu(n,α)
	53 m	^{135m}Cs	781	Ba(n,p)
	82.9 m	^{139}Ba	166	Ba(n,γ)
	9.1 h	$^{135m+g}$Xe	250	Ba(n,α)
	3.19 h	^{90m}Y	480	Y(n,γ)
	18.8 d	^{86}Rb	1077	Y(n,α)
	106.6 d	^{88}Y	1836	Y(n,2n)
	1.65 h	^{61}Co	86	Cu(n,n'α)
	2.52 h	^{65}Ni	1482	Cu(n,p)
	12.9 h	^{64}Cu	1346	Cu(n,2n),(n,γ)
	5.28 y	^{60}Co	1332	Cu(n,α)
$ErBa_2Cu_3O_7$	5.14 m	^{66}Cu	1039	Cu(n,γ)
	6.2 m	^{167}Dy	570	Er(n,α)
	4.18 m	^{89m}Zr	588	Zr(n,2n)
	7.43 m	^{93}Sr	590	Zr(n,α)
	18.7 m	^{94}Y	919	Zr(n,p)
	9.8 m	^{62}Cu	511	Cu(n,2n)
	10.4 m	^{60m}Co	58.6	Cu(n,α)
	13.9 m	^{62}Co	1173	Cu(n,α)
	53 m	^{135m}Cs	781	Ba(n,p)
	2.33 h	^{165}Dy	95	Er(n,α)
	3.1 h	^{167}Ho	347	Er(n,p)
	7.52 h	^{171}Er	308	Er(n,γ)
	26.8 h	^{166}Ho	81/1379	Er(n,p)
	53 m	^{135m}Cs	781	Ba(n,p)

Table 4 continued

	82.9 m	^{139}Ba	166	Ba(n,γ)
	9.1 h	$^{135m+g}$Xe	250	Ba(n,α)
	1.65 h	^{61}Co	86	Cu(n,n'α)
	2.52 h	^{65}Ni	1482	Cu(n,p)
	12.9 h	^{64}Cu	1346	Cu(n,2n),(n,γ)
	5.28 y	^{60}Co	1332	Cu(n,α)

Table 5 Prominent Natural Background Radioactivities, Major γ-ray Energies and Emission Probabilities

Radioactivity Source	γ-ray Energy in KeV (% Emission Probability)@			
^{40}K	1460.8 (10.7)			
^{208}Tl	277.4 (6.8)	510.7 (21.6)	583.1 (85.8)	763.1 (1.6)
	860.4 (12.0)	1093.9 (0.4)	2614.5 (99.8)	
^{212}Pb	115.2 (0.6)	176.6 (0.1)	238.6 (43.1)	300.1 (3.3)
^{212}Bi	727.2 (6.7)	1620.6 (1.6)		
^{214}Pb	295.2 (17.9)	351.9 (34.3)		
^{214}Bi	609.3 (42.6)	768.4 (4.6)	806.2 (1.2)	934.1 (3.0)
	1120.3 (13.9)	1155.2 (1.6)	1238.1 (5.5)	1281.0 (1.4)
	1377.7 (3.8)	1385.3 (0.8)	1401.1 (1.3)	1408.0 (2.4)
	1509.2 (2.0)	1661.3 (1.1)	1729.6 (2.7)	1764.5 (14.6)
	1847.4 (1.9)	2118.6 (1.1)	2204.2 (4.6)	2477.8 (1.4)
^{226}Ra	186.1 (3.5)			
^{228}Ac	129.1 (2.9)	209.4 (4.6)	270.3 (3.8)	328.0 (3.7)
	338.4 (12.0)	463.0 (4.6)	794.8 (4.8)	911.1 (29.0)
	964.6 (5.5)	968.9 (17.5)	1587.9 (3.7)	

@Data are taken from the Table of Radioactive Isotopes [Ref. 24]

Table 6 ***Description of Spectral Conditions and Identifiers***

Experimental Period	Spectral Conditions Location	Identifier	Irradiation Time	Mean '14 MeV' Intensity
December 2, '88	(10, 0) cm	A1	30m	1.70×10^{12} n/s
(Phase IIC: WCC)	(10, 0) cm	A2	9h	8.75×10^{11} n/s
	(82, 5) cm	B1	30m	1.28×10^{12} n/s
	(82, 5) cm	B2	10h	1.12×10^{12} n/s
November 9, '89	(0, 21.9) cm	C1	9h47m	1.88×10^{11} n/s (9.40×10^{8} n/cm/s)*
(Ph IIIA: Bare Line Source)	(40, 21.9) cm	D1	9h47m	1.88×10^{11} n/cm/s (9.40×10^{8} n/cm/s)*
	(100, 21.9) cm	E1	9h47m	1.88×10^{11} n/cm/s (9.40×10^{8} n/cm/s)*
November 21, '89	(0, 23.4) cm	F1	30m	2.42×10^{11} n/s
(Ph IIIA:Point Source inside Annular Blanket)	(0, 22.9) cm	G1	30m	2.42×10^{11} n/s
November 22, '89	(0, 23.4) cm	H1	9h51m5s	1.93×10^{11} n/s (9.66×10^{8} n/cm/s)*
(Ph IIIA: Line Source Driven Annular Blanket)	(0, 28.5) cm	I1	9h51m5s	1.93×10^{11} n/s (9.66×10^{8} n/cm/s)*
	(40, 23.4) cm	J1	9h51m5s	1.93×10^{11} n/s (9.66×10^{8} n/cm/s)*
November 1, '90	(0, 23.4) cm	K1	10h29m40s	1.31×10^{11} n/s (6.55×10^{8} n/cm/s)*
(Ph IIIB: Line Source Driven Annular Blanket with 1" thick graphite armor)	(40, 23.4) cm	L1	10h29m40s	1.31×10^{11} n/s (6.55×10^{8} n/cm/s)*
November 15, '91	(0, 23.4) cm	M1	10h6m33s	2.16×10^{11} n/s (1.08×10^{9} n/cm/s)*
(Ph IIIC: Line Source Driven Annular Blanket with	(0, 21.9) cm	N1	10h6m33s	2.16×10^{11} n/s

*; Source neutron density along the line over 200 cm.

Table 7.1 *Parameters Characterizing Iron Measurements*

Measurement Identifier	Spectral Identifier	IrradiationTime	CoolingTim	CountingTime
FEA11	A1	30m	22.4m	10m
FEA21	A2	9h	3h22.3m	22.4m
FEA22	A2	9h	17h16.2m	39.8m
FEA23	A2	9h	5d13.7h	5h16.9m
FEB11	B1	30m	24m	10m
FEB21	B2	10h	5h1m	44.8m
FEB22	B2	10h	17h16.2m	39.8m
FEC11	C1	9h47m	2h15.5m	10m
FEC12	C1	9h47m	5d13.4h	3h36.7m
FEC13	C1	9h47m	6d14.2h	4h25.0m
FEC14	C1	9h47m	7d22.6h	14h11.8m
FED11	D1	9h47m	2h3.2m	10.5m
FED12	D1	9h47m	5d17.4h	5h14.3m
FEE11	E1	9h47m	1h50m	10m
FEE12	E1	9h47m	3d16.9h	2h
FEF11	F1	30m	33m15s	7.3m
FEF12	F1	30m	2h31.6m	1h13.2m
FEF13	F1	30m	3h50.7m	56.0m
FEF14	F1	30m	21h21.8m	2h12m
FEG11	G1	30m	44m	8.6m
FEG12	G1	30m	1h8.7m	1h17.3m
FEH11	H1	9h51.1m	4h19.6m	14.2m
FEH12	H1	9h51.1m	13h50.3m	30.5m
FEI11	I1	9h51.1m	5h9.9m	25.0m
FEJ11	J1	9h51.1m	4h45.1m	14.2m
FEL11	L1	10h29m40s	3h9.8m	25.4m

Table 7.2 *Parameters Characterizing Nickel Measurements*

Measurement Identifier	Spectral Identifier	IrradiationTime	CoolingTim	CountingTime
NIA11	A1	30m	56.3	30.9m
NIA21	A2	9h	2h26.7m	42.9m
NIA22	A2	9h	16h23.7m	44.7m
NIA23	A2	9h	4d13h	8h41.9m
NIB11	B1	30m	58.8m	26.6m
NIB21	B2	10h	3h52.7m	1h2.8m
NIB22	B2	10h	2d17.6m	4h13.2m
NIC11	C1	9h47m	7h8.7m	16.9m
NIC12	C1	9h47m	18h28.5m	25m
NIC13	C1	9h47m	4d19.9h	2h9.5m
NID11	D1	9h47m	6h45.8m	19.3m
NID12	D1	9h47m	17h14.2m	28.5m
NID13	D1	9h47m	4d22.9h	14h18.9m
NIE11	E1	9h47m	6h20.3m	18.7m
NIE12	E1	9h47m	16h37.5m	32m
NIE13	E1	9h47m	17h20.8m	1h32.3m
NIE14	E1	9h47m	5d17.4h	5h12.8m
NIF11	F1	30m	44m	8.6m
NIF12	F1	30m	2h31.8m	1h13.5m
NIF13	F1	30m	21h21.9m	5h12.7m
NIG11	G1	30m	55.7m	1h29.6m
NIH11	H1	9h51m5s	4h19.8m	18.4m
NIH12	H1	9h51m5s	13h50.6m	30.3m
NII11	I1	9h51m5s	5h10.8m	26.9m
NIJ11	J1	9451m5s	4h45.4m	17.6m
NIK11	K1	10h29m40s	1h12.1m	21.7m
NIK12	K1	10h29m5s	15h58.8m	28.2m
NIK13	K1	10h29m5s	7d14.7h	2h43.1m
NIK14	K1	10h29m5s	23h52.4m	

Table 7.3 *Parameters Characterizing Molybdenum Measurement*

Measurement Identifier	Spectral Identifier	IrradiationTime	CoolingTim	CountingTime
MOA11	A1	30m	46.3m	30.5m
MOA21	A2	9h	1h38.2m	43.8m
MOA22	A2	9h	15h 11.8m	1h5.5m
MOA23	A2	9h	19h42.3m	2h46.7m
MOA24	A2	9h	4d3.7h	15h28.6m
MOB11	B1	30m	58.8m	26.6m
MOB21	B2	10h	2h28.5m	38.2m
MOB22	B2	10h	9h15.8m	4h2.2m
MOC11	C1	9h47m	3h46.8m	11.7m
MOC12	C1	9h47m	4h3.3m	10.8m
MOC13	C1	9h47m	20h47.2m	33.3m
MOC14	C1	9h47m	3d21.7h	15h20.8m
MOD11	D1	9h47m	3h32.5m	10.9m
MOD12	D1	9h47m	20h15.5m	27.3m
MOD13	D1	9h47m	4d13.3h	3h40.7m
MOE11	E1	9h47m	3h18.2m	10.8m
MOE12	E1	9h47m	17h48.2m	35.2m
MOE13	E1	9h47m	4d17.1h	2h37.7m
MOH11	H1	9h51m5s	2h52.7m	33.3m
MOH12	H1	9h51m5s	11h48.1m	30.2m
MOI11	I1	9h51m5s	3h37.3m	33.3m
MOI12	I1	9h51m5s	12h29.2m	33.9m
MOJ11	J1	9h51m5s	6h30.3m	38.8m
MOJ12	J1	9h51m5s	13h13.3m	27.6m
MOJ13	J1	9h51m5s	8d12.1h	3h0.3m
MOK11	K1	10h29m40s	20.8m	13.9m
MOK12	K1	10h29m40s	1h41.9m	24.5m
MOK13	K1	10h29m40s	14h38.5m	35m
MOK14	K1	10h29m40s	6d19.5h	53.4m
MOK15	K1	10h29m40s	7d20.5h	15h19.3m
MOK16	K1	10h29m40s	9h22.8m	

Table 7.4 *Parameters Characterizing Chromium Measurements*

Measurement Identifier	Spectral Identifier	IrradiationTime	CoolingTim	CountingTime
CRA21	A2	9h	1h38.8m	43.0m
CRA22	A2	9h	15h16.8m	1h0.5m
CRB22	B2	10h	2h27.5m	1h19.6m
CRK11	K1	10h29m40s	1h12m	21.6m
CRK12	K1	10h29m40s	20h44.4m	17h0.4m
CRK13	K1	10h29m40s	7d14.7h	2h45.8m

Table 7.5 *Parameters Characterizing SS316 Measurements*

Measurement Identifier	Spectral Identifier	IrradiationTime	CoolingTim	CountingTime
SSA11	A1	30m	37.3m	14.6m
SSA21	A2	9h	1h38.8m	42.4m
SSA22	A2	9h	4h31m	2h46.7m
SSA23	A2	9h	15h16.8m	1h0.5m
SSA24	A2	9h	3d21.8h	13h54.6m
SSB11	B1	30m	39.2m	15.1m
SSB21	B2	10h	3h13.2m	33.9m
SSB22	B2	10h	1d15.9h	21h48.8m

Table 7.6 *Parameters Characterizing AISI316 Measurements*

Measurement Identifier	Spectral Identifier	IrradiationTime	CoolingTim	CountingTime
SSC11	C1	9h47m	4h47.8m	12.9m
SSC12	C1	9h47m	21h24.8m	33.4m
SSC13	C1	9h47m	4d17.5h	2h10.8m
SSC14	C1	9h47m	7d15h	7h23m
SSC15	C1	9h47m	20d14.6h	3h37.4m
SSC16	C1	9h47m	20d22.4h	14h41.4m
SSD11	D1	9h47m	4h33.2m	11.6m
SSD12	D1	9h47m	19h41.2m	30.9m
SSD13	D1	9h47m	4d19.9h	2h8.7m
SSD14	D1	9h47m	20d18.4h	3h35.4h
SSE11	E1	9h47m	4h18.5m	11.9m
SSE12	E1	9h47m	18h59.5m	38.1m
SSE13	E1	9h47m	4d22.4h	14h46.2m
SSH11	H1	9h51m5s	1h37.4m	23.1m
SSH12	H1	9h51m5s	12h29.6m	36.1m
SSI11	I1	9h51m5s	2h12.5m	28.6m
SSI12	I1	9h51m5s	13h13.5m	25.3m
SSK11	K1	10h29m40s	18h9.8m	34.5m
SSK12	K1	10h29m40s	6d21.7h	14h20.9m
SSK13	K1	10h29m40s	14h37.9m	

Table 7.7 *Parameters Characterizing MnCu Alloy Measurements*

Measurement Identifier	Spectral Identifier	IrradiationTime	CoolingTim	CountingTime
MCA11	A1	30m	12.3m	10m
MCA21	A2	9h	2h26.7m	44m
MCA22	A2	9h	16h23.7m	45.7m
MCA23	A2	9h	6d21h	4h50.3m
MCB11	B1	30m	24.3m	10m
MCB21	B2	10h	3h52.7m	1h2.2m
MCB22	B2	10h	3d13.4h	6h44.9m
MCK11	K1	10h29m40s	58.6m	8.3m
MCK12	K1	10h29m40s	15h15.3m	35m
MCK13	K1	10h29m40s	6d20.6h	50.9m

Table 7.8 *Parameters Characterizing Copper Measurements*

Measurement Identifier	Spectral Identifier	IrradiationTime	CoolingTim	CountingTime
CUK11	K1	10h29m40s	20.6m	5.1m
CUK12	K1	10h29m40s	18h49.4m	32.3m
CUK13	K1	10h29m40s	7d17.8h	2h29.6m

Table 7.9 *Parameters Characterizing Tungsten Measurements*

Measurement Identifier	Spectral Identifier	IrradiationTime	CoolingTim	CountingTime
WA11	A1	30m	37.3m	15.5m
WA21	A2	9h	2h26.5m	44.2m
WA22	A2	9h	16h23.4m	45.7m
WA23	A2	9h	2d19.1h	18h22.7m
WB11	B1	30m	39.2m	15.1m
WB21	B2	10h	3h13.5m	33.5m
WB22	B2	10h	4d5.3m	13h32.2m
WC11	C1	9h47m	3h47.5m	10.9m
WC12	C1	9h47m	20h47.5m	33.3m
WC13	C1	9h47m	4d13.3h	3h38.3m
WF11	F1	30m	44.5m	8.2m
WF12	F1	30m	4h57.3m	58.7m
WF13	F1	30m	6h36.5m	14h20m
WG12	G1	30m	55.3m	9.7m
WH11	H1	9h51m5s	1h37.5m	22.4m
WH12	H1	9h51m5s	8d18.5h	2h38.3m
WI11	I1	9h51m5s	2h13m	22.4m
WK11	K1	10h29m40s	20.6m	10.4m
WK12	K1	10h29m40s	2h5.7m	26.5m
WK13	K1	10h29m40s	13h38.4m	32.4m
WK14	K1	10h29m40s	6d19.5h	47m
WK15	K1	10h29m40s	7d20.5h	15h16.3m
WK16	K1	10h29m40s	18d15.8h	20h5.3m

Table 7.10 *Parameters Characterizing Zirconium Measurements*

Measurement Identifier	Spectral Identifier	IrradiationTime	CoolingTim	CountingTime
ZRA11	A1	30m	56.5m	18.9m
ZRA21	A2	9h	2h26.5m	43.5m
ZRA22	A2	9h	17h15.7m	40m
ZRB11	B1	30m	58.3m	27.1m
ZRB21	B2	10h	3h13.5m	33.7m
ZRC11	C1	9h47m	3h33.3m	10m
ZRC12	C1	9h47m	9h21.7m	39.1m
ZRC13	C1	9h47m	19h36m	25.7m
ZRC14	C1	9h47m	3d18.4h	40m
ZRD11	D1	9h47m	8h54.3m	20.5m
ZRD12	D1	9h47m	19h50s	28.3m
ZRD13	D1	9h47m	5d13.4h	19.9m
ZRD14	D1	9h47m	5d14.1h	3h4.5m
ZRE11	E1	9h47m	8h26.9m	24.1m
ZRE12	E1	9h47m	18h28.7m	23.2m
ZRE13	E1	9h47m	3d16.9h	1h20.3m
ZRH11	H1	9h51m5s	3h25.3m	23.5m
ZRH12	H1	9h51m5s	10h1.4m	42.7m
ZRI11	I1	9h51m5s	3h54.3m	18.3m
ZRI12	I1	9h51m5s	10h54.7m	43.6m
ZRK11	K1	10h29m40s	20.9m	26.6m
ZRL11	L1	10h29m40s	2h5.1m	26.1m
ZRL12	L1	10h29m40s	14h14.8m	20.6m
ZRL13	L1	10h29m40s	16h5s	26.1m
ZRL14	L1	10h29m40s	6d19.5h	55.8m
ZRL15	L1	10h29m40s	7d17.9h	18h50s
ZRL16	L1	10h29m40s	14h31.3m	

Table 7.11 *Parameters Characterizing Vanadium Measurements*

Measurement Identifier	Spectral Identifier	IrradiationTime	CoolingTim	CountingTime
VA11	A1	30m	22.3m	10m
VA21	A2	9h	3h42.2m	36.1m
VA22	A2	9h	17h16.2m	39.8m
VB11	B1	30m	24m	10m
VB21	B2	10h	5h1.7m	44.9m
VB22	B2	10h	2d22.4h	14h51.3m
VC11	C1	9h47m	11h47.3m	27m
VC12	C1	9h47m	1d15.6h	4h45.5m
VL11	L1	10h29m40s	1h38m	24m
VL12	L2	10h29m40s	17h15.3m	27m
VL13	L3	10h29m40s	7d17.9h	2h30.1m

Table 7.12 *Parameters Characterizing Aluminum Measurements*

Measurement Identifier	Spectral Identifier	IrradiationTime	CoolingTim	CountingTime
ALA11	A1	30m	1h15.8m	11.4m
ALA21	A2	9h	4h31m	2h46.7m
ALB11	B1	30m	58.3m	27.1m
ALB21	B2	10h	5h52.3m	1h28.5m
ALC11	C1	9h47m	6h46m	39.7m
ALC12	C1	9h47m	7h31m	51.7m
ALC13	C1	9h47m	10h9.2m	1h32.2m
ALD11	D1	9h47m	5h58.2m	40.7m
ALE11	E1	9h47m	5h5m	49.2m
ALF11	F1	30m	23h53m	2h40m
ALF12	F1	30m	1d3.1h	7h15.8m
ALG11	G1	30m	23h52.5m	10h26.3m
ALH11	H1	9h51m5s	9h20.2m	33.3m
ALI11	I1	9h51m5s	10h1.9m	44.3m
ALJ11	J1	9h51m5s	10h55.2m	45.3m
ALK11	K1	10h29m40s	7h37.2m	14.9m
ALL11	L1	10h29m40s	10h47.4m	24.3m

Table 7.13 *Parameters Characterizing Cobalt Measurements*

Measurement Identifier	Spectral Identifier	IrradiationTime	CoolingTim	CountingTime
COA11	A1	30m	37.3m	15m
COA21	A2	9h	3h17.2m	29.2m
COA22	A2	9h	17h15.7m	40.5m
COA23	A2	9h	5d19.2h	3h21.5m
COB11	B1	30m	39.3m	15.1m
COB21	B2	10h	3h53m	1h2.7m
COC11	C1	9h47m	5h10m	44.2m
COC12	C1	9h47m	3d20.3h	1h13.3m
COK11	K1	10h29m40s	1h7.9m	10.3m
COK12	K1	10h29m40s	17h48m	29.9m
COK13	K1	10h29m40s	6d21.7h	14h30.9m
COK14	K1	10h29m40s	5h18.4m	

Table 7.14 *Parameters Characterizing Titanium Measurements*

Measurement Identifier	Spectral Identifier	IrradiationTime	CoolingTim	CountingTime
TIA11	A1	30m	22.3m	10m
TIA21	A2	9h	3h51.5m	29.2m
TIA22	A2	9h	18h11m	1h20.5m
TIB11	B1	30m	24.3m	10m
TIB21	B2	10h	7h27.5m	1h43.4m
TIC11	C1	9h47m	6h46.2m	39.5m
TIC12	C1	9h47m	22h3.4m	17h16.5m
TIH11	H1	9h51m5s	7h34.4m	40.9m
TII11	I1	9h51m5s	8h25.7m	40.9m
TIL11	L1	10h29m40s	1h8m	27.6m
TIL12	L1	10h29m40s	9h9.7m	42.8m
TIL13	L1	10h29m40s	16h32.2m	37.1m
TIL14	L1	10h29m40s	7d12.4h	2h3.3m

Table 7.15 *Parameters Characterizing Niobium Measurements*

Measurement Identifier	Spectral Identifier	IrradiationTime	CoolingTim	CountingTime
NBA21	A2	9h	4h31m	2h46.7m
NBA22	A2	9h	18h49.5m	44.5m
NBB22	B2	10h	13h39m	1h13.7
NBC11	C1	9h47m	9h20.7m	40.2m
NBC12	C1	9h47m	11h45.7m	28.5m
NBC13	C1	9h47m	12h18.5m	28m
NBC14	C1	9h47m	12h50.5m	29.7m
NBD11	D1	9h47m	8h28.2m	46.9m
NBD12	D1	9h47m	10h57.8m	43.5m
NBE11	E1	9h47m	7h31m	51.7m
NBE12	E1	9h47m	10h7m	45.9m
NBF11	F1	30m	1d3.1h	1h25.5m
NBF12	F1	30m	1d4.6h	1h23.4m
NBG11	G1	30m	1d6.2h	2h12.3m
NBG12	G1	30m	1d8.6h	1h44.3m
NBH11	H1	9h51m5s	5d19.6h	1h18.2m
NBH12	H1	9h51m5s	5d21.1h	14h23m
NBI11	I1	9h51m5s	6d11.8h	3h46.5m
NBI12	I1	9h51m5s	6d15.7h	4h1m
NBJ11	J1	9h51m5s	6d19.8h	2h15.3m
NBJ12	J1	9h51m5s	6d22.4h	13h11m
NBK11	K1	10h29m40s	4d19.5h	46.5m
NBL11	L1	10h29m40s	6d12h	1h10.5m

Table 7.16 *Parameters Characterizing Tin Measurements*

Measurement Identifier	Spectral Identifier	IrradiationTime	CoolingTim	CountingTime
SNC11	C1	9h47m	3h4.7m	9.7m
SNC12	C1	9h47m	1d17.6h	1h53.7m
SNC13	C1	9h47m	6d22.6h	15h52m
SND11	D1	9h47m	2h49.7m	10.4m
SND12	D1	9h47m	1d15.6h	2h45.5m
SND13	D1	9h47m	6d19.9h	2h35m
SNE11	E1	9h47m	2h29m	16.9m
SNE12	E1	9h47m	3h5m	24m
SNE13	E1	9h47m	22h3.3m	17h16.8m
SNF11	F1	30m	21.8m	7.8
SNF12	F1	30m	1h8.7m	1h16.7m
SNF13	F1	30m	21h23m	2h7.5m
SNG11	G1	30m	22.3m	7.3m
SNG12	G1	30m	3h50.3m	56.9m
SNJ11	J1	9h51m5s	5h45.9m	35m
SNJ12	J1	9h51m5s	14h33.6m	30m
SNL11	L1	10h29m40s	27.7m	6.7m
SNL12	L1	10h29m40s	1h19.9m	1h12.5m
SNL13	L1	10h29m40s	17h14.6m	27.8m
SNL14	L1	10h29m40s	7d12.5h	1h58.9m
SNL15	L1	10h29m40s	7h51.9m	

Table 7.17 *Parameters Characterizing Lead Measurements*

Measurement Identifier	Spectral Identifier	IrradiationTime	CoolingTim	CountingTime
PBC11	C1	9h47m	12h19.2m	1h1.4m
PBC12	C1	9h47m	3d19.2h	34.2m
PBC13	C1	9h47m	5d22.9h	14h18m
PBF11	F1	30m	12.2m	5.5m
PBF12	F1	30m	4h57.2m	1h30.1m
PBG11	G1	30m	11.5m	6.1m
PBG12	G1	30m	7h17m	13h41m
PBJ11	J1	9h51m5s	9h19.7m	30.8m
PBJ12	J1	9h51m5s	14h33.3m	30m
PBL11	L1	10h29m40s	37.5m	27.6m
PBL12	L1	10h29m40s	2h9.3m	23m
PBL13	L1	10h29m40s	18h47.6m	19.7m
PBL14	L1	10h29m40s	6d20.6h	51.3m

Table 7.18 *Parameters Characterizing Tantalum Measurements*

Measurement Identifier	Spectral Identifier	IrradiationTime	CoolingTim	CountingTime
TAA21	A2	9h	3h17.2m	25.9m
TAA22	A2	9h	18h11.7m	35.4m
TAB21	B2	10h	3h53m	1h2.7m
TAC11	C1	9h47m	5h59m	16m
TAC12	C1	9h47m	3d14.8h	1h52.8m
TAC13	C1	9h47m	7d17h	19h48.6m
TAH11	H1	9h51m5s	7h25.4m	42m
TAI11	I1	9h51m5s	8h25.9m	44.7m
TAK11	K1	10h29m40s	1h37.7m	24.3m
TAK12	K1	10h29m40s	19h25.3m	56.8m
TAK13	K1	10h29m40s	6d20.6h	54.2m
TAK14	K1	10h29m40s	7h28.3m	

Table 7.19 *Parameters Characterizing Silver Measurements*

Measurement Identifier	Spectral Identifier	IrradiationTime	CoolingTim	CountingTime
AGC11	C1	9h47m	2h36.7m	9.2m
AGC12	C1	9h47m	19h37.3m	24.5m
AGC13	C1	9h47m	3d19.2h	55m
AGC14	C1	9h47m	5d22.9h	14h14.3m
AGC15	C1	9h47m	7d14.6h	2h13.4m
AGF11	F1	30m	33.3m	6.9
AGF12	F1	30m	2h31.8m	1h13.5m
AGG11	G1	30m	33.8m	6.8m
AGG12	G1	30m	6h49.5m	14h7.5m
AGJ11	J1	9h51m5s	6h48.8m	50.6m
AGJ12	J1	9h51m5s	11h48.8m	31.7m
AGL11	L1	10h29m40s	46.5m	18.2m
AGL12	L1	10h29m40s	18h49.8m	19h5.5m
AGL13	L1	10h29m40s	7d12.4h	2h4.7m
AGL14	L1	10h29m40s	2d16.7h	

Table 7.20 *Parameters Characterizing Zinc Measurements*

Measurement Identifier	Spectral Identifier	IrradiationTime	CoolingTim	CountingTime
ZNC11	C1	9h47m	2h50.5m	10.2m
ZNC12	C1	9h47m	21h26.3m	32.3m
ZNC13	C1	9h47m	3d19.9h	1h33.3m
ZNC14	C1	9h47m	6d17.2h	2h33.7m
ZNF11	F1	30m	11.7m	5.8m
ZNF12	F1	30m	56.3m	8.7m
ZNF13	F1	30m	4h57.2m	1h42.2m
ZNG11	G1	30m	22.3m	7.2m
ZNG12	G1	30m	3h50.5m	56.6m
ZNJ11	J1	9h51m5s	5h45.3m	37.5m
ZNL11	L1	10h29m40s	32.7m	10.1m
ZNL12	L1	10h29m40s	44.1m	24.2m
ZNL13	L1	10h29m40s	16h31.7m	37.5m
ZNL14	L1	10h29m40s	6d21.7h	14h28.9m
ZNL15	L1	10h29m40s	17h37m	

Table 7.21 *Parameters Characterizing Silicon Measurements*

Measurement Identifier	Spectral Identifier	IrradiationTime	CoolingTim	CountingTime
SIA11	A1	30m	37.3m	15m

Table 7.22 *Parameters Characterizing Yttrium Measurements*

Measurement Identifier	Spectral Identifier	IrradiationTime	CoolingTim	CountingTime
YC11	C1	9h47m	3d14.8h	1h52.2m
YC12	C1	9h47m	6d14.1h	2h50.5m
YC13	C1	9h47m	6d18.9h	2h23.7m

Table 7.23 *Parameters Characterizing Indium Measurements*

Measurement Identifier	Spectral Identifier	IrradiationTime	CoolingTim	CountingTime
INA21	A2	9h	1h38.2m	42.9m
INA22	A2	9h	16h23.7m	45.7m
INB21	B2	10h	2h28.5m	38m
INC11	C1	9h47m	6h20.5m	18.5m
INC12	C1	9h47m	19h1.7m	30m
INC13	C1	9h47m	3d22.3h	14h45.8m
INK11	K1	10h29m40s	2h40m	9m
INL11	L1	10h29m40s	37.4m	7m
INL12	L1	10h29m40s	6h3.7m	21.3m
INL13	L1	10h29m40s	18h21.8m	22.7m
INL14	L1	10h29m40s	7d14.7h	2h53.5m
INL15	L1	10h29m40s	16h6.2m	

Table 7.24 *Parameters Characterizing Magnesium Measurements*

Measurement Identifier	Spectral Identifier	IrradiationTime	CoolingTim	CountingTime
MGA21	A2	9h	3h51.7m	26.3m
MGA22	A2	9h	18h11.7m	31.5m
MGB21	B2	10h	5h2m	44.2m

Table 7.25 *Parameters Characterizing Gold Measurements*

Measurement Identifier	Spectral Identifier	IrradiationTime	CoolingTim	CountingTime
AUA21	A2	9h	3h51.7m	25.9m
AUA22	A2	9h	4h31m	2h46.7m
AUA23	A2	9h	18h49.5m	43.7m
AUA24	A2	9h	19h42m	2h46.7m
AUB21	B2	10h	5h2m	44.2m
AUK11	K1	10h29m40s	1d14.2h	1h27.3m
AUL11	L1	10h29m40s	4d12.1h	1h11.8m

Table 7.26 *Parameters Characterizing $YBa_2Cu_3O_7$ Measurements*

Measurement Identifier	Spectral Identifier	IrradiationTime	CoolingTim	CountingTime
YCA11	A1	30m	1h32m	2h32.9m
YCA12	A1	30m	4h12m	4h31.2m
YCA13	A1	30m	7d2.4h	2h50.4m

Table 7.27 *Parameters Characterizing $ErBa_2Cu_3O_7$ Measurements*

Measurement Identifier	Spectral Identifier	IrradiationTime	CoolingTim	CountingTime
ECA11	A1	30m	1h33m	2h34.3m
ECA12	A1	30m	4h12.5m	4h33.5m
ECA13	A1	30m	11d4.8h	3h34.7m

Table 8 *Identification of Selected Cases*

Measurement Identifier	Spectral Identifier	Irradiation Time	Cooling Time	Counting Time
FEA11	A1	30m	22.4m	10m
FEA25	A2	9h	2d22.1h	15h25.9m
NIA11	A1	30m	56.3m	30.9m
NIA23	A2	9h	4d13h	8h41.9m
NIB22	B2	10h	2d17.6m	4h13.2m
CRA22	A2	9h	15h16.8m	1h0.5m
MOA11	A1	30m	46.3m	30.5m
MOA24	A2	9h	4d3.7h	15h28.6m
SSA24	A2	9h	3d21.8h	13h54.6m
SSC14	C1	9h47m	7d15h	7h23m
MCA11	A1	30m	12.3m	10m
MCA23	A2	9h	16h23.7m	45.7m
MCB22	B2	10h	3d13.4h	6h44.9m
WA23	A2	9h	2d19.1h	18h22.7m
ZRA21	A2	9h	2h26.5m	43.5m
VB22	B2	10h	2d22.4h	14h51.3m
ALB21	B2	10h	5h52.3m	1h28.5m
COA23	A2	9h	5d19.2h	3h21.5m
TIB21	B2	10h	7h27.5m	1h43.4m
NBB21	B2	10h	13h39m	1h13.7m
SNC13	C1	9h47m	6d22.6h	15h52m
PBC11	C1	9h47m	12h19.2m	1h1.4m
TAA21	A2	9h	3h17.2m	25.9m
AGC12	C1	9h47m	19h37.3m	24.5m
ZNC12	C1	9h47m	21h26.3m	32.3m
SIA11	A1	30m	37.3m	15m
YC13	C1	9h47m	6d18.9h	2h23.7m
INA22	A2	9h	16h23.7m	45.7m
MGA21	A2	9h	3h51.7m	26.3m
AUA22	A2	9h	4h31m	2h46.7m
YCA13	A1	30m	7d2.4h	2h50.3m
ECA13	A1	30m	11d4.8h	3h34.7m

Table 9.1: Data for Iron

Measurement ID: **FEA11**

No.	Energy (keV)	γ-emission rate	% Std.dev.
1	511	.29174E+04	4.6
2	847	.10831E+06	3.0
4	1811	.29775E+05	2.8
5	2113	.15533E+05	3.1
6	2523	.11346E+04	6.6
7	2658	.96178E+03	7.1
8	2959	.34592E+03	12.1
9	3370	.18215E+03	18.9

Table 9.2: Data for Iron

Measurement ID: **FEA25**

No.	Energy (keV)	γ-emission rate	% Std.dev.
1	319	.41871E+02	3.8
2	511	.22597E+02	5.5
3	811	.19592E+01	30.3
4	835	.13796E+03	3.0
5	847	.43720E+01	16.0

Table 9.3: Data for Nickel

Measurement ID: **NIA11**

No.	Energy (KeV)	γ-emission rate	% Std.dev.
1	122	.16671E+03	4.1
2	127	.22944E+03	4.6
3	137	.21573E+02	7.5
4	511	.15570E+04	2.2
5	637	.24807E+02	14.2
6	811	.23155E+03	3.5
7	897	.13029E+02	46.4
8	908	.35054E+02	18.1
9	1163	.74094E+02	9.5
10	1172	.23026E+03	6.5
11	1332	.75274E+01	47.9
12	1377	.14961E+04	3.1
13	1757	.13409E+03	5.9
14	1888	.65120E+02	7.9
15	1919	.31754E+03	3.9
16	2003	.20626E+02	13.5
17	2103	.98934E+01	21.6
18	2335	.13988E+01	98.1

Table 9.4: Data for Nickel

Measurement ID: **NIA23**

No.	Energy (KeV)	γ-emission rate	% Std.dev.
1	116	.94223E+02	7.0
2	122	.31433E+04	2.8
3	136	.38782E+03	3.5
4	172	.45030E+02	7.6
5	197	.89729E+02	5.2
6	203	.21655E+02	19.5
7	510	.46908E+04	2.0
8	810	.69569E+04	2.2
9	863	.50641E+02	5.7
10	897	.95165E+01	21.7
11	1098	.16594E+02	20.0
12	1172	.18514E+04	8.4
13	1176	.31422E+01	98.3
14	1291	.12146E+02	16.9
15	1321	.30361E+02	7.8
16	1332	.44789E+02	5.7
17	1374	.51379E+02	6.2
18	1377	.26688E+04	2.9
19	1674	.42259E+02	6.6
20	1757	.19686E+03	3.3
21	1888	.32388E+02	6.0
22	1919	.44976E+03	2.7
23	2803	.52432E+01	14.5

Table 9.5: Data for Nickel

Measurement ID: **NIB22**

No.	Energy (KeV)	γ-emission rate	% Std.dev.
1	122	.36765E+02	4.3
2	127	.16260E+02	7.3
3	137	.56825E+01	13.0
4	511	.14014E+03	2.8
5	811	.16804E+03	2.7
6	1377	.86146E+02	4.2
7	1674	.95851E+00	60.2
8	1757	.45265E+01	19.8
9	1919	.12221E+02	9.7

Table 9.6: Data for Chromium

Measurement ID: **CRA22**

No.	Energy (KeV)	γ-emission rate	% Std.dev.
1	320	.22851E+04	2.1
2	511	.56776E+02	4.8
3	935	.67560E+01	25.2
4	1368	.12830E+02	17.0
5	1811	.15430E+01	63.4
6	2754	.14423E+02	17.3

Table 9.7: Data for Molybdenum

Measurement ID: **MOA11**

No.	Energy (KeV)	γ-emission rate	% Std.dev.
1	141	.90744E+03	3.1
2	172	.18896E+02	46.2
3	181	.29692E+03	3.7
4	192	.72603E+02	24.2
5	263	.56220E+02	11.2
6	307	.63352E+03	2.8
7	335	.10070E+03	13.1
8	352	.12859E+02	85.1
9	366	.56214E+02	11.0
10	460	.72073E+02	8.8
11	481	.22594E+02	24.3
12	511	.79450E+04	2.1
13	545	.43857E+02	12.3
14	568	.14363E+03	5.1
15	591	.41079E+02	13.2
16	644	.38841E+02	12.4
17	658	.13912E+04	2.2
18	684	.84179E+02	7.7
19	695	.12627E+02	46.6
20	714	.67208E+02	12.0
21	722	.53724E+03	3.0
22	739	.47318E+03	3.4
23	766	.11213E+02	31.7
24	778	.44912E+03	2.9
25	787	.66831E+03	2.9
26	791	.60062E+02	9.0
27	810	.34312E+02	16.6
28	823	.24676E+02	23.2
29	833	.65169E+02	7.1
30	849	.51488E+02	9.0
31	879	.33900E+02	12.6
32	909	.11330E+03	4.9
33	920	.27948E+02	14.1
34	934	.94326E+02	5.7
35	970	.76703E+01	41.2
36	996	.15141E+02	23.6
37	1012	.24981E+02	15.4

Table 9.7 continued

38	1024	.23848E+02	16.1
39	1091	.13135E+03	4.8
40	1121	.10965E+02	27.3
41	1168	.12742E+03	4.8
42	1200	.51096E+02	8.8
43	1432	.44664E+02	9.9
44	1436	.19844E+02	20.0
45	1477	.92207E+02	6.9
46	1497	.83454E+01	33.2
47	1511	.66997E+02	6.9
48	1532	.87360E+01	48.7
49	1546	.30084E+02	15.5
50	1555	.50113E+01	47.3
51	1580	.13287E+02	22.0
52	1637	.15284E+02	20.9
53	1701	.69376E+02	7.0
54	1884	.22258E+02	13.4
55	1945	.10178E+02	22.8
56	1956	.42951E+01	47.5
57	1979	.24526E+02	12.6
58	2032	.10365E+02	24.5
59	2615	.14933E+02	15.7
60	2632	.72435E+01	24.0
61	3028	.56603E+01	28.8

Table 9.8: Data for Molybdenum

Measurement ID: **MOA24**

No.	Energy (KeV)	γ-emission rate	% Std.dev.
1	110	.45952E+03	2.5
2	119	.47457E+03	3.2
3	128	.52724E+03	3.5
4	141	.94601E+04	3.4
5	181	.12451E+04	1.7
6	193	.43988E+04	5.6
7	203	.45345E+02	7.1
8	216	.17044E+02	19.2
9	234	.56706E+02	4.0
10	365	.24632E+03	2.4
11	459	.32705E+02	6.6
12	480	.68671E+01	27.0
13	511	.23635E+03	2.4
14	528	.13037E+02	17.0
15	569	.86126E+02	4.6
16	719	.94510E+01	30.7
17	724	.20034E+02	14.8
18	739	.25784E+04	2.7
19	756	.18542E+02	7.6
20	765	.23356E+03	2.5
21	777	.12411E+04	2.4
22	810	.17192E+02	7.2
23	823	.26737E+02	4.9
24	850	.28754E+02	5.2
25	880	.19020E+02	6.2
26	909	.54660E+03	2.3
27	920	.35989E+02	5.3
28	934	.10230E+04	2.7
29	961	.19883E+02	4.9
30	1091	.58736E+02	3.5
31	1200	.23958E+02	4.3
32	1205	.15549E+02	5.5
33	1499	.40355E+01	13.0
34	1661	.14937E+01	25.8
35	1714	.29858E+01	15.7
36	1849	.94408E+01	7.3

Table 9.9: Data for Stainless Steel SS316

Measurement ID: **SSA24**

No.	Energy (KeV)	γ-emission rate	% Std.dev.
1	91	.47085E+03	10.4
2	122	.35015E+03	2.9
3	137	.46804E+02	4.7
4	141	.49838E+03	2.9
5	171	.35853E+01	48.1
6	181	.32569E+02	5.9
7	320	.44043E+03	2.0
8	366	.85152E+01	15.5
9	511	.65625E+03	2.1
10	595	.81945E+01	21.4
11	739	.62849E+02	4.0
12	766	.47647E+01	23.6
13	778	.32294E+02	5.9
14	811	.83918E+03	2.3
15	835	.19007E+03	2.9
16	864	.71710E+01	15.1
17	909	.14223E+02	9.9
18	912	.14946E+01	77.4
19	934	.25136E+02	6.1
20	984	.30997E+01	30.6
21	1099	.52366E+01	24.2
22	1173	.65530E+01	19.3
23	1292	.42015E+01	21.5
24	1312	.35367E+01	24.5
25	1321	.28638E+01	26.2
26	1332	.64257E+01	15.6
27	1377	.40969E+03	3.1
28	1674	.37015E+01	26.2
29	1757	.29554E+02	5.7
30	1919	.62437E+02	3.9
31	2104	.14717E+01	36.1

Table 9.10: Data for Stainless Steel AISI316

Measurement ID: **SSC14**

No.	Energy (KeV)	γ-emission rate	% Std.dev.
1	122	.26851E+02	5.3
2	141	.18321E+02	7.9
3	320	.26606E+02	5.7
4	511	.43943E+02	4.6
5	811	.62750E+02	3.9
6	835	.15266E+02	9.7
7	847	.29903E+01	22.3
8	1377	.30165E+01	34.3

Table 9.11: Data for Mn-Cu Alloy

Measurement ID: **MCA11**
Detector ID: 4F

No.	Energy (KeV)	γ-emission rate	% Std.dev.
1	511	.13872E+06	2.1
2	835	.26891E+03	19.2
3	847	.10479E+05	3.4
4	1164	.40282E+03	20.3
5	1173	.89119E+03	24.7
6	1434	.26187E+04	8.1
7	1482	.16528E+03	36.0
8	1811	.28996E+04	5.5
9	2113	.16981E+04	7.5

Table 9.12: Data for Mn-Cu Alloy

Measurement ID: **MCA23**

No.	Energy (KeV)	γ-emission rate	% Std.dev.
1	122	.20636E+02	10.1
2	199	.53829E+02	7.3
3	205	.15679E+02	23.2
4	511	.33936E+02	12.5
5	811	.36331E+02	8.6
6	835	.42818E+04	2.7
7	847	.35889E+01	25.6
8	1173	.70074E+01	18.1
9	1332	.55330E+01	21.8
10	1377	.42413E+01	27.2

Table 9.13: Data for MnCu Alloy

Measurement ID: **MCB22**

No.	Energy (KeV)	γ-emission rate	% Std.dev.
1	511	.25758E+02	4.9
2	835	.54306E+02	3.8

Table 9.14: Data for Tungsten

Measurement ID: **WA23**

No.	Energy (KeV)	γ-emission rate	% Std.dev.
1	99	.41253E+01	19.7
2	107	.78275E+01	11.2
3	113	.49987E+01	16.7
4	121	.45424E+01	17.1
5	134	.28886E+03	3.2
6	144	.19548E+01	38.9
7	152	.34823E+01	8.5
8	161	.10459E+02	4.2
9	194	.40284E+01	13.0
10	206	.10681E+02	5.6
11	239	.27335E+01	16.5
12	246	.25736E+02	3.1
13	291	.22744E+01	16.3
14	312	.28365E+01	18.2
15	354	.79715E+01	5.6
16	413	.16557E+01	21.2
17	479	.74038E+03	3.0
18	488	.45937E+01	15.7
19	494	.45296E+01	16.0
20	499	.25984E+01	28.0
21	511	.19714E+02	3.2
22	539	.11180E+02	7.1
23	551	.18493E+03	2.3
24	589	.33709E+01	8.5
25	613	.11934E+02	4.1
26	618	.23088E+03	2.4
27	625	.30151E+02	2.9
28	682	.27640E+01	7.8
29	685	.10156E+04	2.7
30	745	.76840E+01	3.7
31	772	.11305E+03	2.5
32	816	.27235E+00	32.3
33	864	.97505E+01	3.0
34	879	.43127E+01	4.1
35	903	.51800E+00	29.2
36	920	.91200E+00	19.1
37	1121	.27890E+01	5.2

Table 9.14 continued

38	1189	.13118E+01	8.9
39	1221	.18300E+01	7.2
40	1231	.10623E+01	13.2

Table 9.15: Data for Zirconium

Measurement ID: **ZRA21**

No.	Energy (KeV)	γ-emission rate	% Std.dev.
1	173	.87664E+03	6.7
2	203	.13546E+05	0.9
3	206	.41739E+03	18.7
4	216	.84968E+02	94.9
5	388	.40923E+04	2.5
6	448	.21444E+03	22.7
7	479	.14473E+05	1.6
8	505	.30813E+03	24.2
9	511	.59298E+05	1.4
10	556	.29527E+04	6.1
11	658	.37359E+03	21.3
12	682	.41734E+03	19.6
13	724	.35503E+03	18.5
14	743	.51639E+03	14.7
15	749	.38144E+03	19.9
16	756	.41116E+03	14.0
17	847	.20624E+03	26.2
18	909	.13922E+06	1.6
19	935	.13326E+04	3.6
20	1024	.52018E+03	5.6
21	1368	.17552E+04	3.1
22	1405	.30918E+03	8.0
23	1621	.10719E+03	13.6
24	1657	.15761E+03	10.4
25	1713	.10450E+04	3.8
26	1745	.19945E+03	10.9
27	2755	.15628E+04	3.8

Table 9.16: Data for Vanadium

Measurement ID: **VB22**

No.	Energy (KeV)	γ-emission rate	% Std.dev.
1	175	.75518E+01	9.2
2	511	.12274E+02	6.9
3	984	.85265E+02	3.3
4	1038	.84750E+02	3.1
5	1213	.22501E+01	25.5
6	1312	.84970E+02	3.2

Table 9.17: Data for Aluminum

Measurement ID: **ALB21**

No.	Energy (KeV)	γ-emission rate	% Std.dev.
1	511	.16935E+03	13.6
2	1368	.76262E+04	2.5
3	2754	.77762E+04	3.1

Table 9.18: Data for Cobalt

Measurement ID: **COA23**

No.	Energy (KeV)	γ-emission rate	% Std.dev.
1	141	.13222E+02	33.1
2	194	.33461E+03	3.8
3	205	.79275E+02	14.1
4	505	.86954E+02	13.7
5	511	.52678E+04	2.9
6	811	.17369E+05	2.2
7	864	.12123E+03	5.0
8	1099	.10581E+04	3.2
9	1173	.33747E+02	9.2
10	1292	.81092E+03	3.3
11	1321	.81487E+02	5.2
12	1332	.29608E+02	8.0
13	1674	.98953E+02	4.9

Table 9.19: Data for Titanium

Measurement ID: **TIB21**

No.	Energy (KeV)	γ-emission rate	% Std.dev.
1	159	.14787E+03	4.2
2	175	.60527E+02	6.7
3	511	.13689E+03	5.4
4	984	.73980E+03	3.4
5	1038	.70518E+03	3.2
6	1213	.17451E+02	22.0
7	1312	.77429E+03	3.2

Table 9.20: Data for Niobium

Measurement ID: **NBB21**

No.	Energy (KeV)	γ-emission rate	% Std.dev.
1	203	.24475E+02	13.0
2	480	.19261E+02	16.3
3	511	.96357E+01	29.0
4	912	.13605E+02	19.1
5	934	.77837E+03	3.1

Table 9.21: Data for Tin

Measurement ID: **SNC13**

No.	Energy (KeV)	γ-emission rate	% Std.dev.
1	102	.16999E+02	3.6
2	110	.83031E+01	5.4
3	144	.11970E+01	4.4
4	148	.14588E+01	4.6
5	159	.60554E+03	3.5
6	172	.24582E+02	2.1
7	186	.31985E+00	29.3
8	245	.28872E+02	2.5
9	315	.20921E+02	4.8
10	336	.36891E+00	30.1
11	391	.30181E+01	5.0
12	417	.14797E+03	3.4
13	511	.24117E+01	6.5
14	564	.82165E+00	15.0
15	911	.41024E+00	32.7
16	968	.31757E+00	38.7
17	1024	.46623E+00	36.3
18	1120	.40034E+00	29.7
19	1764	.96976E+00	14.0
20	2102	.53793E+00	23.2
21	2205	.31634E+00	33.7
22	2250	.13658E+00	53.8
23	2300	.22465E+00	53.9

Table 9.22: Data for Lead

Measurement ID: **PBC11**

No.	Energy (KeV)	γ-emission rate	% Std.dev.
1	279	.27490E+03	3.6
2	401	.10327E+02	20.0
3	511	.10182E+02	19.1

Table 9.23: Data for Tantalum

Measurement ID: **TAA21**

No.	Energy (KeV)	γ-emission rate	% Std.dev.
1	93	.36059E+05	1.4
2	103	.66708E+04	1.6
3	109	.26800E+03	17.4
4	117	.16732E+03	27.1
5	148	.20961E+03	7.6
6	155	.17214E+03	9.1
7	179	.47829E+02	15.7
8	215	.10207E+03	10.2
9	222	.10869E+03	9.8
10	229	.52650E+02	20.0
11	264	.60160E+02	12.1
12	332	.12939E+03	6.3
13	443	.10076E+03	7.3
14	481	.42485E+02	13.0
15	500	.23672E+02	19.5
16	511	.11047E+02	33.3
17	1001	.29476E+02	26.0
18	1121	.47687E+03	3.8
19	1189	.24064E+03	5.3
20	1221	.41088E+03	4.3
21	1231	.14992E+03	7.6
22	1257	.26357E+02	18.6
23	1289	.22798E+02	20.4

Table 9.24: Data for Silver

Measurement ID: **AGC12**

No.	Energy (KeV)	γ-emission rate	% Std.dev.
1	222	.17858E+03	9.3
2	229	.59580E+02	25.3
3	391	.89998E+02	14.0
4	406	.29992E+03	6.1
5	430	.26990E+03	6.7
6	451	.61745E+03	3.9
7	511	.19366E+04	2.7
8	601	.31625E+02	19.3
9	616	.43237E+03	5.7
10	646	.18782E+02	53.2
11	680	.52615E+02	21.9
12	703	.74970E+02	16.5
13	717	.59753E+03	4.2
14	748	.42567E+03	5.4
15	793	.13036E+03	15.0
16	804	.33737E+03	6.9
17	825	.32913E+03	6.2
18	848	.87867E+02	16.1
19	1046	.56849E+03	4.9
20	1128	.24313E+03	7.5
21	1199	.23853E+03	7.6
22	1211	.12892E+02	78.7
23	1223	.15918E+03	10.4
24	1394	.19162E+02	43.4
25	1528	.32277E+03	6.6
26	1573	.14947E+03	10.2
27	1839	.42515E+02	21.4

Table 9.25: Data for Zinc

Measurement ID: **ZNC12**

No.	Energy (KeV)	γ-emission rate	% Std.dev.
1	185	.36667E+02	21.3
2	439	.19651E+03	6.6
3	511	.14863E+04	2.8
4	1116	.51979E+02	17.1

Table 9.26: Data for Silicon

Measurement ID: **SIA11**

No.	Energy (KeV)	γ-emission rate	% Std.dev.
1	146	.46421E+03	49.7
2	171	.16224E+02	51.9
3	511	.15367E+04	31.4
4	844	.14838E+04	19.9
5	1014	.37120E+03	13.6
6	1176	.94203E+02	6.5
7	1196	.74230E+01	39.6
8	1273	.20285E+04	10.0
9	1614	.22516E+02	28.8
10	1641	.14296E+02	37.3
11	1685	.25468E+02	29.0
12	2028	.86329E+02	28.9
13	2128	.38335E+03	26.8
14	2164	.31860E+02	36.2
15	2425	.13712E+03	31.2
16	2637	.85370E+02	32.3
17	3303	.11986E+03	35.8
18	3813	.28354E+02	41.8

Table 9.27: Data for Yttrium

Measurement ID: **YC13**

No.	Energy (KeV)	γ-emission rate	% Std.dev.
1	511	.33202E+02	14.5
2	898	.81857E+03	3.6
3	933	.57971E+01	54.5
4	1836	.91945E+03	3.6

Table 9.28: Data for Indium

Measurement ID: **INA22**

No.	Energy (KeV)	γ-emission rate	% Std.dev.
1	147	.17306E+03	10.8
2	190	.43661E+04	0.7
3	261	.26696E+02	36.9
4	335	.11626E+05	1.3
5	492	.12776E+03	8.5
6	511	.37823E+02	22.9
7	528	.44916E+03	3.8
8	558	.10530E+04	2.4
9	607	.86067E+01	89.2
10	617	.69674E+02	16.6
11	725	.10112E+04	2.7
12	1284	.22003E+02	25.5
13	1300	.54523E+02	14.9
14	1369	.32704E+03	5.3
15	2754	.32881E+03	7.2

Table 9.29: Data for Magnesium

Measurement ID: **MGA21**

No.	Energy (KeV)	γ-emission rate	% Std.dev.
1	511	.10297E+06	1.7
2	1368	.80716E+06	1.9
3	2754	.84604E+06	2.4

Table 9.30: Data for Gold

Measurement ID: **AUA22**

No.	Energy (KeV)	γ-emission rate	% Std.dev.
1	138	.21201E+04	33.5
2	148	.48676E+05	2.9
3	159	.12257E+04	51.3
4	168	.63944E+04	11.8
5	188	.37901E+05	1.4
6	285	.51436E+04	6.6
7	316	.32188E+04	9.8
8	333	.42366E+05	1.7
9	356	.16088E+06	1.4
10	412	.10751E+06	1.5
11	426	.11511E+05	3.5
12	511	.10405E+04	13.8
13	675	.92710E+03	13.8
14	688	.12001E+04	12.0
15	846	.22388E+03	45.2
16	982	.23836E+03	36.1
17	1089	.46626E+03	24.7
18	1368	.48916E+03	23.6

Table 9.31: Data for $YBa_2Cu_3O_7$

Measurement ID: **YCA13**

No.	Energy (KeV)	γ-emission rate	% Std.dev.
1	125	.51616E+00	19.1
2	269	.34470E+01	5.8
3	276	.18413E+01	9.8
4	373	.58160E+00	21.2
5	497	.11858E+01	20.6
6	511	.20583E+01	18.8
7	814	.15438E+01	16.8
8	898	.79508E+02	2.9
9	1048	.55512E+00	26.3
10	1173	.38558E+00	38.1
11	1325	.23439E+01	9.9
12	1836	.90421E+02	2.7
13	2734	.12547E+01	13.0

Table 9.32: Data for $ErBa_2Cu_3O_7$

Measurement ID: **ECA13**
Detector ID: 5S

No.	Energy (KeV)	γ-emission rate	% Std.dev.
1	122	.27881E+02	7.4
2	188	.88249E+01	41.0
3	197	.55587E+02	7.2
4	201	.46350E+02	8.5
5	206	.17748E+02	21.9
6	268	.13987E+02	20.6
7	276	.65877E+01	44.5
8	511	.88338E+02	5.3
9	811	.61934E+02	5.5
10	835	.67066E+04	2.7
11	847	.50841E+01	20.8
12	898	.20480E+03	3.3
13	1173	.10595E+02	12.5
14	1332	.93260E+01	15.7
15	1359	.17571E+01	61.4
16	1377	.10120E+02	14.0
17	1836	.23665E+03	3.2
18	2734	.21099E+01	39.1

Table 10.1 Computed Spectra for Three Locations in REAC Group Structure

Upper Energy (eV)	Lethargy Change (Δu)	Location-wise Spectrum (Flux/Δu) A	B	C
0.924E-01	9.1310	0.170E-08	0.649E-14	0.222E-12
0.152E+00	0.5000	0.202E-07	0.769E-13	0.264E-11
0.251E+00	0.5000	0.126E-07	0.714E-11	0.531E-11
0.414E+00	0.5000	0.209E-07	0.118E-10	0.875E-11
0.683E+00	0.5000	0.224E-07	0.292E-09	0.665E-11
0.113E+01	0.5000	0.369E-07	0.481E-09	0.110E-10
0.186E+01	0.5000	0.412E-07	0.379E-08	0.160E-10
0.306E+01	0.5000	0.679E-07	0.625E-08	0.264E-10
0.504E+01	0.5000	0.100E-06	0.230E-07	0.431E-10
0.832E+01	0.5000	0.150E-06	0.504E-07	0.710E-10
0.137E+02	0.5000	0.230E-06	0.982E-07	0.101E-09
0.226E+02	0.5000	0.342E-06	0.173E-06	0.167E-09
0.373E+02	0.5000	0.467E-06	0.277E-06	0.216E-09
0.614E+02	0.5000	0.620E-06	0.398E-06	0.356E-09
0.101E+03	0.5000	0.108E-05	0.695E-06	0.385E-09
0.167E+03	0.5000	0.148E-05	0.977E-06	0.635E-09
0.275E+03	0.5000	0.198E-05	0.135E-05	0.714E-09
0.454E+03	0.5000	0.207E-05	0.151E-05	0.118E-08
0.749E+03	0.5000	0.246E-05	0.186E-05	0.175E-08
0.123E+04	0.5000	0.286E-05	0.215E-05	0.289E-08
0.203E+04	0.5000	0.345E-05	0.246E-05	0.349E-08
0.240E+04	0.1667	0.340E-05	0.261E-05	0.482E-08
0.284E+04	0.1666	0.320E-05	0.268E-05	0.570E-08
0.335E+04	0.1667	0.313E-05	0.285E-05	0.672E-08
0.553E+04	0.5000	0.409E-05	0.303E-05	0.873E-08
0.912E+04	0.5000	0.474E-05	0.329E-05	0.144E-07
0.150E+05	0.5000	0.545E-05	0.369E-05	0.178E-07
0.199E+05	0.2801	0.719E-05	0.393E-05	0.261E-07
0.255E+05	0.2500	0.715E-05	0.430E-05	0.330E-07
0.409E+05	0.4700	0.771E-05	0.449E-05	0.375E-07
0.674E+05	0.5000	0.952E-05	0.534E-05	0.611E-07
0.111E+06	0.5000	0.122E-04	0.687E-05	0.145E-06
0.183E+06	0.5000	0.171E-04	0.917E-05	0.239E-06
0.302E+06	0.5000	0.199E-04	0.441E-05	0.428E-06
0.388E+06	0.2500	0.306E-04	0.644E-05	0.668E-06
0.498E+06	0.2500	0.321E-04	0.591E-05	0.859E-06
0.639E+06	0.2500	0.411E-04	0.105E-04	0.996E-06
0.821E+06	0.2500	0.511E-04	0.116E-04	0.128E-05
0.111E+07	0.3000	0.501E-04	0.811E-05	0.126E-05
0.135E+07	0.2001	0.570E-04	0.855E-05	0.161E-05

Table 10.1 Continued

0.174E+07	0.2499	0.620E-04	0.909E-05	0.154E-05
0.223E+07	0.2500	0.661E-04	0.870E-05	0.153E-05
0.287E+07	0.2500	0.664E-04	0.902E-05	0.150E-05
0.368E+07	0.2500	0.642E-04	0.635E-05	0.149E-05
0.497E+07	0.3000	0.502E-04	0.460E-05	0.104E-05
0.607E+07	0.2000	0.452E-04	0.498E-05	0.133E-05
0.741E+07	0.2000	0.340E-04	0.518E-05	0.840E-06
0.861E+07	0.1500	0.266E-04	0.512E-05	0.752E-06
0.100E+08	0.1500	0.235E-04	0.538E-05	0.740E-06
0.116E+08	0.1500	0.354E-04	0.553E-05	0.791E-06
0.135E+08	0.1501	0.811E-04	0.122E-04	0.401E-04
0.149E+08	0.1000	0.464E-02	0.506E-04	0.357E-03
0.169E+08	0.1250	0.297E-02	0.264E-04	0.347E-04

Table 10.2(a) Neutron flux spectrum at positions in Phase-IIC

Group No.	Energy Boundary(eV)	Flux at 10cm A	Flux at 82cm B
1	1.64870E+01 - 1.62310E+01	4.99438E-22	3.73488E-24
2	1.62310E+01 - 1.59800E+01	0.00000E-01	4.66207E-25
3	1.59800E+01 - 1.57320E+01	5.26350E-25	2.89839E-25
4	1.57320E+01 - 1.54880E+01	3.28928E-25	2.00991E-25
5	1.54880E+01 - 1.52480E+01	7.01764E-03	5.16859E-05
6	1.52480E+01 - 1.50120E+01	1.09597E-02	8.62624E-05
7	1.50120E+01 - 1.47790E+01	2.00102E-02	1.60079E-04
8	1.47790E+01 - 1.45500E+01	1.15350E-02	1.12816E-04
9	1.45500E+01 - 1.43240E+01	1.62108E-03	4.06286E-05
10	1.43240E+01 - 1.41020E+01	3.20822E-04	2.36639E-05
11	1.41020E+01 - 1.38830E+01	8.54233E-05	1.81667E-05
12	1.38830E+01 - 1.36680E+01	1.62713E-04	1.66834E-05
13	1.36680E+01 - 1.34560E+01	1.16861E-04	1.50631E-05
14	1.34560E+01 - 1.32480E+01	9.01373E-05	1.35737E-05
15	1.32480E+01 - 1.30420E+01	5.90506E-05	1.18539E-05
16	1.30420E+01 - 1.28400E+01	6.76598E-05	1.03259E-05
17	1.28400E+01 - 1.26410E+01	7.92517E-05	9.30106E-06
18	1.26410E+01 - 1.24450E+01	7.63936E-05	8.42283E-06
19	1.24450E+01 - 1.22520E+01	5.11979E-05	7.65603E-06
20	1.22520E+01 - 1.20620E+01	4.30976E-05	7.09210E-06
21	1.20620E+01 - 1.18750E+01	3.56238E-05	6.44678E-06
22	1.18750E+01 - 1.16910E+01	3.55438E-05	6.09311E-06
23	1.16910E+01 - 1.15100E+01	4.99383E-05	6.13017E-06
24	1.15100E+01 - 1.13310E+01	3.84928E-05	5.78273E-06
25	1.13310E+01 - 1.11560E+01	2.37435E-05	5.35284E-06
26	1.11560E+01 - 1.09830E+01	2.26040E-05	5.28925E-06
27	1.09830E+01 - 1.08120E+01	2.64576E-05	5.46391E-06
28	1.08120E+01 - 1.06450E+01	3.36319E-05	5.53807E-06
29	1.06450E+01 - 1.04800E+01	3.32706E-05	5.40959E-06
30	1.04800E+01 - 1.03170E+01	2.63278E-05	5.24218E-06
31	1.03170E+01 - 1.01570E+01	2.26371E-05	5.14050E-06
32	1.01570E+01 - 9.99990E+00	1.98987E-05	5.15268E-06
33	9.99990E+00 - 9.39400E+00	1.87734E-05	4.92129E-06
34	9.39400E+00 - 8.82490E+00	2.08894E-05	4.47418E-06
35	8.82490E+00 - 8.29020E+00	2.75306E-05	4.64219E-06
36	8.29020E+00 - 7.78790E+00	2.10658E-05	4.47965E-06
37	7.78790E+00 - 7.31610E+00	2.16800E-05	4.47876E-06
38	7.31610E+00 - 6.87280E+00	2.66484E-05	4.81281E-06
39	6.87280E+00 - 6.45640E+00	2.66605E-05	4.88972E-06
40	6.45640E+00 - 6.06520E+00	2.75037E-05	4.80286E-06
41	6.06520E+00 - 5.69780E+00	2.37733E-05	4.67707E-06
42	5.69780E+00 - 5.35250E+00	2.48738E-05	4.74177E-06

Table 10.2(a) continued #1

43	5.35250E+00 - 5.02820E+00	2.45248E-05	4.30282E-06
44	5.02820E+00 - 4.72360E+00	2.71756E-05	4.40386E-06
45	4.72360E+00 - 4.43740E+00	2.76878E-05	4.46008E-06
46	4.43740E+00 - 4.16860E+00	3.02530E-05	4.56072E-06
47	4.16860E+00 - 3.91600E+00	3.12170E-05	4.71651E-06
48	3.91600E+00 - 3.67870E+00	3.27541E-05	4.53332E-06
49	3.67870E+00 - 3.45590E+00	3.17727E-05	4.84833E-06
50	3.45590E+00 - 3.24650E+00	3.49459E-05	5.29284E-06
51	3.24650E+00 - 3.04980E+00	3.63893E-05	6.46576E-06
52	3.04980E+00 - 2.86500E+00	3.86149E-05	6.98157E-06
53	2.86500E+00 - 2.69140E+00	3.93946E-05	7.75611E-06
54	2.69140E+00 - 2.52840E+00	4.01866E-05	8.53904E-06
55	2.52840E+00 - 2.37520E+00	4.17973E-05	9.06444E-06
56	2.37520E+00 - 2.23130E+00	4.19650E-05	9.79808E-06
57	2.23130E+00 - 2.09610E+00	4.17186E-05	8.73375E-06
58	2.09610E+00 - 1.96910E+00	3.96626E-05	8.12866E-06
59	1.96910E+00 - 1.84980E+00	4.02804E-05	7.61981E-06
60	1.84980E+00 - 1.73770E+00	4.14676E-05	8.90334E-06
61	1.73770E+00 - 1.53350E+00	3.92124E-05	8.75124E-06
62	1.53350E+00 - 1.35330E+00	4.19806E-05	9.23327E-06
63	1.35330E+00 - 1.19430E+00	3.93846E-05	8.47049E-06
64	1.19430E+00 - 1.05400E+00	3.60514E-05	7.88486E-06
65	1.05400E+00 - 9.30130E-01	3.35991E-05	6.46246E-06
66	9.30130E-01 - 8.20840E-01	3.64270E-05	9.51493E-06
67	8.20840E-01 - 7.24380E-01	3.84772E-05	1.18365E-05
68	7.24380E-01 - 6.39270E-01	3.48357E-05	1.10705E-05
69	6.39270E-01 - 5.64150E-01	3.28974E-05	1.08229E-05
70	5.64150E-01 - 4.97860E-01	3.10034E-05	1.02241E-05
71	4.97860E-01 - 4.39360E-01	2.40712E-05	6.18942E-06
72	4.39360E-01 - 3.87740E-01	2.18790E-05	5.92353E-06
73	3.87740E-01 - 3.42170E-01	2.21696E-05	7.06065E-06
74	3.42170E-01 - 3.01970E-01	2.14734E-05	6.29468E-06
75	3.01970E-01 - 2.66490E-01	1.70113E-05	3.02305E-06
76	2.66490E-01 - 2.35170E-01	1.45599E-05	2.21920E-06
77	2.35170E-01 - 2.07540E-01	1.51479E-05	4.94419E-06
78	2.07540E-01 - 1.83150E-01	1.51036E-05	7.25564E-06
79	1.83150E-01 - 1.61630E-01	1.55696E-05	8.81422E-06
80	1.61630E-01 - 1.42640E-01	1.50582E-05	8.84556E-06
81	1.42640E-01 - 1.25880E-01	1.44735E-05	8.59348E-06
82	1.25880E-01 - 1.11090E-01	1.34256E-05	8.03866E-06
83	1.11090E-01 - 9.80350E-02	1.24946E-05	7.46752E-06
84	9.80350E-02 - 8.65150E-02	1.08165E-05	7.11036E-06
85	8.65150E-02 - 7.63490E-02	1.05063E-05	6.75015E-06
86	7.63490E-02 - 6.73780E-02	9.94884E-06	6.33034E-06
87	6.73780E-02 - 5.94610E-02	9.43496E-06	5.99941E-06

Table 10.2(a) continued #2

88	5.94610E-02 - 5.24740E-02	8.81468E-06	5.66080E-06
89	5.24740E-02 - 4.63080E-02	8.77210E-06	5.46777E-06
90	4.63080E-02 - 4.08670E-02	8.23471E-06	5.22047E-06
91	4.08670E-02 - 3.60650E-02	7.70869E-06	4.98840E-06
92	3.60650E-02 - 3.18270E-02	7.31281E-06	4.74955E-06
93	3.18270E-02 - 2.80870E-02	7.01357E-06	4.08275E-06
94	2.80870E-02 - 2.47870E-02	7.56018E-06	4.86985E-06
95	2.47870E-02 - 2.18740E-02	6.82159E-06	4.40827E-06
96	2.18740E-02 - 1.93040E-02	6.50052E-06	4.27578E-06
97	1.93040E-02 - 1.50340E-02	6.06533E-06	3.94659E-06
98	1.50340E-02 - 1.17090E-02	5.78700E-06	3.85675E-06
99	1.17090E-02 - 9.11860E-03	5.38518E-06	3.65463E-06
100	9.11860E-03 - 7.10160E-03	4.91475E-06	3.40071E-06
101	7.10160E-03 - 5.53070E-03	4.45785E-06	3.27923E-06
102	5.53070E-03 - 4.30730E-03	4.33375E-06	3.16567E-06
103	4.30730E-03 - 3.35460E-03	3.89995E-06	3.02625E-06
104	3.35460E-03 - 2.61250E-03	2.84735E-06	2.84857E-06
105	2.61250E-03 - 2.03460E-03	3.75506E-06	2.70633E-06
106	2.03460E-03 - 1.58460E-03	3.55264E-06	2.55490E-06
107	1.58460E-03 - 1.23410E-03	3.30591E-06	2.40718E-06
108	1.23410E-03 - 9.61100E-04	2.99956E-06	2.23241E-06
109	9.61100E-04 - 5.82930E-04	2.61710E-06	1.96629E-06
110	5.82930E-04 - 3.53570E-04	2.15860E-06	1.65978E-06
111	3.53570E-04 - 2.14450E-04	1.77166E-06	1.35357E-06
112	2.14450E-04 - 1.30070E-04	1.40750E-06	1.06028E-06
113	1.30070E-04 - 7.88910E-05	1.07011E-06	7.94830E-07
114	7.88910E-05 - 4.78500E-05	7.85315E-07	5.68057E-07
115	4.78500E-05 - 2.90230E-05	5.51697E-07	3.84069E-07
116	2.90230E-05 - 1.76030E-05	3.73668E-07	2.44851E-07
117	1.76030E-05 - 1.06770E-05	2.49219E-07	1.46564E-07
118	1.06770E-05 - 6.47580E-06	1.62017E-07	8.18996E-08
119	6.47580E-06 - 3.92780E-06	1.16963E-07	4.19645E-08
120	3.92780E-06 - 2.38230E-06	7.43711E-08	1.94611E-08
121	2.38230E-06 - 1.44490E-06	5.09575E-08	7.96992E-09
122	1.44490E-06 - 8.76400E-07	4.13133E-08	2.81195E-09
123	8.76400E-07 - 5.31560E-07	4.02055E-08	8.29021E-10
124	5.31560E-07 - 3.22410E-07	3.09971E-08	1.79687E-10
125	3.22410E-07 - 1.00100E-11	4.78763E-09	1.37935E-13

Unit of Flux: per/unit lethargy

Table 10.2(b) Neutron flux spectrum at positions in Phase-III line source

Group No.	Energy Boundary(eV)	Flux at(0cm) C	Flux at(40cm) D	Flux at(100cm) E
1	1.64870E+01 - 1.62310E+01	0.00000E-01	0.00000E-01	0.00000E-01
2	1.62310E+01 - 1.59800E+01	0.00000E-01	0.00000E-01	0.00000E-01
3	1.59800E+01 - 1.57320E+01	0.00000E-01	0.00000E-01	0.00000E-01
4	1.57320E+01 - 1.54880E+01	0.00000E-01	0.00000E-01	0.00000E-01
5	1.54880E+01 - 1.52480E+01	2.21715E-05	3.00885E-05	3.68904E-05
6	1.52480E+01 - 1.50120E+01	1.22896E-04	1.40247E-04	1.52718E-04
7	1.50120E+01 - 1.47790E+01	2.54449E-04	2.81296E-04	3.01851E-04
8	1.47790E+01 - 1.45500E+01	4.13554E-04	4.30893E-04	4.43797E-04
9	1.45500E+01 - 1.43240E+01	3.88820E-04	3.91154E-04	3.93844E-04
10	1.43240E+01 - 1.41020E+01	3.01467E-04	3.05498E-04	2.91003E-04
11	1.41020E+01 - 1.38830E+01	3.06803E-04	3.33689E-04	3.02586E-05
12	1.38830E+01 - 1.36680E+01	3.59644E-04	3.43893E-04	3.77488E-06
13	1.36680E+01 - 1.34560E+01	3.62262E-04	3.30062E-04	2.45164E-06
14	1.34560E+01 - 1.32480E+01	2.41109E-04	1.85187E-04	1.98405E-06
15	1.32480E+01 - 1.30420E+01	8.88687E-05	5.02022E-05	1.90904E-06
16	1.30420E+01 - 1.28400E+01	7.58727E-06	5.49986E-06	1.94635E-06
17	1.28400E+01 - 1.26410E+01	4.12964E-06	3.89000E-06	1.93380E-06
18	1.26410E+01 - 1.24450E+01	3.41795E-06	3.16432E-06	1.56700E-06
19	1.24450E+01 - 1.22520E+01	2.69666E-06	2.41763E-06	1.06708E-06
20	1.22520E+01 - 1.20620E+01	2.10403E-06	1.88333E-06	7.49583E-07
21	1.20620E+01 - 1.18750E+01	1.80604E-06	1.62497E-06	6.21650E-07
22	1.18750E+01 - 1.16910E+01	1.48425E-06	1.34322E-06	5.77119E-07
23	1.16910E+01 - 1.15100E+01	1.30103E-06	1.18515E-06	5.00969E-07
24	1.15100E+01 - 1.13310E+01	1.07814E-06	9.94558E-07	4.23234E-07
25	1.13310E+01 - 1.11560E+01	1.01390E-06	9.60242E-07	4.19823E-07
26	1.11560E+01 - 1.09830E+01	8.41378E-07	8.10345E-07	3.90388E-07
27	1.09830E+01 - 1.08120E+01	7.86840E-07	7.62069E-07	3.87440E-07
28	1.08120E+01 - 1.06450E+01	7.96613E-07	7.73813E-07	4.17989E-07
29	1.06450E+01 - 1.04800E+01	7.90250E-07	7.66687E-07	4.39962E-07
30	1.04800E+01 - 1.03170E+01	6.91947E-07	6.61747E-07	3.84365E-07
31	1.03170E+01 - 1.01570E+01	5.77262E-07	5.52099E-07	3.19873E-07
32	1.01570E+01 - 9.99990E+00	5.57404E-07	5.35711E-07	3.16344E-07
33	9.99990E+00 - 9.39400E+00	5.08192E-07	4.89026E-07	2.82106E-07
34	9.39400E+00 - 8.82490E+00	6.46648E-07	6.17308E-07	3.16911E-07
35	8.82490E+00 - 8.29020E+00	7.59107E-07	7.29818E-07	3.97411E-07
36	8.29020E+00 - 7.78790E+00	7.16123E-07	6.97199E-07	4.30693E-07
37	7.78790E+00 - 7.31610E+00	8.00475E-07	7.83781E-07	4.54229E-07
38	7.31610E+00 - 6.87280E+00	9.29785E-07	8.95589E-07	4.88260E-07
39	6.87280E+00 - 6.45640E+00	1.03803E-06	9.82755E-07	4.96388E-07
40	6.45640E+00 - 6.06520E+00	1.11493E-06	1.05388E-06	5.12234E-07
41	6.06520E+00 - 5.69780E+00	1.09938E-06	1.03572E-06	5.14449E-07
42	5.69780E+00 - 5.35250E+00	1.11757E-06	1.05382E-06	5.28671E-07

Table 10.2(b) continued #1

43	5.35250E+00 - 5.02820E+00	1.14332E-06	1.08222E-06	5.59110E-07
44	5.02820E+00 - 4.72360E+00	1.27025E-06	1.20785E-06	6.12041E-07
45	4.72360E+00 - 4.43740E+00	1.31633E-06	1.24678E-06	6.39629E-07
46	4.43740E+00 - 4.16860E+00	1.39835E-06	1.32780E-06	6.63746E-07
47	4.16860E+00 - 3.91600E+00	1.41557E-06	1.33149E-06	6.69344E-07
48	3.91600E+00 - 3.67870E+00	1.50555E-06	1.41463E-06	6.97096E-07
49	3.67870E+00 - 3.45590E+00	1.54227E-06	1.45252E-06	7.20155E-07
50	3.45590E+00 - 3.24650E+00	1.63323E-06	1.54138E-06	7.64028E-07
51	3.24650E+00 - 3.04980E+00	1.66133E-06	1.56711E-06	7.61343E-07
52	3.04980E+00 - 2.86500E+00	1.78383E-06	1.67103E-06	7.91872E-07
53	2.86500E+00 - 2.69140E+00	1.73367E-06	1.62557E-06	7.89883E-07
54	2.69140E+00 - 2.52840E+00	1.64812E-06	1.55123E-06	7.66872E-07
55	2.52840E+00 - 2.37520E+00	1.67927E-06	1.57627E-06	7.68810E-07
56	2.37520E+00 - 2.23130E+00	1.60705E-06	1.51419E-06	7.41501E-07
57	2.23130E+00 - 2.09610E+00	1.54200E-06	1.45107E-06	7.04471E-07
58	2.09610E+00 - 1.96910E+00	1.52724E-06	1.43510E-06	6.99271E-07
59	1.96910E+00 - 1.84980E+00	1.61727E-06	1.51683E-06	7.33860E-07
60	1.84980E+00 - 1.73770E+00	1.56930E-06	1.47486E-06	7.13367E-07
61	1.73770E+00 - 1.53350E+00	1.46758E-06	1.37266E-06	6.62552E-07
62	1.53350E+00 - 1.35330E+00	1.58588E-06	1.48968E-06	7.23603E-07
63	1.35330E+00 - 1.19430E+00	1.52624E-06	1.43060E-06	6.93405E-07
64	1.19430E+00 - 1.05400E+00	1.45340E-06	1.36517E-06	6.55968E-07
65	1.05400E+00 - 9.30130E-01	1.41534E-06	1.33333E-06	6.43785E-07
66	9.30130E-01 - 8.20840E-01	1.41993E-06	1.33571E-06	6.46401E-07
67	8.20840E-01 - 7.24380E-01	1.41654E-06	1.33410E-06	6.45266E-07
68	7.24380E-01 - 6.39270E-01	1.32464E-06	1.24278E-06	5.99323E-07
69	6.39270E-01 - 5.64150E-01	1.21918E-06	1.14732E-06	5.56259E-07
70	5.64150E-01 - 4.97860E-01	1.14751E-06	1.08005E-06	5.24293E-07
71	4.97860E-01 - 4.39360E-01	1.02953E-06	9.59706E-07	4.62331E-07
72	4.39360E-01 - 3.87740E-01	9.28734E-07	8.71199E-07	4.18774E-07
73	3.87740E-01 - 3.42170E-01	9.07154E-07	8.52382E-07	4.04397E-07
74	3.42170E-01 - 3.01970E-01	8.06393E-07	7.57912E-07	3.62125E-07
75	3.01970E-01 - 2.66490E-01	7.16653E-07	6.73187E-07	3.22765E-07
76	2.66490E-01 - 2.35170E-01	6.31299E-07	5.94122E-07	2.87102E-07
77	2.35170E-01 - 2.07540E-01	5.56635E-07	5.21879E-07	2.50828E-07
78	2.07540E-01 - 1.83150E-01	4.71792E-07	4.43543E-07	2.14708E-07
79	1.83150E-01 - 1.61630E-01	4.15947E-07	3.91013E-07	1.88002E-07
80	1.61630E-01 - 1.42640E-01	3.45947E-07	3.28410E-07	1.63406E-07
81	1.42640E-01 - 1.25880E-01	3.16717E-07	3.00006E-07	1.48002E-07
82	1.25880E-01 - 1.11090E-01	2.96908E-07	2.75786E-07	1.32147E-07
83	1.11090E-01 - 9.80350E-02	2.28326E-07	2.13598E-07	1.06114E-07
84	9.80350E-02 - 8.65150E-02	1.41641E-07	1.33004E-07	6.52287E-08
85	8.65150E-02 - 7.63490E-02	1.12987E-07	1.06194E-07	5.26917E-08
86	7.63490E-02 - 6.73780E-02	9.34875E-08	8.84329E-08	4.46442E-08
87	6.73780E-02 - 5.94610E-02	8.23734E-08	7.75366E-08	3.89872E-08

Table 10.2(b) continued #2

88	5.94610E-02 - 5.24740E-02	7.16961E-08	6.71173E-08	3.39171E-08
89	5.24740E-02 - 4.63080E-02	6.23686E-08	5.92773E-08	2.95163E-08
90	4.63080E-02 - 4.08670E-02	5.24855E-08	5.00680E-08	2.57390E-08
91	4.08670E-02 - 3.60650E-02	4.18602E-08	4.04719E-08	2.20251E-08
92	3.60650E-02 - 3.18270E-02	3.86103E-08	3.70440E-08	1.94309E-08
93	3.18270E-02 - 2.80870E-02	3.24034E-08	3.20481E-08	1.79920E-08
94	2.80870E-02 - 2.47870E-02	2.86957E-08	2.82735E-08	1.66269E-08
95	2.47870E-02 - 2.18740E-02	3.37027E-08	3.20812E-08	1.68733E-08
96	2.18740E-02 - 1.93040E-02	2.44350E-08	2.35493E-08	1.27618E-08
97	1.93040E-02 - 1.50340E-02	1.88821E-08	1.82557E-08	1.01772E-08
98	1.50340E-02 - 1.17090E-02	1.40432E-08	1.36996E-08	7.96762E-09
99	1.17090E-02 - 9.11860E-03	1.20777E-08	1.18509E-08	7.07858E-09
100	9.11860E-03 - 7.10160E-03	9.61246E-09	9.05089E-09	5.06899E-09
101	7.10160E-03 - 5.53070E-03	1.04676E-08	9.83621E-09	4.83765E-09
102	5.53070E-03 - 4.30730E-03	6.84512E-09	6.57240E-09	3.50245E-09
103	4.30730E-03 - 3.35460E-03	5.15859E-09	5.03726E-09	2.68818E-09
104	3.35460E-03 - 2.61250E-03	4.09783E-09	3.89641E-09	2.15674E-09
105	2.61250E-03 - 2.03460E-03	3.15531E-09	3.11564E-09	2.08121E-09
106	2.03460E-03 - 1.58460E-03	4.28208E-09	4.10202E-09	2.28189E-09
107	1.58460E-03 - 1.23410E-03	2.98569E-09	2.84428E-09	1.46182E-09
108	1.23410E-03 - 9.61100E-04	2.18489E-09	2.10949E-09	1.12074E-09
109	9.61100E-04 - 5.82930E-04	2.17775E-09	2.06641E-09	1.18214E-09
110	5.82930E-04 - 3.53570E-04	8.89363E-10	8.75277E-10	5.57150E-10
111	3.53570E-04 - 2.14450E-04	5.20647E-10	5.20739E-10	3.43559E-10
112	2.14450E-04 - 1.30070E-04	7.74695E-10	7.60573E-10	4.49672E-10
113	1.30070E-04 - 7.88910E-05	2.72289E-10	2.68035E-10	1.23897E-10
114	7.88910E-05 - 4.78500E-05	1.29384E-10	1.25308E-10	5.43291E-11
115	4.78500E-05 - 2.90230E-05	6.66295E-11	6.50619E-11	3.22533E-11
116	2.90230E-05 - 1.76030E-05	3.54746E-11	3.45529E-11	1.91558E-11
117	1.76030E-05 - 1.06770E-05	1.96846E-11	1.87962E-11	1.23538E-11
118	1.06770E-05 - 6.47580E-06	1.13671E-11	1.10910E-11	7.38059E-12
119	6.47580E-06 - 3.92780E-06	7.00863E-12	6.97629E-12	4.59041E-12
120	3.92780E-06 - 2.38230E-06	4.06024E-12	4.08025E-12	2.78807E-12
121	2.38230E-06 - 1.44490E-06	2.40655E-12	2.41899E-12	1.69684E-12
122	1.44490E-06 - 8.76400E-07	1.40419E-12	1.41247E-12	1.02067E-12
123	8.76400E-07 - 5.31560E-07	8.26399E-13	8.31619E-13	6.03980E-13
124	5.31560E-07 - 3.22410E-07	4.82935E-13	4.85934E-13	3.54418E-13
125	3.22410E-07 - 1.00100E-11	3.76587E-14	3.80084E-14	2.78161E-14

Unit of Flux: per/unit lethargy

Table 10.2(c) Neutron flux spectrum at positions in Phase-IIIA(point source)

Group No.	Energy Boundary(eV)	Flux at#1(FW0cm) F	Flux at#2(Li2O) G
1	1.64870E+01 - 1.62310E+01	0.00000E-01	0.00000E-01
2	1.62310E+01 - 1.59800E+01	0.00000E-01	0.00000E-01
3	1.59800E+01 - 1.57320E+01	0.00000E-01	0.00000E-01
4	1.57320E+01 - 1.54880E+01	0.00000E-01	0.00000E-01
5	1.54880E+01 - 1.52480E+01	0.00000E-01	0.00000E-01
6	1.52480E+01 - 1.50120E+01	0.00000E-01	0.00000E-01
7	1.50120E+01 - 1.47790E+01	1.09519E-06	1.14203E-06
8	1.47790E+01 - 1.45500E+01	6.13510E-06	4.96585E-06
9	1.45500E+01 - 1.43240E+01	3.54624E-05	3.12982E-05
10	1.43240E+01 - 1.41020E+01	3.24167E-03	2.90565E-03
11	1.41020E+01 - 1.38830E+01	5.46171E-03	4.91755E-03
12	1.38830E+01 - 1.36680E+01	1.96387E-04	2.21274E-04
13	1.36680E+01 - 1.34560E+01	1.47030E-04	1.31959E-04
14	1.34560E+01 - 1.32480E+01	8.54540E-05	7.53285E-05
15	1.32480E+01 - 1.30420E+01	5.23358E-05	5.39638E-05
16	1.30420E+01 - 1.28400E+01	4.22832E-05	4.56054E-05
17	1.28400E+01 - 1.26410E+01	3.51712E-05	3.71989E-05
18	1.26410E+01 - 1.24450E+01	2.60671E-05	3.14812E-05
19	1.24450E+01 - 1.22520E+01	2.17788E-05	2.92633E-05
20	1.22520E+01 - 1.20620E+01	2.04651E-05	2.76160E-05
21	1.20620E+01 - 1.18750E+01	1.95273E-05	2.48701E-05
22	1.18750E+01 - 1.16910E+01	1.82402E-05	2.18284E-05
23	1.16910E+01 - 1.15100E+01	1.80687E-05	2.01340E-05
24	1.15100E+01 - 1.13310E+01	1.95348E-05	2.09007E-05
25	1.13310E+01 - 1.11560E+01	2.39879E-05	2.53282E-05
26	1.11560E+01 - 1.09830E+01	2.75166E-05	2.96369E-05
27	1.09830E+01 - 1.08120E+01	2.40426E-05	2.70474E-05
28	1.08120E+01 - 1.06450E+01	1.92268E-05	2.25686E-05
29	1.06450E+01 - 1.04800E+01	1.73494E-05	2.13154E-05
30	1.04800E+01 - 1.03170E+01	1.62228E-05	2.08756E-05
31	1.03170E+01 - 1.01570E+01	1.59604E-05	2.14550E-05
32	1.01570E+01 - 9.99990E+00	1.77758E-05	2.39059E-05
33	9.99990E+00 - 9.39400E+00	2.37672E-05	3.04079E-05
34	9.39400E+00 - 8.82490E+00	3.06918E-05	3.36266E-05
35	8.82490E+00 - 8.29020E+00	2.85052E-05	2.95181E-05
36	8.29020E+00 - 7.78790E+00	2.64878E-05	2.61940E-05
37	7.78790E+00 - 7.31610E+00	2.00317E-05	1.96656E-05
38	7.31610E+00 - 6.87280E+00	1.80706E-05	1.81623E-05
39	6.87280E+00 - 6.45640E+00	1.93654E-05	2.09891E-05
40	6.45640E+00 - 6.06520E+00	2.33027E-05	2.51437E-05
41	6.06520E+00 - 5.69780E+00	2.76529E-05	2.89220E-05
42	5.69780E+00 - 5.35250E+00	3.00245E-05	3.08396E-05

Table 10.2(c) continued #1

43	5.35250E+00 - 5.02820E+00	3.11810E-05	3.05667E-05
44	5.02820E+00 - 4.72360E+00	3.23933E-05	3.12330E-05
45	4.72360E+00 - 4.43740E+00	3.28029E-05	3.15102E-05
46	4.43740E+00 - 4.16860E+00	3.31430E-05	3.21213E-05
47	4.16860E+00 - 3.91600E+00	3.48431E-05	3.42172E-05
48	3.91600E+00 - 3.67870E+00	3.71672E-05	3.60346E-05
49	3.67870E+00 - 3.45590E+00	4.02457E-05	3.86607E-05
50	3.45590E+00 - 3.24650E+00	4.35215E-05	4.17937E-05
51	3.24650E+00 - 3.04980E+00	4.78140E-05	4.66014E-05
52	3.04980E+00 - 2.86500E+00	5.16604E-05	5.02046E-05
53	2.86500E+00 - 2.69140E+00	5.63260E-05	5.48364E-05
54	2.69140E+00 - 2.52840E+00	5.96984E-05	5.83400E-05
55	2.52840E+00 - 2.37520E+00	6.21557E-05	6.04420E-05
56	2.37520E+00 - 2.23130E+00	6.66797E-05	6.45486E-05
57	2.23130E+00 - 2.09610E+00	6.30491E-05	6.05439E-05
58	2.09610E+00 - 1.96910E+00	6.16979E-05	5.89424E-05
59	1.96910E+00 - 1.84980E+00	6.14771E-05	5.84261E-05
60	1.84980E+00 - 1.73770E+00	6.91839E-05	6.63572E-05
61	1.73770E+00 - 1.53350E+00	6.94811E-05	6.65899E-05
62	1.53350E+00 - 1.35330E+00	7.54766E-05	7.20884E-05
63	1.35330E+00 - 1.19430E+00	7.65491E-05	7.18923E-05
64	1.19430E+00 - 1.05400E+00	7.43377E-05	6.95589E-05
65	1.05400E+00 - 9.30130E-01	7.07911E-05	6.51178E-05
66	9.30130E-01 - 8.20840E-01	8.17201E-05	7.89633E-05
67	8.20840E-01 - 7.24380E-01	9.55436E-05	9.37493E-05
68	7.24380E-01 - 6.39270E-01	9.83101E-05	9.38857E-05
69	6.39270E-01 - 5.64150E-01	8.73577E-05	8.50210E-05
70	5.64150E-01 - 4.97860E-01	7.89529E-05	7.74338E-05
71	4.97860E-01 - 4.39360E-01	6.09023E-05	5.68453E-05
72	4.39360E-01 - 3.87740E-01	5.38656E-05	5.13623E-05
73	3.87740E-01 - 3.42170E-01	6.90746E-05	6.53894E-05
74	3.42170E-01 - 3.01970E-01	6.09422E-05	5.80290E-05
75	3.01970E-01 - 2.66490E-01	3.72340E-05	3.38600E-05
76	2.66490E-01 - 2.35170E-01	2.90705E-05	2.61898E-05
77	2.35170E-01 - 2.07540E-01	4.04227E-05	4.05436E-05
78	2.07540E-01 - 1.83150E-01	4.63940E-05	5.00757E-05
79	1.83150E-01 - 1.61630E-01	6.47764E-05	6.64048E-05
80	1.61630E-01 - 1.42640E-01	5.04130E-05	5.59409E-05
81	1.42640E-01 - 1.25880E-01	7.25933E-05	7.03459E-05
82	1.25880E-01 - 1.11090E-01	5.69187E-05	5.75929E-05
83	1.11090E-01 - 9.80350E-02	4.38622E-05	4.73955E-05
84	9.80350E-02 - 8.65150E-02	4.86529E-05	4.97429E-05
85	8.65150E-02 - 7.63490E-02	5.24969E-05	5.13546E-05
86	7.63490E-02 - 6.73780E-02	4.22766E-05	4.35346E-05
87	6.73780E-02 - 5.94610E-02	3.84988E-05	4.00451E-05

Table 10.2(c) continued #2

88	5.94610E-02 - 5.24740E-02	3.29856E-05	3.50042E-05
89	5.24740E-02 - 4.63080E-02	3.56193E-05	3.64503E-05
90	4.63080E-02 - 4.08670E-02	3.16963E-05	3.28032E-05
91	4.08670E-02 - 3.60650E-02	2.76749E-05	2.94152E-05
92	3.60650E-02 - 3.18270E-02	2.38604E-05	2.62611E-05
93	3.18270E-02 - 2.80870E-02	8.87510E-06	1.60726E-05
94	2.80870E-02 - 2.47870E-02	4.77896E-05	4.05247E-05
95	2.47870E-02 - 2.18740E-02	2.84624E-05	2.81530E-05
96	2.18740E-02 - 1.93040E-02	2.22579E-05	2.35780E-05
97	1.93040E-02 - 1.50340E-02	1.44763E-05	1.74808E-05
98	1.50340E-02 - 1.17090E-02	2.04486E-05	2.06170E-05
99	1.17090E-02 - 9.11860E-03	1.73262E-05	1.78451E-05
100	9.11860E-03 - 7.10160E-03	1.20504E-05	1.35248E-05
101	7.10160E-03 - 5.53070E-03	1.32567E-05	1.38941E-05
102	5.53070E-03 - 4.30730E-03	1.35768E-05	1.35491E-05
103	4.30730E-03 - 3.35460E-03	1.30567E-05	1.28350E-05
104	3.35460E-03 - 2.61250E-03	1.07142E-05	1.08802E-05
105	2.61250E-03 - 2.03460E-03	8.98934E-06	9.31269E-06
106	2.03460E-03 - 1.58460E-03	8.75690E-06	8.66661E-06
107	1.58460E-03 - 1.23410E-03	7.22536E-06	7.26021E-06
108	1.23410E-03 - 9.61100E-04	5.13398E-06	5.47507E-06
109	9.61100E-04 - 5.82930E-04	4.05851E-06	4.15251E-06
110	5.82930E-04 - 3.53570E-04	2.21262E-06	2.38155E-06
111	3.53570E-04 - 2.14450E-04	1.98758E-06	1.83224E-06
112	2.14450E-04 - 1.30070E-04	1.08641E-06	1.03770E-06
113	1.30070E-04 - 7.88910E-05	5.61834E-07	5.27927E-07
114	7.88910E-05 - 4.78500E-05	2.69998E-07	2.49412E-07
115	4.78500E-05 - 2.90230E-05	1.16038E-07	1.03868E-07
116	2.90230E-05 - 1.76030E-05	4.50585E-08	3.87423E-08
117	1.76030E-05 - 1.06770E-05	1.57546E-08	1.29317E-08
118	1.06770E-05 - 6.47580E-06	5.05224E-09	3.91037E-09
119	6.47580E-06 - 3.92780E-06	1.51334E-09	1.10546E-09
120	3.92780E-06 - 2.38230E-06	4.27105E-10	2.94040E-10
121	2.38230E-06 - 1.44490E-06	1.18789E-10	7.68633E-11
122	1.44490E-06 - 8.76400E-07	3.44983E-11	2.09586E-11
123	8.76400E-07 - 5.31560E-07	1.12844E-11	6.47442E-12
124	5.31560E-07 - 3.22410E-07	4.38553E-12	2.33586E-12
125	3.22410E-07 - 1.00100E-11	8.54487E-12	3.79483E-12

Unit of Flux: per/unit lethargy

Table 10.2(d) Neutron flux spectrum in Phase-IIIA(line source)

Group No.	Energy Boundary(eV)	Flux at(FW0cm) H	Flux at(Li2O) I	Flux at(FW40cm) J
1	1.64870E+01 - 1.62310E+01	0.00000E-01	0.00000E-01	0.00000E-01
2	1.62310E+01 - 1.59800E+01	0.00000E-01	0.00000E-01	0.00000E-01
3	1.59800E+01 - 1.57320E+01	0.00000E-01	0.00000E-01	0.00000E-01
4	1.57320E+01 - 1.54880E+01	0.00000E-01	0.00000E-01	0.00000E-01
5	1.54880E+01 - 1.52480E+01	1.03799E-05	1.42869E-06	1.69772E-05
6	1.52480E+01 - 1.50120E+01	6.92793E-05	1.51125E-05	9.23765E-05
7	1.50120E+01 - 1.47790E+01	1.57865E-04	4.50244E-05	1.98629E-04
8	1.47790E+01 - 1.45500E+01	2.77778E-04	9.77876E-05	3.28254E-04
9	1.45500E+01 - 1.43240E+01	2.97572E-04	1.37091E-04	3.29366E-04
10	1.43240E+01 - 1.41020E+01	2.57564E-04	1.39759E-04	2.79464E-04
11	1.41020E+01 - 1.38830E+01	2.89956E-04	1.53146E-04	3.08014E-04
12	1.38830E+01 - 1.36680E+01	2.73438E-04	1.47930E-04	2.94652E-04
13	1.36680E+01 - 1.34560E+01	2.65229E-04	1.26497E-04	2.83862E-04
14	1.34560E+01 - 1.32480E+01	1.67238E-04	8.30025E-05	1.65149E-04
15	1.32480E+01 - 1.30420E+01	7.02008E-05	5.34389E-05	5.89542E-05
16	1.30420E+01 - 1.28400E+01	2.40077E-05	3.90578E-05	2.01542E-05
17	1.28400E+01 - 1.26410E+01	1.86170E-05	3.26255E-05	1.57141E-05
18	1.26410E+01 - 1.24450E+01	1.67750E-05	2.76725E-05	1.35674E-05
19	1.24450E+01 - 1.22520E+01	1.53454E-05	2.37107E-05	1.19531E-05
20	1.22520E+01 - 1.20620E+01	1.41363E-05	2.04112E-05	1.09623E-05
21	1.20620E+01 - 1.18750E+01	1.29243E-05	1.73332E-05	1.02477E-05
22	1.18750E+01 - 1.16910E+01	1.17137E-05	1.49514E-05	9.49356E-06
23	1.16910E+01 - 1.15100E+01	1.09756E-05	1.32349E-05	9.11671E-06
24	1.15100E+01 - 1.13310E+01	1.05232E-05	1.21613E-05	8.94091E-06
25	1.13310E+01 - 1.11560E+01	1.00914E-05	1.13095E-05	8.75339E-06
26	1.11560E+01 - 1.09830E+01	9.83673E-06	1.08300E-05	8.56600E-06
27	1.09830E+01 - 1.08120E+01	9.87064E-06	1.06825E-05	8.57080E-06
28	1.08120E+01 - 1.06450E+01	9.76566E-06	1.03078E-05	8.49278E-06
29	1.06450E+01 - 1.04800E+01	9.42974E-06	9.74207E-06	8.18634E-06
30	1.04800E+01 - 1.03170E+01	9.01702E-06	9.25229E-06	7.78414E-06
31	1.03170E+01 - 1.01570E+01	8.82053E-06	8.94145E-06	7.62231E-06
32	1.01570E+01 - 9.99990E+00	9.15687E-06	8.97070E-06	8.03049E-06
33	9.99990E+00 - 9.39400E+00	9.77074E-06	9.23386E-06	8.67587E-06
34	9.39400E+00 - 8.82490E+00	1.01694E-05	9.30085E-06	9.35630E-06
35	8.82490E+00 - 8.29020E+00	9.68960E-06	9.11653E-06	9.09179E-06
36	8.29020E+00 - 7.78790E+00	8.74439E-06	8.83510E-06	8.23619E-06
37	7.78790E+00 - 7.31610E+00	7.65549E-06	8.35407E-06	7.21802E-06
38	7.31610E+00 - 6.87280E+00	7.58617E-06	8.49830E-06	7.07721E-06
39	6.87280E+00 - 6.45640E+00	8.30318E-06	8.56012E-06	7.69489E-06
40	6.45640E+00 - 6.06520E+00	9.16030E-06	8.67158E-06	8.58896E-06
41	6.06520E+00 - 5.69780E+00	9.79976E-06	8.61862E-06	9.34518E-06
42	5.69780E+00 - 5.35250E+00	1.04909E-05	8.84717E-06	1.01126E-05

Table 10.2(d) continued #1

43	5.35250E+00 - 5.02820E+00	1.02992E-05	8.11896E-06	1.01874E-05
44	5.02820E+00 - 4.72360E+00	1.05856E-05	8.19327E-06	1.05936E-05
45	4.72360E+00 - 4.43740E+00	1.09312E-05	8.34990E-06	1.09927E-05
46	4.43740E+00 - 4.16860E+00	1.13484E-05	8.55204E-06	1.14103E-05
47	4.16860E+00 - 3.91600E+00	1.19173E-05	8.80819E-06	1.19851E-05
48	3.91600E+00 - 3.67870E+00	1.23349E-05	8.61372E-06	1.25209E-05
49	3.67870E+00 - 3.45590E+00	1.32606E-05	9.28617E-06	1.34477E-05
50	3.45590E+00 - 3.24650E+00	1.45045E-05	1.01065E-05	1.46876E-05
51	3.24650E+00 - 3.04980E+00	1.65988E-05	1.21974E-05	1.66060E-05
52	3.04980E+00 - 2.86500E+00	1.80559E-05	1.32510E-05	1.80922E-05
53	2.86500E+00 - 2.69140E+00	1.96710E-05	1.45933E-05	1.96692E-05
54	2.69140E+00 - 2.52840E+00	2.10449E-05	1.58724E-05	2.09883E-05
55	2.52840E+00 - 2.37520E+00	2.22112E-05	1.67702E-05	2.22451E-05
56	2.37520E+00 - 2.23130E+00	2.41414E-05	1.81437E-05	2.42356E-05
57	2.23130E+00 - 2.09610E+00	2.26246E-05	1.63532E-05	2.29250E-05
58	2.09610E+00 - 1.96910E+00	2.19894E-05	1.55225E-05	2.24388E-05
59	1.96910E+00 - 1.84980E+00	2.17824E-05	1.48041E-05	2.23672E-05
60	1.84980E+00 - 1.73770E+00	2.48871E-05	1.74176E-05	2.52721E-05
61	1.73770E+00 - 1.53350E+00	2.48936E-05	1.74036E-05	2.52668E-05
62	1.53350E+00 - 1.35330E+00	2.73098E-05	1.87419E-05	2.77705E-05
63	1.35330E+00 - 1.19430E+00	2.75212E-05	1.76755E-05	2.83520E-05
64	1.19430E+00 - 1.05400E+00	2.68920E-05	1.68637E-05	2.77239E-05
65	1.05400E+00 - 9.30130E-01	2.54552E-05	1.41321E-05	2.66363E-05
66	9.30130E-01 - 8.20840E-01	3.14462E-05	2.13930E-05	3.13738E-05
67	8.20840E-01 - 7.24380E-01	3.78328E-05	2.73462E-05	3.72626E-05
68	7.24380E-01 - 6.39270E-01	3.89858E-05	2.68309E-05	3.93059E-05
69	6.39270E-01 - 5.64150E-01	3.57792E-05	2.66471E-05	3.52914E-05
70	5.64150E-01 - 4.97860E-01	3.28415E-05	2.53874E-05	3.21489E-05
71	4.97860E-01 - 4.39360E-01	2.41460E-05	1.53926E-05	2.47436E-05
72	4.39360E-01 - 3.87740E-01	2.17472E-05	1.48365E-05	2.18032E-05
73	3.87740E-01 - 3.42170E-01	2.82834E-05	1.83149E-05	2.85750E-05
74	3.42170E-01 - 3.01970E-01	2.52265E-05	1.63144E-05	2.53143E-05
75	3.01970E-01 - 2.66490E-01	1.45403E-05	7.70055E-06	1.51802E-05
76	2.66490E-01 - 2.35170E-01	1.11599E-05	5.60856E-06	1.17290E-05
77	2.35170E-01 - 2.07540E-01	1.75369E-05	1.25464E-05	1.67058E-05
78	2.07540E-01 - 1.83150E-01	2.17724E-05	1.87766E-05	1.94035E-05
79	1.83150E-01 - 1.61630E-01	2.96502E-05	2.38629E-05	2.78018E-05
80	1.61630E-01 - 1.42640E-01	2.48345E-05	2.39853E-05	2.15733E-05
81	1.42640E-01 - 1.25880E-01	3.24087E-05	2.49940E-05	3.20986E-05
82	1.25880E-01 - 1.11090E-01	2.71126E-05	2.38061E-05	2.56116E-05
83	1.11090E-01 - 9.80350E-02	2.22645E-05	2.21583E-05	1.97483E-05
84	9.80350E-02 - 8.65150E-02	2.37941E-05	2.16943E-05	2.22635E-05
85	8.65150E-02 - 7.63490E-02	2.53615E-05	2.13488E-05	2.46701E-05
86	7.63490E-02 - 6.73780E-02	2.16871E-05	2.00890E-05	2.00912E-05
87	6.73780E-02 - 5.94610E-02	1.99971E-05	1.91210E-05	1.83113E-05

Table 10.2(d) continued #2

88	5.94610E-02 - 5.24740E-02	1.76050E-05	1.79413E-05	1.57498E-05
89	5.24740E-02 - 4.63080E-02	1.84625E-05	1.74827E-05	1.71579E-05
90	4.63080E-02 - 4.08670E-02	1.68240E-05	1.65786E-05	1.53942E-05
91	4.08670E-02 - 3.60650E-02	1.51387E-05	1.56388E-05	1.34925E-05
92	3.60650E-02 - 3.18270E-02	1.35149E-05	1.46528E-05	1.16401E-05
93	3.18270E-02 - 2.80870E-02	8.12163E-06	1.22705E-05	4.26029E-06
94	2.80870E-02 - 2.47870E-02	2.12005E-05	1.53527E-05	2.37888E-05
95	2.47870E-02 - 2.18740E-02	1.51889E-05	1.37756E-05	1.43744E-05
96	2.18740E-02 - 1.93040E-02	1.26554E-05	1.29504E-05	1.12303E-05
97	1.93040E-02 - 1.50340E-02	9.27463E-06	1.12162E-05	7.23877E-06
98	1.50340E-02 - 1.17090E-02	1.11900E-05	1.07315E-05	1.04338E-05
99	1.17090E-02 - 9.11860E-03	9.80932E-06	9.74770E-06	8.94903E-06
100	9.11860E-03 - 7.10160E-03	7.36655E-06	8.66729E-06	6.18517E-06
101	7.10160E-03 - 5.53070E-03	7.65282E-06	7.88637E-06	6.87172E-06
102	5.53070E-03 - 4.30730E-03	7.57699E-06	7.28511E-06	7.12447E-06
103	4.30730E-03 - 3.35460E-03	7.28517E-06	6.69176E-06	6.93242E-06
104	3.35460E-03 - 2.61250E-03	6.23602E-06	5.96468E-06	5.73431E-06
105	2.61250E-03 - 2.03460E-03	5.34586E-06	5.23487E-06	4.83040E-06
106	2.03460E-03 - 1.58460E-03	5.05454E-06	4.65361E-06	4.75122E-06
107	1.58460E-03 - 1.23410E-03	4.27213E-06	4.01736E-06	3.94898E-06
108	1.23410E-03 - 9.61100E-04	3.21213E-06	3.32384E-06	2.80568E-06
109	9.61100E-04 - 5.82930E-04	2.49036E-06	2.38207E-06	2.26183E-06
110	5.82930E-04 - 3.53570E-04	1.42178E-06	1.51005E-06	1.22940E-06
111	3.53570E-04 - 2.14450E-04	1.12958E-06	9.63039E-07	1.13923E-06
112	2.14450E-04 - 1.30070E-04	6.45444E-07	5.44731E-07	6.28729E-07
113	1.30070E-04 - 7.88910E-05	3.34663E-07	2.74317E-07	3.29073E-07
114	7.88910E-05 - 4.78500E-05	1.57437E-07	1.21735E-07	1.58484E-07
115	4.78500E-05 - 2.90230E-05	6.60819E-08	4.68032E-08	6.86250E-08
116	2.90230E-05 - 1.76030E-05	2.48438E-08	1.53807E-08	2.68152E-08
117	1.76030E-05 - 1.06770E-05	8.41115E-09	4.27238E-09	9.49724E-09
118	1.06770E-05 - 6.47580E-06	2.58448E-09	9.93449E-10	3.06762E-09
119	6.47580E-06 - 3.92780E-06	7.31487E-10	1.92136E-10	9.18962E-10
120	3.92780E-06 - 2.38230E-06	1.95008E-10	3.06254E-11	2.58861E-10
121	2.38230E-06 - 1.44490E-06	4.97412E-11	4.03969E-12	7.00045E-11
122	1.44490E-06 - 8.76400E-07	1.25308E-11	4.46026E-13	1.88243E-11
123	8.76400E-07 - 5.31560E-07	3.32458E-12	4.31876E-14	5.36591E-12
124	5.31560E-07 - 3.22410E-07	9.70483E-13	4.60715E-15	1.74001E-12
125	3.22410E-07 - 1.00100E-11	1.45776E-12	3.83303E-15	3.15547E-12

Unit of Flux: per unit lethargy

Table 10.2(e) Neutron flux spectrum in Phase-IIIB(line source)

Group No.	Energy Boundary(eV)	Flux at#1(Li20cm) K	Flux at#2(40cm) L
1	1.64870E+01 - 1.62310E+01	0.00000E-01	0.00000E-01
2	1.62310E+01 - 1.59800E+01	0.00000E-01	0.00000E-01
3	1.59800E+01 - 1.57320E+01	0.00000E-01	0.00000E-01
4	1.57320E+01 - 1.54880E+01	0.00000E-01	0.00000E-01
5	1.54880E+01 - 1.52480E+01	1.70686E-06	1.86626E-06
6	1.52480E+01 - 1.50120E+01	1.76951E-05	1.81567E-05
7	1.50120E+01 - 1.47790E+01	5.26439E-05	5.37870E-05
8	1.47790E+01 - 1.45500E+01	1.14346E-04	1.15303E-04
9	1.45500E+01 - 1.43240E+01	1.58826E-04	1.59636E-04
10	1.43240E+01 - 1.41020E+01	1.60195E-04	1.58981E-04
11	1.41020E+01 - 1.38830E+01	1.77292E-04	1.76864E-04
12	1.38830E+01 - 1.36680E+01	1.66430E-04	1.67049E-04
13	1.36680E+01 - 1.34560E+01	1.41861E-04	1.39448E-04
14	1.34560E+01 - 1.32480E+01	9.20133E-05	8.68312E-05
15	1.32480E+01 - 1.30420E+01	5.53268E-05	5.08525E-05
16	1.30420E+01 - 1.28400E+01	3.79614E-05	3.57445E-05
17	1.28400E+01 - 1.26410E+01	3.07073E-05	2.92009E-05
18	1.26410E+01 - 1.24450E+01	2.58792E-05	2.47630E-05
19	1.24450E+01 - 1.22520E+01	2.24001E-05	2.14971E-05
20	1.22520E+01 - 1.20620E+01	1.96220E-05	1.88599E-05
21	1.20620E+01 - 1.18750E+01	1.72171E-05	1.65444E-05
22	1.18750E+01 - 1.16910E+01	1.54727E-05	1.48402E-05
23	1.16910E+01 - 1.15100E+01	1.42623E-05	1.36514E-05
24	1.15100E+01 - 1.13310E+01	1.35599E-05	1.29607E-05
25	1.13310E+01 - 1.11560E+01	1.30151E-05	1.24393E-05
26	1.11560E+01 - 1.09830E+01	1.27701E-05	1.22121E-05
27	1.09830E+01 - 1.08120E+01	1.28267E-05	1.22774E-05
28	1.08120E+01 - 1.06450E+01	1.26678E-05	1.21242E-05
29	1.06450E+01 - 1.04800E+01	1.22521E-05	1.17329E-05
30	1.04800E+01 - 1.03170E+01	1.17350E-05	1.12993E-05
31	1.03170E+01 - 1.01570E+01	1.12306E-05	1.08919E-05
32	1.01570E+01 - 9.99990E+00	1.11945E-05	1.09151E-05
33	9.99990E+00 - 9.39400E+00	1.14572E-05	1.12495E-05
34	9.39400E+00 - 8.82490E+00	1.17835E-05	1.15739E-05
35	8.82490E+00 - 8.29020E+00	1.10169E-05	1.07116E-05
36	8.29020E+00 - 7.78790E+00	9.43002E-06	9.15624E-06
37	7.78790E+00 - 7.31610E+00	8.57159E-06	8.33471E-06
38	7.31610E+00 - 6.87280E+00	9.45204E-06	9.15838E-06
39	6.87280E+00 - 6.45640E+00	9.82353E-06	9.52937E-06
40	6.45640E+00 - 6.06520E+00	9.57088E-06	9.30307E-06
41	6.06520E+00 - 5.69780E+00	9.57694E-06	9.30579E-06
42	5.69780E+00 - 5.35250E+00	9.61043E-06	9.34348E-06

Table 10.2(e) continued #1

43	5.35250E+00 - 5.02820E+00	8.91373E-06	8.66945E-06
44	5.02820E+00 - 4.72360E+00	9.07407E-06	8.83398E-06
45	4.72360E+00 - 4.43740E+00	9.31403E-06	9.08104E-06
46	4.43740E+00 - 4.16860E+00	9.50912E-06	9.28111E-06
47	4.16860E+00 - 3.91600E+00	9.97741E-06	9.73954E-06
48	3.91600E+00 - 3.67870E+00	9.76006E-06	9.53210E-06
49	3.67870E+00 - 3.45590E+00	1.03172E-05	1.00775E-05
50	3.45590E+00 - 3.24650E+00	1.11556E-05	1.08911E-05
51	3.24650E+00 - 3.04980E+00	1.34006E-05	1.30655E-05
52	3.04980E+00 - 2.86500E+00	1.42149E-05	1.38505E-05
53	2.86500E+00 - 2.69140E+00	1.58572E-05	1.54352E-05
54	2.69140E+00 - 2.52840E+00	1.74625E-05	1.69868E-05
55	2.52840E+00 - 2.37520E+00	1.84729E-05	1.79610E-05
56	2.37520E+00 - 2.23130E+00	1.98081E-05	1.92541E-05
57	2.23130E+00 - 2.09610E+00	1.83133E-05	1.77993E-05
58	2.09610E+00 - 1.96910E+00	1.74521E-05	1.69627E-05
59	1.96910E+00 - 1.84980E+00	1.69540E-05	1.64710E-05
60	1.84980E+00 - 1.73770E+00	1.95380E-05	1.89729E-05
61	1.73770E+00 - 1.53350E+00	1.95198E-05	1.89394E-05
62	1.53350E+00 - 1.35330E+00	2.09160E-05	2.02774E-05
63	1.35330E+00 - 1.19430E+00	1.99396E-05	1.93160E-05
64	1.19430E+00 - 1.05400E+00	1.91700E-05	1.85625E-05
65	1.05400E+00 - 9.30130E-01	1.66270E-05	1.60900E-05
66	9.30130E-01 - 8.20840E-01	2.35401E-05	2.27604E-05
67	8.20840E-01 - 7.24380E-01	2.89004E-05	2.79065E-05
68	7.24380E-01 - 6.39270E-01	2.78534E-05	2.68596E-05
69	6.39270E-01 - 5.64150E-01	2.72129E-05	2.62227E-05
70	5.64150E-01 - 4.97860E-01	2.58795E-05	2.49118E-05
71	4.97860E-01 - 4.39360E-01	1.67919E-05	1.61479E-05
72	4.39360E-01 - 3.87740E-01	1.63814E-05	1.57440E-05
73	3.87740E-01 - 3.42170E-01	2.00675E-05	1.92581E-05
74	3.42170E-01 - 3.01970E-01	1.80664E-05	1.73198E-05
75	3.01970E-01 - 2.66490E-01	9.15450E-06	8.77288E-06
76	2.66490E-01 - 2.35170E-01	6.91396E-06	6.62340E-06
77	2.35170E-01 - 2.07540E-01	1.47660E-05	1.41276E-05
78	2.07540E-01 - 1.83150E-01	2.06318E-05	1.97272E-05
79	1.83150E-01 - 1.61630E-01	2.52689E-05	2.41501E-05
80	1.61630E-01 - 1.42640E-01	2.44908E-05	2.34073E-05
81	1.42640E-01 - 1.25880E-01	2.54907E-05	2.43009E-05
82	1.25880E-01 - 1.11090E-01	2.35684E-05	2.24562E-05
83	1.11090E-01 - 9.80350E-02	2.17211E-05	2.06783E-05
84	9.80350E-02 - 8.65150E-02	2.14663E-05	2.03899E-05
85	8.65150E-02 - 7.63490E-02	2.10848E-05	2.00183E-05
86	7.63490E-02 - 6.73780E-02	1.98742E-05	1.88125E-05
87	6.73780E-02 - 5.94610E-02	1.90331E-05	1.79857E-05

Table10.2(e) continued #2

88	5.94610E-02 - 5.24740E-02	1.78634E-05	1.68738E-05
89	5.24740E-02 - 4.63080E-02	1.75932E-05	1.66046E-05
90	4.63080E-02 - 4.08670E-02	1.68026E-05	1.58316E-05
91	4.08670E-02 - 3.60650E-02	1.59205E-05	1.49812E-05
92	3.60650E-02 - 3.18270E-02	1.49465E-05	1.40501E-05
93	3.18270E-02 - 2.80870E-02	1.17303E-05	1.10454E-05
94	2.80870E-02 - 2.47870E-02	1.66180E-05	1.56199E-05
95	2.47870E-02 - 2.18740E-02	1.44402E-05	1.35372E-05
96	2.18740E-02 - 1.93040E-02	1.37379E-05	1.28586E-05
97	1.93040E-02 - 1.50340E-02	1.17014E-05	1.09449E-05
98	1.50340E-02 - 1.17090E-02	1.16973E-05	1.09190E-05
99	1.17090E-02 - 9.11860E-03	1.07587E-05	1.00215E-05
100	9.11860E-03 - 7.10160E-03	9.33474E-06	8.68597E-06
101	7.10160E-03 - 5.53070E-03	8.82428E-06	8.19645E-06
102	5.53070E-03 - 4.30730E-03	8.40646E-06	7.79167E-06
103	4.30730E-03 - 3.35460E-03	7.90014E-06	7.31161E-06
104	3.35460E-03 - 2.61250E-03	7.17017E-06	6.62094E-06
105	2.61250E-03 - 2.03460E-03	6.36055E-06	5.86501E-06
106	2.03460E-03 - 1.58460E-03	5.88344E-06	5.41254E-06
107	1.58460E-03 - 1.23410E-03	5.23661E-06	4.80771E-06
108	1.23410E-03 - 9.61100E-04	4.38871E-06	4.02398E-06
109	9.61100E-04 - 5.82930E-04	3.39030E-06	3.10629E-06
110	5.82930E-04 - 3.53570E-04	2.25932E-06	2.06378E-06
111	3.53570E-04 - 2.14450E-04	1.61523E-06	1.47443E-06
112	2.14450E-04 - 1.30070E-04	1.08622E-06	9.85973E-07
113	1.30070E-04 - 7.88910E-05	6.76686E-07	6.11188E-07
114	7.88910E-05 - 4.78500E-05	3.99499E-07	3.58887E-07
115	4.78500E-05 - 2.90230E-05	2.25646E-07	2.01619E-07
116	2.90230E-05 - 1.76030E-05	1.23037E-07	1.09447E-07
117	1.76030E-05 - 1.06770E-05	6.52238E-08	5.78294E-08
118	1.06770E-05 - 6.47580E-06	3.35641E-08	2.96836E-08
119	6.47580E-06 - 3.92780E-06	1.66114E-08	1.46642E-08
120	3.92780E-06 - 2.38230E-06	7.79519E-09	6.87346E-09
121	2.38230E-06 - 1.44490E-06	3.40618E-09	3.00080E-09
122	1.44490E-06 - 8.76400E-07	1.36486E-09	1.20077E-09
123	8.76400E-07 - 5.31560E-07	4.86290E-10	4.27706E-10
124	5.31560E-07 - 3.22410E-07	1.47478E-10	1.29633E-10
125	3.22410E-07 - 1.00100E-11	1.16669E-13	1.03394E-13

Unit of Flux: per unit lethargy

Table 11.1

Comparison of Measured and Computed Decay γ Emissions/s/g of Material per 10^{12} source neutron/s
(Phase IIC)

Material	Measure-ment Identifier	Distance from Source	Irradiation Time	Cooling Time	Counting Time	C/E REAC-2	C/E DKRICF	C/E THIDA
Fe	FEA11	10 cm	30 m	22.4 m	10 m	0.85	0.98	0.91
	FEA21	10 cm	9 h	2h 22.3m	22.4 m	1.00	1.17	1.06
	FEA26	10 cm	9 h	5d 13.7h	5h 16.9m	0.95	1.00	1.02
	FEB11	82 cm	30 m	24.0 m	10 m	1.10	1.22	1.06
	FEB21	82 cm	10 h	5h 1m	44.8m	1.01	1.13	- - -
	FEB22	82 cm	10 h	17h16.2m	39.8m	0.98	1.14	0.97
Ni	NIA11	10 cm	30 m	56.3 m	30.9 m	1.10	1.18	0.88
	NIA21	10 cm	9 h	2h 26.7m	42.9 m	1.13	1.24	1.01
	NIA22	10 cm	9 h	16h 23.7m	44.7 m	1.17	1.24	1.01
	NIA23	10 cm	9 h	4d 13hk	8h 41.9m	1.30	1.04	- - -
	NIB11	82 cm	30 m	58.8 m	26.6 m	1.89	2.02	1.17
	NIB21	82 cm	10 h	3h 52.7m	1h 2.8m	1.12	1.20	0.88
	NIB22	82 cm	10 h	2d 16.6h	4h 13.2m	1.39	1.23	1.09
Mo	MOA11	10 cm	30 m	46.3 m	30.5 m	6.99	2.55	1.22
	MOA21	10 cm	9 h	1h 38.2m	43.8 m	2.09	1.55	1.51
	MOA22	10 cm	9 h	15h 11.8m	1h 5.5m	1.21	1.22	1.21
	MOA23	10 cm	9 h	19h 42.3m	2h 46.7m	1.37	1.42	1.14
	MOA24	10 cm	9 h	4d 3.7h	15h 28.6m	1.18	1.22	- - -
	MOB11	82 cm	30 m	58.8 m	26.6 m	3.30	1.85	1.11
	MOB24	82 cm	10 h	2h 28.85m	38.2 m	5.40	1.26	- - -
	MOB22	82 cm	10 h	9h 15.8m	4h 2.2m	3.57	1.41	- - -
SS316	SSA11	10 cm	30 m	36.3 m	14.6m	0.86	0.95	0.98
	SSA21	10 cm	9 h	1h 38.8m	42.4 m	0.92	1.06	0.92
	SSA22	10 cm	9 h	4h 31m	2h 46.7m	1.04	1.20	0.97
	SSA23	10 cm	9 h	15h 16.8m	1h 0.5m	1.14	1.23	0.98
	SSA24	10 cm	9 h	3d 21.8h	13h 54.6m	1.35	1.14	- - -
	SSB11	82 cm	30 m	39.2 m	15.1 m	1.11	1.16	1.15
	SSB21	82 cm	10 h	3h 13.2m	33.9 m	0.84	0.88	0.94
	SSB22	82 cm	10 h	1d15h53m	21h 48.8m	1.24	1.16	0.79

Table 11.2

Comparison of Measured and Computed Decay γ Emissions/s/g of Material per 10^{12} source neutron/s
(Phase IIC)

Material	Measure-ment Identifier	Distance from Source	Irradiation Time	Cooling Time	Counting Time	C/E REAC-2	C/E DKRICF	C/E THIDA
Nb	NBA21	10 cm	9 h	4h 31m	2h 46.7m	1.27	0.87	0.75
	NBA22	10 cm	9 h	18h 49.5m	44.5 m	1.09	1.05	0.88
	NBB21	82 cm	10 h	13h 39m	1h 13.7m	1.25	1.13	0.82
Co	COA11	10 cm	30 m	37.3 m	15 m	0.84	1.03	0.85
	COA21	10 cm	9 h	3h 17.2m	29.2 m	1.40	1.27	1.11
	COA22	10 cm	9 h	17h 15.7m	40.5 m	2.13	1.24	1.11
	COA23	10 cm	9 h	5d 19h 9m	3h 21.5m	2.10	1.23	- - -
	COB11	82 cm	30 m	39.3 m	15.1 m	1.51	1.58	1.23
	COB21	82 cm	10 h	3h 53m	1h 2.7m	1.40	1.16	- - -

Table 11.3

Comparison of Measured and Computed Decay γ Emissions/s/g of Material per 10^{12} source neutron/s

Material	Measure-ment Identifier	Distance from Source	Irradiation Time	Cooling Time	Counting Time	C/E REAC-2	C/E DKRICF	C/E THIDA
V	VA11	10 cm	30 m	22.3 m	10 m	1.06	1.35	0.90
	VA21	10 cm	9 h	3h 42.2m	36.1 m	1.57	3.38	1.59
	VA22	10 cm	9 h	17h16.2m	39.8m	1.55	3.35	1.59
	VB11	82 cm	30 m	24 m	10 m	1.31	1.81	1.09
	VB21	82 cm	10 h	5h 1.7m	44.9 m	1.44	3.18	1.40
	VB22	82 cm	10 h	2d22h26m	14h 51.3m	1.41	3.11	1.20
Ti	TIA11	10 cm	30 m	22.3 m	10 m	1.69	1.24	0.72
	TIA21	10 cm	9 hh	3h 51.5m	29.2 m	1.28	1.15	0.75
	TIA22	10 cm	9 h	18h 11m	d1h 20.5m	1.16	1.12	----
	TIB11	82 cm	30 m	24.3 m	10 m	1.73	1.62	0.58
	TIB21	82 cm	10 h	7h 27.5m	1h 43.4m	1.24	1.43	0.56
W	WA11	10 cm	30 m	37.3 m	15.5 m	3.07×10^{2}	0.20	0.99*(2.19)
	WA21	10 cm	9 h	2h 26.5m	44.2 m	2.55	2.86×10^{-2}	0.82*(2.38)
	WA22	10 cm	9 h	16h 23.4m	45.7m	2.28	1.27×10^{-2}	0.76*(2.38)
	WA23	10 cm	9 h	2d19h3.5m	18h 22.7m	2.05	4.05×10^{-2}	0.70*(2.26)
	WB11	82 cm	30 m	39.2 m	15.1 m	1.38×10^{1}	7.00×10^{-3}	0.65*(2.11)
	WB21	82 cm	10 h	3h 13.5m	33.5 m	2.26	4.88×10^{-4}	0.96*(3.17)
	WB22	82 cm	10 h	4d 5.3m	13h 32.2m	2.59	2.35×10^{-3}	0.91*(2.99)
Zr	ZRA11	10 cm	30 m	56.5 m	18.9 m	4.13	0.82	1.21
	ZRA21	10 cm	9 h	2h 26.5m	43.5 m	5.58	1.08	- - -
	ZA22	10 cm	9 h	17h 15.7m	40.0 m	5.81	1.16	- - -
	ZRB11	82 cm	30 m	58.3 m	27.1 m	4.30	0.88	1.13
	ZRB21	82 cm	10 h	3h 13.5m	33.7 m	4.10	0.83	1.31
MnCu	MCA11	10 cm	30 m	12.3 m	10 m	3.35	3.42	1.04
	MCA21	10 cm	9 h	2h 26.7m	44.0 m	1.75	1.19	0.83
	MCA22	10 cm	9 h	16h 23.7m	45.7 m	1.21	0.29	0.26
	MCA23	10 cm	9 h	6d20h59m	4h 50.3m	1.09	1.11	- - -
	MCB11	82 cm	30 m	24.3 m	10 m	2.52	2.42	1.49
	MCB21	82 cm	10 h	3h 52.7m	1h 2.2m	2.19	2.03	1.40
	MCB22	82 cm	10 h	3d13h28m	6h 44.9m	1.24	1.00	0.80
Cr	CRA21	10 cm	9 h	1h 38.8m	43.0 m	2.95	1.35	0.55
	CRA22	10 cm	9 h	15h 16.8m	1h 0.5m	1.54	1.05	0.88
	CRB21	82 cm	10 h	2h 27.5m	1h 19.6m	2.95	1.67	0.64

* Bracketed numbers were obtained with original γ-yields which were inaccurate for some γ's. Starred numbers are with corrected γ-yields.

Table 11.4

Comparison of Measured and Computed Decay γ Emissions/s/g or Material per 10^{12} source nertron/s (Phase IIC)

Material	Material Identifier	Distance from Source	Irradiation Time	Cooling Time	Counting Time	C/E REAC-2	C/E DKRICF	C/E THIDA
Al	ALA11	10 cm	30 m	1h 15.8m	11.4 m	0.98	1.02	1.17
	ALA21	10 cm	9 h	4h 31m	2h 46.7m	0.88	0.92	1.06
	ALB11	82 cm	30 m	58.3 m	27.1 m	1.34	1.39	1.05
	ALB21	82 cm	10 h	5h 52.3m	1h 28.5m	1.03	1.07	1.12
Si	SIA11	10 cm	30 m	37.3 m	15 m	2.80	1.08	1.14
Mg	MGA21	10 cm	9 h	3h 51.7m	26.3 m	1.16	1.07	0.99
	MGA22	10 cm	9 h	18h 11.7m	31.5 m	1.08	1.00	---
	MGB21	82 cm	10 h	2h 28.5m	44.2 m	1.37	1.28	1.25
In	INA21	10 cm	9 h	1h 38.2m	42.9 m	1.06	1.08	---
	INA22	10 cm	9 h	16h 23.7m	45.7 m	2.62	0.18	---
	INB21	82 cm	10 h	2h 28.5m	38 m	1.11	1.52	---
Ta	TAA21	10 cm	9 h	3h 17.2m	28.2 m	3.56	0.35	---
	TAA22	10 cm	9 h	18h 11.7m	35.4 m	2.03	0.83	---
	TAB21	82 cm	10 h	3h 53m	1h 2.7m	1.74	1.53	0.19
Au-thick	AUA21	10 cm	9 h	3h 51.7m	25.9 m	1.71	0	---
	AUA23	10 cm	9 h	18h 49.5m	43.7 m	2.16	0	---
	AUB21	82 cm	10 h	5h 2m	44.2 m	6.43	0	---
Au-thin	AUA22	10 cm	9 h	4h 31m	2h 46.7m	1.33	0	---
	AUA24	10 cm	9 h	19h 42m	2h 46.7m	1.57	0	---
$YBa_2Cu_3O_7$	YCA11	10 cm	30 m	1h 32m	2h 32.9m	0.97	0.31	---
	YCA12	10 cm	30 m	4h 12m	4h31.2m	0.73	4.38×10^{-2}	---
	YCA13	10 cm	30 m	7d2h26.1m	2h 50.4m	0.72	1.30×10^{-3}	---
$ErBa_2Cu_3O_7$	BCA11	10 cm	30 m	1h 33m	2h 24.3m	6.20	1.06	---
	BCA12	10 cm	30 m	4h 12.5m	4h 33.5m	7.69	1.30	---
	BCA13	10 cm	30 m	11d4h47m	3h 34.7m	0.58	0.12	---

Table 11.5
Variation of C/E for Integrated Decay γ Emission rates for Different Source Conditons (Iron Samples)

Material	Material Identifier	Source Conditon	Mean Distance from target[a](cm)	Irradiation Time	Cooling Time	C/E REAC2	C/E DKRICF
Fe	FEC11	Bare Line	0	9h47m	2h15.5m	1.10	1.19
Fe	FED11	Bare Line	40	9h47m	1h50m	1.17	1.03
Fe	FEE11	Bare Line	100	9h47m	1h50m	1.17	1.03
Fe	FEF11	Point Source	0	30m	33ml5s	0.97	1.04
Fe	FEG11	Point Source	40	30m	44m	1.26	1.40
Fe	FEH11	Line+Blkt.	0 (1.5cmFW)	9h51m	4h19.6m	1.14	1.21
Fe	FEI11	Line+Blkt.	0 (5cmLi_2O)	9h51m	5h9.9m	1.12	1.19
Fe	FEJ11	Line+Blkt.	40 (1.0cmFW)	9h51m	4h45.1m	1.02	1.09
Fe	FEA21	Point Source (PhaseIIC)	10cm from target	9h	3h22.3m	1.00	1.17

a It stands for axial distance. Bracketed numbers indicate radial distance from axis

Table 11.6
Variation of C/E for Integrated Samples inside Annular Blanket Assembly Driven by Line Source (Irradiation Time = 9h51m)

Material	Material Identifier	Location	Cooling Time	C/E REAC2	C/E DKRICF
Fe	FEH11	#H	4h19.6m	1.14	1.21
Ni	NIH11	#H	1h37.4m	1.20	1.26
AISI316	SSH11	#H	1h37.4m	1.20	1.26
Mo	MOH11	#H	2h52.7m	4.29	1.58
W	WH11	#H	1h37.5m	1.34	4.56e-03
Pb	PBJ11	#J	9h19.7m	2.51	1.09
Zn	ZNJ11	#J	5h45.3m	1.83	2.69e-02
Zr	ZRI11	#J	3h54.3m	4.08	1.04
Ag	AGJ11	#J	6h30.8m	0.0102	0.974
Sn	SNJ11	#J	5h45.9m	2.63	0.438
Ta	TAH11	#H	7h35.4m	2.25	1.97
Al	ALJ11	#J	10h55.2m	0.97	0.97
Nb	NBH11	#H	5d19.6h	0.999	0.997
Ti	TIH11	#H	7h34.4m	1.68	1.86

Table 12 Major Radioactive Products and Source Reactions in Tungsten

Half-life	Product	γ-ray Energies (keV)	Major Reactions
10.5m	^{186}Ta	122,198,215,308,418,738	^{186}W(n,p)^{186}Ta
49.5m	^{185}Ta	174	^{186}W(n,n'p/d)^{185}Ta
64m	^{183}Hf	459,784	^{186}W(n,α)^{183}Hf
8.7h	^{184}Ta	111,161,215,227,243,253,318, 384,414,461,537,792,895,903, 921,1110,1174	^{184}W(n,p)^{184}Ta
23.9h	^{187}W	134,480,552,618,625,686,745, 773,865,879	^{186}W(n,γ)^{187}W
5.1d	^{183}Ta	99,108,162,246,292,312	^{183}W(n,p)^{183}Ta ^{184}W(n,n'p/d)^{183}Ta
42.4d	^{181}Hf	482	^{184}W(n,α)^{181}Hf
115d	^{182}Ta	1121,1189,1221,1231	^{182}W(n,p)^{182}Ta ^{183}W(n,n'p/d)^{182}Ta

* One of the tungsten samples detected appreciable counting rate for ^{24}Na γ-rays (1369 & 2754 KeV)

Strategy of Benchmark Study on Induced Radioactivity Calculation

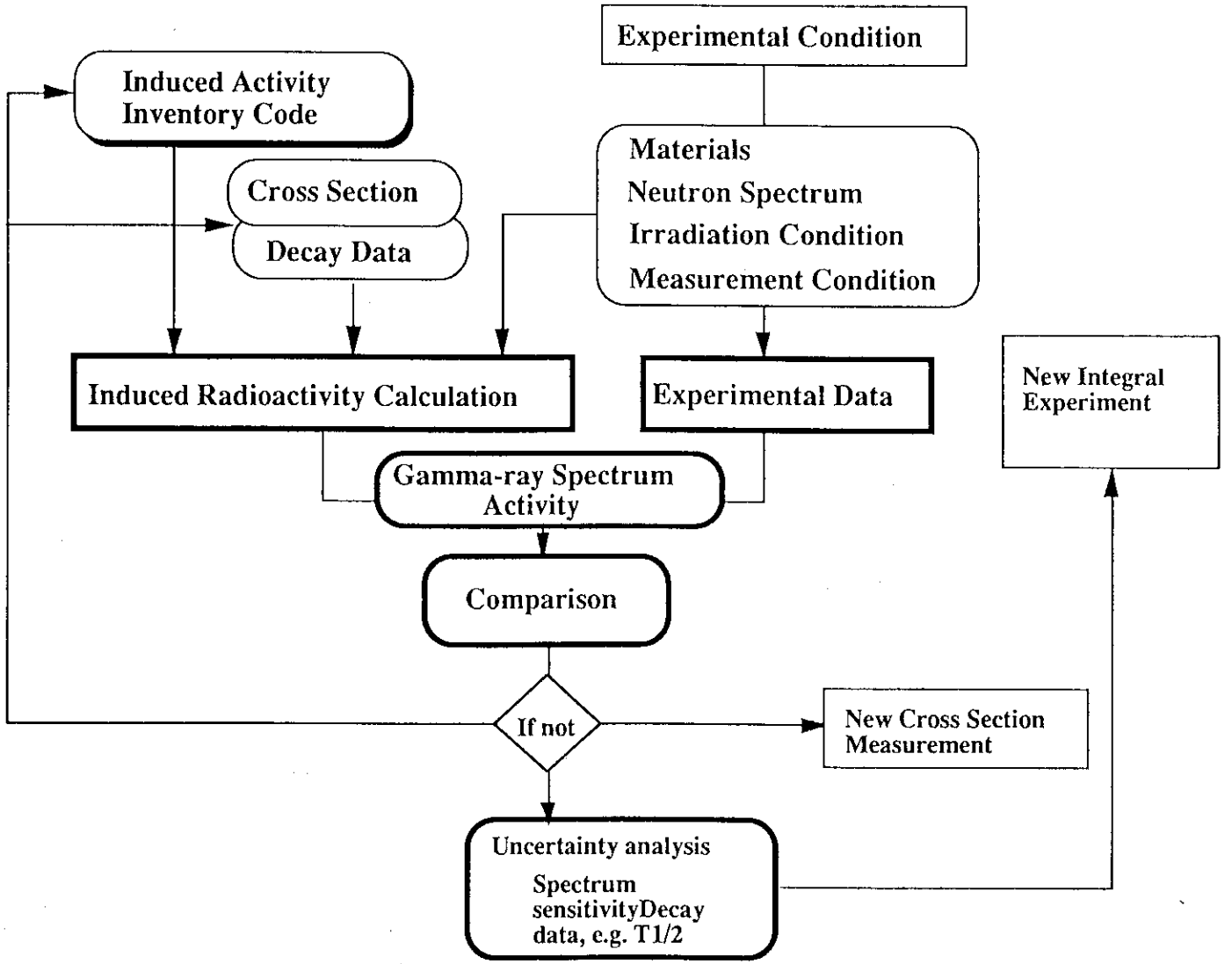

Fig. 1 Overview of the induced radioactivity data testing.

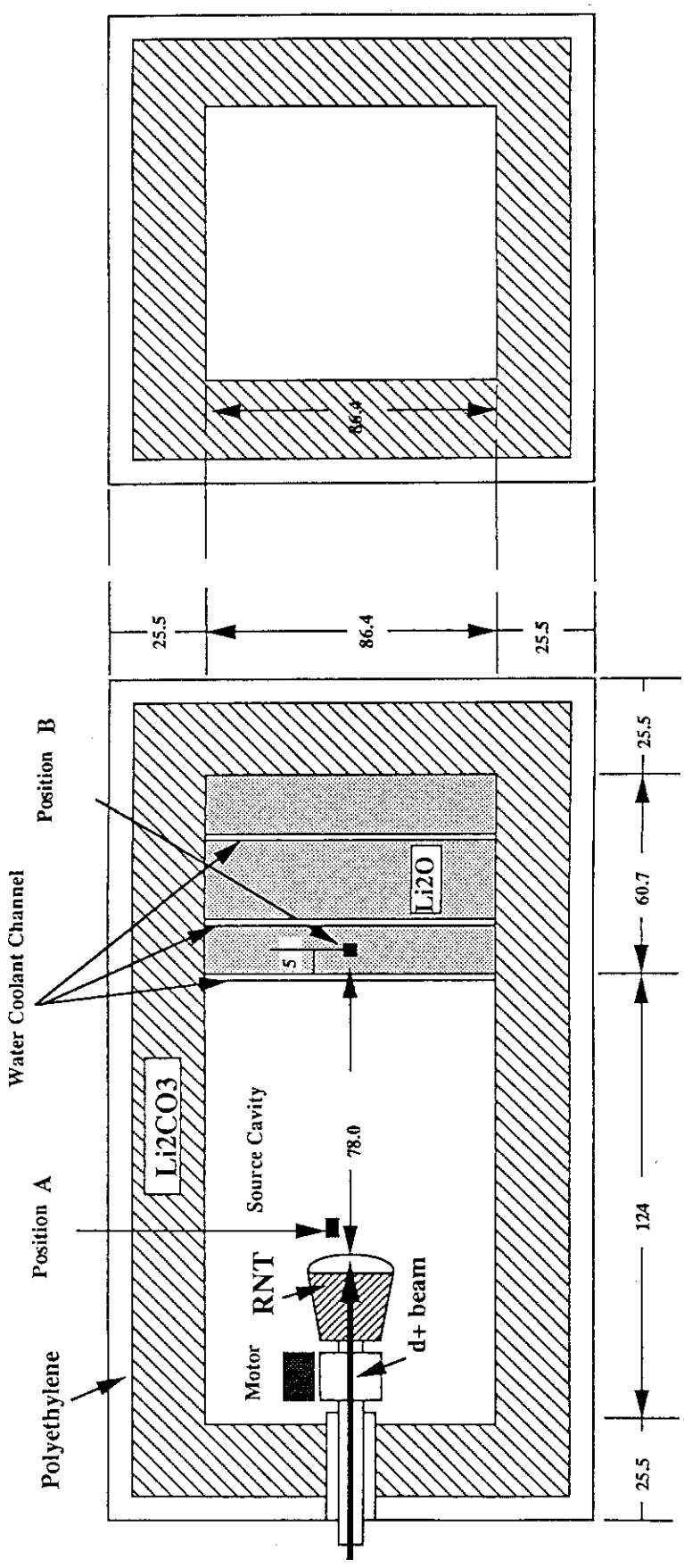

Phase-IIC Experimental System

Fig. 2 Schematic view of experimental arrangement of samples in coolant channel assembly of Phase IIC.

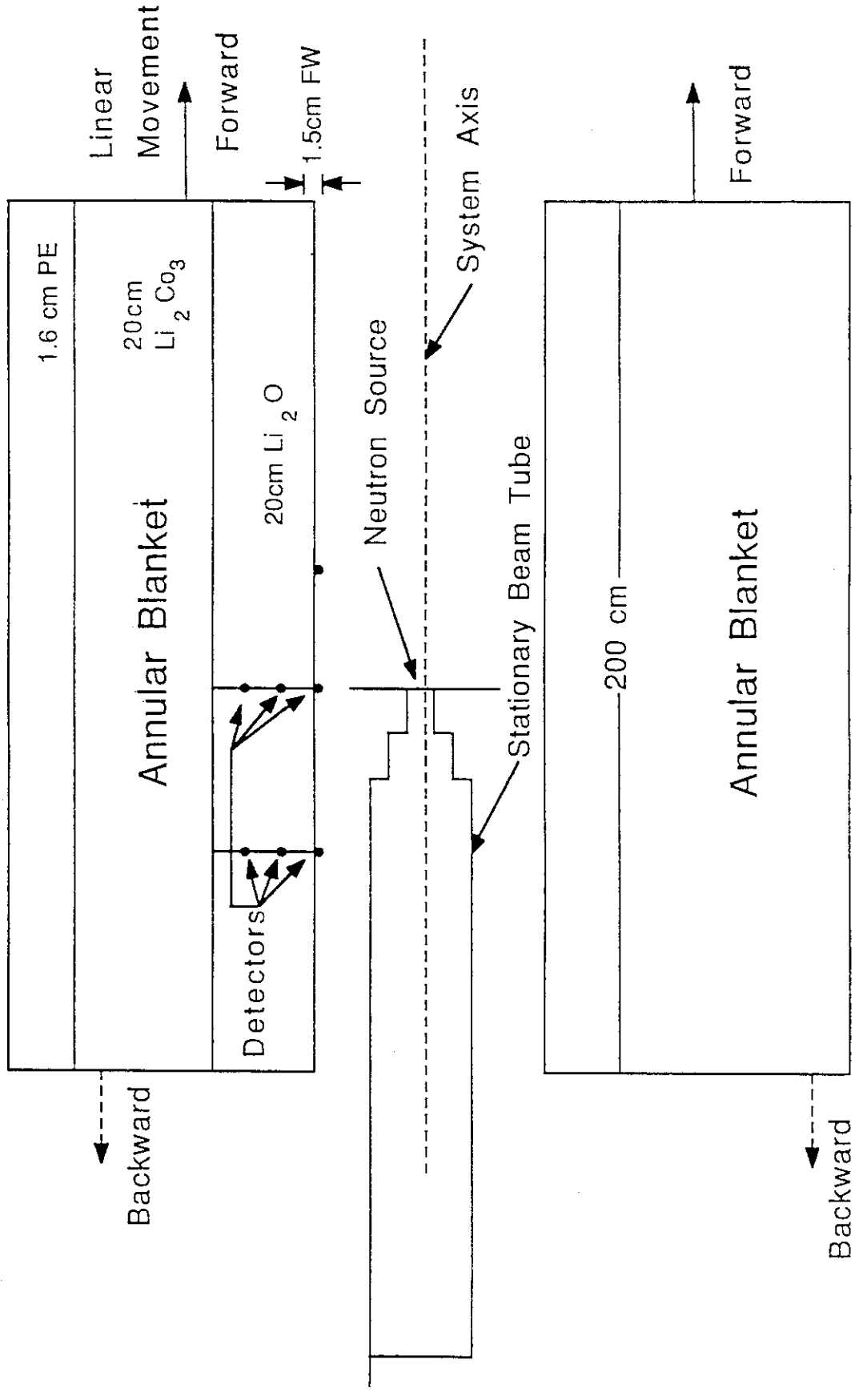

Fig. 3 Line source simulation in Phase III and sample locations for induced activity measurements.

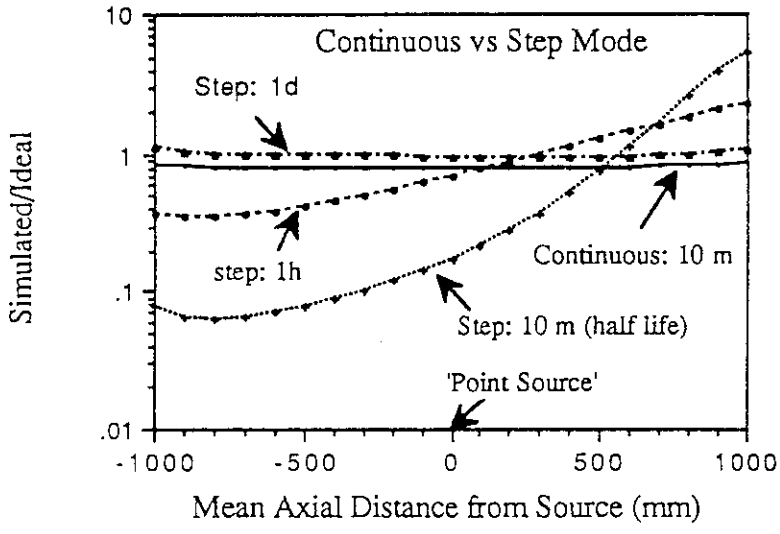

Fig. 4 Effect of product half-life on ratio of activation rate for simulated line source to that for an "ideal" line source: continuous versus step mode.

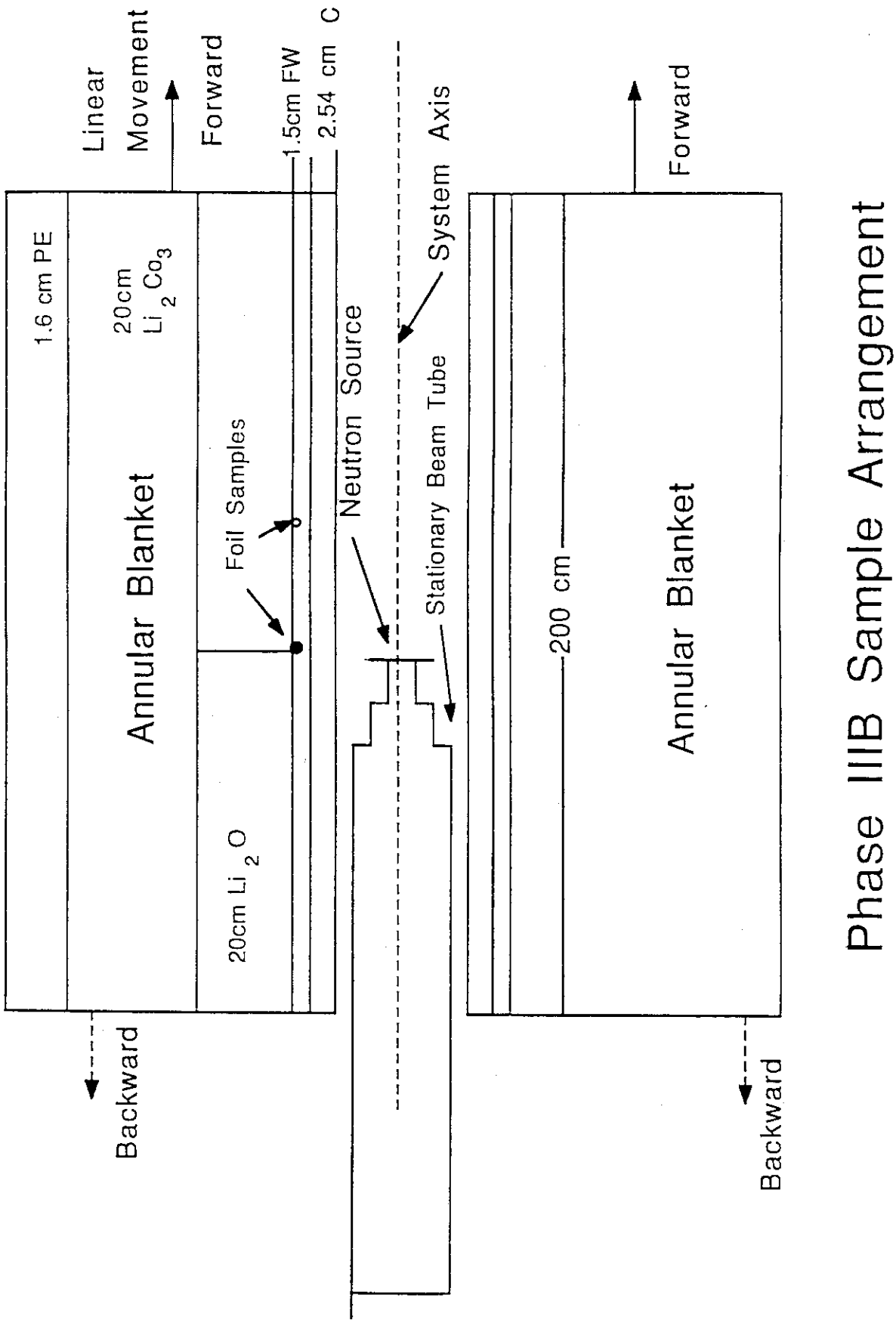

Fig. 5 Sample locations in Phase IIIB assembly.

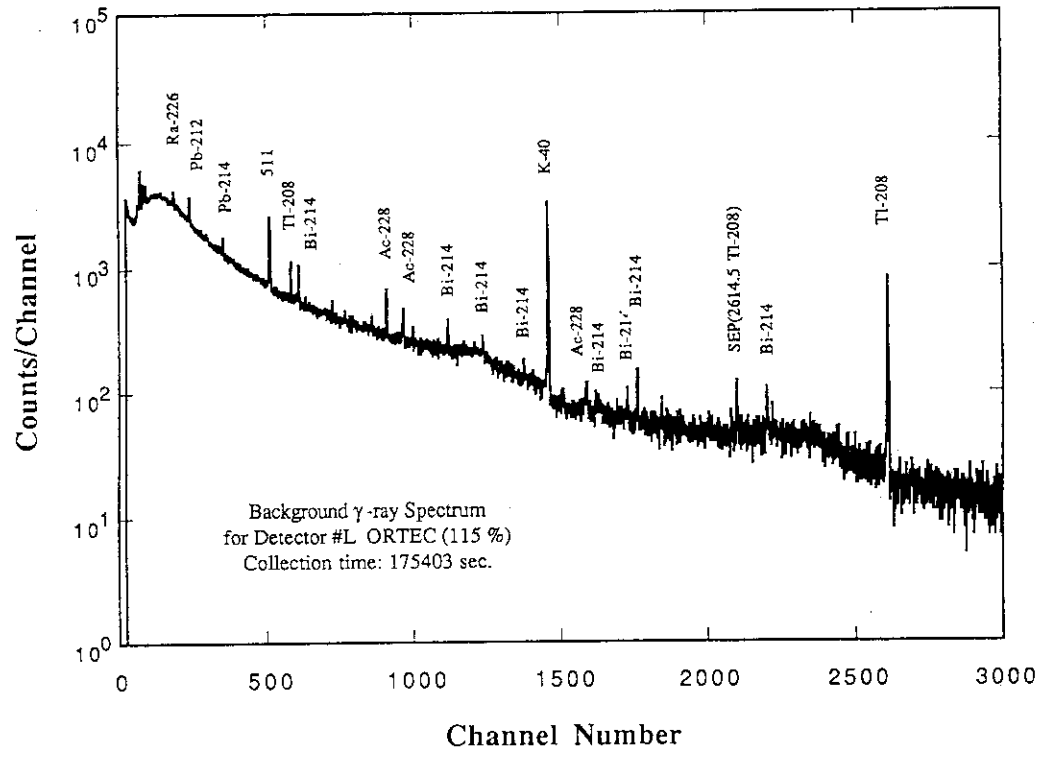

Fig. 6 Background γ-ray spectrum for detector #L.

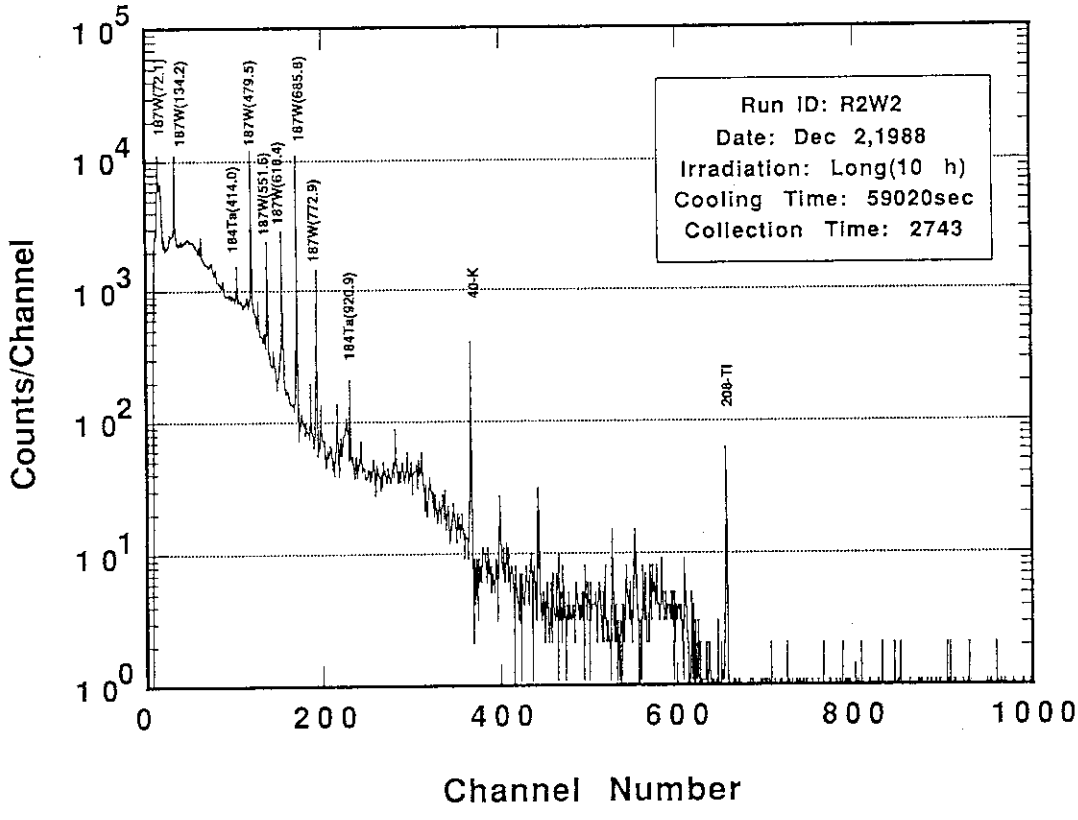

Fig. 7 Measured γ-ray spectrum of tungsten.

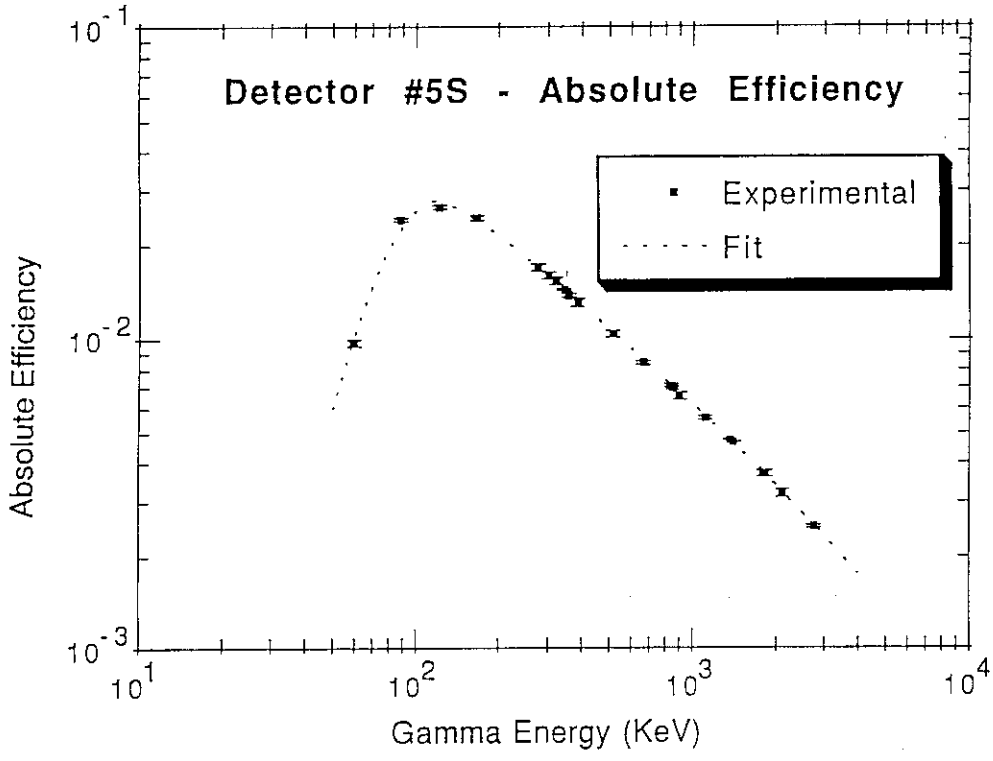

Fig. 8.1 Absolute γ-ray detection efficiency as a function of γ-ray energy of Detector #5S

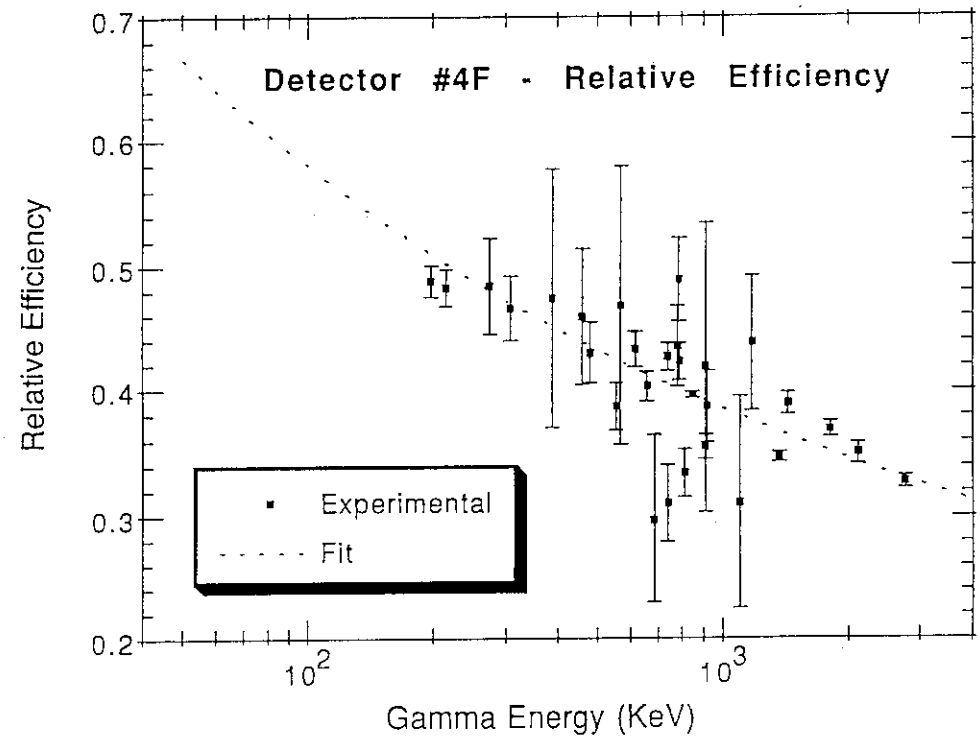

Fig. 8.2 Relative efficiency of Detector #4.

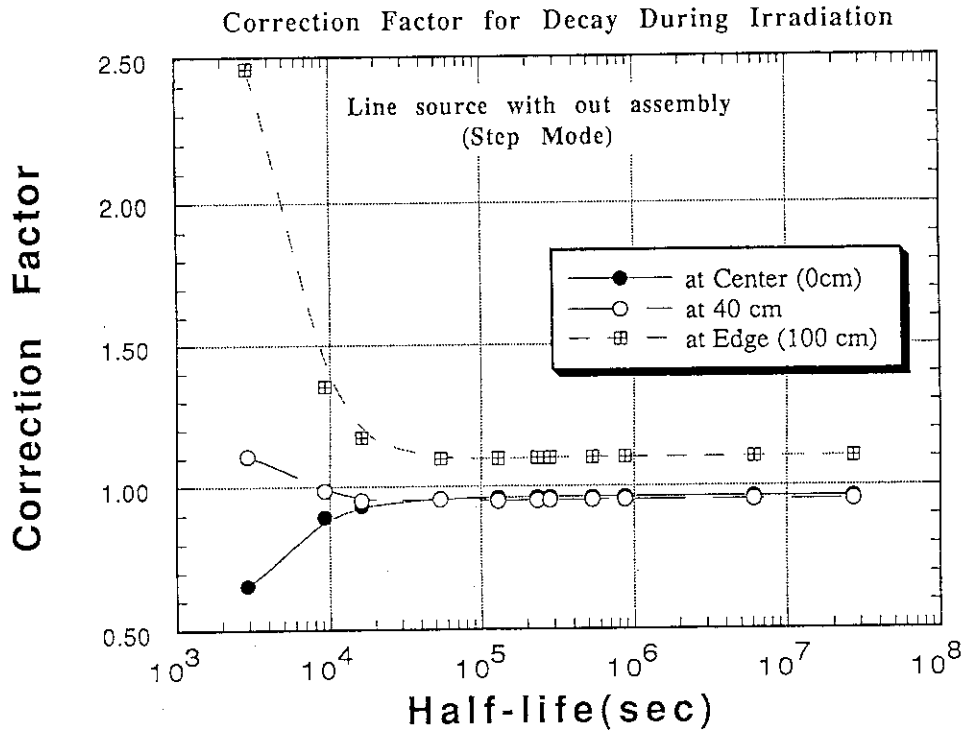

Fig. 9.1 Correction factor for half-lives with respect to sample position in the line source configuration without assembly.

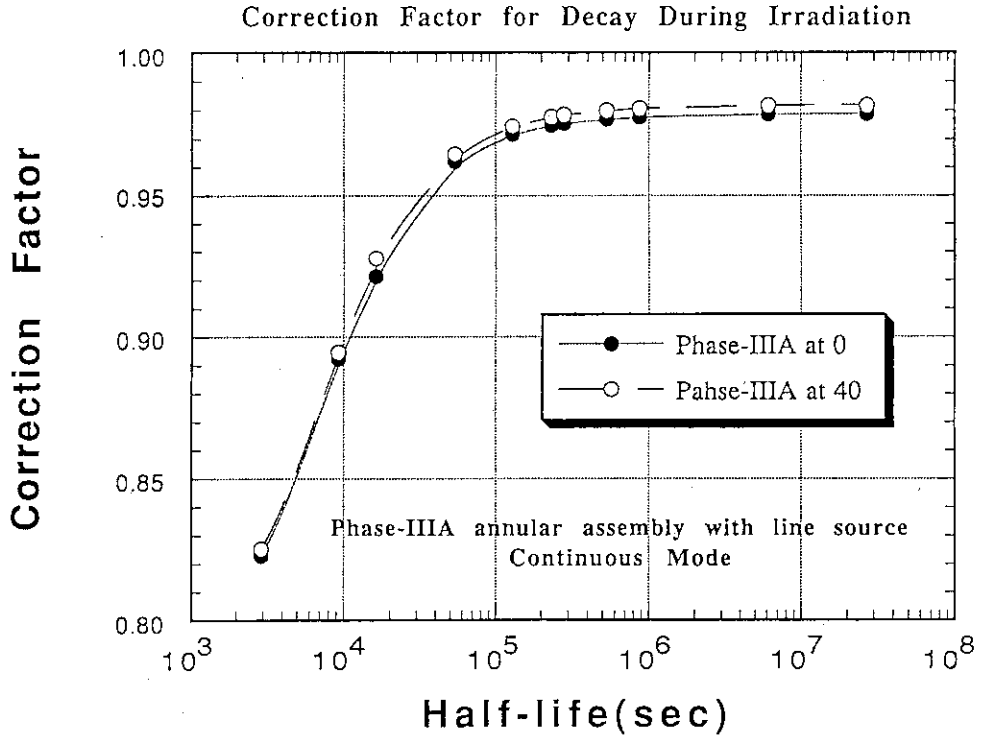

Fig. 9.2 Correction factor for half-lives with respect to sample position in the line source configuration with the Phase-IIIA assembly.

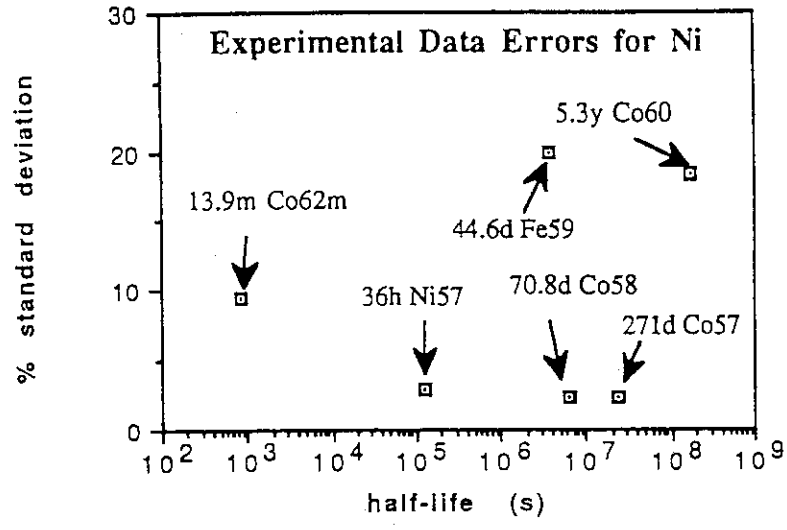

Fig. 10 Experimental error(%) vs product half-life for a nickel sample (Phase IIC; tr=30m/9h, tcool=56m/2h27m, tcount=31m/43m).

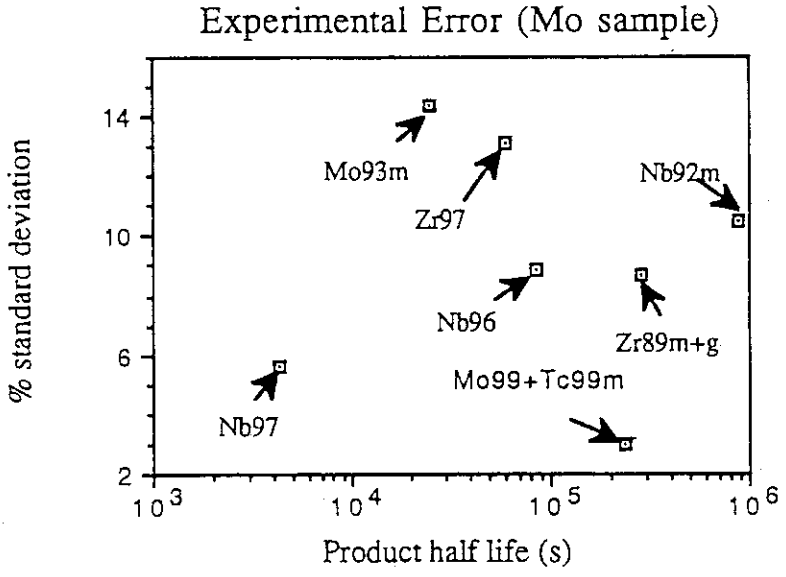

Fig. 11 Experimental error(%) vs product for half-life a molybdenum sample (Phase IIIA; tr=30m, tcool=3h18m, tcount=10.8m).

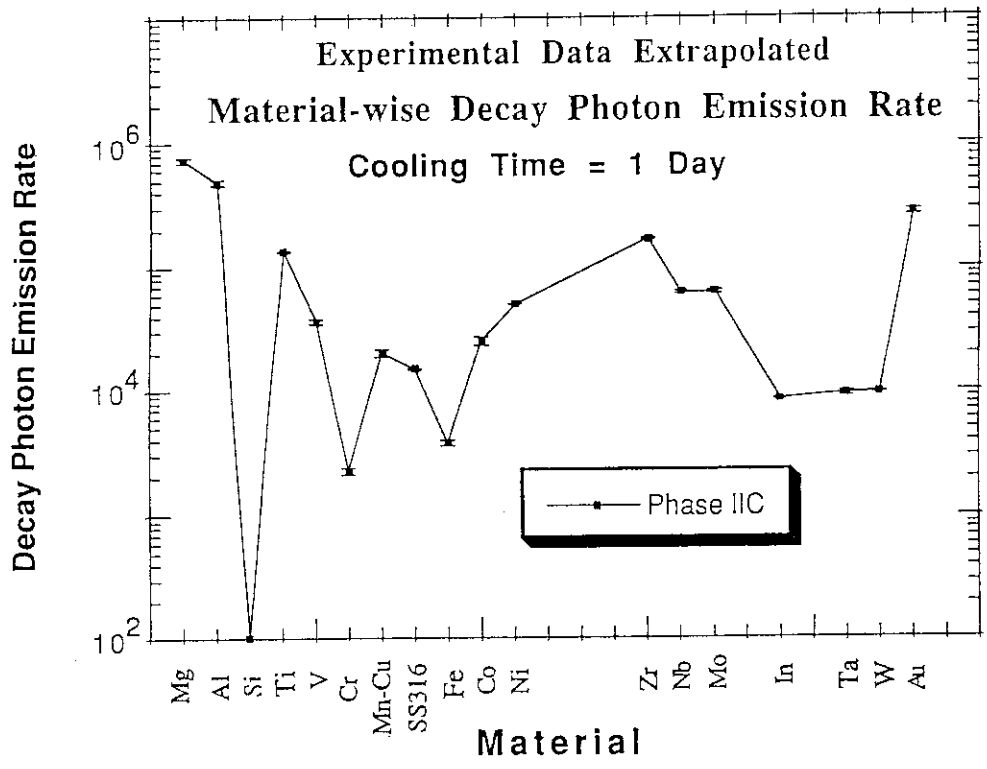

Fig. 12.1 Decay γ emission rate/s/g versus Z of sample for ~1 day cooling time in Phase IIC experiment.

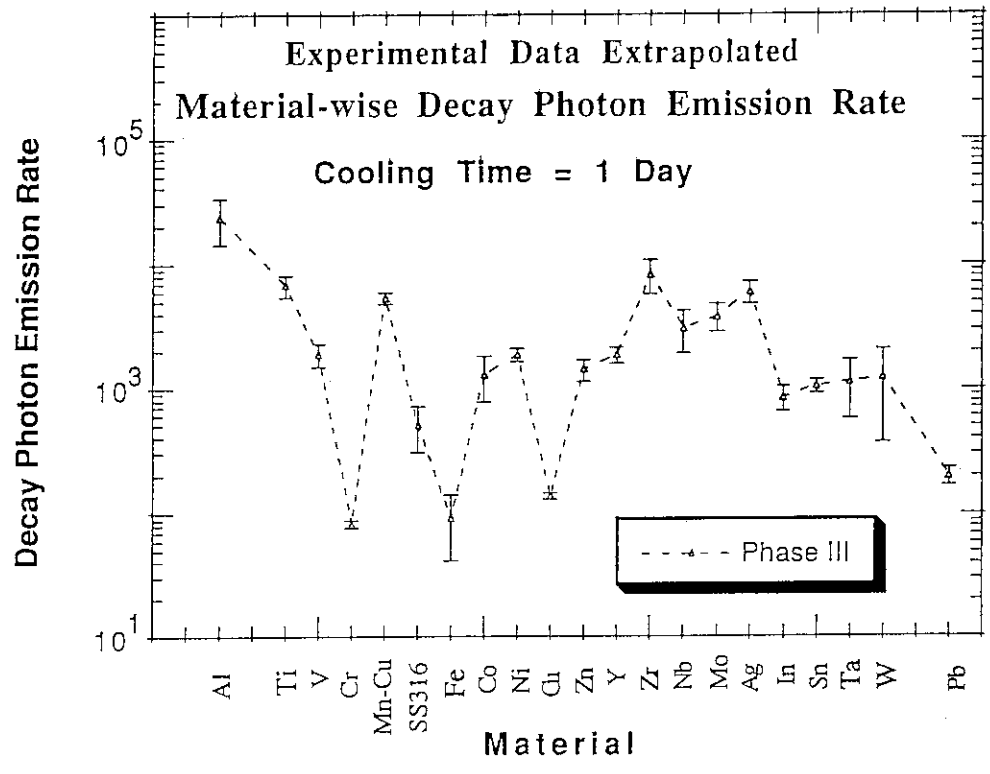

Fig. 12.2 Decay γ emission rate/s/g versus Z of sample for ~1 day cooling time in Phase III experiment.

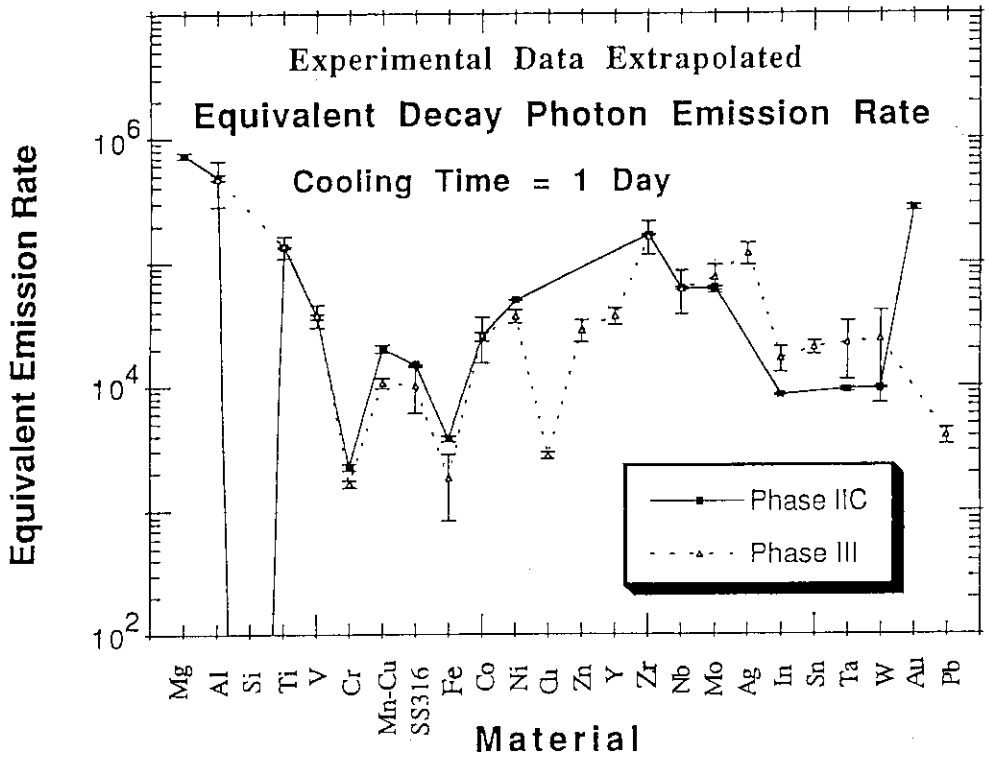

Fig. 12.3 Equivalent decay γ emission rate/s/g versus Z of sample for ~1 day cooling time.

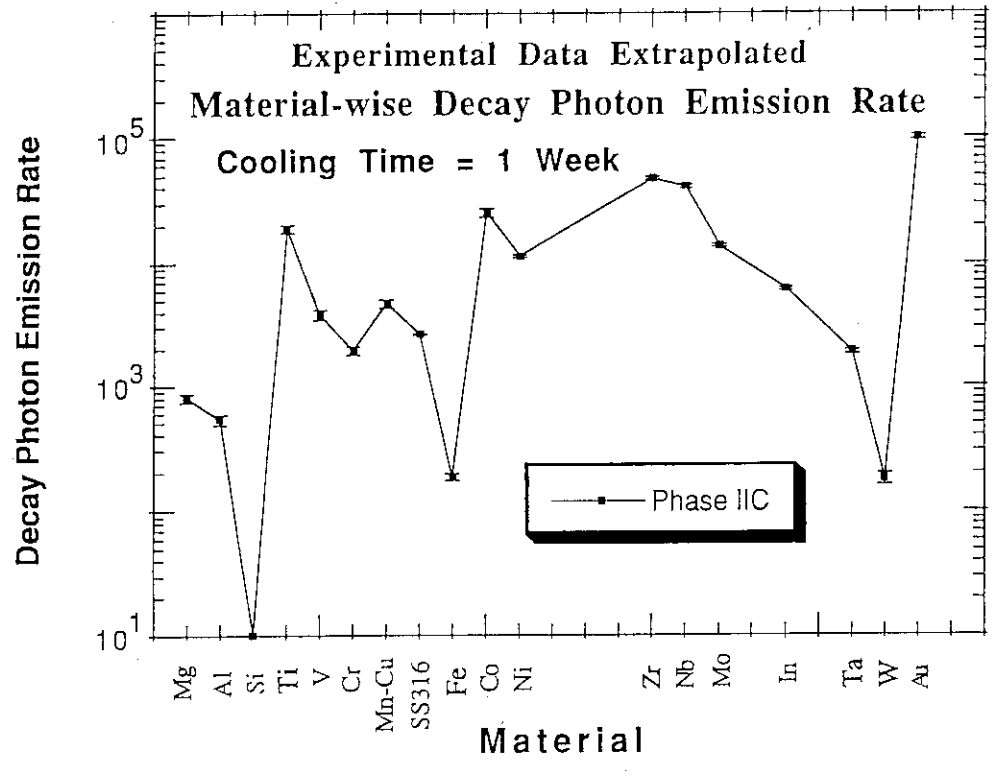

Fig. 13.1 Decay γ emission rate/s/g versus Z of sample for ~1 week cooling time in Phase IIC experiment.

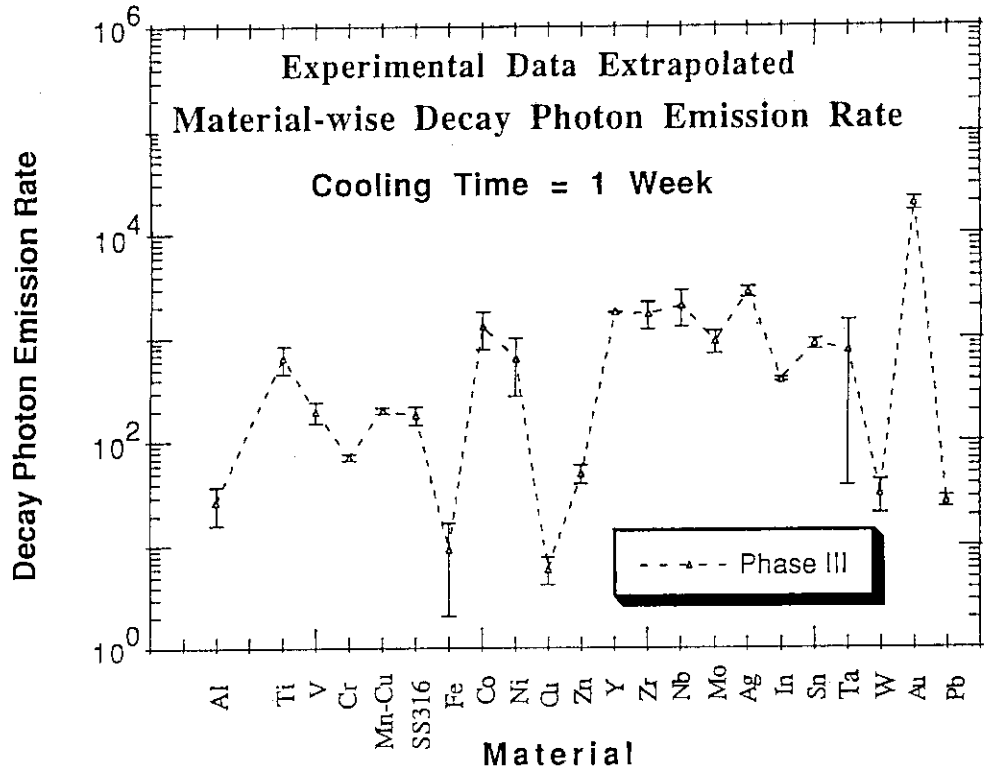

Fig. 13.2 Decay γ emission rate/s/g versus Z of sample for ~1 week cooling time in Phase III experiment.

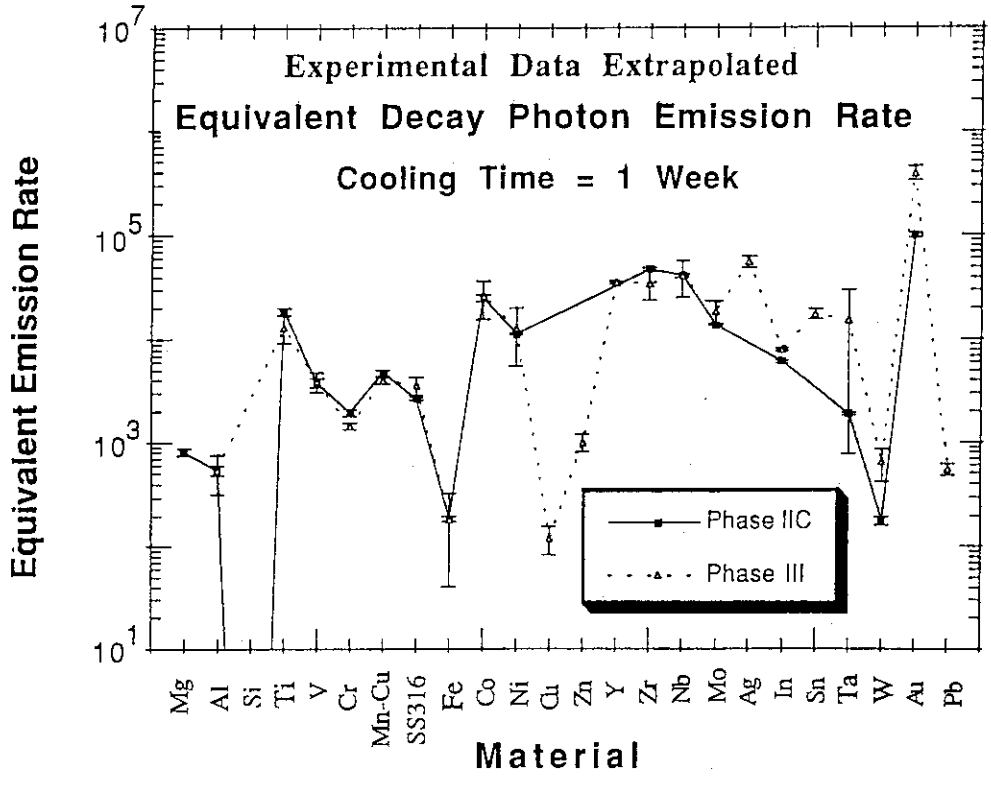

Fig. 13.3 'Equivalent' decay γ emission rate/s/g versus Z of sample for ~1 week cooling time.

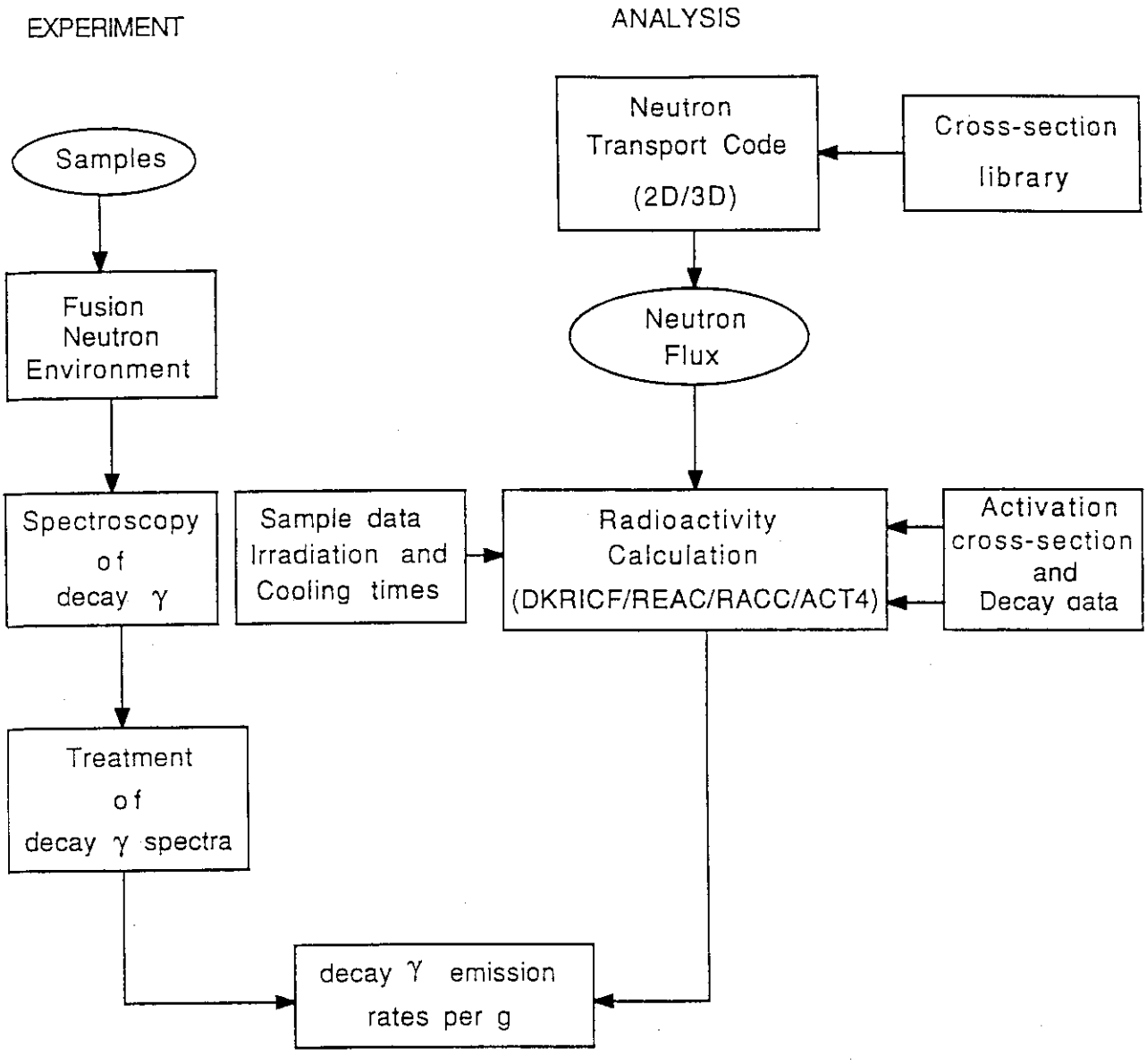

Fig. 14 Flow chart of experiment and calculation.

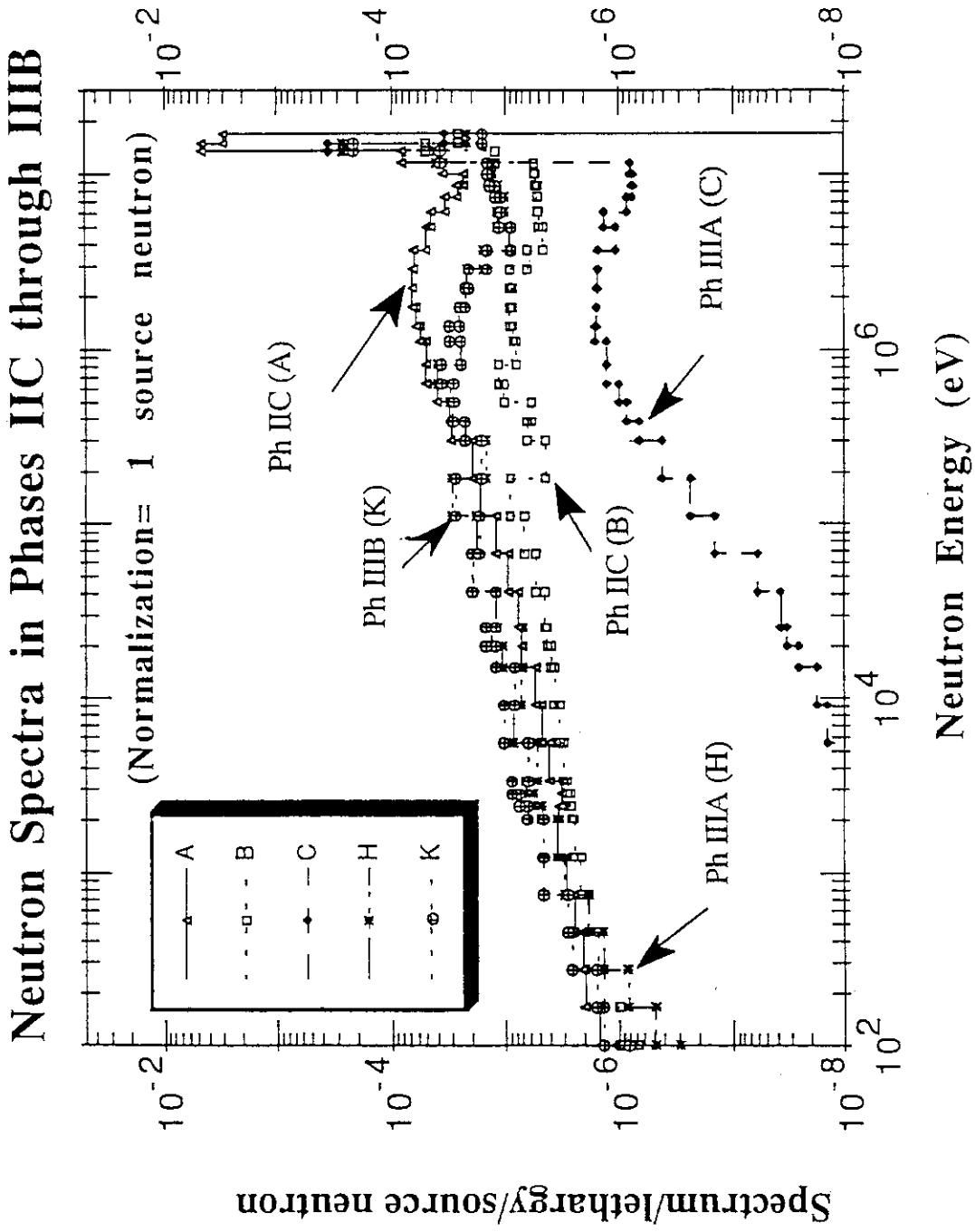

Fig. 15 Computed neutron energy spectra per unit lethargy for experiments in Phase IIC through IIIB.

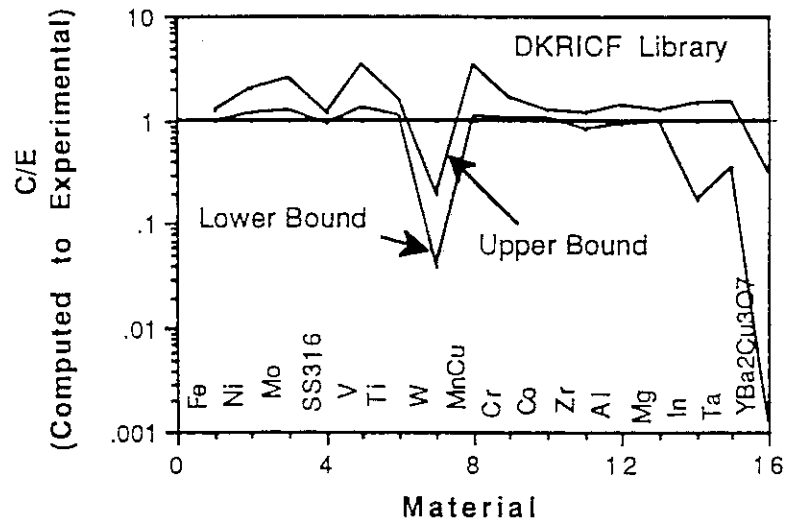

Fig. 16.1 Measured and DKRICF computed decay γ integrated decay rate: comparison.

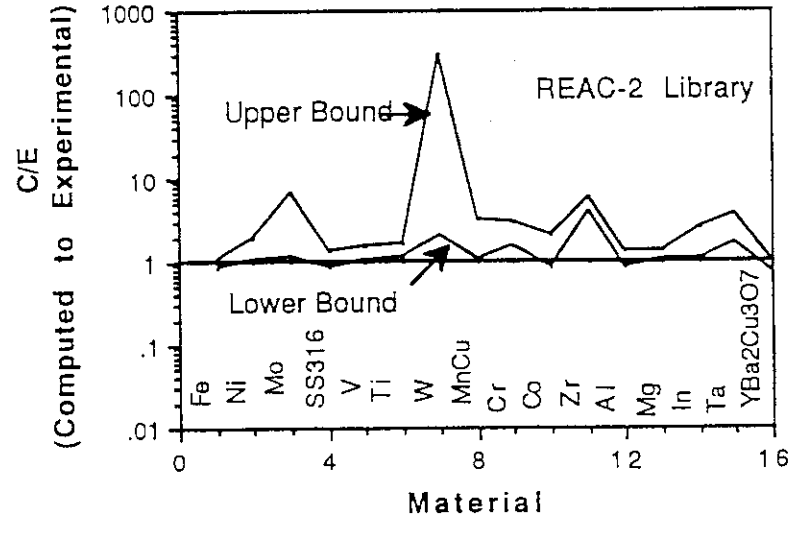

Fig. 16.2 Measured and REAC-2 computed decay γ integrated decay rate: comparison.

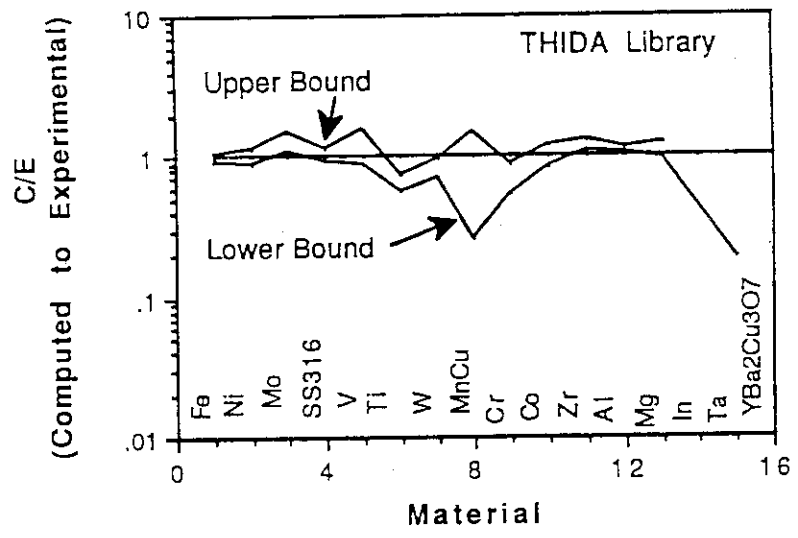

Fig. 16.3 Measured and THIDA-2 computed decay γ integrated decay rate: comparison.

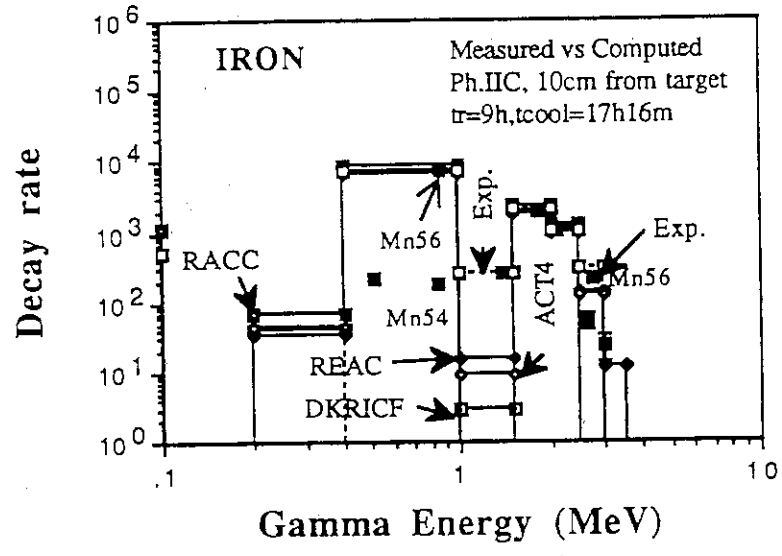

Fig. 17.1 Decay γ-emission rate spectra per g for iron: measurement vs. computation (tr=9h, tcool=17h16m).

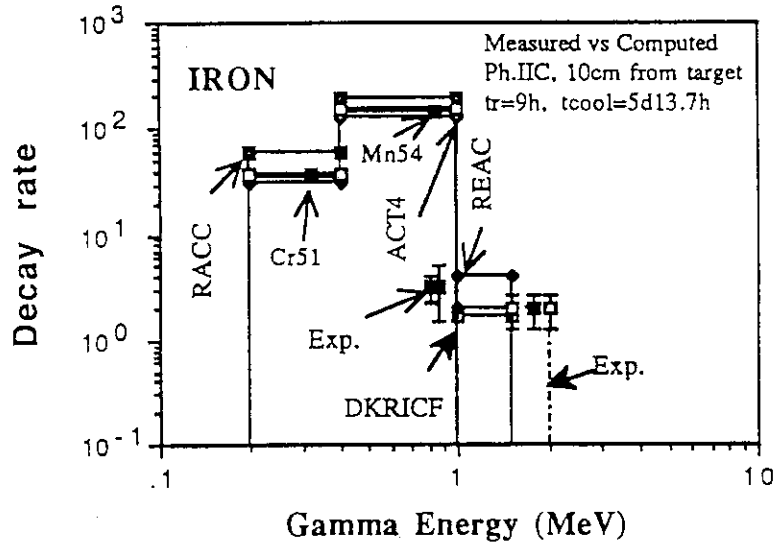

Fig. 17.2 Decay γ-emission rate spectra per g for iron: measurement vs. computation (tr=9h, tcool=5d13.7h).

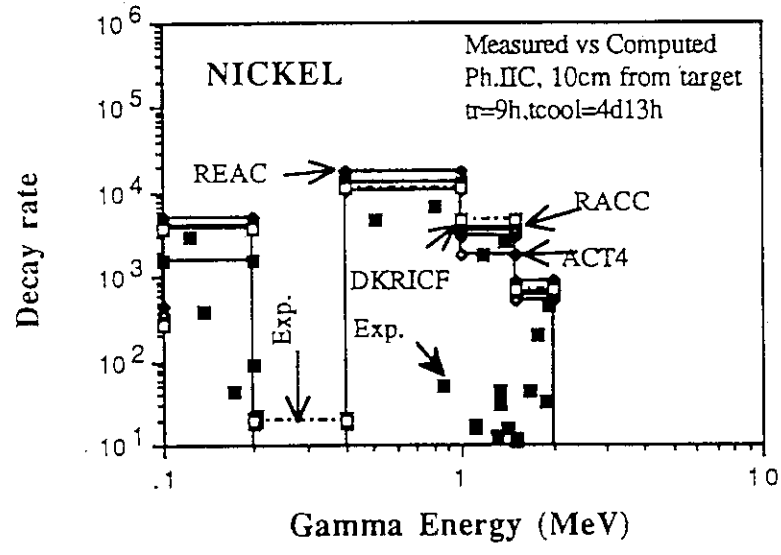

Fig. 17.3 Decay γ-emission rate spectra per g for nickel: measurement vs. computation (tr=9h, tcool=4d13h).

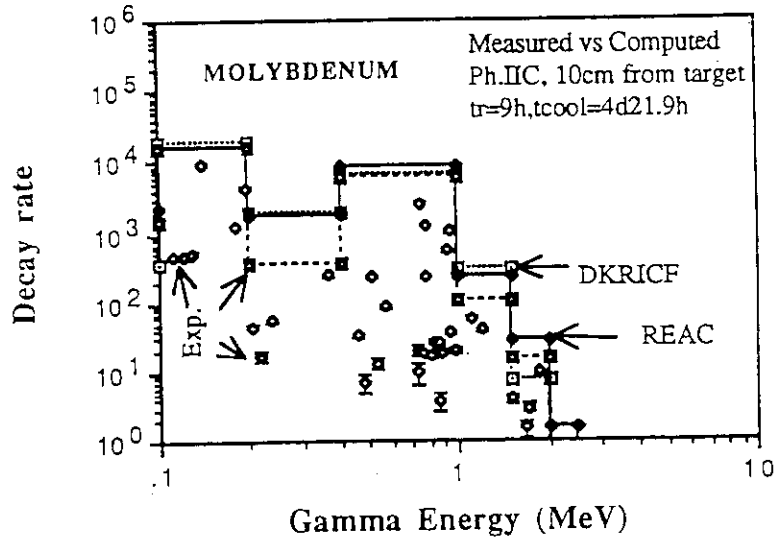

Fig. 17.4 Decay γ-emission rate spectra per g for molybdenum: measurement vs. computation (tr=9h, tcool=4d21.9h).

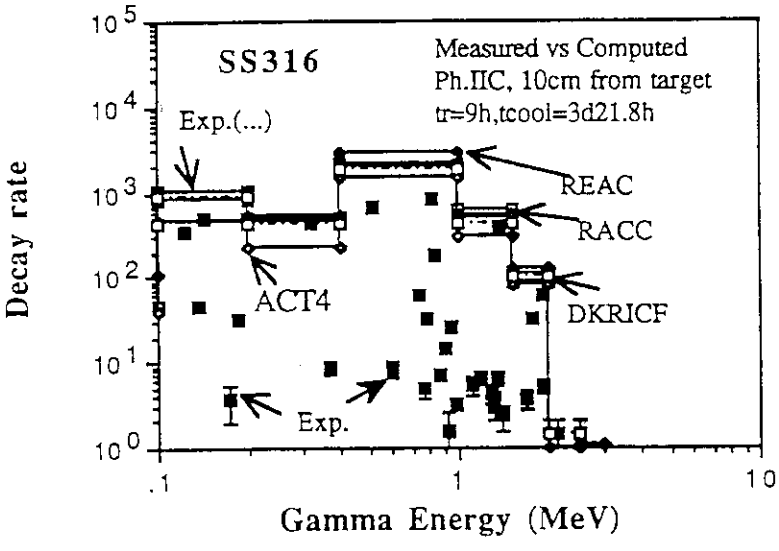

Fig. 17.5 Decay γ-emission rate spectra per g for stainless steel: measurement vs. computation (tr=9h, tcool=3d21.8h).

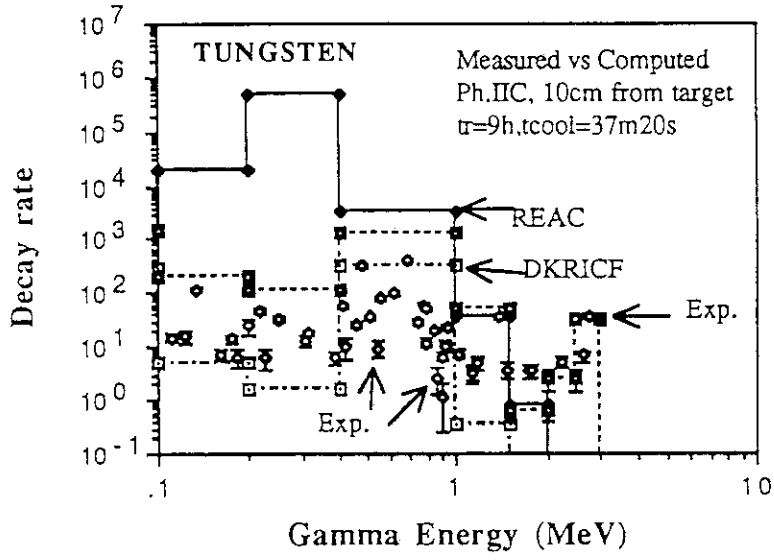

Fig. 17.6 Decay γ-emission rate spectra per g for tungsten: measurement vs. computation (tr=9h, tcool=37m20s).

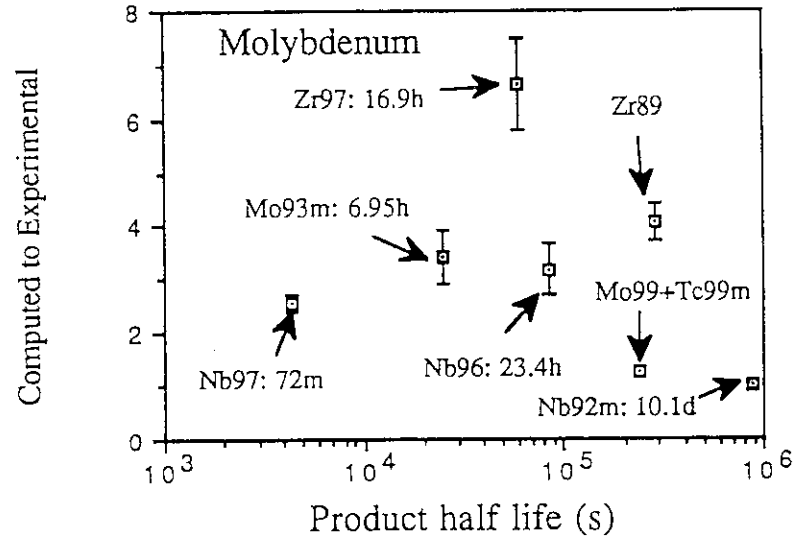

Fig. 18.1 Computed to experimental ratio (C/E) of decay γ-emission rates as a function of product half life for a molybdenum sample (Phase IIIA, REAC-2 computation).

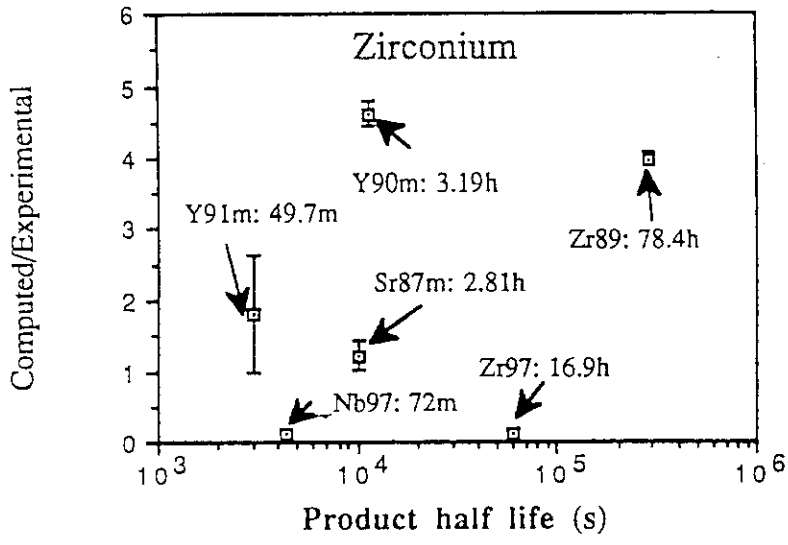

Fig. 18.2 Computed to experimental ratio (C/E) of decay γ-emission rates as a function of product half life for a zirconium sample (Phase IIIA, REAC-2 computation).

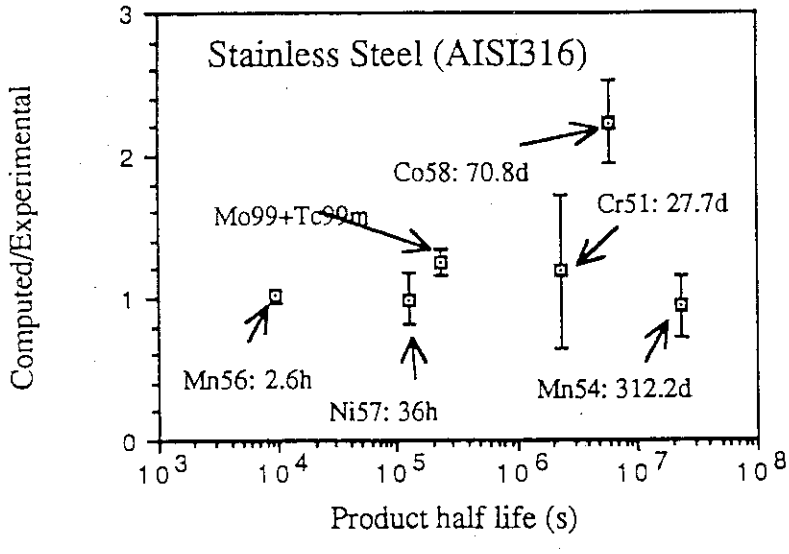

Fig. 18.3 Computed to experimental ratio (C/E) of decay γ-emission rates as a function of product half life for a aisi316 sample (Phase IIIA, REAC-2 computation).

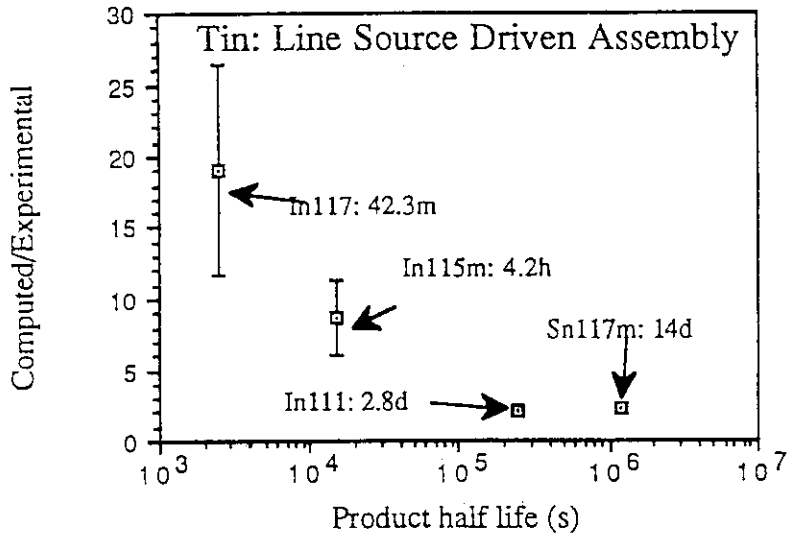

Fig. 18.4 Computed to experimental ratio (C/E) of decay γ-emission rates as a function of product half life for a tin sample (Phase IIIA, REAC-2 computation).

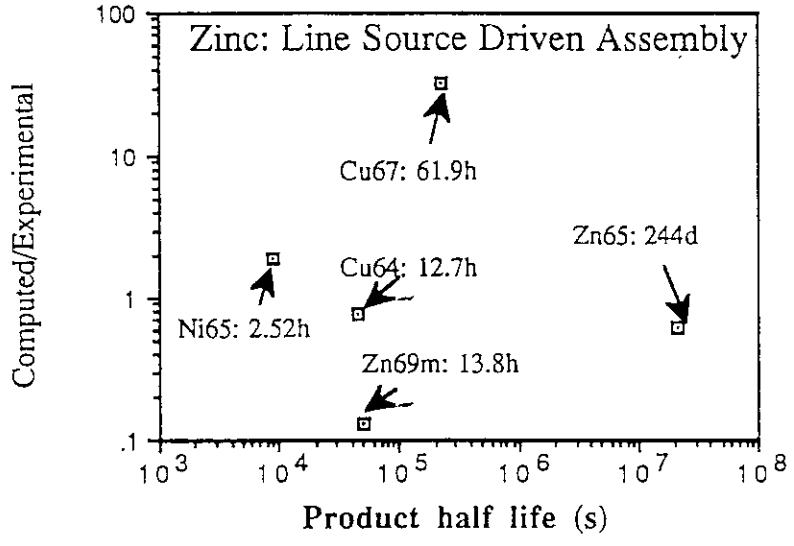

Fig. 18.5 Computed to experimental ratio (C/E) of decay γ-emission rates as a function of product half life for a zinc sample (Phase IIIA, REAC-2 computation).

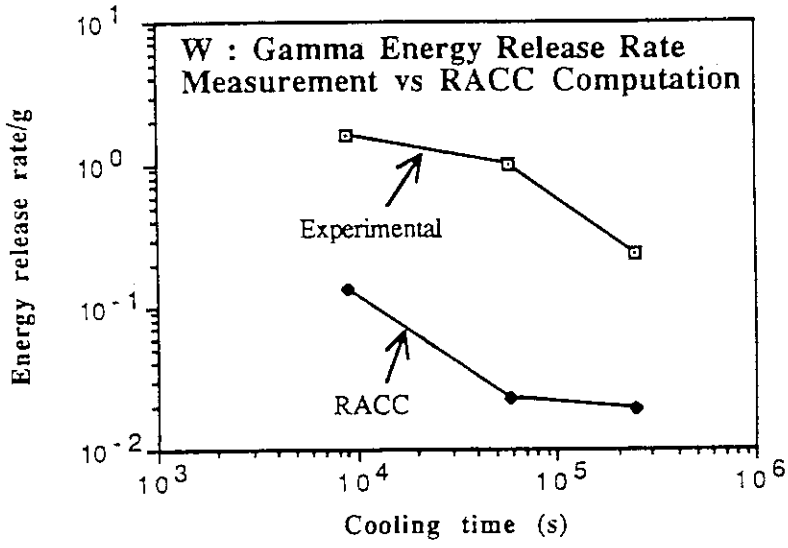

Fig. 19 Gamma-ray energy release rate per g, nW/g, as a function of cooling time from a tungsten sample irradiated at '10 cm' location for 9h.

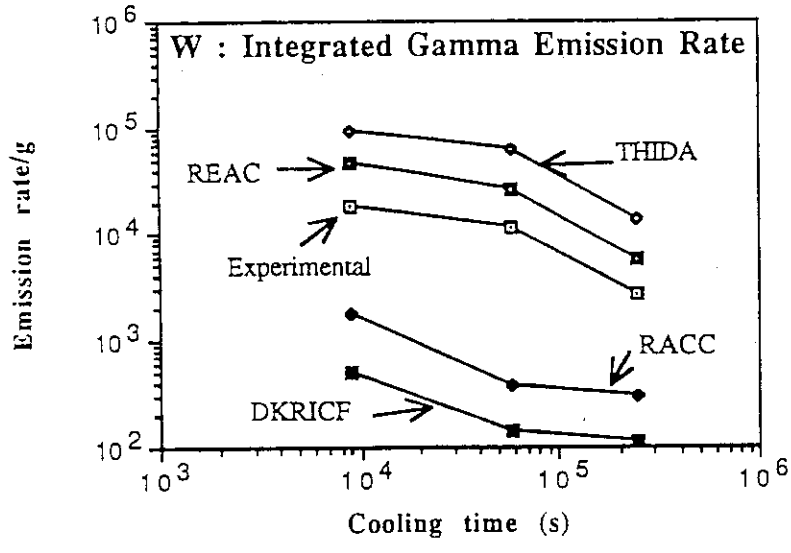

Fig. 20 Integrated decay γ emission rate (100 keV - 3 MeV) as a function of cooling time for a tungsten sample irradiated for 9h.

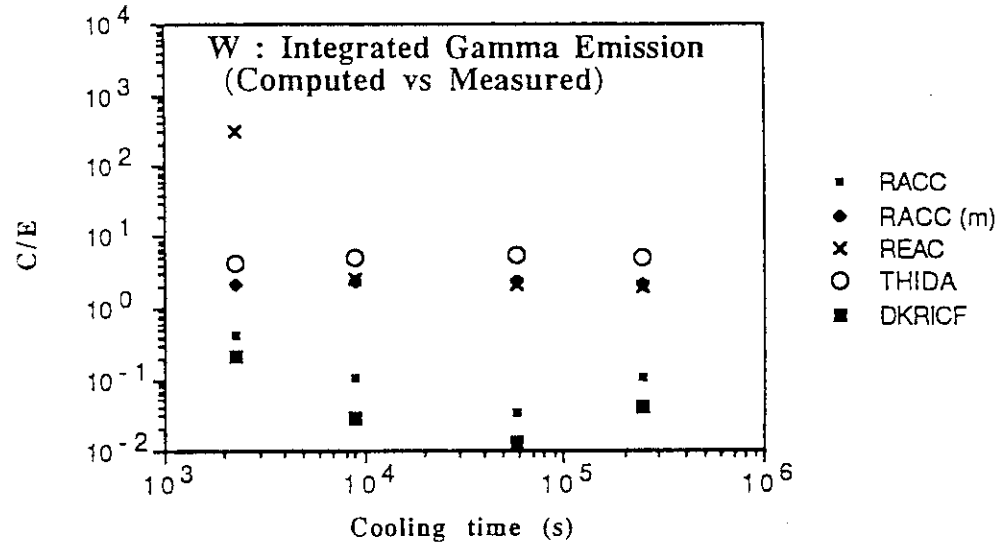

Fig. 21 C/E ratios for integrated decay γ-emission rates obtained from various radioactivity code systems.

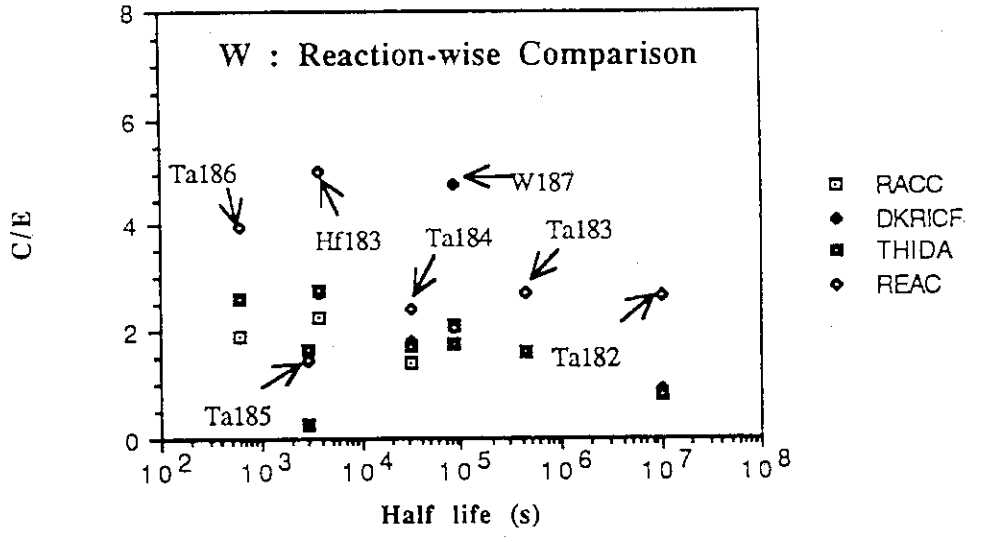

Fig. 22 C/E ratios for reaction rates from all four codes as a function of product half life.

APPENDICES:

Associated publications

A.1 "Radioactivity and Nuclear Heating Measurements for Fusion Applications," by A. Kumar, M.A. Abdou, Y. Ikeda, C. Konno in *Symposium of Fusion Technology 1990*, 872-876, edited by B.E. Keen, M. Huguet, R. Hemsworth, Elsevier Science Publishers (1991).

A.2 "Experiment on Induced Activities and Decay-Heat in Simulated D-T Neutron Fields: JAERI/USDOE Collaborative Program on Fusion Neutronics," by Y. Ikeda, C. Konno, T. Nakamura, A. Kumar, M.A. Abdou, *Fusion Technology*, **19** (1991) pp.1961-1966

A.3 "Analysis of Induced Activities Measurements Related to Decay-Heat in Phase IIC Experimental Assembly: USDOE/JAERI Collaborative Program on Fusion Neutronics Experiments," by A. Kumar, M.A. Abdou, Y. Ikeda, T. Nakamura, *Fusion Technology*, **19** (1991) pp.1909-1918.

A.4 "Experiments and Analysis for Measurements of Decay-Heat Related Induced Activities in Simulated Line Source Driven D-T Neutron Fields of Phase IIIA: USDOE/JAERI Collaborative Program on Fusion Neutronics," by A. Kumar, M.Z. Youssef, Y. Ikeda and C. Konno, *Fusion Technology*, **19** (1991) pp.1859-1866.

A.5 "Experimental Verification of the Current Data and Methods for Induced Radioactivity and Decay Heat Calculation in D-T Fusion Reactors," by Y. Ikeda, C. Konno, Y. Oyama, T. Nakamura, A. Kumar, M.Z. Youssef, and M.A. Abdou, *Fusion Engineering and Design*, **18** (1991) pp.387-395 .

A.1

FUSION TECHNOLOGY 1990
B.E. Keen, M. Huguet, R. Hemsworth (editors)
Elsevier Science Publishers B.V., 1991

RADIOACTIVITY AND NUCLEAR HEATING MEASUREMENTS FOR FUSION APPLICATIONS

Anil KUMAR, Mohamed A. ABDOU

University of California,
Los Angeles, CA 90024-1597, USA

Yujiro IKEDA, Chikara KONNO

Japan Atomic Energy Research Institute
Tokai-mura, Ibaraki-ken 319-11, Japan

Induced radioactivity has been measured in samples of Fe, Ni, Cr, Mo, SS316, MnCu alloy, Co, V, Ti, Nb, W, Pb, Sn, Zn, Ag, Ta, Al, Si, Mg, In, Zr, $YBa_2Cu_3O_7$ and $ErBa_2Cu_3O_7$ in fusion neutron environment for different irradiation and cooling times. Analysis shows up inadequacies of activation and decay data of leading radioactivity calculation codes. Large discrepancies are observed for W, Mo, Zr, V and MnCu alloy though integrated decay γ-emission rates agree within 30% for Fe and SS316. Long half life measurements are still in progress. Nuclear heat deposition rate measurements have been made in small probes of Fe, Cu, graphite, Al and W. The analysis shows discrepancies of as much as 40% between measured and computed rates.

1. INTRODUCTION

Induced activity and nuclear heat deposition rates are among the most important parameters qualifying design of a fusion machine including its vacuum vessel and other components[1]. A range of structural and other materials are under consideration for next-step devices like ITER, CIT and NET. Prompt and decay heating rates are subject to large uncertainties as there is very little supporting experimental data base existing at the moment.

A program was planned and executed over the last two years for experimental verification of the data base and computer codes presently used for calculation of radioactivity and nuclear heating in fusion device design[2-5]. The measurements were carried out in 1988 and 1989 at fusion neutronics source facility of JAERI within the framework of USDOE/JAERI collaborative program on fusion neutronics[6]. The experiments on induced radioactivity were conducted inside prototypical blanket assemblies. The materials investigated in these experiments include: Fe, Ni, Cr, Mo, SS316, Mn, Cu, Co, V, Ti, Nb, Ta, Al, Si, In, Zr, $YBa_2Cu_3O_7$, $ErBa_2Cu_3O_7$. In addition , an experiment was conducted in June 1989 under average fluence of 7×10^{14} n/cm^2 for accumulating activation data on long half life radioactive isotopes, with half-lives ranging from 13.3 y (^{153}Eu) to 0.72 My (^{26}Al).

2. RADIOACTIVITY EXPERIMENTS

Experimental measurements have been conducted at fusion neutronics source facility (FNS) of JAERI over last few years inside prototypical fusion blanket assemblies within the framework of USDOE/JAERI collaborative program on fusion breeder neutronics[6].The measured quantities have consisted of tritium breeding ratio, neutron energy spectrum, foil activation rates and gamma heating rates. First measurements related to induced decay γ activity were conducted within this program during phase IIC in fall 1988.

Though entire phase IIC experimental program consisted of carrying out measurements in each of two prototypical blanket assemblies[7-8]- beryllium edge-on and coolant channel assemblies- the radioactivity measurements were conducted only inside 'coolant channel' assembly. This assembly had three polyethylene (PE) channels implanted in test section made of Li_2O bricks. Two spatial locations were chosen so as to have significantly different neutron energy spectra- the two locations being at 10 cm (in air) and 82 cm (5 cm inside Li_2O section) distance from the target center of 'rotating neutron target' (RNT) source. The materials irradiated included: Fe, Cr, Ni, Mo, SS316, MnCu alloy, V, Ti, Co, Al, Si, Zr, Nb, W, Au, In, Mg, Ta, $YBa_2Cu_3O_7$ and $ErBa_2Cu_3O_7$. Of these, $YBa_2Cu_3O_7$ and $ErBa_2Cu_3O_7$(on substrate of yttria stabilized zirconia) are known high temperature superconductors, and Au, In, Mg, Fe, Al, Nb, and Ta were also intended to serve as dosimetry foils for monitoring neutron energy spectrum. Two separate irradiations were carried out to cover each of these locations. Two foil packets were irradiated at each location to separately cover: (i) shorter half life products (less than 1 hour half life), (ii) longer half life products (1 hour to 5 year half life). Each irradiation period consisted of initial half an hour irradiation followed by pulling out of one of the two packets. The γ−spectroscopy of the foils in this

packet were to cover primarily shorter half life products. The full irradiation perids were 9 and 10 hours respectively for the locations at 10 and 82 cm, logging average source neutron intensities of 8.75 10^{11} and 1.12 10^{12} n/s.The γ−spectroscopy of each sample was done using three intrinsic germanium detectors and for multiple cooling periods ranging from 20 m to 10 d.

The availability of clean D-T neutron source environment coupled with high intensity at rotating neutron target (RNT) at FNS was considered to be an asset for a high-fluence activation in June 1989 for obtaining cross-section data on long half life isotopes. Foil packages, each consisting of samples of Al, Re, Ho, W, Mo, Dy, Ir, Tb, Ag, ^{151}Eu, ^{153}Eu and Hf, were kept one each at 0, 45 and 75^0 with respect to beam-axis; the front end of a package was at a distance of around 22 mm from the target-center whereas the back-end was 49 mm away. The fourth package was kept at a distance of 12 cm and at an angle of around 115^0 with respect to the beam axis. Multiple Nb and Zr foils were placed inside each package to monitor neutron fluence (through Nb) and neutron spectrum (through Zr/Nb ratio). The foil packages were irradiated over 4 days for a total duration of 32 hours and total neutron yield of 1.3 10^{17} n.. This yield amounts to a fluence of 1.66 10^{15} n/cm^2 (first foil) to 3 10^{14} n/cm^2 for the packages in the forward direction; the average fluence being ~7 10^{14} n/cm^2. The isotopes of interest and their half lives are: ^{153}Eu (13.3 y), ^{178m2}Hf (31 y), ^{150m}Eu (35.8 y), ^{108m}Ag (127 y), ^{158}Tb (150 y), ^{192m}Ir (241 y), ^{166m}Ho (1200 y), ^{94}Nb (20.3 Ky), ^{186m}Re (0.2 My) and ^{26}Al (0.72 My). The γ−spectroscopy of these foils is still continuing.

Phase IIIA experiments of the collaborative program were conducted in fall 1989. This phase is especially noteworthy for the landmark implementation of line source concept employing a point D-T neutron source[9-10]. The line source simulation was achieved by moving detectors/blanket assembly back and forth along the beam axis with respect to the fixed point neutron source. The induced radioactivity experiments were conducted both with bare line source and with a blanket assembly. The materials covered in the experiments included: Fe, Ni, Mo, SS316, W, Al, Sn, Ta, Zr, Nb, Ag, Pb, Zn, Ti, V, Co and In. The length of the simulated line source was set at 200 cm. The average source intensities obtained were 1.11 10^9 and 9.66 10^8 n/s /cm with and without assembly for irradiation periods of 9h47m and 9h51m respectively.

3. NUCLEAR HEATING EXPERIMENTS

Nuclear heating rates were measured using microcalorimetric technique in june and december 1989. Bead (point-size) thermistors and platinum RTD's were employed as thermal sensors inside probes made of Fe, Cu, W, Al and C (graphite). High sensitivity digital nanovoltmeter (model 181 from Keithley) formed integral part of the measurement circuit for picking up temperature change rates as low as 5 μ^0K/s. The irradiation stability of thermistors was found excellent for fluence as high as 2.9 x 10^{14} n/cm^2 during the qualifying tests in june 1989. We did not check the stability at a higher fluence as there were plans to work much below this value in the experiments to follow. Four types of thermistors were employed, having 25 ^{0}C resistances of 2.252 KΩ, 10 KΩ, 22 KΩ, and 30 KΩ . A platinum RTD had resistance of 100 Ω at 0 ^{0}C. Temperanure coefficient of resistance for a thermistor and a platinum RTD were -4.4 x 10^{-2} per ^{0}C (at 25 ^{0}C) and 3.6 10^{-3} per ^{0}C (at 0 ^{0}C) respectively. Measurements were made on probes of iron, aluminum, copper and graphite. Each probe consisted of a cylindrical core of 20 mm height and 20 mm diameter sitting symmetrically inside a 1 mm thick jacket that had external diameter and height of 32 mm each. Polystyrene stubs provide thermal insulation between the core and the jacket. Three locations were chosen for placing the thermistors inside a core: front, middle and back; two locations were used for the RTD's: in the central planes of first and second halves of each core. During measurements each probe was kept inside a vacuum chamber. Distance of the core of a probe from the neutron source ranged from 6.3 to 7.7 cm. The source neutron intensity varied from 1.9 to 1.1 10^{12} n/s through experiments with all these probes. Generally, neutron source intensity was modulated such that there were 3 to 10 minute duration spaced pulses.

Additional nuclear heat deposition rate measurements were carried out during phase IIIA of the collaborative program in fall 1989. Two generic kinds of experiments were scheduled: (1) single probe experiments using composite or single block structure probe (Fe, Cu, C, W, Al); the objective consisted in examining the reproducibility of earlier (June 1989) experiments, (2) multiple probe experiments employing many smaller size single probes in a much larger host medium; two host media, e.g., iron, graphite, housed single probes made of graphite, tungsten, iron/copper; the underlying objective was to obtain spatial distribution of heat deposition rates and possibly extract its neutron and gamma heating

components. Both kinds of measurements were conducted with probe kept inside an evacuated vacuum chamber.

4. RESULTS AND DISCUSSION

Analysis of the experiments on induced radioactivity and nuclear heat deposition rate measurements has been carried out after obtaining neutron and gamma spectra from two transport codes DOT4.3 (two-dimensional and deterministic)[11] and MCNP-3B (three-dimensional and Monte Carlo)[12] with cross-section data[13] based on ENDF/B-V. The induced radioactivity computations were then carried out using REAC-2[5], DKRICF[3], RACC[2], and THIDA-2[4]. The THIDA-2 analysis is patterned after reference 14.

4.1 Induced Radioactivity

The experimental data was treated to obtain decay gamma emission rate per g of irradiated material per normalizing source strength of 10^{12} n/s. Correction for self-absorption of γ spectra in each sample was also applied.

The neutron energy spectra at 10 and 82 cm locations is significantly different, e.g, there are only 66% neutrons above 100 KeV at later location as against 97% for the former. The maximum fluences at the two locations were 3.5 10^{13} n/cm^2 and 2.4 10^{12} n/cm^2 respectively. Figures 1a to 1c show comparison of calculated (C) to measured (E) integrated decay gamma emission rates for different materials for the three radioactivity codes DKRICF, REAC-2 and THIDA-2 respectively. The γ-energy range covered goes from 100 KeV to 3.5 MeV. Only upper and lower bounds are shown- embracing all the cooling periods for each material. The largest discrepancies are seen for DKRICF and REAC-2 codes. Regarding THIDA-2 results, the discrepancies are usually lower. For SS316, in particular, the results reported earlier (ref. 14) are reinforced. The largest discrepancies have been observed for tungsten in both REAC-2 and DKRICF, even as the origins are widely different. C/E for DKRICF ranges from 4.88 10^{-4} to 0.20; it ranges from 2.05 to 307 for REAC-2. The large discrepancies for DKRICF originate from the absence of decay data for ^{186}Ta, ^{187}W and ^{181}W. As for REAC-2, the discrepancies are due to inadequate decay/cross-section data for production of γs from ^{179m}W, ^{187}W, ^{184}Ta, ^{183}Hf, ^{182m}Hf, and ^{180m}Hf. For SS316 and Fe all the three codes agree within 25% as for the integrated decay gamma emission rates. Mo, Zr, MnCu (80% Mn+20% Cu alloy), Ta, $YBa_2Cu_3O_7$ and V also show up large discrepancies.

The discrepancies on γ−spectra are, in general, much higher. Figures 2 to 6 display typical comparison of

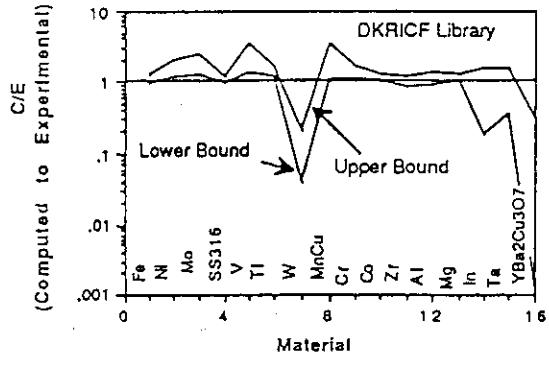

Figure 1a

Comparison of Measured and DKRICF computed decay γ emission rates

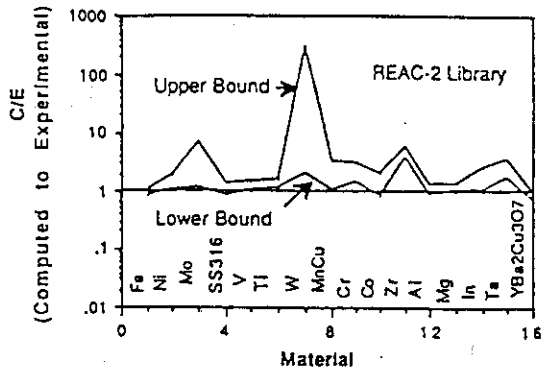

Figure 1b

Comparison of Measured and REAC-2 computed decay γ emission rates

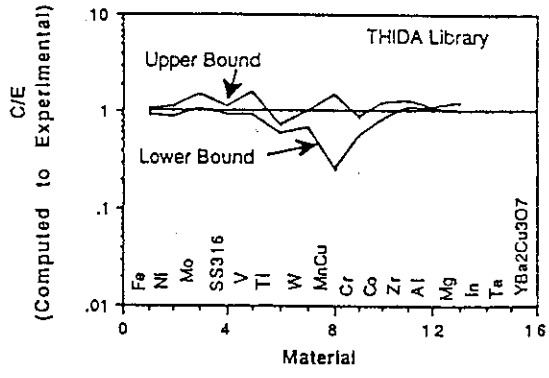

Figure 1c

Comparison of Measured and THIDA-2 computed decay γ emission rates

measured and computed decay γ−emission rates for Fe, SS316, Ni, and W. 'tr ' stands for irradiation period and tcool ' denotes sample cooling time after irradiation. It is obvious that significant revision of REAC-2 and DKRICF code systems would be called for to get reasonable agreement between the measured and computed γ−spectra.

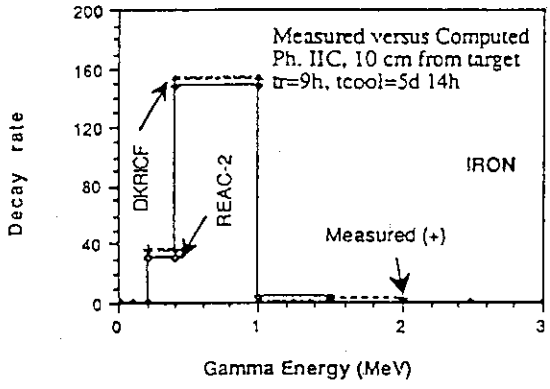

Figure 2

Comparison of Measured and computed decay γ emission spectra for Iron Sample

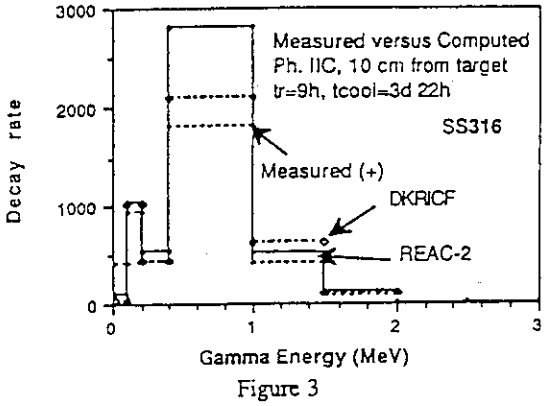

Figure 3

Comparison of Measured and computed decay γ emission spectra for SS316 Sample

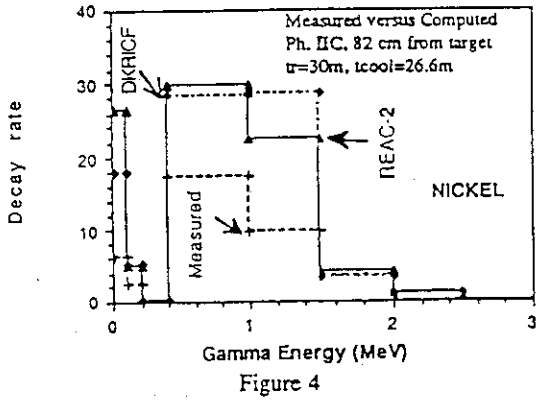

Figure 4

Comparison of Measured and computed decay γ emission spectra for Nickel Sample (cooling time = 26.6 m)

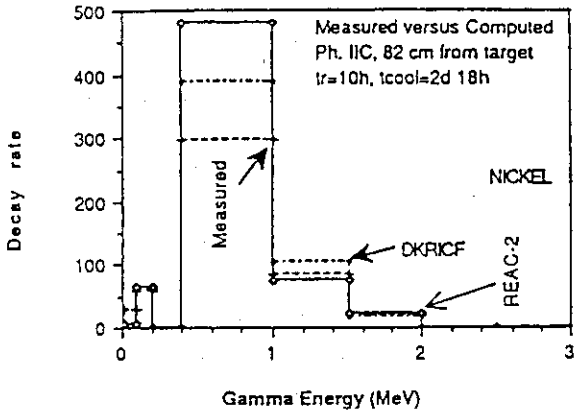

Figure 5

Comparison of Measured and computed decay γ emission spectra for Nickel Sample (cooling time = 2 d 18 h)

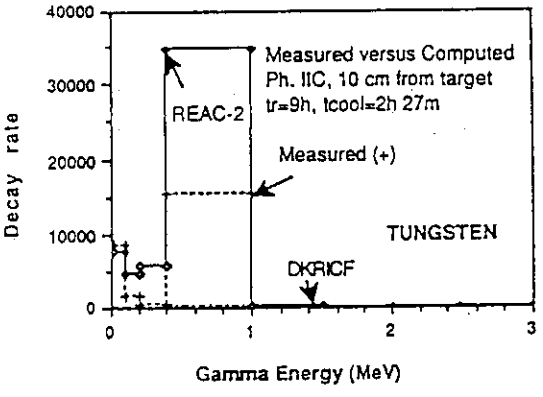

Figure 6

Comparison of Measured and computed decay γ emission spectra for Tungsten Sample

4.2 Nuclear Heat Deposition

Various sensors kept inside a probe in vacuum chamber gave very close values for heat deposition rate. This is understandable as relatively small size of a probe allowed rapid equilibration of initial thermal gradients inside the probe. The heat deposition rate was averaged over the probe dimensions so as to compare it to measured value. Figures 7 and 8 show typical resistance change per cycle (length = 30 s) for a thermistor and a RTD sensor kept inside an iron probe.

The analysis of the measurements of june 1989 showed that the computed and measured data agreed within 40%. It is interesting to point out that measured rates of temperature change, normalized to 10^{12} source neutrons per s, were respectively 18, 20, 39 and 16 μ^0K/s for Fe, Al, C (graphite) and Cu probes. These are rather small

rates, showing up the sensitivity of the experimental equipment and procedure.

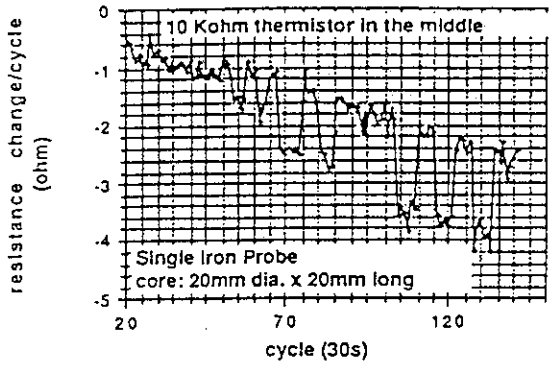

Figure 7

Nuclear heat deposition in an Iron probe: response of a thermistor

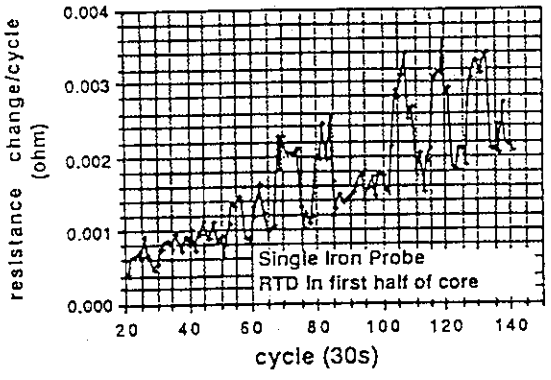

Figure 8

Nuclear heat deposition in an Iron probe: response of an RTD

5. CONCLUSIONS

Experimental measurements of induced radioactivity and nuclear heat deposition rates in fusion neutron environment have been carried out and compared to analysis made with two and three dimensional transport codes and different decay radioactivity codes. Integrated decay gamma emission spectra is found to agree within 30% for SS316 and Fe samples. However, larger deviations are found for W and some other materials. The discrepancies for decay γ−spectra are found to be much larger. The activation cross sections and decay data libraries asscociated with REAC-2 and DKRICF code systems need to be given a closer look with a view to improve the agreement between measured and computed data. The nuclear heat deposition rates have been measured in probes of Fe, graphite, Cu, Al and W. The measured and computed rates differ considerably. Additional measurements will help in accumulating the data bases for both induced radioactivity and nuclear heat deposition so as to permit an early and extensive revision of the basic nuclear data.

ACKNOWLEDGEMENTS

This work was supported by U.S. DOE grant No. DE-FG0388ER52150 and Japan Atomic Energy Research Institute.

REFERENCES

1. R.W. Conn et al.,Nuclear Technology, 26 (1985) 391.
2. J. Jung, "Theory and Use of the Radioactivity Code RACC," ANL/FPP/TM-122, Argonne National Laboratory (1979).
3. D.L. Henderson and O. Yasar, "A Radioactivity and Dose Rate Calculation Code Package," Vol. 1 and 2, RSIC computer code collection, CCC-323 (April 1987).
4. Y. Seki et al.,"THIDA-2: An Advanced Code System for Calculation of Transmutation, Activation, Decay Heat and Dose Rate," RSIC computer code collection, CCC-410 (April 1987).
5.F.M. Mann,"REAC*2: Users Manual and Code Description," WHC-EP-0282, Westinghouse Hanford Company (1989).
6. T. Nakamura and M.A. Abdou,"Overview of JAERI/U.S.DOE Collaborative Program on Fusion Blanket Neutronics," Proc. Int. Symp. on Fusion Blanket Nuclear Technology, Tokyo (April 11-15, 1988).
7. A. Kumar et al., Fusion Technology, 15 (1989) 1309.
8. M.Z. Youssef et al., to be presented at 9th topical meeting on the Technology of Fusion Energy, 7-11 October, 1990, Oak Brook, USA.
9. Y. Oyama et al., ibid.
10. M.Z. Youssef et al., ibid.
11. W.A. Rhoades and R.L. Childs,"DOT-IV Version 4.3: One and Two Dimensional Transport Code System," RSIC computer code collection, CCC-429 (May 1984).
12. J.F. Briesmeister, editor,"MCNP- A General Monte Carlo Code for Neutron and Photon Transport: Version 3A," report no. LA-7396-M, Rev. 2 (Sep. 1988), alongwith MCNP3B newsletter dated July 18, 1988, Los Alamos National Laboratory.
13. R.E. MacFarlane,"TRANSX-CTR: A Code for Interfacing MATXS Cross Section Libraries to Nuclear Transport Codes for Fusion Systems Analysis," report no. LA-9863-MS, Los Alamos National Laboratory (Feb. 1984).
14. Y. Ikeda et al., Fusion Technology, 8 (1985) 1466.

A.2

EXPERIMENT ON INDUCED ACTIVITIES AND DECAY-HEAT IN SIMULATED D-T NEUTRON FIELDS: JAERI/USDOE COLLABORATIVE PROGRAM ON FUSION NEUTRONICS

Y. Ikeda, C. Konno and T. Nakamura
Department of Reactor Engineering,
Japan Atomic Energy Research Institute
Tokai-mura, Ibaraki-ken 319-11 Japan
0292-82-6016

A. Kumar and M. A. Abdou
University of California, Los Angeles
Los Angeles, CA 90024
U.S.A.
213-825-8266

ABSTRACT

An experiment of Induced radioactivity and decayheat has been conducted in the framework of JAERI/USDOE collaborative program on the fusion blanket neutronics. Sixteen different materials have been irradiated in two typical DT neutron fields simulating spectra at the first wall and blanket regions of a fusion reactor. Induced radioactivity production profiles for both short and long irradiation times were analyzed by detecting associated γ-ray energy spectra. Energy release rate in material was characterized on the basis of the γ-ray emission data measured as well as β-ray contribution estimated. In this experimental study, focuses were placed not only on providing benchmark data for verification of the calculation code and nuclear data, but also on a comparative study for providing a guide line for the material selection concerning the dose rate as well as the decayheat after shutdown in the near term DT fusion devices.

INTRODUCTION

Accurate estimation of radioactivity induced by DT neutron reactions is of importance because of its impact on nuclear design of DT burning fusion devices, e. g., ITER and FER. To meet the data requirement from the reactor design, an integral experiment has an important role to examine uncertainties in the calculation code and associated activation data. Benchmark experiments have been reported previously on the induced activities for SS-316 and concrete components [1−4] verifying the THIDA code system.[5]

Up to now, there have been much progress in the design and broad choice of the materials in the next generation fusion testing devices have been proposed. Thus, it is urgent requirement to establish more systematic data base pertinent to the induced radioactivity and decayheat assessment.

An integral experiment was conducted at the FNS facility[6] in the framework of JAERI/USDOE collaborative program on fusion neutronics during Phase-IIC[7]: the system for the coolant channel effect consisted of Li_2O breeder blanket with a first wall enclosed by Li_2CO_3 with Polyethylene layer. The objectives of the experiment are to provide data for verifying radioactivity calculation codes, and to investigating the suitability of different materials in meeting the selection criteria based on low activation and decayheat considerations. The major independent variables considered in this study are materials, neutron spectrum, the operation time and the time after shutdown. Using experimental data, comparative investigation as material wise are performed in terms of γ-ray emission rate and total energy release rate as a function of neutron spectrum and irradiation and cooling time. The accompany paper[8] is treating successive experimental analysis using codes of THIDA2[9], REAC2[10] and DKRICF.[11]

EXPERIMENTS

Materials

Materials considered in the present study includes not only substantial structural materials of Iron, Nickel, Chromium, but the other potential materials of Aluminum, Silicon, Titanium, Molybdenum, etc.. Aiming at making a systematic experimental data base, sixteen different materials were chosen. In Table 1, they are shown together with their densities. To simplify the successive analysis, materials were to be single element rather than alloy. Only SS-316 and MnCu alloy(Mn 80%, Cu 20%) were selected because that SS-316 is one of most promising structural materials and Mn can not stand by itself as a metallic foil. The size of the sample was 5 mm in dia. by 1 mm in thickness except for Cr, Al, Si and W, which have dimensions of 12.7 mm in dia. by 0.1 mm in thickness for Al and W, and 10 mm^2 by 1 mm in thickness for Cr and Si.

Table 1. Materials tested and their densities

Material name	Density(g/cm^3)
Fe	7.86
W	19.35
Mo	10.2
V	5.87
SS-316	7.82
Ni	8.80
MnCu	8.60
Co	8.71
Zr	6.49
Ti	4.50
Si	2.42
Al	2.70
Nb	8.57
Ta	16.6
Mg	1.74
Cr	7.14

Neutron Fields

Since neutron spectrum dependence on the radioactivity production is the fundamental parameter for the present investigation, the spectrum at the irradiation position is needed to be close to the realistic fusion neutron environment. The configuration of the Phase-IIC experimental assembly was chosen for this experiment. The system consisted of Li_2O breeder blanket with a first wall enclosed by 200 mm Li_2CO_3 with 50 mm polyethylene. The DT neutron source was located in the cavity of the enclosure, at 780 mm distance from the first wall of the Li_2O region. The cross sectional view of the system is shown in Fig. 1 along with two irradiation positions. The first sample location was set at 100 mm distance from the neutron source at 30º with respect to the incident d^+ beam direction. The other one was located at 50 mm depth in the Li_2O region. As the first position(A) was close to the DT neutron source, it is expected that the neutron spectrum simulates a typical one at first wall region. The second position(B) provided simulation of typical spectrum inside tritium breeder blanket,Li_2O. Figure 2 illustrates neutron spectra calculated by DOT3.5 with GICX40 nuclear library,[12] which are to be used in the successive experimental analysis.[8] The spectrum inside the cavity includes neutron components reflected by the surrounding materials so that the field is expected reasonably to simulate the fusion radiation environment.

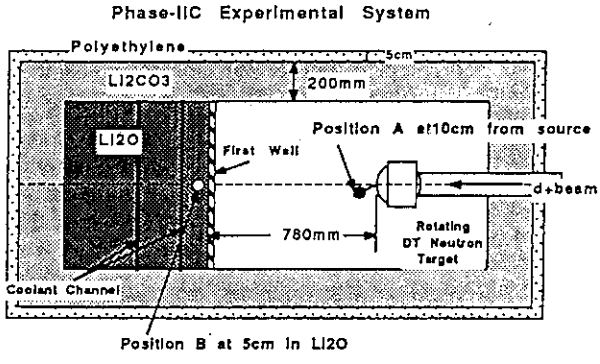

Fig. 1 The cross sectional view of Phase-IIC experimental system configuration and irradiation sample positions.

Irradiations

One of parameters to be investigated here is a dependence of radioactivity on the time(the operation and cooling after shutdown). It is of importance because of inherent time dependent nature of the radioactivity. The variation in the plasma burning time and timing for the access after shutdown are very crucial to setup the experimental scenario for the testing of the devices.

Two irradiation times for 30 m and about 10 h were taken to respectively emphasize shorter and longer half-live products. The irradiation times for each irradiation runs are shown in Table 2 together with neutron source strengths. It is reasonably accepted to assume that the irradiation length for 30 min to 10 hours corresponds to the operation duration expected in the first stage of the testing devices.

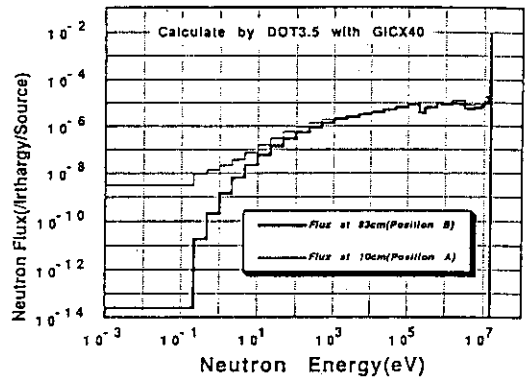

Fig. 2 Neutron energy spectra at the positions A and B calculated by DOT3.5 with GICX40 library.

Table 2. Irradiation times and neutron source strengths

Run No.	Position	Irradiation Time	Source Strength
1	A	30 m	1.740×10^{12}/sec
2	A	10 h	9.046×10^{11}/sec
3	B	30 m	1.298×10^{12}/sec
4	B	11 h	1.022×10^{12}/sec

γ-ray spectrum measurements

After irradiation, samples were extracted from the system and γ-ray spectra were measured with four Ge detectors at cooling times ranging from10 m to 5 h for the short irradiation and 1 h to 7 days for the long irradiation. The data of cooling time and counting time for each run are described in detail in the accompany paper.[8] The γ-ray spectrum of Tungsten for the long irradiation at position A is shown in Fig. 3 as an example of the spectrum. The spectra measured were analyzed by a code BOB[13] to obtain γ-ray counts. Corrections for sum-peak, γ-ray self- absorption in the samples, material density, detector efficiency and neutron flux fluctuation were applied to obtain γ-ray spectra per unit volume. When the irradiation time is longer than the half-lives of the activities induced, correction for the neutron flux fluctuation during irradiation can not be negligible to keep assumption for the uniform strength irradiations.

Experimental errors estimated in the data processing are summarized in Table 3.

Table 3. Experimental error

Error sources	Estimated value
Counting statistics	0.1 to 50 % for single γ-ray 0.1 to 3 % for integrated
Detector efficiency	2.5% for standard detector 3 - 4 % for relative detector
Self-absorption	1 - 2 %
Neutron flux fluctuation	0.5 - 2 %
Sum peak corrections	1 - 2 %

RESULTS

Materials Wise Observation

Identification of the decaying nuclide was performed using the decay γ-ray energy and relationship of their branching ratio.[14] In this section, the main contribution of activities for all spectra are described for each material.

Fe: For spectra at a cooling time less than 10 h by both short and long irradiations, ^{56}Mn(T1/2=2.579h), the product by the reaction of ^{56}Fe(n,p), has the largest contribution to the total γ-ray emission. The fraction of ^{54}Mn(T1/2=312d), the product of ^{54}Fe(n,p), increases as the cooling time increases longer than 1 day. No other activity was observed in this measurement. There was no significant spectrum dependence in those activity production rate except in the difference in the neutron flux level with respect to the distance to the source. This was due to that both production reactions are threshold type so that only the high energy neutron component contributed to the activity production.

Ni: Main contribution comes from ^{57}Ni(T1/2=36h), the product of ^{58}Ni(n,2n), in all spectra. In spectra for the short irradiation runs, ^{62m}Co(T1/2=13.9m), the product of ^{62}Ni(n,p), gave several % fraction to the total. For the long irradiation runs, ^{60}Co(T1/2=5.271y), product of ^{60}Ni(n,p), was observed though its contribution was small less than 1 %. The other nuclides observed were ^{57}Co(T1/2=271d) and ^{58}Co(T1/2=70.8d), the products from the decay of ^{57}Ni + ^{58}Ni(n,np), and ^{58}Ni(n,p), respectively.

Cr: Spectra were measured only for the long irradiations. The 320 keV γ-line from ^{51}Cr (T1/2=27.7d), the product of ^{50}Cr(n,γ) and ^{52}Cr(n,2n), was observed in both spectra. However, there was high intensity γ-line due to ^{34m}Cl(T1/2=32m), which was produced by ^{35}Cl(n,2n). This fact indicated that there was a certain amount of Cl as an unexpected impurity, which might be used as a coating material for Cr foil.

Co: The ^{56}Mn, the products of ^{59}Co(n,α), contributed 95 to 100 % and 10 to 80 % in spectra for the short and long irradiations, respectively. Contribution rate varied with the cooling time. The other nuclide observed were ^{59}Fe(T1/2=44.6d) and ^{58}Co, products of ^{59}Co(n,p) and ^{59}Co(n,2n), respectively. The ^{60}Co of ^{59}Co(n,γ) was observed in the spectrum for the long irradiation at the position B.

Ti: In the spectrum for the short irradiation at position A, annihilation 511 keV g-ray associated with β^+ decay of ^{45}Ti(T1/2=3.1h), products of ^{46}Ti(n,2n), occupied 40 % contribution to the total. The contribution of 511 kev γ-ray decreased to 6 % in the spectrum at position B. This is due to the fact that the direct 14 MeV neutron flux at position B is lower by two orders than that at position A. The ^{48}Sc(T1/2=43.7h), the product of ^{48}Ti(n,p) and ^{49}Ti(n,np) gave the largest contribution through all measurements. The other nuclide observed in the spectra for the long irradiation were ^{47}Sc (T1/2=3.42d) and ^{46}Sc(T1/2=83.8d), products of ^{47}Ti(n,p)+^{48}Ti(n,np) and ^{46}Ti(n,p)+^{47}Ti(n,np), respectively.

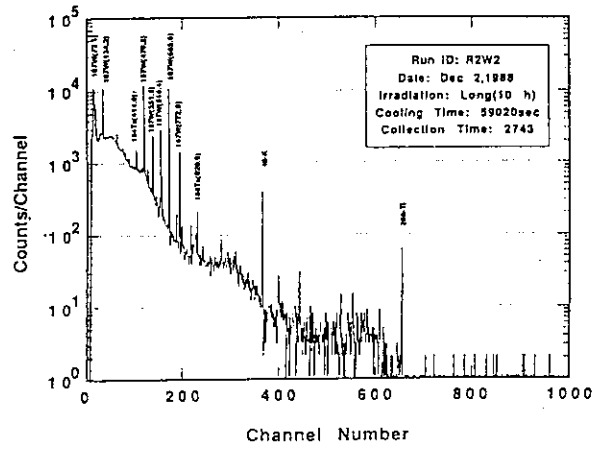

Fig. 3 Measured γ-ray spectrum of W sample for the long irradiation at position A.

V: In spectra for the short irradiations at both positions, ^{51}Ti(T1/2=5.76m) gave the largest contribution of 60 to 80 % to the total and the next one was ^{48}Sc, the product of ^{51}V(n,α), showing about 20 % contributions. In the spectrum for the short irradiation at position B, ^{52}V, the product of ^{51}V(n,γ) was observed, the contribution of which was 18%, while only 1% in the spectrum at position A. This fact indicated the softness of the neutron spectrum at position B. In the spectra for the long irradiations, only ^{48}Sc was observed.

Mg: Only spectra for the long irradiation runs were measured. Almost all contribution arose by ^{24}Na (T1/2=15.02h), the products of ^{24}Mg(n,p)+^{25}Mg (n,np).

Al: As the same situation as in the Mg, ^{24}Na, the product of ^{27}Al(n,α) dominated all spectra.

Si: Silicon is known as the low activation material because the reaction cross sections for the 14 MeV neutron are rather small and only short lived activities are produced. In this study, we could measure the spectrum only for the short irradiation at position A. Major activities were ^{27}Mg(T1/2=9.46m) and ^{29}Al(T1/2=6.6m), products of ^{30}Si(n,α) and ^{29}Si(n,p)+^{30}Si(n,np), respectively. They had contributions of 25 and 20 % to the total, respectively. However, as observed in the spectra for Cr, there were intense γ-lines from ^{34m}Cl which contributed 55 % of the total.

MnCu: The spectrum for the short irradiation at position A gave strong annihilation γ-ray with 90 % contribution of the total γ-ray intensity. This was due to ^{62}Cu(T1/2=9.73m), the product of ^{63}Cu(n,2n). In the spectra at long cooling time, ^{64}Cu(T1/2=12.7h), the product of ^{65}Cu(n,2n) + ^{63}Cu(n,γ), became the main source for the aniihillation γ-ray. At position B, ^{56}Mn, the product of ^{55}Mn(n,γ) had a contribution of 85 % for the short irradiation. For the long irradiation and long cooling time, ^{54}Mn, the product of ^{55}Mn(n,2n), dominated the spectrum with 70 % contribution.

Zr: Through all spectra, γ-ray from ^{89}Zr(T1/2=78.4h), the product of ^{90}Zr(n,2n), showed large

contributions of about 70 % to the total intensity. For the short irradiation, about 20 % contribution by ^{90m}Y(T1/2=3.19h), the product of ^{90}Zr(n,p) was observed. As the other activities, ^{87}Sr(T1/2=2.8h), ^{91}Sr(T1/2=9.5h), ^{91m}Y(T1/2=49.7m) and ^{92}Y(T1/2=3.54h) were identified. At position B for the long irradiation, a contribution of 9 % by ^{97}Zr(T1/2=1.6h), the production of ^{96}Zr(n,γ), was observed.

Nb: Gamma-lines from ^{92m}Nb(T1/2=10.5d), the product of ^{93}Nb(n,2n) dominated the spectrum in all cases. The other activity of ^{90m}Y(T1/2=3.19h), the product of ^{93}Nb(n,α), gave contributions of 1 to 15 %.

Mo: The main activity was ^{99}Mo(T1/2=66.02h), the product of ^{98}Mo(n,γ)+^{100}Mo(n,2n) and ^{99m}Tc (T1/2=6.02h), the product of associated decay of ^{99}Mo. THe same type of decay chain occurred in ^{101}Mo(T1/2=14.6m),the product of ^{100}Mo(n,γ), and ^{101m}Tc(T1/2=14.2m), which were observed in the spectrum for the short irradiation at position B. In the spectrum for the short irradiation at position A, annihilation γ-ray occupied 50 % of the total intensity. The source of the annihilation was estimated to be mainly ^{91m}Mo(T1/2=15.5m), the product of ^{92}Mo(n,2n). The contribution decreased to be 17 % in the spectrum at position B. Other activities observed were ^{98m}Nb(T1/2=51m), ^{97}Nb(T1/2=72m), ^{96}Nb(T1/2=23.4h), ^{93m}Mo(T1/2=6.9h) and ^{92m}Nb, the products of ^{98}Mo(n,p), ^{97}Mo(n,p), ^{96}Mo(n,p), ^{92}Mo(n,γ)+^{94}Mo(n,2n) and ^{92}Mo(n,p),respectively.

Ta: Only spectrum for the long irradiation at position B was measured. Dominant activities were ^{182}Ta (T1/2=115d), the product of ^{181}Ta(n,γ), and ^{180m}Ta(T1/2=8.1h), the product of ^{181}Ta(n,2n), which gave contribution of 74 and 26 %. respectively.

W: Through all spectra, ^{187}W(T1/2=23.9h), the product of ^{186}W(n,γ), gave the largest contribution of more than 70 % to the total γ-ray intensities. Especially, it had more than 90 % contribution in the spectrum at position B. The other γ-lines were due to ^{184}Ta (T1/2=8.7h), the product of ^{184}W(n,p), ^{186}Ta(T1/2=10.5m), the product of ^{186}W(n,p), and ^{183}Ta (T1/2=5.1d), the product of ^{183}W(n,p).

SS-316: This is an alloy of Fe, Ni, Cr, Mn and Mo. The major activity was ^{56}Mn; the product of ^{56}Fe(n,p), showing contribution more than 90 % in the spectra at cooling time less than 1 day. For the short irradiation, ^{49}Cr(T1/2=42.1m) was observed. Though the Mo constituent in SS-316 is small less than 3 %, γ-lines from ^{99}Mo and $^{99\mu}$Tc were clearly detected. Other γ-lines from ^{57}Ni, ^{58}Co, ^{57}Co were observed.

DISCUSSION

It is primarily of importance to select materials which reduce the dose rate and decayheat after shutdown to the tolerable levels to meet the criteria from the safety point of view. In this study, an attempt was made to extract a guide line from the experiment for that purpose. In order to make a direct comparative study, the γ-ray emission rates at various cooling times were modified by using half-lives to be those at certain cooling times (at 1800 sec and 54000 sec for the short and long irradiations, respectively). These data were analyzed from view points of difference in neutron spectra at the irradiation positions and difference in irradiation time (short and long). Figure 4 shows ratios of γ-ray emission rate materials at position B to those at position A. In addition, the total energy release rate data are obtained directly from γ-ray emission rate data and indirectly from the β-ray branching ratio data taken from the Table of Isotopes.[13] The ratios Both γ-ray emission rates and energy release corresponding tc respective irradiation runs are given in Figs. 5.1 to 5.4.

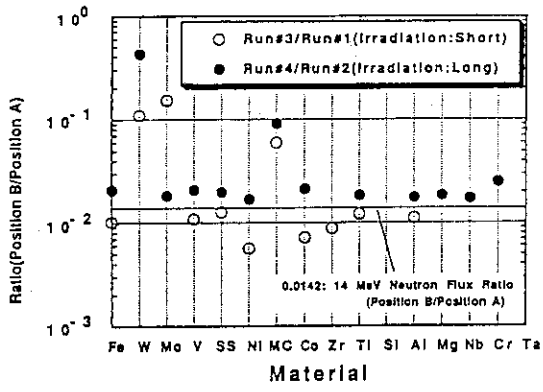

Fig. 4 Ratios of γ-ray emission rate materials at position B to those at position A.

Neutron spectrum dependence

The ratios shown in Fig. 4 indicates the dependence of the γ-ray emission rates on the spectrum change for the materials. The ratios for almost all materials except W, Mo and MnCu in the both irradiations fall in the range from 0.008 to 0.02. Although the ratios at position B give slightly higher value systematically than those at position A, they are very close to the ratio of 0.014 for the neutron fluxes above 10 MeV at position A and B. This fact suggested that the radioactivity productions are governed by the reactions with primary DT neutrons in many materials.

As noted in the section for γ-ray spectrum observation, the presence of (n,γ) reaction obviously becomes dominant for several materials at position B where the 14 MeV neutron fraction is less than 10 % of the total and flux below 1 MeV occupy more than 50 %. It is significant for the materials of W, Mo and MnCu, the γ-ray spectrum of which are governed by ^{187}W, ^{99}Mo and ^{56}Mn, the products of (n,γ) reaction, respectively.

As a result, it is concluded that not only 14 MeV neutrons, but also neutron reflected by the materials are highly important in the radioactivity assessment.

Time dependence on the γ-ray emission rate

Comparisons of Fig 5.1 with 5.2 and Fig. 5.3 with 5.4, give the irradiation and cooling time dependencies on the γ-ray emission rate as a function of material. For the short irradiation at position A, Fe gives the highest γ-ray emission rate. MnCu, SS-316, Al and Co follow the Fe. On the other hand, for the long irradiation, Al and Mg show the largest value and Fe, SS-316 and MnCu give quite low value. This trend is reasonably accepted by considering the half-lives of the dominant activities and production cross

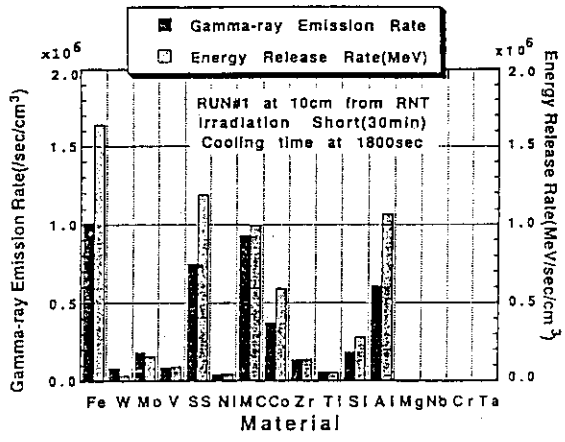

Fig. 5.1 Gamma-ray emission rates and energy release rates for the short irradiation, after 1800 sec cooling time, at position A.

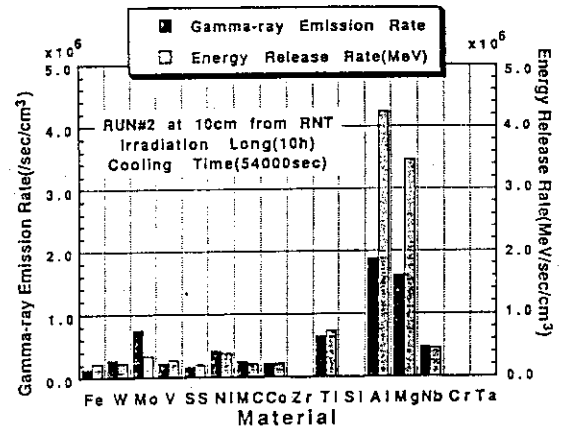

Fig. 5.2 Gamma-ray emission rates and energy release rates for the long irradiation, after 54000 sec cooling time, at position A.

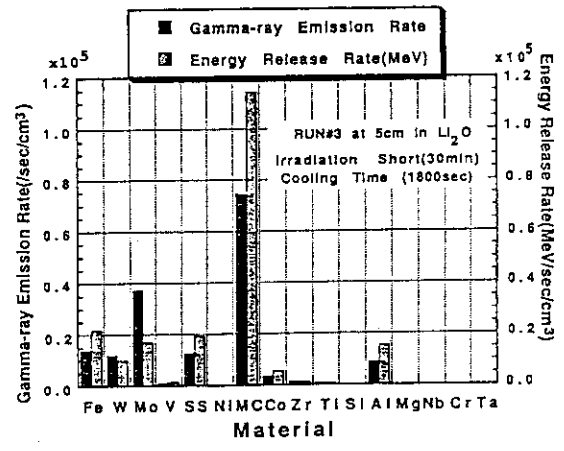

Fig. 5.3 Gamma-ray emission rates and energy release rates for the short irradiation, after 1800 sec cooling time, at position B.

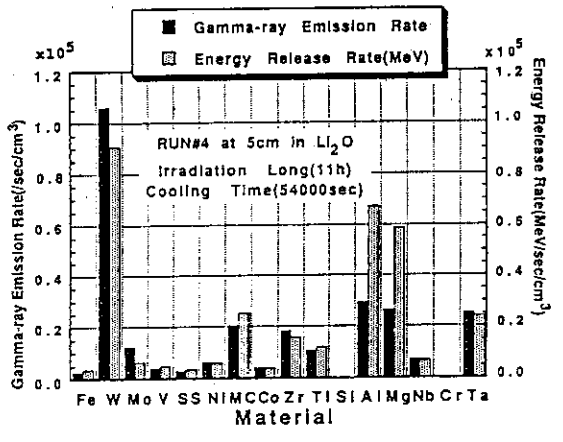

Fig. 5.4 Gamma-ray emission rates and energy release rates for the long irradiation, after 54000 sec cooling time, at position B.

section for the 14 MeV neutrons: the production of $^{24}Na(T1/2=15.02h)$ in Al and Mg was not saturated even after 10 h irradiation, beside the production of $^{56}Mn(T1/2=2.579h)$ in Fe, SS-316 and Mn and the production of $^{62}Cu(T1/2=9.73m)$in Cu were already saturated. The same trend are found in the case at position B except W. The increase in the γ-ray emission rate for the long irradiation is due to the same reason as in Al case; the half-life of ^{187}W, dominant activity in W, is 23.9h so that that the production is not saturated after 11h irradiation. The increase rate in the γ-ray is almost in proportion to the total neutron fluence.

Decayheat consideration

As shown in Fig 5.1 to 5.4, the values of energy release rates are, in general, in proportion to the intensity of γ-ray emissions. However, Al, Mg, Fe, SS-316 and Co give much larger energy release rates with respect to their γ-ray emission rates in comparison with the other materials. This is simply due to that the ^{24}Na and ^{56}Mn, the dominant activities, emit high energy γ-rays.

Up to now, we devoted discussion on the basis of the γ-ray emission. However, it is worthwhile to consider the β-ray contribution to the energy deposition. Bate energy release rate was deduced from the γ-ray intensity in corporation with the β-decay branching ration per disintegration. Table 4 gives the ratio of the fractions of β-ray in the total energy release rates for respective irradiation runs. It is evident that β-ray have considerable amounts of contribution to the total energy release in a number of materials. They range from a few % to 50 % of the total. They fall, in general, around 20 to 30 % to the

total. The lowest β-contribution was observed in Cr, and next is Ni. The fraction varied with irradiation time as well as cooling times. Especially, the MnCu in the short irradiation at position A presented the highest β-ray fraction, because of high Q-β value(3.9 MeV) of ^{62}Cu. In general, the short lived activity tends to have high Q-β value. This fact indicates the significant importance in the decayheat consideration in the short time range. Thus, productions of short life activities should be taken account into the material selection criteria though the activity disappear in quite short time range. In particular, it is very crucial in operation of fusion device in testing phase because the frequent personnel access for the maintenance is expected and also there should be a large possibility for the accidental failure of the reactor in the early stage of the operation.

Table 4. Contribution of β-ray to the total decay heat

Materials	β-ray contribution(%)			
	Run#1	Run#2	Run#3	Run#4
Fe	28.4	28.7	29.4	26.8
W	29.1	33.3	33.1	33.6
Mo	26.8	24.7	16.0	25.0
V	51.0	9.8	46.4	10.0
SS-316	28.9	24.1	29.3	22.1
Ni	11.6	5.0	5.1	5.2
MnCu	45.4	32.7	30.7	31.0
Co	28.9	22.0	29.9	9.8
Zr	36.9	----	34.6	11.1
Ti	15.2	10.9	17.0	11.0
Si	32.4	----	----	- - - -
Ta	----	----	----	- - - -

Impurity control

As observed in the spectra of materials of Si and Cr, it happened to yield intensive γ-rays from the unexpected products in the impurities. In some case it is possible to have activities more than 50 % of the total when cross sections of the impurity are orders of magnitude larger than the materials of interest: in soft neutron spectrum, the (n,γ) reaction is significant, while in the 14 MeV dominant field, the (n,2n) reaction takes place with large probability. The results for the Si and Cr are good evidence for this problems we experienced in this study.

CONCLUSION

The present integral experiment provided data for the verification of the radioactivity calculation code and data. Since all profiles of the radioactivity production and decay are governed by the neutron spectrum and their half-lives, the present analysis provides basic indices for the material selection concerning γ-ray emission characteristics relevant to the dose rate and decayheat estimation in the near term DT fusion device.

ACKNOWLEDGEMENTS

The US activities are supported by the US Department of Energy, Office of Fusion Energy.

REFERENCES

1. Y. Ikeda et al.,"An Experimental Study of Induced Activity in Type 316 Stainless Steel by Irradiation in D-T Neutron Fields," JAERI-M 83-177 (1983).
2. Y. Ikeda, et al.,"Measurements of Induced Activity in Type 316 Stainless Steel by Irradiation in D-T Neutron Fields," Fusion Technology., 8, 1466 (1985).
3. K. Oishi, et al.,"Experiment and Analysis of Induced Activities in Concrete Irradiated by 14 MeV Neutrons," Fusion Technology., 10, 579 (1986).
4. K. Oishi, et al.,"Measurement and Analysis of Induced Activities in Concrete Components Irradiated by 14 MeV Neutrons," to be published in Fusion Technology.
5. H. Iida and M. Igarashi,"THIDA Code System for Calculation of the Exposure Dose Rate Around a Fusion Device," JAERI-M 8019 (1978).
6. T. Nakamura, et al.,"A D-T Neutron Source for Fusion Neutronics Experiments as the JAERI," Proc. 7th Int. Conf. Ion Sources and Ion-Assisted Technology and 4th Int. Conf. Ion and Plasma-Assisted Techniques, Kyoto, Japan, Sep. 12-16, 1983.
7. Y. Oyama, et al.,"Measured Characteristics of Be Multi-Layered and Coolant Channel Blankets: Phase-IIC Experiments of the JAERI/USDOE Collaborative on Fusion Neutronis," Presented in this Meeting.
8. A. Kumar, et al.,"Analysis of Induced Activities Measurements Related to Decayheat in Phase-IIC Experimental Assembly: JAERI/USDOE Collaborative Program," Presented in this Meeting.
9. Y. Seki, et al., "THIDA-2: An Advanced Code System for Calculation of Transmutation, Activation, Decay Heat and Dose Rate", JAERI-1301 (1985).
10. F. M. Mann, " REAC2: Status of Codes and Libraries", Technology of Fusion Energy, 8th Topical Meeting, October 1988, Salt Lake City, Fusion Technology, March 1989.
11. D. L. Henderson and O. Yasar,"DKR-ICF: A Radioactivity and Dose Rate Calculation Code Package," Vol. 1 and 2, UWFDM-714 (1986).
12. Y. Seki and H. Iida,"Coupled 42-Group Neutron and 21-Group Gamma-ray Cross Section Sets for Fusion Reactor Calculations," JAERI-M 8818 (1980)
13. H. Baba,"Usage of the BOB 7-Series Program for the Analysis of Ge(Li) Gamma-ray Spectra," JAERI-M 7017 (1977).
14. C. M. Lederer and V. S. Shirley,"Table of Isotopes," Seventh Edition, John Wiley and Sons, Inc., New York (1978).

A.3

ANALYSIS OF INDUCED ACTIVITIES MEASUREMENTS RELATED TO DECAY HEAT IN PHASE IIC EXPERIMENTAL ASSEMBLY: USDOE /JAERI COLLABORATIVE PROGRAM ON FUSION NEUTRONICS EXPERIMENTS

A.Kumar, M.A.Abdou
School of Engineering and Applied Science
University of California at Los Angeles (UCLA)
Los Angeles,California 90024, USA

Y.Ikeda, T.Nakamura
Japan Atomic Energy Research Institute
Tokai, Ibaraki 319-11, Japan

ABSTRACT

The selection of materials and design options for fusion device components depends crucially on the level of radioactivity and decayheat induced in the components subject to D-T neutron irradiation. An experimental program was carried out to obtain decay γ emission spectra from samples of Fe, Ni, Cr, MnCu alloy, Ti, Mo, Zr, Ta, W, Si, Mg, Al, V, Nb, SS316, $YBa_2Cu_3O_7$ and $ErBa_2Cu_3O_7$, which were subjected to simulated fusion neutron environment. Cooling times obtained ranged from 10 min to 7 days. The experimental results have been analyzed using four leading radioactivity codes: DKRICF, REAC, RACC and THIDA. The integrated decay γ emission rates (over 100 KeV to 3 MeV) have been compared in addition to decay γ emission spectra. It is observed that : (i) generally, much better agreement is found between computed (C) and experimentally measured (E) values for integrated γ emission rates as against the detailed γ spectra, (ii) C/E ratios for integrated γ emission rates are found to range from 0.001 to 300, though most of the ratios cluster between 1 to 2. Significant discrepancies are obtained on C/E ratios for a number of cases for the four codes used above. Most of the observed discrepancies are due to (a) missing or wrong fundamental decay γ–ray data, e.g., (1) missing decay data in DKRICF for ^{186}Ta, ^{187}W, ^{181}W, ^{90m}Y, ^{86}Rb, ^{88}Y, etc., (2) wrong decay γ–intensities for W products in THIDA, (b) inaccurate activation cross sections, e.g., for V, Zr, Mo in DKRICF, RACC, REAC, (c) errors on computed neutron energy spectra, (d) various experiment related factors, essentially poor counting statistics for weak neutron induced reactions.

I. INTRODUCTION

Induced radioactivity level is an important parameter for characterizing design of a fusion machine. All materials used therein are subject to production of induced activity as soon as they are exposed to fusion neutrons. Currently, there is a large uncertainty associated with the activation and decay data bases of radioactivity calculation codes, e.g., DKRICF[1], RACC[2], REAC[3] and THIDA[4], due to rather narrow experimental data base for materials under consideration for fusion devices, e.g., ITER[5], NET[6] and FER[7]. An experiment to validate these codes was conducted to obtain γ-ray spectra emerging from a number of materials, e.g., Fe, Ni, Cr, Mn, Ti, Mo, Zr, Ta, W, Si, Mg, Al, V, Cu, Nb, SS316, Au, In, Mg, Al, Nb, Ta, $YBa_2Cu_3O_7$ and $ErBa_2Cu_3O_7$, which were subjected to simulated fusion neutron environment[8-9]. Of these, $YBa_2Cu_3O_7$ and $ErBa_2Cu_3O_7$ (on substrate of yttria stabilized zirconia) are known high temperature superconductors, and Au, In, Mg, Fe, Al, Nb, and Ta were also intended to serve as dosimetry foils for monitoring neutron energy spectrum. The experiment was performed during phase IIC of USDOE/JAERI collaborative program on fusion neutronics. Samples of different materials were irradiated at two locations, at 10 and 82 cm from target, inside coolant channel assembly of phase IIC[10-11]. Figure 1 shows the schematic of the arrangement.

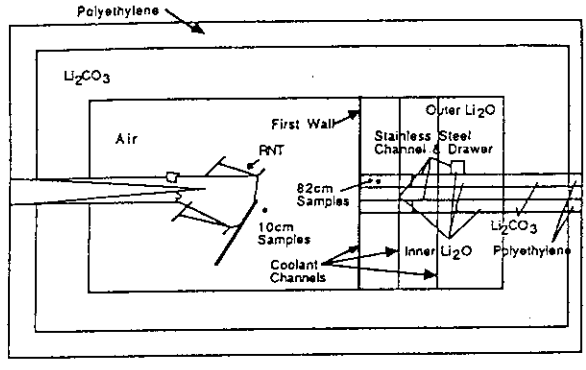

Figure 1: Schematic arrangement of samples in Phase IIC coolant channel assembly.

Two separate irradiation programs were executed to cover each of the two locations. Two foil packets were irradiated at each location to individually focus on: (i)shorter half life products (less than 1 hour half life), (ii)longer half life products (1 hour to 5 year half life). Each irradiation program consisted of initial half an hour irradiation followed by pulling out of one of the two packets. The γ-spectroscopy of the foils in this packet was to cover primarily shorter half life products. The total irradiation periods were 9 and 10 hours respectively for the locations at 10 and 82 cm, logging average source neutron intensities of $8.75.10^{11}$ and $1.12.10^{12}$ n/s. The γ-spectroscopy of each sample was done using four intrinsic germanium detectors and for multiple cooling periods ranging from 20 m to 10 d. Three detectors were relatively calibrated with respect to an absolutely calibrated standard detector.

The experimental data was treated to obtain spectra of decay γ emission rate per g of the irradiated specimen (see Section II). These quantities were also computed using leading radioactivity calculation packages: DKRICF, REAC,

RACC, THIDA (Section III). The measured and computed decay γ-emission rates were then intercompared (Section IV).

II. TREATMENT OF EXPERIMENTAL DATA

Figure 2 is a flow diagram depicting what is broadly involved in intercomparison of measured and computed decay γ spectra. γ pulse-height spectrum for a sample for a each cooling time is processed by a spectrum analysis code BOB75[12] to obtain gamma ray intensity spectrum. Then background is subtracted. The resulting spectrum is then corrected for detector efficiency and attenuation of decay γ's emitted in a sample. Variation of source neutron intensity during irradiation is accounted for to finally obtain decay γ emission rate per g for a normalizing source neutron intensity of 10^{12} n/s. It is to be added that standard deviation on each γ-peak is a function of many parameters, e.g., neutron flux, counting time, waiting time, counting efficiency, activation cross-section, half-life of γ-peak emitter, γ-yield etc. It is insufficient to characterize this standard deviation by a single factor, even as, γ-emitters with longer half lives can be expected to carry larger errors. It is interesting to look at Fig. 3 that shows % standard deviation as a function of product half life for a nickel sample irradiated at 10 cm distance from target for 9 hours. It is hard to extract any systematic trends as a function of a single parameter as already outlined earlier.

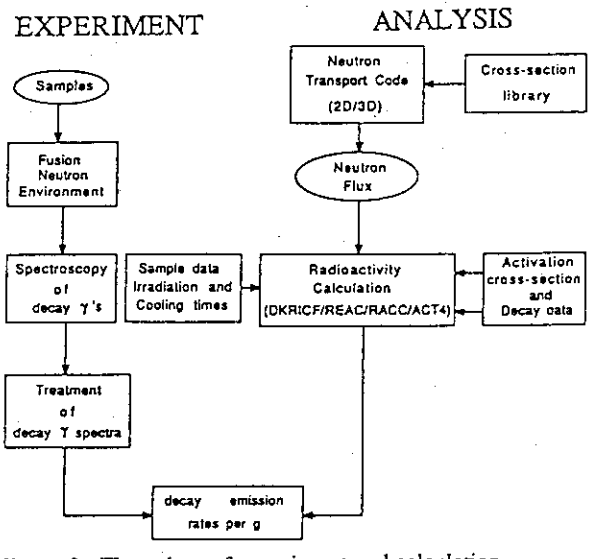

Figure 2: Flow chart of experiment and calculation.

III. ANALYSIS

As shown in Figure 2, analysis to obtain decay γ emission rate involves a multi-step procedure. A two or three dimensional transport code is employed to get neutron energy distribution, i.e.,neutron flux, at spatial locations of samples. Geometry and material composition of irradiation environment are important inputs for this calculation. Next stage involves computation of decay γ emission spectrum using a radioactivity calculation code. Neutron flux, sample composition, irradiation and cooling (or shutdown) times are required input data for this stage. Decay and activation cross-section libraries form part of the code used. Leading codes used for this purpose include DKRICF, REAC, RACC and THIDA. In fact, THIDA is a code system that includes neutron flux calculating modules too. However, its central module is ACT4 that calculates induced radioactivity and associated quantities.

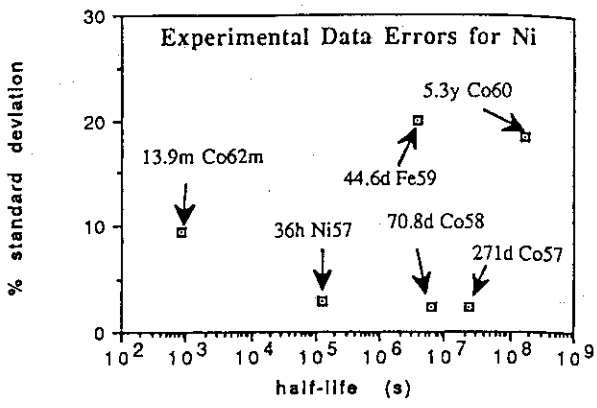

Figure 3: Percent Standard deviation on measured decay γ emission rate as a function of product half life for a nickel sample

Table 1

Radioactive Products from Stainless Steel and Tungsten Samples

(3m < half life < 5 y)

Sample-material	Half-life	Product	γ-energy (dominant)	Reaction
SS316	3.76 m	^{52}V	1434 KeV	^{55}Mn(n,α); ^{52}Cr(n,p)
	5.8 m	^{51}Ti	320 KeV	^{54}Cr(n,α)
	8.5 m	^{53}Fe	378 KeV	^{54}Fe(n,2n)
	10.5 m	^{60m}Co	58.6 KeV	^{60}Ni(n,p)
	13.9 m	^{62}Co	1173 KeV	^{62}Ni(n,p)
	14.6 m	^{101}Mo	192 KeV	^{100}Mo(n,γ)
	15.5 m	^{91}Mo	1634 KeV	^{92}Mo(n,2n)
	41.9 m	^{49}Cr	91 KeV	^{50}Cr(n,2n)
	51.5 m	^{98m}Nb	723/787 KeV	^{100}Mo(n,t),^{98}Mo(n,p)
	72 m	^{97}Nb	658 KeV	Mo(n,p), (n,n'p),(n,d)
	1.65 h	^{61}Co	67 KeV	Ni(n,n'p), (n,α)
	2.52 h	^{65}Ni	1482 KeV	^{64}Ni(n,γ)
	2.58 h	^{56}Mn	847 KeV	^{56}Fe(n,p);^{55}Mn(n,γ)
	18.9 h	^{97}Zr	743 KeV	^{100}Mo(n,α)
	23.4 h	^{96}Nb	569/778 KeV	Mo(n,p),(n,n'p)
	36 h	^{57}Ni	1373 KeV	^{58}Ni(n,2n)
	78.4 h	^{89}Zr	909 KeV	^{92}Mo(n,α)
	10.14 d	^{92m}Nb	935 KeV	^{92}Mo(n,p)
	15.97 d	^{48}V	984 KeV	^{50}Cr(n,t)
	27.7 d	^{51}Cr	320 KeV	^{54}Fe(n,α);^{52}Cr(n,2n)
	44.6 d	^{59}Fe	1099 KeV	^{62}Ni(n,α)
	70.8 d	^{58}Co	811 KeV	^{58}Ni(n,p)
	271 d	^{57}Co	122 KeV	^{58}Ni(n,n'p),(n,d)
	312.2 d	^{54}Mn	835 KeV	^{54}Fe(n,p); ^{55}Mn(n,2n)
	5.27 y	^{60}Co	1332 KeV	^{60}Ni(n,p)
W	10.5 m	^{186}Ta	198 KeV	^{186}W(n,p)
	49.5 m	^{185}Ta	178 KeV	^{186}W(n,n'p), (n,d)
	64 m	^{183}Hf	784 KeV	^{186}W(n,α)
	23.9 h	^{187}W	480 KeV	^{186}W(n,γ)
	5 d	^{183}Ta	246 KeV	^{183}W(n,p)
	115 d	^{182}Ta	1121 KeV	^{182}W(n,p)
	121 d	^{181}W	136 KeV	^{180}W(n,γ)

Table 2
Chemical Composition of Primary Impurities in the Samples Used in Induced Activity Irradiations of December, 1988

Sample Material	Chemical Composition by Maximum weight %
Iron (Fe)	99.92 Fe, 0.059 Mn, 0.02 C
Nickel (Ni)	99.97 Ni, 0.016 C
Molybdenum (Mo)	99.93, 0.03 W, 0.01 Fe
Stainless Steel@ (SS316)	66.22 Fe, 17.75 Cr, 11.60 Ni, 2.08 Mo, 1.33 Mn, 0.42 Si, 0.19 Co, 0.34 Cu, 0.06 V
Manganese Copper Alloy+ (MnCu)	79.78 Mn, 19.66 Cu, 0.46 Ni, 0.07 Fe
Vanadium (V)	99.82 V, 0.044 Si, 0.03 Ta, 0.03 O, 0.013 Mo, 0.01 Zr, 0.01 Fe, 0.01 Al, 0.01 Hf
Titanium (Ti)	99.79 Ti, 0.12 O, 0.06 Fe, 0.02 C
Aluminum (Al)	99.97 Al, 0.006 Mg
Cobalt (Co)	99.95 Co, 0.04 Ni
Tungsten (W)	99.97 W, 0.008 Si
Niobium (Nb)	99.91 Nb, 0.018 Ta, 0.01 Zr
Zirconium (Zr)	99.76 Zr, 0.10 Fe, 0.09 Si, 0.03 Ti
Indium (In)	99.99 In, 0.003 Cu
Tantalum (Ta)	99.98 Ta, 0.007 Fe
Magnesium (Mg)	99.78 Mg, 0.10 Al, 0.07 Zr, 0.02 Mn, 0.01 Si

Two calculational schemes were followed for analysis. First scheme related to use of externally evaluated neutron flux with four radioactivity codes: DKRICF, REAC, RACC and ACT4. The flux was obtained in a two step process: (1)source neutron energy and angular distribution was obtained by 3D MCNP[13] modeling of rotating neutron target (RNT) of fusion neutronics source (FNS) facility , (2)source neutron distribution from MCNP was input to RUFF[14] and DOT4.3[15] code system to compute spatial distribution of neutron flux. 30 group MATXS5 cross-section library of LANL was used for neutron transport. The neutron flux was also obtained by full-fledged MCNP caculation and was found to match the flux via the foregoing approach. As neutron energy group boundaries are different for the radioactivity codes used, flux transformation from one group structure to another was carried out subject to total neutron flux conservation. It is evident that this will add to total numerical error entailed in decay rate computation. However, it should not amount to more than a percent for most of the cases. The second calculational scheme is similar to the one in reference 16, wherein THIDA code is employed for whole analysis.

Multitude of neutron induced reactions and range of product half lives can be gauged from Table 1 which lists γ-emitting radioactive products, of half life from 3m to 5y, for stainless steel and tungsten samples. Primarily, dominant γ-energies are shown. In all, more than 150 γ-emitting products are of interest, covering all samples. Table 2 lists compositions of various foil materials. These compositions have been provided by commercial suppliers of these samples.

IV. RESULTS AND DISCUSSION

Tables 3a to 3d summarize results of comparison of integrated, from 100 KeV through 3 MeV, decay γ-emission rates per g normalized to source intensity of 10^{12} n/s. The computed results from REAC-2, DKRICF and THIDA-2 are included. RACC results generally follow same trends as those from DKRICF, though spectral distributions of decay γ-emission rates differ at times. Large deviations in C/E (Computed/Experimental) ratio are observed for Mo, W, MnCu alloy, Cr, Zr, Ta and $YBa_2Cu_3O_7$. Tables 3a to 3c show upper and lower bounds of C/E ratios for integrated decay emission rates for the three codes as a function of irradiated material. Though C/E ratios for Fe, Ni, Mo, SS316 and many other materials behave reasonably well, large discrepancies are seen for spectral distributions. Figures 5a to 5f typically bring home this aspect. The materials covered include Iron, Nickel, Molybdenum, Stainless Steel (SS316) and Tungsten. The experimental data displayed is of two kinds: energy-group integrated for direct comparison, and gamma-ray peak-wise data for detailed break-down. tr and tcool respectively stand for irradiation and cooling times.Table 4 lists important radioactive products and gamma rays observed during measurements for some of the materials. Specific observations follow for few materials.

IV.A. Iron

^{56}Mn dominates for short cooling times, ^{54}Mn takes over at longer cooling times; other contributors include ^{51}Cr and ^{58}Co (nickel impurity). Some samples showed also presence of nickel/aluminum/magnesium impurities. REAC and ACT4 (a component module of THIDA) have, generally, more reliable γ-emission data. RACC cross-section data for ^{56}Fe(n,p)^{56}Mn are closest to published experimental ones. γ-yield data is generally the lowest for ACT4 even as the activation cross-sections are quite close to others. DKRICF lacks γ-yield data for gamma-rays carrying more than 2.5 MeV. In spite of all these differences, the evaluated and measured reaction rates for ^{56}Mn, ^{54}Mn and ^{51}Cr agree within 15%, even though, the softer spectrum, at distance of 82 cm from target, tends to raise C/E ratios.

IV.B. Nickel

^{62m}Co and ^{57}Ni dominate at short cooling times. At longer cooling times, ^{58}Co, ^{57}Co, ^{57}Ni, ^{59}Fe, ^{60}Co dominate. REAC strongly overestimates (by at least a factor of 2) contributions from ^{58}Co and ^{59}Fe. Also ^{57}Co is overestimated by as much as 25%. C/E for ^{57}Co for DKRICF is in the range of 0.97 to 1.08 for all cases; C/E for ^{58}Co ranges from 0.0.97 to 1.24; C/E for ^{59}Fe is 0.82 for DKRICF as against 2.61 for REAC2; C/E for ^{60}Co is 0.83 as against 1.63 for REAC2.

IV.C. Molybdenum

For short cooling times, ^{97}Nb, ^{98m}Nb, ^{99}Mo,^{99m}Tc, ^{96}Nb, ^{101}Mo, ^{101}Tc, ^{93m}Mo and ^{91}Mo contribute predominantly. ^{99m}Tc and ^{101}Tc respectively result from β$^-$ decays of ^{99}Mo and ^{101}Mo. Longer cooling times see dominance of ^{99}Mo, ^{99m}Tc, ^{96}Nb, ^{97}Nb and ^{89}Zr. ^{91}Mo

Table 3a
Comparison of Measured and Computed Decay γ Emissions/s/g of Material per 10^{12} source neutron/s

Material	Distance from Source	Irradiation Time	Cooling Time	Counting Time	C/E REAC-2	C/E DKRICF	C/E THIDA
Fe	10 cm	30 m	22.4 m	10 m	0.85	0.98	0.91
	10 cm	9 h	3h 22.3m	22.4 m	1.00	1.17	1.06
	10 cm	9 h	5d 13.7h	5h 16.9m	0.95	1.00	1.02
	82 cm	30 m	24.0 m	10 m	1.10	1.22	1.06
	82 cm	10 h	5h 1m	44.8 m	1.01	1.13	---
	82 cm	10 h	17h16.2m	39.8 m	0.98	1.14	0.97
Ni	10 cm	30 m	56.3 m	30.9 m	1.10	1.18	0.88
	10 cm	9 h	2h 26.7m	42.9 m	1.13	1.24	1.01
	10 cm	9 h	16h 23.7m	44.7 m	1.17	1.24	1.01
	10 cm	9 h	4d 13h	8h 41.9m	1.30	1.04	---
	82 cm	30 m	58.8 m	26.6 m	1.89	2.02	1.17
	82 cm	10 h	3h 52.7m	1h 2.8m	1.12	1.20	0.88
	82 cm	10 h	2d 17.6h	4h 13.2m	1.39	1.23	1.09
Mo	10 cm	30 m	46.3 m	30.5 m	6.99	2.55	1.22
	10 cm	9 h	1h 38.2m	43.8 m	2.09	1.55	1.51
	10 cm	9 h	15h 11.8m	1h 5.5m	1.21	1.22	1.21
	10 cm	9 h	19h 42.3m	2h 46.7m	1.37	1.42	1.14
	10 cm	9 h	4d 3.7h	15h 28.6m	1.18	1.22	---
	82 cm	30 m	58.8 m	26.6 m	3.39	1.85	1.11
	82 cm	10 h	2h 28.5m	38.2 m	5.40	1.26	---
	82 cm	10 h	9h 15.8m	4h 2.2m	3.57	1.41	---
SS316	10 cm	30 m	37.3 m	14.6 m	0.86	0.95	0.98
	10 cm	9 h	1h 38.8m	42.4 m	0.92	1.06	0.92
	10 cm	9 h	4h 31m	2h 46.7m	1.04	1.20	0.97
	10 cm	9 h	15h 16.8m	1h 0.5m	1.14	1.23	0.98
	10 cm	9 h	3d 21.8h	13h 54.6m	1.35	1.15	---
	82 cm	30 m	39.2 m	15.1 m	1.11	1.16	1.15
	82 cm	10 h	3h 13.2m	33.9 m	0.84	0.88	0.94
	82 cm	10 h	1d15h53m	21h 48.8m	1.24	1.16	0.79

Table 3b
Comparison of Measured and Computed Decay γ Emissions/s/g of Material per 10^{12} source neutron/s

Material	Distance from Source	Irradiation Time	Cooling Time	Counting Time	C/E REAC-2	C/E DKRICF	C/E THIDA
Nb	10 cm	9 h	4h 31m	2h 46.7m	1.27	0.87	0.75
	10 cm	9 h	18h 49.5m	44.5 m	1.09	1.05	0.88
	82 cm	10 h	13h 39m	1h 13.7m	1.25	1.13	0.82
Co	10 cm	30 m	37.3 m	15 m	0.84	1.03	0.85
	10 cm	9 h	3h 17.2m	29.2 m	1.40	1.27	1.11
	10 cm	9 h	17h 15.7m	40.5 m	2.13	1.24	1.11
	10 cm	9 h	5d19h9m	3h 21.5m	2.10	1.23	---
	82 cm	30 m	39.3 m	15.1 m	1.51	1.58	1.23
	82 cm	10 h	3h 53m	1h 2.7m	1.40	1.16	---

Table 3c
Comparison of Measured and Computed Decay γ Emissions/s/g of Material per 10^{12} source neutron/s

Material	Distance from Source	Irradiation Time	Cooling Time	Counting Time	C/E REAC-2	C/E DKRICF	C/E THIDA
V	10 cm	30 m	22.3 m	10 m	1.06	1.35	0.90
	10 cm	9 h	3h 42.2m	36.1 m	1.57	3.38	1.59
	10 cm	9 h	17h 16.2m	39.8 m	1.55	3.35	1.59
	82 cm	30 m	24 m	10 m	1.31	1.81	1.09
	82 cm	10 h	5h 1.7m	44.9 m	1.44	3.18	1.40
	82 cm	10 h	2d22h26m	14h 51.3m	1.41	3.11	1.20
Ti	10 cm	30 m	22.3 m	10 m	1.69	1.24	0.72
	10 cm	9 h	3h 51.5m	29.2 m	1.28	1.15	0.74
	10 cm	9 h	18h 11m	1h 20.5m	1.16	1.12	- - -
	82 cm	30 m	24.3 m	10 m	1.73	1.62	0.58
	82 cm	10 h	7h 27.5m	1h 43.4m	1.24	1.43	0.67
W	10 cm	30 m	37.3 m	15.5 m	3.07×10^{2}	0.20	0.99*(2.19)
	10 cm	9 h	2h 26.5m	44.2 m	2.55	2.86×10^{-2}	0.82*(2.38)
	10 cm	9 h	16h 23.4m	45.7 m	2.28	1.27×10^{-2}	0.76*(2.38)
	10 cm	9 h	2d19h3.5m	18h 22.7m	2.05	4.05×10^{-2}	0.70*(2.26)
	82 cm	30 m	39.2 m	15.1 m	1.38×10^{1}	7.00×10^{-3}	0.65*(2.11)
	82 cm	10 h	3h 13.5m	33.5 m	2.26	4.88×10^{-4}	0.96*(3.17)
	82 cm	10 h	4d 5.3m	13h 32.2m	2.59	2.35×10^{-3}	0.91*(2.99)
Zr	10 cm	30 m	56.5 m	18.9 m	4.13	0.82	1.21
	10 cm	9 h	2h 26.5m	43.5 m	5.58	1.08	- - -
	10 cm	9 h	17h 15.7m	40.0 m	5.81	1.16	- - -
	82 cm	30 m	58.3 m	27.1 m	4.30	0.88	1.13
	82 cm	10 h	3h 13.5m	33.7 m	4.10	0.83	1.31
MnCu	10 cm	30 m	12.3 m	10 m	3.35	3.42	1.04
	10 cm	9 h	2h 26.7m	44.0 m	1.75	1.19	0.83
	10 cm	9 h	16h 23.7m	45.7 m	1.21	0.29	0.26
	10 cm	9 h	6d20h59m	4h 50.3m	1.09	1.11	- - -
	82 cm	30 m	24.3 m	10 m	2.52	2.42	1.49
	82 cm	10 h	3h 52.7m	1h 2.2m	2.19	2.03	1.40
	82 cm	10 h	3d13h28m	6h 44.9m	1.24	1.00	0.80
Cr	10 cm	9 h	1h 38.8m	43.0 m	2.95	1.35	0.55
	10 cm	9 h	15h 16.8m	1h 0.5m	1.54	1.05	0.88
	82 cm	10 h	2h 27.5m	1h 19.6m	2.95	1.67	0.64

*several γ-rays 'unreasonably' overestimated in the library are suppressed

contribution is strongly overestimated by REAC. C/E ratios for this isotope are 328 and 307 respectively in 1.5-2 and 2.5-3 MeV ranges respectively. Other products are strongly underestimated by REAC. It is seen from experimental data that ratio of γ-yields for 778 to 569 KeV peaks from ^{96}Nb is 3.1 instead of 1.74 (see ref. 17); it is to be added here that quite possibly the balance of contribution for 778 KeV peak pertains to 66h ^{99}Mo. Respective C/E ratios for different products for REAC2 and DKRICF are: (1)^{93m}Mo: 200/1.11, (2)^{96}Nb: 2.04/3.49, (3)^{99}Mo: 1.08/1.11, (4)$^{89m+g}$Zr: 6/1.35, (5)^{97}Nb: 2.68/2.57, (6)^{95}Nb: 2/2.5, (7)^{95m}Nb: 0.77/0.20, (8)^{92m}Nb: 0.90/0.90, (9)^{95}Zr: 0.87/0.86.

IV.D. MnCu Alloy

^{56}Mn, ^{62}Cu, ^{52}V, ^{62m}Co and ^{65}Ni are most important contributors for short cooling times. ^{54}Mn dominates larger cooling times. 511 KeV γ from ^{62}Cu is overestimated by a factor of more than 3 by REAC2 and DKRICF. C/E ratios are found considerably larger than 1 for ^{56}Mn. In fact, even for other materials, there is a general trend for the codes to predict larger C/E ratios for (n,γ) reactions in presence of softer neutron energy spectrum (at 82 cm from target). REAC gives C/E ratios close to 1 for ^{54}Mn. DKRICF and REAC generally agree between themselves from 0.1 to 2.5 MeV.

Table 3d
Comparison of Measured and Computed Decay γ Emissions/s/g of Material per 10^{12} source neutron/s

Material	Distance from Source	Irradiation Time	Cooling Time	Counting Time	C/E REAC-2	C/E DKRICF	C/E THIDA
Al	10 cm	30 m	1h 15.8m	11.4 m	0.98	1.02	1.17
	10 cm	9 h	4h 31m	2h 46.7m	0.88	0.92	1.06
	82 cm	30 m	58.3 m	27.1 m	1.34	1.39	1.05
	82 cm	10 h	5h 52.3m	1h 28.5m	1.03	1.07	1.12
Si	10 cm	30 m	37.3 m	15 m	2.80	1.08	1.14
Mg	10 cm	9 h	3h 51.7m	26.3 m	1.16	1.07	0.99
	10 cm	9 h	18h 11.7m	31.5 m	1.08	1.00	---
	82 cm	10 h	5h 2m	44.2 m	1.37	1.28	1.25
In	10 cm	9 h	1h 38.2m	42.9 m	1.06	1.08	---
	10 cm	9 h	16h 23.7m	45.7 m	2.62	0.18	---
	82 cm	10 h	2h 28.5m	38 m	1.11	1.52	---
Ta	10 cm	9 h	3h 17.2m	28.2 m	3.67	0.35	---
	10 cm	9 h	18h 11.7m	35.4 m	2.03	0.83	---
	82 cm	10 h	3h 53m	1h 2.7m	1.74	1.53	0.19
Au-thick	10 cm	9 h	3h 51.7m	25.9 m	1.71	0	---
	10 cm	9 h	18h 49.5m	43.7 m	2.16	0	---
	82 cm	10 h	5h 2m	44.2 m	6.43	0	---
Au-thin	10 cm	9 h	4h 31m	2h 46.7m	1.33	0	---
	10 cm	9 h	19h 42m	2h 46.7m	1.57	0	---
$YBa_2Cu_3O_7$	10 cm	30 m	1h 32m	2h 32.9m	0.97	0.31	---
	10 cm	30 m	4h 12m	4h 31.2m	0.73	4.38×10^{-2}	---
	10 cm	30 m	7d2h26.1m	2h 50.4m	0.72	1.30×10^{-3}	---
$ErBa_2Cu_3O_7$	10 cm	30 m	1h 33m	2h 34.3m	6.20	1.06	---
	10 cm	30 m	4h 12.5m	4h 33.5m	7.69	1.30	---
	10 cm	30 m	11d4h47m	3h 34.7m	0.58	0.12	---

IV.E. Chromium

Dominant contributors are ^{51}Cr and ^{49}Cr. 847 and 1811 KeV peaks of ^{56}Mn are also detected- Fe/Mn impurity is expected. Unidentified peaks at 147, 563, 573 and 601 KeV were observed. ^{48}V contribution was absent. However, REAC predicts a large contribution from this isotope; γ-yield data appears acceptable. As a result, C/E (=6.2) is strongly overpredicted in 0.4-1 MeV range. DKRICF has C/E of 2.2 for the same range. REAC yields C/E of 2.63 for ^{49}Cr, whereas DKRICF yields a value of 0.96.

IV.F. Stainless Steel (SS316)

^{56}Mn contributes overwhelmingly at short cooling times. At larger cooling times, ^{99}Mo, ^{99m}Tc, ^{51}Cr, ^{58}Co, ^{57}Ni, and ^{54}Mn are leading contributors. C/E trends for individual contributors are same as discussed before for Fe, Ni, Cr and Mo.

IV. G. Vanadium

Short cooling times bring leading contibutions from ^{51}Ti, ^{52}V and ^{48}Sc. Larger cooling times bring out total dominance of ^{48}Sc. C/E ratios, from REAC, are 1.01 and 0.86 respectively for ^{51}Ti and ^{52}V at 10 cm location. C/E ratio of 1.5 is found for the same location for ^{48}Sc by the same code. For DKRICF, C/E for ^{48}Sc is ~3.

IV. H. Zirconium

^{89}Zr, ^{87m}Sr, ^{90m}Y, ^{94}Y, ^{92}Y and ^{91}Sr contribute at short cooling times. Larger cooling times bring out predominance of ^{89}Zr and ^{90m}Y. REAC largely overpredicts C/E (factor of 4 to 5) for both ^{89}Zr and ^{90m}Y. For ^{91m}Y, C/E is 1.7. However, C/E for ^{87m}Sr is close to 1 for REAC and is just 0.4 for DKRICF. Nevertheless, DKRICF has good agreement with the experimental data otherwise.

Table 4:

Important Radioactive Products and Prominent Gamma-ray Peaks

Irradiated Material	Products/γ-ray peaks
Fe	8.5m ^{53}Fe: 378 KeV 2.6h ^{56}Mn: 847/1811/2113/2523/2658 /2960/3370 KeV 27.7d ^{51}Cr: 320 KeV 44.6d ^{59}Fe: 143/192/334.8/1099/1292 KeV 312.2d ^{54}Mn: 835 KeV
Cr	41.9m ^{49}Cr: 91/153/1362/1423/1508/1515 /1570 KeV 15.97d ^{48}V: 984/1312/2240 KeV 27.7d ^{51}Cr
Ni	13.9m ^{62m}Co: 778/875/1129/1164/1173/ 1719/2004/2105 KeV 2.5h ^{65}Ni: 366/1116/1482/1623/1725 KeV 36h ^{57}Ni: 127/1377/1757/1919 KeV 44.6d ^{59}Fe: 143/192/1099/1292 KeV 70.8d ^{58}Co: 811/864/1674 KeV 271d ^{57}Co: 122/137/692 KeV 5.27y ^{60}Co: 1173/1332 KeV
MnCu alloy	8.76m ^{52}V: 1332/1434/1531 KeV 9.8m ^{62}Cu: 511/876/1173 KeV 13.9m ^{62m}Co, 2.6h ^{56}Mn, 2.52h ^{65}Ni 12.9h ^{64}Cu: 1346 KeV 312.2d ^{54}Mn, 5.27y ^{60}Co
Mo	14.2m ^{101}Tc: 127/184/307/545 KeV 14.6m ^{101}Mo: 192/409/506/591/696/934/ 1013/1161/1251/2032 KeV 15.5m ^{91}Mo: 1582/1634/2632 KeV 51.5m ^{98m}Nb: 173/355/645/714/723/787/ 792/824/834/996/1169/1432/1511 KeV 72m ^{97}Nb: 658/1025/1269/1516 KeV 6.95h ^{93m}Mo: 263/685/1477 KeV 16.9h ^{97}Zr: 355/508/743/1148 KeV 23.4h ^{96}Nb: 460/569/778/1091/1200 KeV 66h ^{99}Mo: 141/181/366/739/778 KeV 6.02h ^{99m}Tc: 141 KeV 78.4h ^{89}Zr: 909/1621/1657/ 1713/1745 KeV 87h ^{95m}Nb: 204/786 KeV 10.14d ^{92m}Nb: 913/935/1848 KeV 35d ^{95}Nb: 766 KeV 64d ^{95}Zr: 724/757 KeV

Table 4 (Continued)

W	10.5m ^{186}Ta: 122/198/215/274/308/418/615/738 KeV 64m ^{183}Hf: 459/398/784/1470 KeV 23.9h ^{187}W: 134/480/552/618/ 689/773 KeV 5d ^{183}Ta: 246/354 KeV 115d ^{182}Ta: 155/222/230/264/266/1121/1189/1221/ 1231/1257 KeV
Ta	5.5h ^{180m}Hf: 93/215/332/443/501 KeV 8h ^{180m}Ta: 93/103 KeV 115d ^{182}Ta
Zr	18.7m ^{94}Y: 551/919/1139 KeV 49.7m ^{91m}Y: 556 KeV 72m ^{97}Nb: 658 KeV 2.81h ^{87m}Sr: 388 KeV 3.19h ^{98m}Y: 203/480 KeV 3.54h ^{92}Y: 449/935/1405 KeV 9.48h ^{91}Sr: 556/653/750/1024 KeV 16.9h ^{97}Zr: 743 KeV 78.4h $^{89m+g}$Zr: 909/1713 KeV 64d ^{95}Zr: 724/757 KeV
Ti	5.8m ^{51}Ti: 320/609/929 KeV 3.1h ^{45}Ti: 720 KeV 3.9h ^{44}Sc: 1157 KeV 43.7h ^{48}Sc: 175/984/1038/1213/1312 KeV 3.42d ^{47}Sc: 159 KeV 83.8d ^{46}Sc: 889/1121 KeV

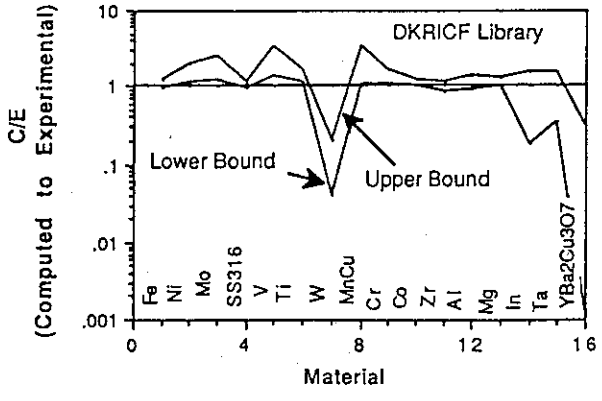

Figure 4a: Measured and DKRICF computed decay γ integrated decay rate: Comparison

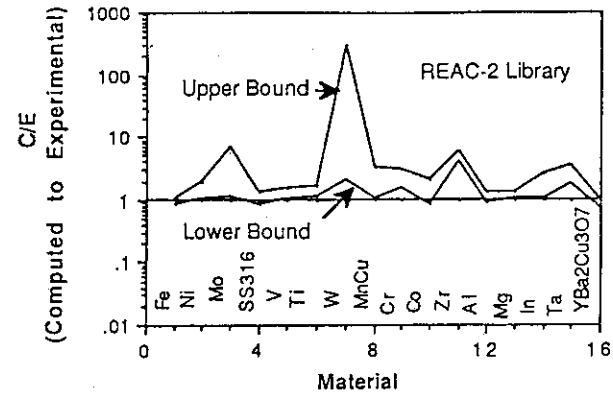

Figure 4b: Measured and REAC-2 computed decay γ integrated decay rate: Comparison

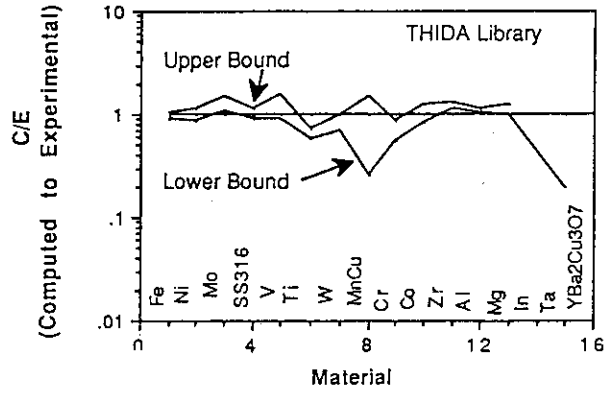

Figure 4c: Measured and THIDA-2 computed decay γ integrated decay rate: Comparison

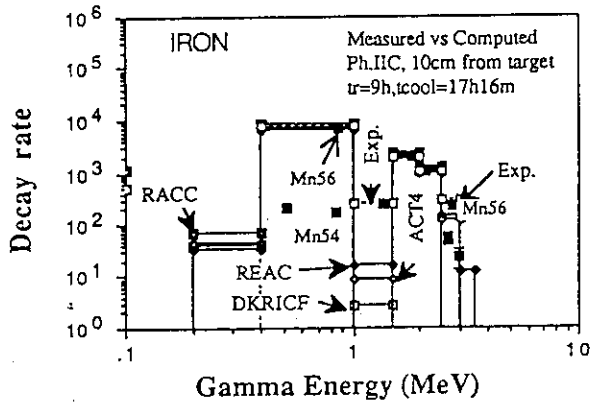

Figure 5a: Decay γ-emission rate spectrua per g for Iron: Measurement vs. Computation (tr = 9h, tcool = 17h16m)

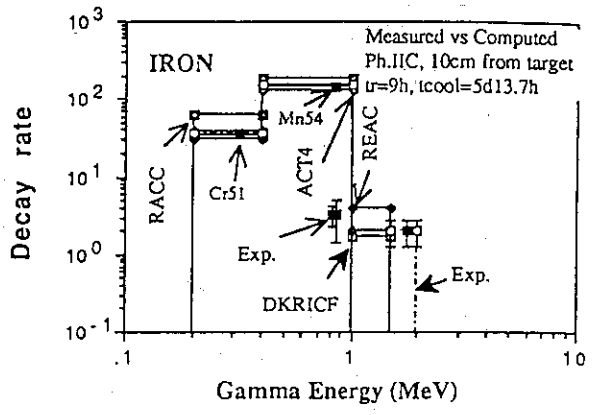

Figure 5b: Decay γ emission rte spectra per g from Iron (Cooling time = 5d13.7h): Measurement vs. Computation (tr = 9h)

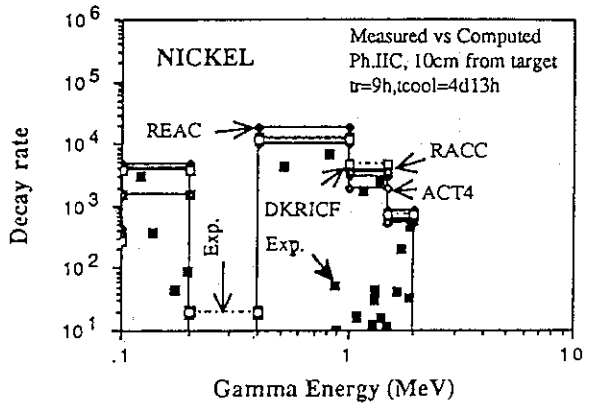

Figure 5c: Decay γ emission rate spectra per g from Nickel: Measurement vs. Computation (tr = 9h, tcool = 4d13h)

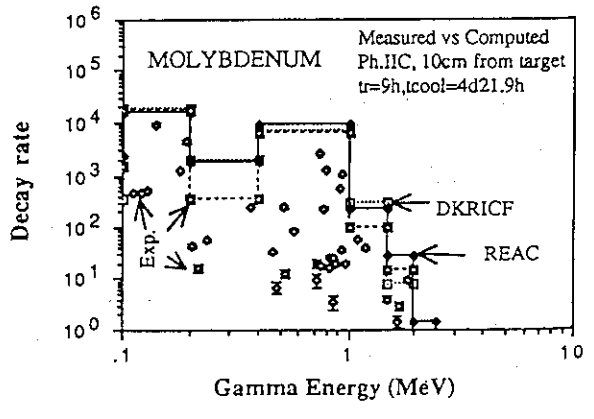

Figure 5d: Decay γ emission rate spectra per g from Molybdenum: Measurement vs. Computation (tr = 9h, tcool = 4d21.9h)

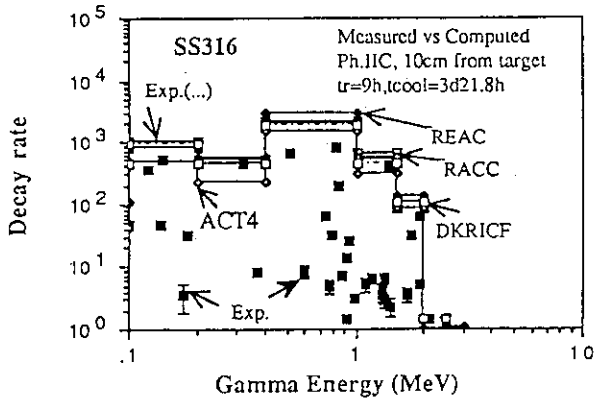

Figure 5e: Decay γ emission rate spectra per g from Stainless Steel: Measurement vs. Computation (tr = 9h, tcool = 3d21·8h)

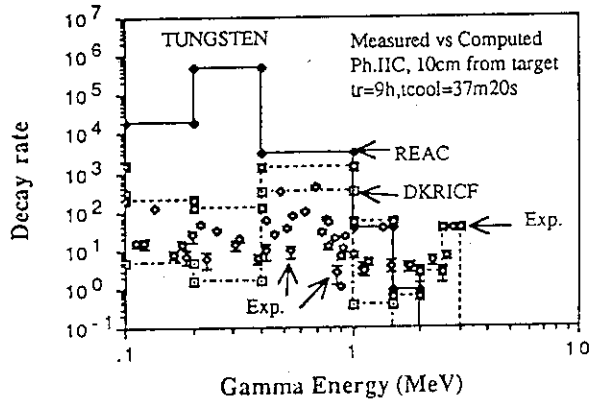

Figure 5f: Decay γ emission rate spectra per g from Tungsten Measurement vs. Computation

IV.I. Tungsten

^{187}W, ^{186}Ta and ^{183}Hf dominate short cooling time measurements. For larger cooling times, predominant contributor ^{187}W is backed up by ^{183}Ta and ^{182}Ta. One sample indicates the presence of Na/Al/Mg impurity. Tabulated γ-yield data[17] does not match with measured relative ratios for various γ peaks emitted by ^{186}Ta and ^{183}Hf. Further investigation is called for. DKRICF lacks decay data for ^{186}Ta, ^{187}W and ^{181}W. REAC analysis shows ^{179m}W ($t_{1/2}$=6.4m, 0.03% 289 KeV, 0.19% 282 KeV, 0.22% 239 KeV, 0.32% 120 KeV and 0.61% 102 KeV) as making dominant contributions for both short and long cooling times; γ-yield data is 2 to 3 orders higher in decay data library of REAC2. Also, ^{182m}Hf, ^{184}Ta, ^{183}Hf, ^{180m}Hf are strongly overestimated by REAC. γ-yields are found to be grossly overestimated for many products in THIDA.

IV.J. Tantalum

^{180m}Ta, ^{180m}Hf and ^{182}Ta dominate identifiable contributions to measured data. There are unidentified peaks at 110, 117, 148, 482, 500 and 1001 KeV. REAC strongly overestimates in 0.2-0.4 MeV (factor of 5) and 0.4-1.0 MeV (factor of 7) energy ranges.

IV.K. $YBa_2Cu_3O_7$

^{135m}Ba($t_{1/2}$=28.7h), ^{139}Ba, $^{135m+g}Xe$ and ^{90m}Y make largest identifiable contributions at short cooling times. There appears to be ^{87m}Sr peak at 388 KeV. Other contributors include ^{65}Ni, ^{62}Cu, ^{62m}Co, ^{64}Cu and ^{88}Y. At larger cooling times, ^{88}Y dominates the scene. REAC lacks decay data for ^{139}Ba, ^{133m}Ba, ^{135m}Ba and $^{135m+g}Xe$. DKRICF lacks decay data for Ba, Xe and Y. C/E ratios for ^{65}Ni, ^{62}Cu and ^{62m}Co deviate considerably from unity even though they are not crucial contributors to overall decay γ-emission rates.

V. CONCLUSIONS

Integrated and spectral decay γ-emission rates from fusion neutron induced radioactive materials have been measured and computed using four leading radioactivity codes. Large discrepancies have been revealed for many materials even for integrated rates. These materials include Ni, Mo, V, Ti, W, MnCu alloy, Cr, Si, In, Ta, Co, $YBa_2Cu_3O_7$ and Zr. Larger discrepancies are observed for spectral rates for practically all the materials. Inadequate experimental statistics is partly to blame in so far as contributions from weaker neutron-induced reactions are concerned. Largely, it is activation cross-sections and decay data that are inadequate and need large scale improvement. C/E results from THIDA are found to be most promising as a whole. RACC broadly follows DKRICF results though there are significant differences when it comes to the details of the spectral rates. Regarding both REAC and DKRICF, it is to be said that γ–yield data needs further improvement, though former scores over the latter in many respects. DKRICF lacks yield data for gamma peaks lying above 2.5 MeV except for some well-known exceptions. A thorough updating is required. Also, in general, the activation cross-sections for (n,γ) reactions need improvement as there is a systematic trend for larger C/E in softer spectra obtaining at '82cm' location.

DKRICF related observations meriting immediate attention follow: γ–yield data is missing for a large number of isotopes. For example, decay data is absent for Y, ^{186}Ta, ^{187}W, ^{181}W, Ba and Xe. For MnCu alloy, ^{62}Cu was overestimated by a factor of 3. For V, ^{48}V contribution is strongly overestimated. For Zr, ^{91m}Y contribution is severely underestimated.

REAC related observations can be summarized as follows: For V, ^{48}Sc and ^{49}Cr are strongly overestimated. For Ni, ^{57}Co, ^{58}Co, ^{59}Fe are too much overestimated. For Mo, ^{91}Mo is strongly overestimated and ^{101}Mo, ^{99}Mo, ^{98m}Nb, ^{97}Nb, ^{93m}Nb are underestimated. For MnCu alloy, ^{62}Cu is overestimated by as much as by a factor of 3. For Zr, ^{89m}Y decay/cross-section data needs early look. The discrepant data leads to large and unconvincing

overestimation. Also, ^{89}Zr and ^{91m}Y are strongly overestimated. For W, ^{179m}W yields abnormally large contribution for both short and long cooling times; major factor appears to be γ-yield data which is 2 to 3 orders higher. In addition, both decay and activation cross-section data for ^{182m}Hf, ^{184}Ta, ^{183}Hf and ^{180m}Hf need attention for doing away with strong overestimation.

Decay heat released in the form of γ's is directly calculable from the experimental data analyzed in this work. We have evaluated this quantity too. The broad C/E trends are similar to those for total decay γ-rates produced in Tables 3a to 3d, even though, the products with harder γ spectra gain upper hand. However, the analysis reported herein is more helpful in deciphering the problem radioactive products, and, of course, the decay/cross-section data of the radioactivity codes used for the analysis.

ACKNOWLEDGEMENTS

This effort is supported by the United States Department of Energy, Office of Fusion Energy under Grant No. DE-F603-86ER52124.

REFERENCES

1. D.L. HENDERSON and O. YASAR, "A Radioactivity and Dose Rate Calculation Code Package," Vol. 1 and 2, RSIC computer code collection, CCC-323 (April 1987).

2. J. JUNG, "Theory and Use of the Radioactivity Code RACC," ANL/FPP/ TM-122, Argonne National Laboratory (1979).

3. F. M. MANN, "REAC*2: Users Manual and Code Description, " WHC-EP-0282, Westinghouse Hanford Company (1989).

4. Y. SEKI et al., "THIDA-2: An Avanced Code System for Calculation of Transmutation, Activation, Decay Heat and Dose Rate," RSIC computer code collection, CCC-410 (April 1987).

5. K. TOMABECHI, "International Thermonuclear Experimental Reactor, ITER, " Fusion Engineering and Design , 8, 43 (1989)

6. J. DARVAS, "The European Fusion Nuclear Technology Effort," Fusion Engineering and Design, 8, 61 (1989).

7. S. TAMURA and FER design team," Design Study o Fusion Experimental Reactor at JAERI," Fusion Engineering and Design, 8, 29 (1989).

8. A. KUMAR et al., "Radioactivity and Nuclear Heating Measurements for Fusion Applications," paper presented a 16th symposium on fusion technology held 3-7 September 1990, Abingdon, U.K.

9. Y. IKEDA et al., "Experiments on Induced Activities related to Decayheat in Simulated D-T Neutron Fields: JAERI/USDOE Collaborative Program on Fusion Neutronics Experiments," paper to be presented at this meeting.

10. Y. OYAMA et al., "Measured Characteristics of Be Multi-layered and Coolant Channel Blankets: Phase IIC Experiments of the JAERI/USDOE Collaborative Program on Fusion Neutronics," paper to be presented at this meeting.

11. M.Z. YOUSSEF et al., "Analysis for Heterogeneous Blankets and Comparison to Measurements: Phase IIC Experiments of the USDOE/JAERI Collaborative Program on Fusion Neutronics," paper to be presented at this meeting.

12. H. BABA, "Gamma-ray Spectrum Analysis Code for Ge(Li) Detectors," RSIC code package PSR-84 (1978); also, JAERI-M 7017, Japan Atomic Energy Research Institute (1977).

13. J.F . BRIESMEISTER, editor, "MCNP- A General Monte Carlo Code for Neutron and Photon Transport: Version 3A," report no. LA-7396-M, Rev. 2 (Sep. 1988), alongwith MCNP3B newsletter dated July 18, 1988, Los Alamos National Laboratory.

14. L.P. KU and J. KOLIBAL, "RUFF- A Ray Tracing Program to Generate Uncollided Flux and First Collision Moments for DOT 4, A User's Manual, EAD-R-16, Plasma Physics Laboratory, Princeton University (1980).

15. W.A. RHOADES and R. L. CHILDS, "DOT-IV Version 4.3: One and Two Dimensional Transport Code Collection, CCC-429 (May 1984).

16. Y. IKEDA et al., "Measurements of Induced Activity in Type 316 Stainless Steel by Irradiation in D-T Neutron Fields," Fusion Technology, 8, 1466 (1985).

17. C.M. LEDERER and V. SHIRLEY, editors, "Table of Isotopes," 7th edition, John Wiley & Sons, Inc., New York (1978).

A.4

EXPERIMENTS AND ANALYSIS FOR MEASUREMENTS OF DECAY HEAT RELATED INDUCED ACTIVITIES IN SIMULATED LINE SOURCE DRIVEN D-T NEUTRON FIELDS OF PHASE IIIA: USDOE/JAERI COLLABORATIVE PROGRAM ON FUSION NEUTRONICS

A.Kumar, M.Z.Youssef
University of California at Los Angeles,
Los Angeles,California 90024-1597, USA

Y.Ikeda, C.Konno, Y. Oyama
Japan Atomic Energy Research Institute
Tokai, Ibaraki 319-11, Japan

ABSTRACT

The recently concluded phase IIIA experiments of the USDOE/JAERI collaborative program mark a watershed in that a D-T line source was simulated by moving detectors/annular Li_2O blanket-assembly with respect to a stationary point source. Three experiments were conducted in three stages during this phase: (i) source characterization (step-mode, 10 cm step, 9h47m duration, 3 sample locations), (ii) in-situ short irradiation (stationary assembly, 30m duration, 2 sample locations), (iii) in-situ long irradiation (continuous-mode, 9h51m duration, 3 sample locations). The sample-materials included: Fe, Ni, Mo, SS316, W, Ta, Zr, Al, Sn, Ag, Pb, Zn, Nb, Ti, V, Co and In. The sample locations inside the phase IIIA assembly were so chosen as to monitor (a) the impact of lack of line source simulation on decay γ-radioactivity, (b) the influence of SS304 first wall, (c) the role of neutron spectral degradation in the annular Li_2O fusion blanket assembly. The experimental results demonstrate that : (1) continuous-mode operation provides better simulation of line source even for radioactive products of half lives as low as ~10 min, (2) the decay γ-emission rates generally drop as one moves away from the center of simulated line source (length=2 meters), (3) the presence of surrounding annular blanket leads to larger enhancements in the γ-emission rates ascribable to reactions induced by energy-degraded neutrons.

The analysis of these measurements shows up discrepancies for most of the materials. DKRICF lacks decay data for many isotopes. For example, decay data is absent for Y, ^{186}Ta, ^{187}W, and ^{181}W. For Zr, ^{91m}Y contribution is severely underestimated.Severe underestimation hits Zn and Sn (especially ^{117m}Sn and ^{111}In).

REAC2 related more important observations can be summarized as follows: For Mo, ^{91}Mo is strongly overestimated and ^{101}Mo, ^{99}Mo, ^{98m}Nb, ^{97}Nb, ^{93m}Nb are underestimated. For Zr, $^{89m+g}$Zr , ^{90m}Y and ^{91m}Y are strongly overestimated. For W, ^{179m}W yields abnormally large contribution for both short and long cooling times. The data base for Zn needs complete overhaul as for some isotopes there is strong overestimation (^{65}Ni, ^{67}Cu and ^{69}Zn), while yet for others, there is severe underestimation (^{69m}Zn, ^{65}Zn and ^{64}Cu).

I. INTRODUCTION

A simulated line source concept was implemented during phase IIIA experiments, conducted during fall 1989, of USDOE/JAERI collaborative program on fusion breeder neutronics[1-2]. This was for the first time that a line source was experimentally realized beginning with a point source. The extended source thus obtained creats a whole lot of possibilities in that it allows closer simulation of a fusion machine conditions. More realistic source neutron spatial distribution gives rise to more realistic neutron energy spectrum in or out of annular blanket assembly that is to be driven by this simulated line source. Hence, there is an ideal environment for carrying out induced radioactivity experiments related to decay-heat . Multiple measurements were planned and carried out using this novel neutron source facility. Three kinds of experimental measurements were carried out and the irradiated materials included: Fe, Ni, Mo, Stainless Steel (AISI316), W, Ta, Zr, Al, Sn, Ag, Pb, Zn, Nb, Ti, V, Co and In. This work follows its precursor[3-4] carried out during December 1988 phase IIC.

II. EXPERIMENTS

The line source simulation was realized by step or continuous mode[1-2], Detector/assembly are moved by a predetermined spatial step at a time and held at each new position for predetermined time-interval in the step mode. In continuous mode, detector/assembly are constantly moved back and forth at a predetermined speed except very close to the ends. Figure 1 shows schematic of the simulation. Three different environments were chosen for radioactivity measurements: (i)bare line source, (ii)point source inside stationary assembly, (iii)line source driving an annular assembly. The objectives behind this selection are discussed in what follows. It is to outlined here that all these experiments were conducted in large target room with 80^0 beamline. The nominal source intensity for stationary source is 2×10^{11} n/s (for 2 mA beam current), it is an order of magnitude lower than what was available with rotating target neutron source (RNT) in target room#2 during earlier phases. The counting statistics suffers considerably and hence adversely affects accumulation of data on weaker radioactive isotopes.

The degree of achievement of 'ideal' line source simulation attainable through the step and continuous modes is brought out through Fig. 2. By 'Ideal' line source, we

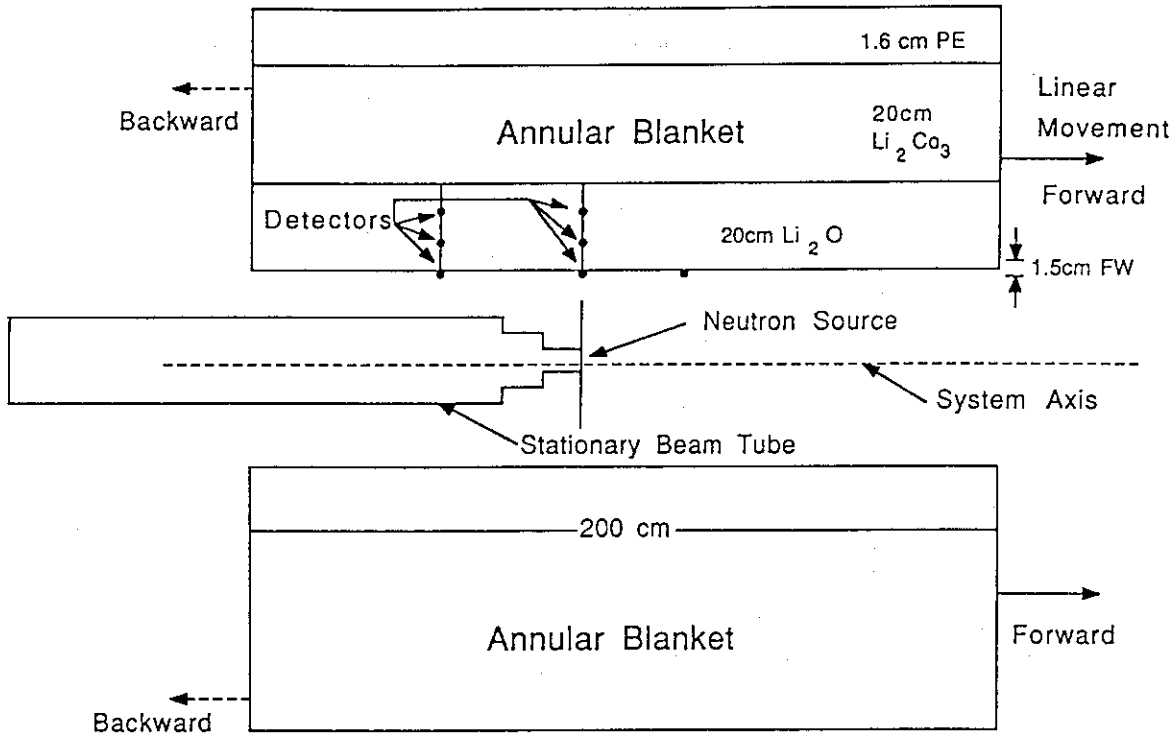

Figure 1: Schematic of simulated line source driven annular blanket assembly of Phase IIIA experiment

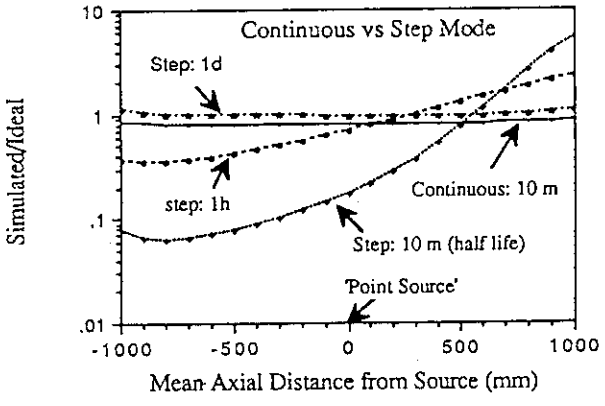

Figure 2: Effect of product half life on ratio of activation rate for simulated line source to that for an "Ideal" line source: continuous versus Step Mode

imply a simulated source that is free from effects of limited speed on any foil activation rate. It is possible only if the moving system attains infinite speed. Fig. 2 shows the ratio of simulated to 'ideal' activation rates as a function of mean axial distance, from the fixed point source, of an irradiated foil. The foil is considered placed at 21.9 cm radial distance from the centerline passing through the target. For continuous mode, the actual temporal profiles of source intensity and deck (or foil) position during 'line source driven assembly' experiment (see Sec. II.C.) have been factored in; product half life is taken to be 10 m. In the actu experiment, an average cycle length of ~ 11 minutes wa realized over 54 cycles for a total irradiation period o 9h51m5s. This corresponds to an average speed o movement of 6.1 mm/s. It is to be seen that simulation i close to ideal for a foil located with mean istance of 30 to 4(cm on either side of the stationary target. Figure 2 alsc shows the degree of simulation obtainable with stepwis mode for a product of half life ranging from 10m to 1d actual source intensity and position data realized during 'lin source without assembly' experiment (see Sec. II.A.) have been factored in. The deviation is much larger for shorter half lives. During this experiment, a spatial step of 10 cm was selected , for a total of 41 irradiations of 13 minutes each and total experiment time of 9h47m; only one spatia cycle was executed. It is to be noted that even for 1 h hali life product, the deviation from line source is considerable.

II.A. Line Source without Assembly

Three sets of foil packets were irradiated at three initial axial distances of 0, 60 and 100 cm from the target towards its back-side; the corresponding mean distances from the target during irradiation period are 0, 40 and 100 cm; radial distance from the system axis was 21.9 cm .The foil materials common to the three sets included: Zr, AISI316, Mo, Sn, Ni and Fe. In addition, thinner Nb and Al foils were used for source neutron dosimetry. The set at 100 cm contained additional foils of Co, Ti, V, In, Ta, W, Y, Ag, Pb and Zn. Some product isotopes of interest are shown in Table 1 (refer to 3 & 4 for additional information). The foils were attached to a stand resting on a movable deck. This deck was moved 10 cm in a step and there was 13 minute irradiation at each step. Only one cycle could be completed

during irradiation period of 9h47m. The decay γ spectroscopy was done using three available intrinsic germanium detectors at FNS. Two of these were relative detectors whereas the third one was used as absolute detector with its γ detection efficiency known better than 2% in the energy range of 100 KeV to 3 MeV at a standard sample-detector distance. Generally, more than one cooling time was covered for each foil. The cooling times varied from foil to foil and ranged from 1h50m to 7d22h37m20s. The average source intensity obtained amounts to 1.11 10^9 n/s/cm.

II.B. Point Source Driven Assembly

The movable deck was held stationary during the first irradiation with the annular assembly on November 21, that was intended for shorter half life product isotopes; the irradiation lasted half an hour only. The source was all the time located at the center of the stationary assembly. Two sets of foils were irradiated for half an hour at initial axial distances of 0 and 40 cm from the target. The set at 40 cm was kept behind 10 mm thick layers of SS304. The other set was kept just behind 15 mm thick SS304 in the central radial drawer. Each set contained foils of Sn, Zn, Pb, Ag, Ni, Fe and W. In addition, two foils of Nb and one foil of Al were included for source neutron dosimetry. Because of lowering of neutron flux due to line source simulation, on the one hand, and relatively low source neutron strength, on the other hand, it was decided to have irradiation inside stationary assembly. It is clear that this configuration represents only a point source inside annular assembly of phase IIIA. However, this type of neutron energy spectrum was realized for the first time in this collaborative program. only two cooling times per sample were covered. The lowest cooling time was 11m30s for a lead sample, the highest one was 21h21m55s for a nickel sample.

II.C. Line Source Driven Assembly

The line source simulation was carried out in continuous mode for 54 cycles during total irradiation time of 9h51m5s. The assembly was initially located such that its farthest end was cooincident with the target; thereafter assembly was moved such that this end of the assembly was always within 0 to 2m of the stationary target. Three sets of foils were irradiated: 2 sets were in the central radial drawer at an initial axial distance of 100 cm from the target and the remaining set was at an initial axial distance of 60 cm from the target. One of the sets in the central drawer was just behind the 15 mm thick SS304 layers; the second set was inserted just behind first 2" thick Li_2O block. These two locations were chosen so as to provide different neutron energy spectra. The last set was placed behind 10 mm thick SS304 layers. The first two sets had identical sample composition: AISI316, Ti, Ta, Mo, Zr, Fe, Ni and W. The third set contained: Sn, Zn, Pb, Ag, Ni, Fe and Mo. In addition, all the three sets contained source neutron dosimetry foils of Nb (2 each) and Al (1 each). Generally, one cooling time per sample was covered. cooling time varied from sample to sample and ranged from the lowest of 1h37m25s for a AISI316 sample to the highest of 14h33m20s for a lead sample. The source intensity averaged to 9.66 10^8 n/s/cm.

II. D. Treatment of Experimental Data

γ pulse-height spectrum for a sample for a each cooling time is processed by a spectrum analysis code BOB75[5] to obtain gamma ray intensity spectrum[3]. Then background is subtracted. The resulting spectrum is then corrected for detector efficiency and attenuation of decay γ's emitted in a sample. Variation of source neutron intensity during irradiation is accounted for to finally obtain decay γ emission rate per g for a normalizing source neutron intensity of 10^{12} n/s. For simulated line source (step/continuous mode) correction is applied to account for decay during intervening period for step mode and also to account for decay during movement for continuous mode as the speed of movement is not totally uniform over a cycle itself and the speed is quite low, as already described above.

Regarding error estimation on experimental measurements, it is to be recognized that a number of parameters affect counting statistics. The primary parameters include: neutron flux, half life of γ-emitter, detector efficiency, cooling time, counting time, activation cross-section and atom density. It is impossible to give a single figure for even one sample material as is amply brought out in Fig. 3 that shows percent standard deviation on decay rates for different products as a function of half life for a molybdenum sample irradiated in 'point source driven assembly' experiment. Irradiation (tr), cooling(tcool) and counting (tcount) times are 30m, 3h18.2m and 10.75m respectively. It is to be noted that only most prominent γ-peaks for a given emitter are included; in addition, 66h ^{99}Mo peak at 141 KeV carries contribution from 6.02h ^{99m}Tc too. Error varies from 3.0% for ^{99}Mo(+^{99m}Tc) to 14.4% for 6.95h ^{93m}Mo.

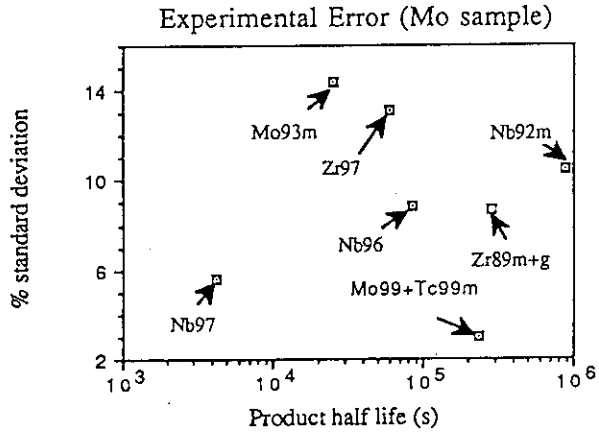

Figure 3: Experimental error as a function of product half life for a molybdenum sample

II.E. Trends of Experimental Results

Radioactive isotopic products of half lives ranging from 2m to 5y were targeted. Three intrinsic germanium detectors were employed for γ spectroscopy. One of these detectors was used as a standard for remaining ones which were employed as relative detectors. Experimentally, identification of a γ emitting radioactive nuclide was done looking at γ energy and its decay as a function of cooling time.

Table 1: Longer Half-life Products from some samples

(30 m < half life < 5.3 y)

Sample-material	Half-life	Product	γ-energy	Reaction
Zn	38.1 m	^{63}Zn	670 KeV	(n,2n)
	2.52 h	^{65}Ni	1482 KeV	(n,α)
	13.8 h	^{69m}Zn	439 KeV	(n,2n)
	61.9 h	^{67}Cu	185 KeV	(n,p),(n,d), (n,n'p)
	244 d	^{65}Zn	1116 KeV	(n,2n),(n,γ)
Sn	35 m	^{111}Sn	1152 KeV	(n,2n)
	40 m	^{123m}Sn	160 KeV	(n,2n),(n,γ)
	48.6 m	^{111m}Cd	245 KeV	(n,α)
	54.1 m	^{116m1}In	417 KeV	(n,p)
	2.4 h	^{117}Cd	273 KeV	(n,α)
	3.4 h	^{117m}Cd	1066 KeV	(n,α)
	4.5 h	^{115m}In	336 KeV	(n,p),(n,d), (n,n'p)
	53.4 h	^{115}Cd	336 KeV	(n,α)
	9.63 d	^{125}Sn	1066 KeV	(n,γ)
	14 d	^{123}Sn	1089 KeV	(n,2n)
	44.8 d	^{115m}Cd	934 KeV	(n,α)
	453 d	^{109}Cd	88 KeV	(n,α)
Pb	66.9 m	^{204m}Pb	899/912KeV	(n,n')
	52.02 h	^{203}Pb	279 KeV	(n,2n)
	12.23 d	^{202}Tl	440 KeV	(n,t)
	46.76 d	^{203}Hg	279 KeV	(n,α)
Ag	24 m	^{106}Ag	512/295KeV	(n,2n)
	130 m	^{106m}Rh	512/717 KeV	(n,α)
	13.43 h	^{109}Pd	88 KeV	(n,p)
	8.5 d	^{108m}Ag	512/717 KeV	(n,2n)
	252 d	^{110m}Ag	707/658 KeV	(n,γ)
	127 y	^{108m}Ag	434/723 KeV	(n,2n)

II.E.1. Material-wise Highlights

For some of the irradiated materials, dominant contributors to decay γ emission rates are summarized as follows:

Iron: For cooling times less than 10h, ^{56}Mn ($t_{1/2}$=2.6h) dominates. For larger cooling times, ^{54}Mn ($t_{1/2}$=312d) assumes growing ascendancy. No significant neutron energy spectrum dependence was seen as both these products result from high threshold (n,p) reaction.

Nickel: ^{62m}Co (13.9m) and ^{57}Ni (36h) dominate for short cooling times. ^{58}Co(70.8d),^{57}Co(271d), ^{57}Ni, ^{59}Fe(44.6d) and ^{60}Co(5.3y) take over at larger cooling times.

Chromium: 320KeV γ line from ^{51}Cr (27.7d) dominates for long irradiation and cooling times. NaCl and Fe/Mn impurities seem to be present as ^{24}Na(15h), ^{35m}Cl(32m) and ^{56}Mn(2.6h) contribute as much as 3% to the total decay γ emission rate for cooling period of 1.5h. For cooling period of 15h only ^{24}Na contributes- less than 1% only.

Molybdenum: Major contributors for short cooling times are ^{101}Mo(14.6m), ^{101}Tc(14.2m) , ^{97}Nb(1.2h), ^{98m}Nb(51m), ^{99}Mo(66h), ^{99m}Tc(6h), ^{96}Nb(23.4h), and ^{93m}Mo(6.9h). ^{101}Tc results from β⁻ decay of ^{101}Mo, and ^{99m}Tc is produced by β⁻ decay of ^{99}Mo. Longer cooling times see dominance of ^{99}Mo, ^{99m}Tc, ^{96}Nb, ^{97}Nb and ^{89}Zr.

Stainless Steel (AISI316): It is an alloy of Fe, Ni, Cr, Mn and Mo. ^{56}Mn contributes overwhelmingly at cooling times less than a day. At larger cooling times, ^{99}Mo, ^{99m}Tc, ^{51}Cr, ^{58}Co, ^{57}Ni and ^{54}Mn are leading contributors.

Cobalt: For cooling periods of less than 5h, ^{56}Mn- pro of ^{59}Co(n,γ)^{56}Mn reaction- made dominating contribut as much as 95% for irradiation period of 30m and coo period of 37m. The other contributing isotopes incl ^{59}Fe(44.6d), ^{58}Co(70.8d) and ^{60}Co(5.3y), the last iso was noticeable at locations having larger component of sc neutrons.

Tungsten: ^{187}W(23.9h), ^{186}Ta (10.5m) and ^{183}Hf(6 dominate short cooling times. For larger cooling tim predominant contributor ^{187}W is backed up by ^{183}Ta(and ^{182}Ta(115d).

Zirconium: ^{89}Zr(78.4h), ^{87m}Sr(2.8h), ^{90m}Y(3.2 ^{94}Y(18.7m), ^{92}Y(3.5h) and ^{91}Sr(9.5h) contribute for sh cooling times. Larger cooling times bring into foc predominance of ^{89}Zr and ^{90m}Y(3.2h).

Tantalum: ^{180m}Ta(8h), ^{180m}Hf(5.5h) annd ^{182}Ta(11 dominate γ emission rate.

Lead: ^{203}Pb(52h) and ^{204m}Pb(67m) dominate at shor cooling times. ^{203}Pb dominates at larger cooling times.

Tin: At shorter cooling times, ^{123m}Sn(40m) dominate other contributors include ^{117}In(42.3m), ^{116m1}In(54.1m ^{117}In(1.93h), ^{111}In(2.8d) and ^{117m}Sn(14d). At larg cooling times, ^{117m}Sn dominates.

Zinc: Annihilation peak at 511KeV dominates at sho cooling times. Other significant contributors incluc ^{63}Zn(38m), ^{66}Cu(5.1m), ^{69m}Zn(13.8h) and ^{65}Ni(2.52h). A larger cooling times, apart from annihilation peak, leadir contributors are ^{69m}Zn, ^{67}Cu(61.9h), ^{65}Zn(244d) ^{64}Cu(12.7h) and ^{65}Ni.

Titanium: At short cooling times, 511KeV annihilation from ^{45}Ti(3.1h) and ^{48}Sc(43.7h) γ's dominate the measur emission rates. At longer cooling times, other contributor include ^{47}Sc(3.42d) and ^{46}Sc(83.8d).

Vanadium: At shorter cooling times, ^{51}Ti(5.8m) dominate the emission rate followed by ^{48}Sc(43.7h). Also, ^{52}V (3.8m) was observed. For longer cooling times, ^{48}Sc dominated the scene single handedly.

Aluminum: ^{24}Na(15h) dominated the decay γ spectra at larger cooling times.

Silver: At short cooling times, a peak at 511-512 KeV dominates. This peak gets large contributions from ^{106}Ag(24m), ^{106m}Rh(130m) and ^{106m}Ag(8.5d). At larger cooling times, a large number of γ lines from ^{106m}Ag dominate the emission rate.

II.E.2. Parametric Dependence

Spectrum dependence of γ emission rates is mostly seen only in those materials that have dominating isotopes resulting from (n,γ) reactions. High threshold reactions, e.g. (n,n'), (n,p), (n,n'p), (n,d), (n,2n), are essentially governed by harder part of the spectrum. Comparing the integrated γ-

emission rates (between 100 KeV to 3MeV), it is found that for short irradiation time (30m), Fe, AISI316, Al and Co give leading rates in that order. However, the trend changes for ~10h irradiation to: Al, Fe, and AISI316. This is understandable as ^{24}Na (15h) production rate was unsaturated during 30m irradiation but almost saturated during ~10h irradiation.

γ component of total energy release rate was obtained from γ emission rate spectrum for each material. Comparison of γ energy release rates at same irradiation and cooling times shows that for short (30m) irradiation time, Fe, AISI316, Al dominate in that order. For larger irradiation and cooling times, the trend is different: for hard spectrum (without blanket), ~10h irradiation and 15h cooling time Al domination is meekly followed by Mo and Ti; for softer spectrum (with surrounding blanket) ~10h irradiation and 15h cooling time, W, Al, Ta, and Zr contribute in that order.

Total energy release rates, directly related to decayheat, were derived from measured γ emission rates and deduced β emission rates (using known branching ratios and average beta energy release per disintegration). It turns out that β contribution varies widely from material to material and it ranges from 0 to 50%. The lowest beta contribution is observed for Cr followed by Ni. The beta fraction varies both with irradiation and cooling times. V dominance at short irradiation and cooling times under hard spectrum is followed by Zr, AISI316, Co and Fe. At larger irradiation and cooling time , W lead is followed by Fe, Mo, AISI316 and Co. Generally, it is observed that short lived isotopes make dominating contributions towards β energy release at shorter cooling times. This fact underlines the important role of accurate determination of short lived activities in the selection of materials for fusion devices that would be required to be accessed by personnel after relatively short operation time.

III. ANALYSIS

Analysis to obtain decay γ emission rate involves a multi-step procedure[3]. A two or three dimensional transport code is employed to get neutron energy distribution, i.e.,neutron flux, at spatial locations of samples. Geometry and material composition of irradiation environment are important inputs for this calculation. Next stage involves computation of decay γ emission spectrum using a radioactivity calculation code. Neutron flux, sample composition, irradiation and cooling (or shutdown) times are required input data for this stage. Decay and activation cross-section libraries form part of the code used. Leading codes used for this purpose include DKRICF[6], REAC[7], RACC[8] and THIDA[9]. The flux was obtained in a two step process: (1)source neutron energy and angular distribution was obtained by 3D MCNP[10] modeling of line source/point source of fusion neutronics source (FNS) facility , (2)source neutron distribution from MCNP was input to RUFF[11] and DOT4.3[12] code system, with 30 group MATXS5 cross-section library of LANL, to compute spatial distribution of neutron flux.

Table2: Chemical Compositions of the Irradiated Samples

Sample Material	Chemical Composition by Maximum weight %
Iron (Fe)	99.92 Fe, 0.059 Mn, 0.02 C
Nickel (Ni)	99.97 Ni, 0.016 C
Molybdenum (Mo)	99.93, 0.03 W, 0.01 Fe
Stainless Steel (AISI 316-goodfellow)	68.6 Fe, 16.5 Cr, 11.30 Ni, 2.12 Mo, 1.46 Mn
Manganese Copper	79.78 Mn, 19.66 Cu, 0.46 Ni, 0.07 Fe Alloy + (MnCu)
Vanadium (V)	99.82 V, 0.044 Si, 0.03 Ta, 0.032 O, 0.013 Mo, 0.01 Zr, 0.01 Fe, 0.01 Al, 0.01 Hf
Titanium (Ti)	99.79 Ti, 0.12 O, 0.06 Fe, 0.02 C (Reactor-expt)
Aluminum (Al)	99.97 Al, 0.006 Mg
Cobalt (Co)	99.95 Co, 0.04 Ni
Tungsten (W)	99.97 W, 0.008 Si
Niobium (Nb)	99.89 Nb, 0.027 Ta, 0.01 Zr
Zirconium (Zr)	99.83 Zr, 0.07 Fe, 0.07 Cr, 0.01 N, 0.01 C, 0.01 Hf
Indium (In)	99.97 In, 0.009 Pb
Tin (Sn)	99.87 Sn, 0.02 Cu, 0.02 Sb, 0.02 Pb, 0.01 Fe, 0.01 Ni, 0.01 Co, 0.01 S, 0.01 As, 0.01 Bi
Tantalum (Ta)	99.89 Ta, 0.03 Cd, 0.01 Zr, 0.01 Ti, 0.01 W, 0.01 Si
Lead (Pb)	99.95 Pb, 0.023 Bi, 0.016 Sn,0.005 Ag, 0.005 Cu, 0.001 Ti
Silver (Ag)	99.95 Ag, 0.043 Cu, 0.003 Fe, 0.003 Zn, 0.0006 Pb
Zinc (Zn)	99.95 Zn, 0.038 Pb, 0.006 Cu, 0.004 Cd, 0.002 Sn, 0.0004 Ag
Titanium (Ti) (Goodfellow)	99.6 Ti, 0.013 O, 0.003 Al, 0.003 Cr, 0.003 Mn, 0.003 Ni, 0.003 V, 0.002 Fe
Iron (Fe thin)	99.93 Fe, 0.01 H, 0.01 O

IV. RESULTS AND DISCUSSION

Tables 3 provide a typical intercomparison of computed (C) to measured (E) ratio for different source conditions for iron samples. Quantity being compared here is integrated decay γ emission rate per s per g for a normalizing source strength of 10^{12} n/s. Though there are some changes in C/E values for REAC and DKRICF codes, it is clear that, given rather untested nature of wide body of decay and cross section data of these codes, the change from one spectral environment to another does not bring out any drastic change. Hence, in what follows, we shall generally be presenting results for samples kept inside annular assembly of phase IIIA driven by simulated line source. But, broad conclusions deduced therefrom quite possibly are applicable to other spectral environments too.

Table 4 depicts C/E ratios for Fe, Ni, AISI (stainless steel), Mo, W, Pb, Zn, Zr, Ag, Sn, Ta, Al , and Nb. The reasons for discrepancies for iron, nickel, molybdenum, stainless steel, zirconium, tungsten and tantalum have already been enumerated in a companion paper[3] and are recalled in the following section. Aluminum and niobium show excellent agreement between computations and measurements for both the codes. This gives confidence in the evaluated neutron spectra used in the decay radioactivity codes.

Table 3: Variation of C/E for Integrated Decay γ Emission rates for Different Source Conditions

Material	Source Condition	Mean Distance from target[a] (cm)	Irradiation Time	Cooling Time	C/E REAC2	C/E DKRICF
Fe	Bare Line	0	9h47m	2h15.5m	1.10	1.19
Fe	Bare Line	40	9h47m	2h3.2m	1.13	1.23
Fe	Bare Line	100	9h47m	1h50m	1.17	1.03
Fe	Point Source	0	30m	33m15s	0.97	1.04
Fe	Point Source	40	30m	44m	1.27	1.40
Fe	Line+Blkt.	0 (1.5cm FW)	9h51m	4h19.6m	1.14	1.21
Fe	Line+Blkt.	0 (5cm Li2O)	9h51m	5h9.9m	1.12	1.19
Fe	Line+Blkt.	40 (1.0cm FW)	9h51m	4h45.1m	1.02	1.09
Fe	Point Source (Phase IIC)	10cm from target	9h	3h22.3m	1.00	1.17

a It stands for axial distance. Bracketed numbers indicate radial distance from axis

Table 4: Variation of C/E for Integrated Samples inside Annular Blanket Assembly Driven by Line Source

(tr=9h51m)

Material	Location	Cooling Time	C/E REAC2	C/E DKRICF
Fe	#A	4h19.6m	1.14	1.21
Ni	#A	4h19.8m	1.22	1.53
AISI	#A	1h37.4m	1.20	1.26
Mo	#A	2h52.7m	4.29	1.58
W	#A	1h37.5m	1.34	4.56e-03
Pb	#C	9h19.7m	2.51	1.09
Zn	#C	5h45.3m	1.83	2.69e-02
Zr	#C	3h54.3m	4.08	1.04
Ag	#C	6h30.8m	0.0102	0.974
Sn	#C	5h45.9m	2.63	0.438
Ta	#A	7h35.4m	2.25	1.97
Al	#C	10h55.2m	0.97	0.97
Nb	#A	5d19.6h	0.999	0.997
Ti	#A	7h34.4m	1.68	1.86

a For #A, mean axial position with respect to fixed source is 0 cm, radial position is behind 1.5cm FW in central drawer
For #B, mean axial position with respect to fixed source is 0 cm, radial position is located behind first 5 cm of Li2O
For #C, mean axial position with respect to fixed source is +40 cm, radial position is behind 1 cm FW

Figures 4 to 8 display C/E for Mo, Zr, AISI, Sn and Zn for REAC2 code system. Figure 4 for Mo corresponds to bare line source driven experiment for a sample at mean axial location of +100 cm; tr and tcool are 9h47m and 3h18.2m. C/E's for Mo for different products are: (1)^{99}Mo: 1.25, (2)^{96}Nb: 3.18, (3)^{97}Nb: 2.56, (4)^{97}Zr: 6.64, (5)$^{89m+g}$Zr: 4.07, (6)^{92m}Nb: 1.02. Figure 5 for Zr corresponds to 'line source driven assembly' experiment wherein a Zr sample was located at position B, i.e., 5 cm inside Li_2O zone in the central drawer; tr, tcool are 9h51m and 3h54.3m respectively. C/E values for different products are: (1)^{90m}Y: 4.6, (2)^{87m}Sr: 1.22, (3)^{91m}Y: 1.82, (4)^{97}Nb: 0.10, (5)^{97}Zr: 9.7x10^{-2}, (6)$^{89m+g}$Zr.

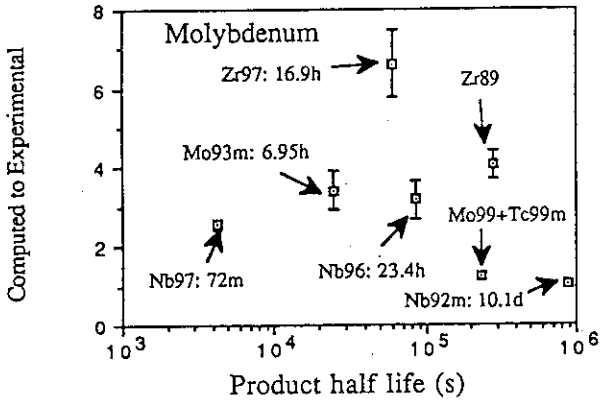

Figure 4: Computed to Experimental (C/E) of decay γ emission rates as a function of product half life for a molybdenum sample

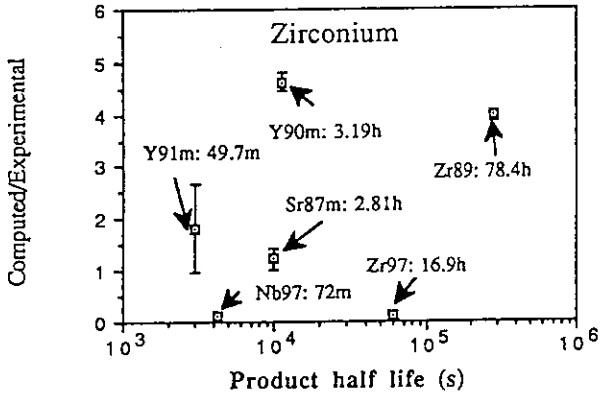

Figure 5: C/E ratio of decay γ emission rates as a function of product half life for a zirconium sample

Figure 6 for stainless steel (AISI) represents C/E's for an AISI sample located at position B in 'line source driven assembly' experiment; tcool is 13h13.5m. C/E values are: (1) ^{57}Co: 0.94, (2)^{51}Cr: 1.18, (3)^{57}Co: 2.23, (4)^{54}Mn: 0.58, (5)^{56}Mn: 1.02, (6)^{57}Ni: 0.96. Figure 7 refers to a Sn sample located at location C, i.e., at 40 cm axial distance from the mid-point of the assembly in line source driven experiment.; tcool is 3h45.9m. Tin data does have problems with both the codes. In DKRICF, ^{117m}Sn and ^{111}In are largely underestimated. REAC shows total absence of ^{116m1}In ($t_{1/2}$=54.1 m, 417 KeV). In addition, ^{117m}Sn and ^{111}In are strongly overestimated.

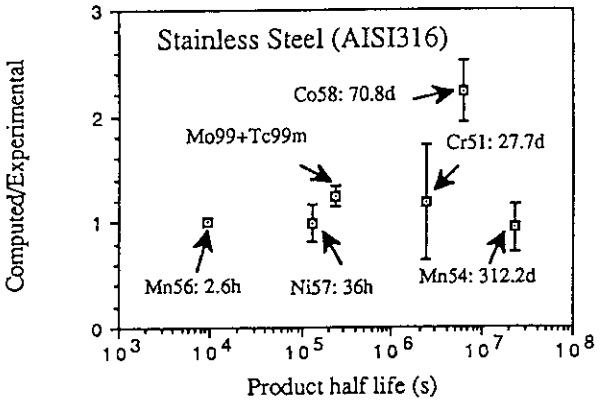

Figure 6: C/E ratio of decay γ emission rates as a function of product half life for a stainless steel (AISI) sample

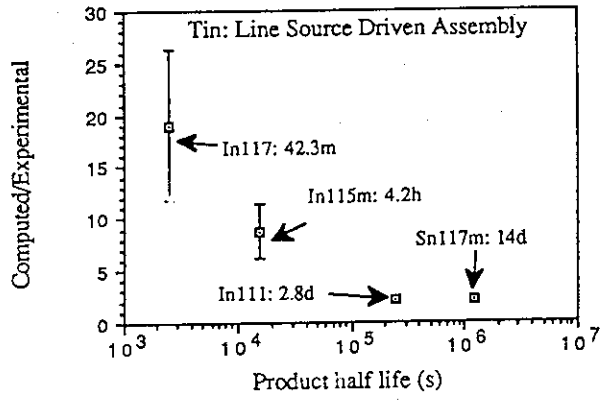

Figure 7: C/E as a function of half life for a tin sample

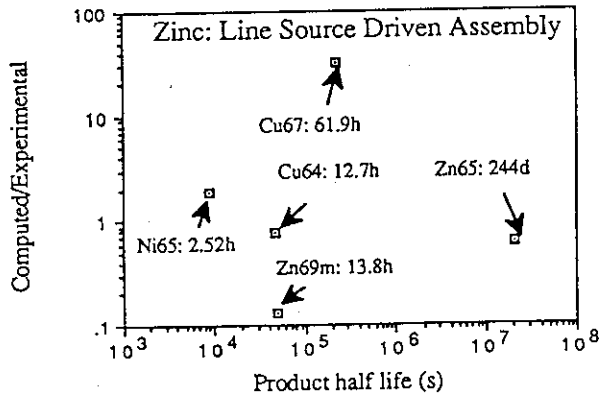

Figure 8: C/E versus product half life for a zinc sample

Figure 8 refers to a Zn sample kept at position C in 'line source driven assembly' experiment and cooled for 5h45.3m. Zinc data has serious problems for both DKRICF and REAC. ^{67}Cu, ^{69m}Zn and ^{64}Cu contributions are practically absent in DKRICF. REAC severely overestimates ^{65}Ni (factor of 1.9), ^{67}Cu (factor of 32) , and ^{69}Zn (absent in experimental data). It largely underestimates ^{69m}Zn (C/E=0.13), ^{65}Zn(C/E=0.62), and ^{64}Cu (C/E=0.78).

Lead C/E values for REAC are too high. The reason for this discrepancy lies in overestimation of ^{203}Pb production by a factor of 2.3. ^{204m}Pb is also strongly overestimated though it does not show up much contribution in our experiments.

Silver data appear to be acceptable for DKRICF. However, the absence of decay data of ^{106m}Ag severely handicaps REAC results, resulting in abysmally low values of C/E even at rather low cooling times.

V. CONCLUSIONS

Integrated and spectral decay γ-emission rates from fusion neutron induced radioactive materials have been measured and computed using leading radioactivity codes. Large discrepancies have been revealed for many materials even for integrated rates. These materials include Ni, Mo, Ti, W, In, Ta, Co, Zr, Pb, Zn, Ag, and Sn. Larger discrepancies are observed for spectral rates for practically all the materials. Inadequate experimental statistics is partly to blame in so far as contributions from weaker neutron-induced reactions are concerned. Largely, it is activation cross-sections and decay data that are inadequate and need large scale improvement. RACC broadly follows DKRICF results though there are significant differences when it comes to the details of the spectral rates. Regarding both REAC and DKRICF, it is to be said that γ−yield data needs further improvement, though former scores over the latter in many respects. DKRICF lacks yield data for gamma peaks lying above 2.5 MeV except for some well-known exceptions. A thorough updating is required. Also, in general, the activation cross-sections for (n,γ) reactions need improvement as there is a systematic trend for larger C/E in softer spectra.

DKRICF related observations meriting immediate attention follow: γ−yield data is missing for a large number of isotopes. For example, decay data is absent for Y, ^{186}Ta, ^{187}W, and ^{181}W. For Zr, ^{91m}Y contribution is severely underestimated. Severe underestimation hits Zn and Sn (especially ^{117m}Sn and ^{111}In).

REAC related observations can be summarized as follows: For Ni, ^{57}Co, ^{58}Co, ^{59}Fe are too much overestimated. For Mo, ^{91}Mo is strongly overestimated and ^{101}Mo, ^{99}Mo, ^{98m}Nb, ^{97}Nb, ^{93m}Nb are underestimated. For Zr, ^{89}Zr , ^{90m}Y and ^{91m}Y are strongly overestimated. For W, ^{179m}W yields abnormally large contribution for both short and long cooling times. This is largely due to 2 to 3 orders higher γ-yield data in the library. In addition, both decay and activation cross-section data for ^{182m}Hf, ^{184}Ta, ^{183}Hf and ^{180m}Hf need attention for doing away with strong overestimation. The data base for Zn needs complete overhaul as for some isotopes there is strong overestimation (^{65}Ni, ^{67}Cu and ^{69}Zn), while yet for others, there is severe underestimation (^{69m}Zn, ^{65}Zn and ^{64}Cu). Tin data needs also to be freshly investigated as ^{117m}Sn and ^{111}In are strongly overestimated. Silver too receives poor treatment from REAC as the dominant contributor ^{106m}Ag is not credited with any decay γ contribution.

ACKNOWLEDGEMENTS

This effort is supported by the United States Department of Energy, Office of Fusion Energy under Grant No. DE-F603-86ER52124.

REFERENCES

1. T. NAKAMURA et al., "A Line D-T Neutron Source Facility for Annular Blanket Experiment: Phase IIIA of the JAERI/USDOE Collaborative Program on Fusion Neutronics," paper to be presented at this meeting.
2. Y. OYAMA et al., "Annular Blanket Experiment Using a Line D-T Neutron Source: Phase IIIA of the JAERI/USDOE Collaborative Program on Fusion Neutronics," paper to be presented at this meeting.
3. A. KUMAR et al., "Analysis of Induced Activities' Measurements Related to Decayheat in Phase IIC Experimental Assembly: JAERI/USDOE Collaborative Program on Fusion Neutronics Experiments," paper to be presented at this meeting.
4. Y. IKEDA et al., "Experiments on Induced Activities related to Decayheat in Simulated D-T Neutron Fields: JAERI/USDOE Collaborative Program on Fusion Neutronics Experiments," paper to be presented at this meeting.
5. H. BABA, "Gamma-ray Spectrum Analysis Code for Ge(Li) Detectors," RSIC code package PSR-84 (1978); also, JAERI-M 7017, Japan Atomic Energy Research Institute (1977).
6. D.L. HENDERSON and O. YASAR, "A Radioactivity and Dose Rate Calculation Code Package," Vol. 1 and 2, RSIC computer code collection, CCC-323 (April 1987).
7. J. JUNG, "Theory and Use of the Radioactivity Code RACC," ANL/FPP/ TM-122, Argonne National Laboratory (1979).
8. F. M. MANN, "REAC*2: Users Manual and Code Description, " WHC-EP-0282, Westinghouse Hanford Company (1989).
9. Y. SEKI et al., "THIDA-2: An Avanced Code System for Calculation of Transmutation, Activation, Decay Heat and Dose Rate," RSIC computer code collection, CCC-410 (April 1987).
10. J.F . BRIESMEISTER, editor, "MCNP- A General Monte Carlo Code for Neutron and Photon Transport: Version 3A," report no. LA-7396-M, Rev. 2 (Sep. 1988), alongwith MCNP3B newsletter dated July 18, 1988, Los Alamos National Laboratory.
11. L.P. KU and J. KOLIBAL, "RUFF- A Ray Tracing Program to Generate Uncollided Flux and First Collision Moments for DOT 4, A User's Manual, EAD-R-16, Plasma Physics Laboratory, Princeton University (1980).
12. W.A. RHOADES and R. L. CHILDS, "DOT-IV Version 4.3: One and Two Dimensional Transport Code Collection, CCC-429 (May 1984).

A.5

Fusion Engineering and Design 18 (1991) 387–395
North-Holland

Experimental verification of the current data and methods for induced radioactivity and decay heat calculation in D–T fusion reactors

Y. Ikeda, C. Konno, Y. Oyama, T. Nakamura
Japan Atomic Energy Research Institute, Tokai-mura, Ibaraki-ken 319-11, Japan

A. Kumar, M.Z. Youssef, M.A. Abdou
University of California, Los Angeles, Los Angeles CA 90024-1579, USA

Induced radioactivities and decay heat are of significant importance in the nuclear design of a near-term D–T fusion device from the view point of the safety consideration. In the framework of the JAERI/USDOE collaborative program on fusion neutronics, extensive experimental efforts have been devoted to verify the validity of the calculation code systems THIDA-2, REACT-2 and DKR-ICF. In the previous study, it was clearly pointed out that there were large discrepancies for several important materials between the experiment and the calculation in terms of γ-ray emission rates. This paper investigated the major sources of these large discrepancies. In addition to the previous ones, the analysis was carried out by THIDA-2 using an updated cross-section library. As a result, the following was pointed out: (1) The calculation of THIDA with the new activation cross-section library gave better agreement with experiment, especially for MnCu, W, Mo and V. As far as the higher neutron energy range above 1.0 MeV is concerned, all calculation code systems offer reasonable prediction accuracy. (2) For MnCu. W and Ta, uncertainty in the neutron spectrum was the main source for the large discrepancies because low-energy neutrons were very sensitive to the capture reaction products of ^{64}Cu, ^{187}W and ^{182}Ta.

1. Introduction

Induced radioactivity in fusion structural materials is of importance in terms of decay-heat, dose rate, and radioactive waste estimation. Extensive efforts have been addressed concerning the compilation of cross-section data and calculation code development. In order to arrive at the target accuracy for the parameters relevant to the activation, several experiments using many structural materials have been conducted in the framework of fusion neutronics studies [1–6]. They have investigated the adequacy of the cross-section data as well as the calculation codes to predict induced activities in the simulated D–T neutron environment at rather short time ranges from 10 min to several days after irradiation. In particular, the systematic experiments in the framework of the JAERI/USDOE collaborative program [4–6], have addressed serious problems: there were sever discrepancies among results obtained by different code systems, THIDA-2 [7], REAC-2 [8] and DKR-ICF [9], which are currently available and large deviations in the comparison of experiment and calculations were observed for materials like Mo, W, MnCu, Ta, V, etc. [5,6].

In this paper, we have investigated the sources of the discrepancies between calculation and experiment focusing on the adequacy of the activation cross-section data libraries. It was concluded that the main source of the uncertainty in the calculation arose mainly from inadequacy of the activation cross-section data. Also the uncertainty in the low-energy neutron flux calculation impacted on the accuracy of induced activity prediction.

2. Outline of experiments

An integral experiment of radioactivity and decay-heat was conducted at the FNS facility [10] in the framework of the JAERI/USDOE collaborative program on fusion neutronics during Phase-IIC [11] and Phase-IIIA [12]. The objectives of the experiment were to provide data for verifying radioactivity calculation codes, and to investigate the suitability of different

materials in meeting the selection criteria based on low activation and decay-heat considerations.

The Phase-IIC system consisted of an Li_2O breeder blanket with a first wall enclosed by 200 mm Li_2CO_3 with 50 mm polyethylene. A D–T point neutron source was located in the cavity of the enclosure, at 780 mm instance from the first wall of the Li_2O region. The Phase-IIIA system was featured by a new concept of a 2 m long pseudo line source with annular blanket assembly consisting of a 15 mm thick SS-304 first wall, and 400 mm thick Li_2O, 200 mm thick Li_2CO_3 and 50 mm polyethylene reflector zones. Detailed descriptions for both system were given in refs. [11] and [12].

As the first position (A) was close to the D–T neutron source in Phase-IIC, it is expected that the neutron spectrum simulates a typical one in the first wall region. The second position (B) provided simulation of a typical spectrum inside the tritium breeder blanket, Li_2O. With the line D–T neutron source configuration, the third position (C) was located at the center of the Phase-IIIA system at 5 mm depth in the Li_2O region. Neutron spectra at the three positions are shown in fig. 1.

The twenty materials used in the present study were Mg, Al, Si, Ti, V, Cr, MnCu alloy, Fe, Co, Ni, SS-316, Zn, Zr, Nb, Mo, Ag, Sn, Ta, W, and Pb. These samples were irradiated in the D–T neutron fields. After irradiation, decay γ-ray spectra were measured with Ge detectors. The gamma-ray emission rate in each sample material was deduced to be compared with the calculations. In table 1, the notations of the systems are tabulated along with the irradiation times and typical cooling times, which corresponded to the experimental conditions.

Table 1
Abbreviated notation of the cases to the experiments

Notation	System	Irradiation time	Cooling time
AS	Phase-IIC	30 m	30 m–1 hr
AL-1	Phase-IIC	10 hr	1hr–3 hr
AL-2	–	–	10 hr–3 d
BS	Phase-IIC	30 m	30 m–1 hr
BL-1	Phase-IIC	10 hr	1 hr–3 hr
BL-2	–	–	10 hr–3 d
C	Phase-IIIA	10 hr	1 hr–10 hr

3. Experimental analysis

The experimental analysis has been carried out by the currently available code systems THIDA-2, REAC-2 and DKR-ICF. Since the cross-section library of THIDA-2 has been recently updated, the experimental analysis has been carried out using the new version of library. The THIDA code system involves neutron flux calculation by DOT3.5 with the GICX40 [13] data library based on ENDF/B-VI and induced activity calculation by ACT4 with an activation cross-section

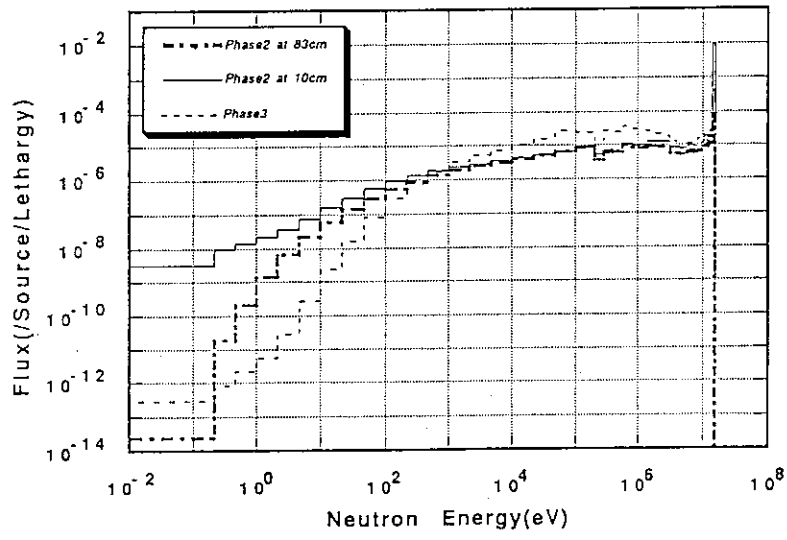

Fig. 1. Neutron spectra at position A, B and C calculated by DOT3.5 with GICX40.

library, CROSSLIB. In order to avoid uncertainties associated with the decay of activities during collecting time, THIDA computed the integrated γ-ray intensities per unit volume and an individual γ-ray energy spectrum during counting in order to avoid uncertainty in tracing all the decaying activities. The annihilation γ-ray is the case to be considered. The code systems REAC and DKR-ICF employed the MCNP for neutron transport calculation, using nuclear data libraries based on ENDF/B-V. Induced activities were generated using their own activation cross-section libraries. For REAC-2 and DKR-ICF, the ratio of computed to experimental value (C/E) was given for the integrated γ-ray emission rate per gram at the moment when γ-ray counting started.

From now, notations of THIDA-Old, THIDA-New, REAC and DKR-ICF indicate the induced activity calculations by using corresponding codes and libraries, respectively.

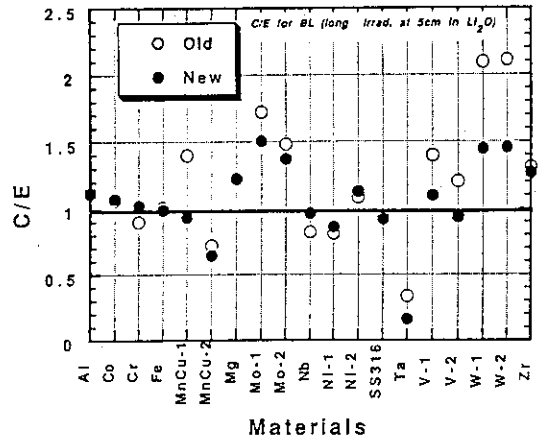

Fig. 2. The C/E values corresponding to both THIDA-Old and THIDA-New for the case of BL.

4. Discussion

4.1. Comparison of THIDA-New with THIDA-Old

In fig. 2, C/E values in the case of BL are plotted against the materials as a function of the cases. One of major topics is the improvement of the calculation accuracy in THIDA-New with respect to THIDA-Old. Figure 3 gives the direct change of the final γ-ray spectrum for W in the case AS. It was recognized that almost all γ-ray emission rates in THIDA-New were different from those in THIDA-Old.

Table 2
Experimental errors in ±% for the integrated γ-ray intensities

Materials	Cases						
	AS	Al-1	AL-2	BS	BL-1	BL-2	C
Mg	–	3.2	3.2	–	3.3	3.8	–
Al	3.0	3.7	–	10	3.3	–	6.5
Si	3.5	–	–	–	–	–	–
V	2.9	4.4	4.4	8.2	5.2	6.1	–
Ti	3.2	3.7	3.8	16	4.9	–	6.4
Cr	–	3.3	3.4	–	6.1	–	–
MnCu	3.2	3.6	3.7	4.1	3.5	4.8	–
Fe	3.0	3.5	4.9	4.0	3.8	6.6	3.2
Co	3.1	3.0	3.7	4.2	3.7	4.0	–
Ni	3.4	3.3	3.6	12	3.8	5.0	6.7
Zn	–	–	–	–	–	–	5.3
Zr	3.3	–	–	10	3.7	–	5.9
Nb	–	3.7	3.7	–	3.3	3.8	4.1
Mo	3.9	4.0	3.6	6.6	3.3	3.9	5.2
Ag	–	–	–	–	–	–	4.7
Sn	–	–	–	–	–	–	5.9
Ta	–	–	–	–	–	3.1	7.8
W	3.8	3.8	4.5	4.8	3.4	4.1	5.1

Major sources for the error are due to γ-ray counting statistics, detector efficiency (2.5%) and neutron source determination (2.0%). Contributions from other uncertainties were relatively small, less than 1%.

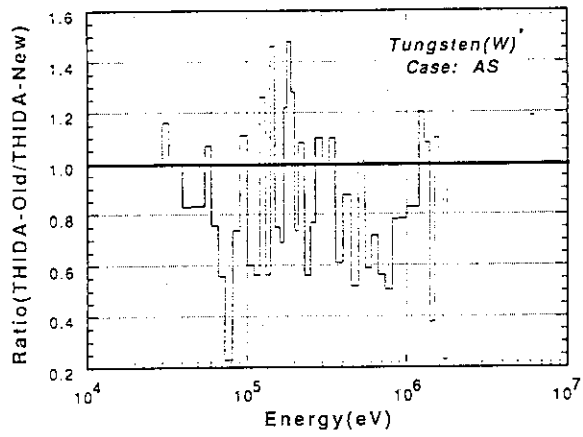

Fig. 3. The ratio of the γ-ray energy spectrum for W calculated by THIDA-Old to that by THIDA-New.

4.2. Discussion on each activity C/E

Here, we focused only on the major radioactivities in typical irradiation and γ-ray counting conditions because numbers of experimental cases were so lager to be covered. Much care was taken in the material cases which exhibited significant discrepancies among the calculations as well as experiments. Ranges of experimental errors are summarized in table 2 in order to make the discussion quantitative. Since almost all experimental errors were less than ±10% as show in table 2, it was anticipated that C/E values without errors gave a reasonably adequate basis for the discussion. In the following, material wise the studies are given.

4.2.1. Al

The activity of ^{24}Na, the product of the ^{27}Al (n, α)^{24}Na reaction, was dominant in all cases. The C/E values of all calculations were very close to 1.0 for all cases. This demonstrated the reasonable treatment in the analysis procedure of the neutron spectrum to the final γ-ray spectrum as long as the high energy part was concerned. This is a good indication for the monitoring of the system code performance because of less uncertainty in the activation cross-section and well known decay properties.

4.2.2. Mg

The C/E for magnesium looked good though there was a systematic overestimation of 18 to 37% for the case BL for all codes. This overestimation could be explained by the D–T neutron energy spectrum at the sample position and the overestimation of the cross-section of ^{24}Mg(n, p)^{24}Na in all libraries. The actual neutron peak energy at the sample position A and B were estimated 14.6 MeV from the D–T reaction kinematics. However, the cross-section was given as an averaged value for the 14 MeV region, resulting in the some overestimation. Recent experiments gave the cross-sections for this reaction to be 167 mb and 183 mb at 14.9 and 14.5 MeV, respectively, corresponding to the position of B and A. Substitution of this new cross-section value gives better agreement.

4.2.3. Si

Only one data set for the case of AS was available for silicon. The dominant activities were ^{27}Mg(50%) and ^{29}Si(50%). A very large discrepancy between calculations by THIDA-Old and -New was observed, where calculation with the New version gave much smaller values than that with Old. DKR-ICF and THIDA-Old showed reasonable agreement with experiment as shown in table 3. However, THIDA-New and REAC2 gave large underestimation and overestimation. From the investigation of the these particular reaction cross-sections given also in table 3, apparently, the cross-sections of THIDA-New are too small for both reactions. This leads to unreasonable underestimation. For the ^{29}Si(n, p)^{29}Al reaction cross-section at 14 MeV, however, values in both REAC2 and DKR-ICF seemed too high by more than a factor of two. Thus it should be noted that the agreement obtained using DKR-ICF could not be simply the evidence for the activation cross-section verification. The overestimation in REAC2 could be attributable to the existence of the other reactions which unreasonably contributed to the activity in silicon. The cross-sections in the THIDA2-New library should be corrected.

4.2.4. V

The new version of the cross-section in THIDA gave much improvement in the C/E ratios as shown in

Table 3
C/E values for silicon and cross-sections at 14.5 MeV for each library

	THIDA-Old	THIDA-New	REAC-2	DKR-ICF	FNS
C/E	0.81	0.39	2.8	1.08	–
Reaction	Cross-section (mb)				
^{30}Si(n, α)^{27}Mg	86	40	84	90	80
^{29}Si(n, p)^{29}Al	230	80	240	280	135

Table 4
C/E values for vanadium cases

Case	THIDA-Old	THIDA-New	REAC-2	DKR-ICF
AS	0.88	0.78	1.06	1.35
AL-1	1.59	1.22	1.57	3.4
BS	1.09	1.03	1.3	1.8
BL-2	1.40	1.10	1.4	3.1

table 4. This is mainly due to the improvement of the cross-section for $^{51}V(n, \alpha)^{48}Ti$ being 16.2 mb which is close to the experimental data at FNS [14]: the old value at 14 MeV was 20% larger than the new one which is very consistent with the currently available experimental data at FNS. The overestimations in the REAC2 and DKR-ICF calculations by 40% and a factor of three, respectively, are also explained by too large cross-section values, 24.3 mb and 45.2 mb, respectively. It should be noted that there was no corresponding γ-ray peak to the activity of ^{47}Sc in the measurement though calculation presented prominent lines for all calculations. The cross-sections for this reaction were evaluated from reaction systematic or theoretical prediction because of lack of experimental data at 14 MeV. As far as the experimental evidence showed, the cross-section must be subjected to measurement.

4.2.5. Ti

Both THIDA calculations with the Old and New libraries gave identical results showing good agreement with experimental values. This is reflected by the identical cross-section values at 14 MeV for the main contributing reactions of $^{48}Ti(n, p)^{48}Sc$ and $^{47}Ti(n, p)^{47}Sc$. However, REAC2 and DKR-ICF overestimated the experimental values in general by 15–86% although the cross-sections seem consistent with data in THIDA as well as the experimental value at FNS [14]. This unexplainable problem remaines to be solved in the near future. Only the case BS short cooling time less than 30 min submitted the problem of underestimation in THIDA, whereas REAC2 and DKR-ICF overestimated it by 73 and 62%, respectively. This trend can be attributed to the improper cross-section for $^{46}Ti(n, 2n)^{45}Ti$. In this case, ^{45}Ti gave around 40% contribution to the total.

4.2.6. Cr

The results of THIDA-New and DKR-ICF were in good agreement with experiments. However, REAC2 showed a large overestimation by more than 50%. The improvement in C/E of the New library to that of the Old one was simply due to change in the cross-sections of $^{52}Cr(n, 2n)$ and $^{50}Cr(n, 2n)$ which produce major contributing activities of ^{51}Cr and ^{49}Cr, respectively.

4.2.7. Fe

The induced activities in iron were obviously dominated by ^{56}Mn at the short cooling time less than several hours. At one day after irradiation, ^{54}Mn becomes the only prominent contributor to the radioactivity. By the same reason for the aluminum case, C/E tends to be around 1.0.: the cross-sections for the major production reactions $^{56}Fe(n, p)$ and $^{54}Fe(n, p)$ have been well evaluated because of their importance in dosimetry application. The results for all cases are also positively supporting the validity of all code systems with the neutron transport calculations as far as the high neutron energy range above 1 MeV was concerned.

4.2.8. Co

Acceptable results in C/E values were found for cobalt. The improvement in C/E by using THIDA-New calculation indicated the properness of the cross-sections for $^{59}Co(n, \alpha)$.

4.2.9. SS-316

There was generally good agreement between the experiments and all three calculations for all cases of SS-316, within 20%. As verified previously in the Li_2O assembly [1], the same level of confidence in the calculation had been provided by THIDA, resulting in excellent consistency to each other.

4.2.10. Ni

For nickel, there was general agreement between calculations and experiments for all cases. Only calculations by REAC2 and DKR-ICF for the cases of BS gave an unreasonable overestimation by a factor of two.

4.2.11. MnCu

The case MnCu suffered by very complicated trends for the C/E's as shown in fig. 4. The C/E's differ case by case (neutron spectrum, irradiation time and cooling time). Apparently, there was inconsistency among the three codes. In the case AS, THIDA with both Old and New libraries overestimated by 60% and REAC2 and DKR-ICF overestimated by more than a factor of three. This overestimation was dominantly (more than 90%) contributed by the 511 keV annihilation γ-ray

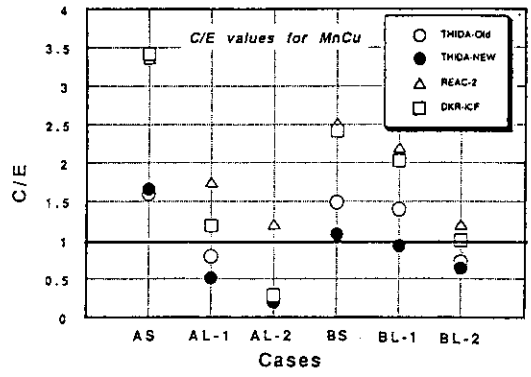

Fig. 4. The C/E values of MnCu alloy for all cases.

from ^{62}Cu, the product of ^{63}Cu(n, 2n)^{62}Cu. The cross-section values at 14 MeV for this reaction are 500, 539, 658 and 633 mb for THIDA-Old, THIDA-NEW, REAC2 and DKR-ICF, respectively. Though these values are slightly higher than the experimental value at FNS, it can not explain the overestimation. As one possible reason, the insufficient detector efficiency for this particular annihilation γ-ray which is distributed broadly due to the high energy β^+ emission around the MnCu samples. Still it is required to investigate the extremely large C/E's the for REAC and DKR.

A sudden drop in C/E was observed for the cases AL-1 and AL-2, where ^{56}Mn and ^{64}Cu dominated the γ-ray emissions. Although measurements gave 52 and 81% contributions by ^{64}Cu in AL-1 and AL-2, respectively, calculations of THIDA underestimated them by a magnitude of more than one order. Since the cross-section for ^{65}Cu(n, 2n)^{64}Cu has been well studied and data at 14 MeV in all libraries are identical, small C/E values were attributable to the underestimation in the ^{63}Cu(n, γ)^{64}Cu reaction, which is sensitive to the low-energy neutrons. In the case BS where ^{56}Mn gave 82% contribution, THIDA-NEW gave a reasonable C/E of 1.08. This result demonstrated the feasibility of the cross-section for ^{55}Mn(n, γ) for the neutron spectrum in Li_2O where the low-energy neutron flux was depressed due to the large resonance absorption at 250 keV by ^{6}Li(n, α). It may reduce the uncertainty in the low-energy neutron capture reaction of ^{55}Mn(n, γ). The C/E of 0.97 assigned by THIDA-NEW calculation in BL-1 where ^{56}Mn gave 90%, supported the adequacy in the prediction of ^{56}Mn. In the case of BL-2 at 3 days after irradiation, where the ^{64}Cu had 33% weight, C/E values tend to decrease. This is also explained by the underestimation in the ^{64}Cu in the calculation.

4.2.12. Zn

The 511 keV γ-line from ^{64}Cu, the product of ^{64}Zn(n, p)^{64}Cu, was the major contributor in the case C. THIDA-Old and -NEW tended to underestimate and overestimate the experiment by 10% and 30%, respectively. The cross-section values at 14 MeV for this reaction in the libraries of Old and NEW are 110 mb and 172 mb, respectively. The recent measurement at FNS gave 135 mb for this reaction cross-section [14]. These differences seemed to reflect the C/E trend.

4.2.13. Nb

One of the standard dosimetry reactions, ^{93}Nb(n, 2n)^{92m}Nb leaded the induced decay γ-rays. Current cross-sections around 14 MeV evaluated tend to be around 460 mb. All codes predicted reasonably the experiments in all cases. However, the C/E's for THIDA-Old systematically gave underestimation of the experiment by 10–15%. The reason was simply due to lack of the reaction of ^{93}Nb(n, α)^{90m}Y($T_{1/2}$ = 3.6 h) which contributed 15% of the total γ-ray intensity.

4.2.14. Mo

The C/E values are given in table 5. By careful checking of the γ-ray branching for the THIDA decay data, a serious mistake was found in the ^{99}Mo decay gamma branching: it gave 90% branching for the 141 keV from ^{99}Mo though that value should be negligibly small. This was the main source for the overestimations for the cases of AL, BL and C, where ^{99}Mo and ^{99m}Tc dominated the γ-ray intensities. For the cases at short cooling time, agreement seemed good between THIDA-New and experiments. However, the 54% 511 γ-ray from ^{91}Mo, product of ^{92}Mo(n, 2n), in the measurement in these cases was underestimated by a factor of two. Thus, it can be said that the agreements were the results of compensation due to the underestimation and overestimation. It is apparent that REAC2 has some trouble in the library which includes unnecessarily large cross-sections giving the main contribution.

Table 5
C/E values for molybdenum cases

Case	THIDA-Old	THIDA-New	REAC-2	DKR-ICF
AS	1.23	1.03	7.0	2.6
AL-2	1.5	1.35	2.1	1.6
BS	1.13	1.08	3.5	1.9
BL-2	1.5	1.37	3.6	1.4
C	1.7	1.5	4.3	1.6

4.2.15. Zr

The THIDA calculation tended to overestimate the measurements by 20–30%. This overestimation arose in the 909 kev γ-lines prediction. This may cause the inadequate decay chain treatment for ^{89m}Y, daughter nuclide of ^{89}Sr which is produced by the reaction of ^{92}Zr(n, α). THIDA calculation gave a comparable intensity of the 909 keV γ-line from ^{89m}Y. However, such a large contribution from ^{89m}Y is not realistic, because the half-life of ^{89}Sr is 53 d and the cross-section of ^{92}Zr(n, α) should be small, around 10 mb, in comparison with the cross-section of ^{90}Zr(n, 2n)^{89}Zr. Subtraction of the contribution from ^{89m}Y in the calculation gives excellent improvement in *C/E*.

4.2.16. Sn

Gamma-ray energy spectrum analysis gave no clear correspondence between calculation and measurement. This is due to miss assignment of the reaction of ^{116}Sn(n, p)^{116m}In in the THIDA-New library: THIDA dropped the correspondence to the product of ^{116m}In of 54.2 m, which was the major contributor in the measured γ-ray spectrum. On the other hand, calculation gave a very high intensity for the 158 keV line emitted by ^{111m}In, the product of ^{112}Sn(n, np). The THIDA calculation gave a large cross-section of 36.8 mb for this reaction, a value which seems too high from the reaction cross-section systematic.

4.2.17. Ag

For the Ag in case C, there was reasonable agreement between calculation and experiments as shown in fig. 5. REAC2 did not include the corresponding cross-section or decay γ-ray source.

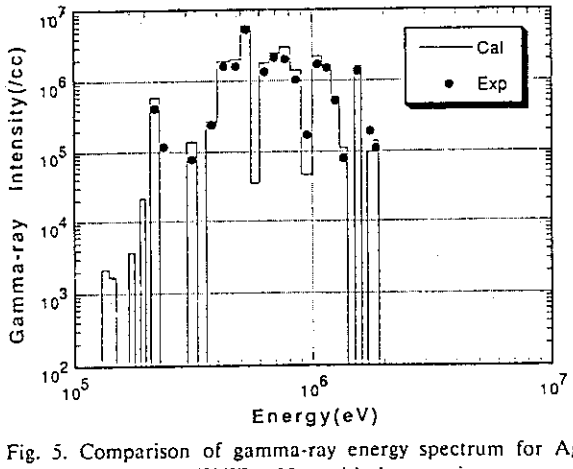

Fig. 5. Comparison of gamma-ray energy spectrum for Ag calculated by THIDA-New with the experiment.

Table 6
C/E values for Tungsten cases

Case	THIDA-Old	THIDA-New	REAC-2	DKR-ICF
AS	1.5	0.97	307	0.2
AL-2	1.6	0.91	2.6	0.03
BS	1.5	1.05	14	0.01
BL-2	2.1	1.45	2.6	0.002
C	1.12	0.97	1.3	0.005

4.2.18. W

In table 6, the *C/E* values are shown. There were no corresponding decay data of prominent activities of ^{187}W, ^{186}Ta and ^{183}Hf in DKR-ICF resulting in very small *C/E* values for all cases. On the contrary, REAC2 showed extremely high *C/E*'s for cases with short cooling time. This was mainly due to an improperly large cross-section for ^{180}W(n, 2n)^{179}W in the library. THIDA-New presented significant improvement in the *C/E* ratios for all cases with respect to THIDA-Old. This decrease in *C/E* is attributed to the lowered cross-section value of the ^{186}W(n, γ) resonance capture at 20 eV in THIDA-New. However, the branchings for 239 and 114 keV γ-rays from ^{187}W, which are dominant contributors in the calculation, were unreasonably larger by more than a factor of 100 in the THIDA decay library. After the correction for the incorrect γ-ray branching ratio, *C/E* became around 0.75 for all cases. Thus it could concluded that the products by the (n, γ) reaction tended to be underestimated as shown for ^{64}Cu in MnCu cases.

4.2.19. Pb

Leading activity of ^{203}Pb was produced by the reaction of ^{204}Pb(n, 2n), though the abundance of ^{204}Pb is small, 1.4%. THIDA-NEW and DKR-ICF gave reasonable *C/E*'s. An overestimation in REAC2 may caused by the duplication of the cross-sections for ^{204}Pb(n, 2n)^{204g}Pb and ^{204}Pb(n, 2n)^{204m}Pb.

4.2.20. Ta

Contrary to the W cases, very small *C/E*'s in THIDA were found. This was partly due to missing branchings for 41.3, 100.1, 152.4 and 222.1 keV γ-rays from ^{182}Ta which should have 74% contribution to the total. Although correction for these data improves the *C/E*'s, still the calculation underestimated the experiment by about 50%. This is also attributable to the uncertainty in the capture reaction calculation process as seen in cases of ^{63}Cu(n, γ) and ^{186}W(n, γ).

Finally, referring to $^{197}Au(n, \gamma)^{198}Au$ the reaction rate was systematically underestimated by 40–50% in the Phase-IIC cavity through the analysis by DOT3.5 and MORSE-DD. It was concluded that the low-energy neutron spectra in the Phase-IIA and IIB should be softer than those from the calculations [15]. Thus, the underestimation in the codes for some products by (n, γ) reactions is attributable for the neutron transport insufficiencies.

5. Summary and conclusion

The adequacy of the code systems used was assured by the integral test on the reaction products for ^{24}Na, ^{56}Mn, ^{92m}Nb, the cross-section of which were assumed well evaluated with sufficient accuracy. Also, the reasonable C/E values indicated that the neutron energy spectrum above 1 MeV could be reasonable for each code.

We have encountered serious improper data bases associated with the decay γ-ray branching ratios. This may be simply because of unexpected human error in making such a large data library. But it would be very important because many design calculations have been carried out giving the criticality of specific items of concern without noticing the incorrectness of the data. In this context, emphasis should be placed on the importance of integral experiments for verifying codes and data.

The experimental analyses for induced radioactivities in various spectra indicated inadequacy for considerable large numbers of the activation cross-section data in the currently available libraries. The present study has clearly pointed out the specific reactions which gave rather poor C/E's. Thus, we could reach a reasonable solution or acceptable levels of the adequacy in the data base as long as the threshold type reactions were taking into account. One serious problem associated with inadequate prediction in the products of (n, γ) reactions, however, is still left to be verified.

Acknowledgement

US activity for this work was supported by the US Department of Energy.

References

[1] Y. Ikeda, Y. Seki, H. Maekawa, Y. Oyama and T. Nakamura, Measurements of induced activity in Type 316 stainless steel by irradiation in D–T neutron fields, Fusion Technol. 8 (1985) 1466–1471.

[2] K. Oishi, y. Ikeda, C. Konno, H. Maekawa and T. Nakamura, Experiment and analysis of induced activities in concrete irradiated by 14 MeV neutrons, Fusion Technol. 10 (1986) 579–584.

[3] K. Oishi, y. Ikeda, C. Konno and T. Nakamura, Measurement and analysis of induced activities in concrete components irradiated by 14 MeV neutrons, Fusion Technol. 18 (1990) 291–309.

[4] Y. Ikeda, A. Kumar, C. Konno, T. Nakamura and M.A. Abdou, Experiment on induced activities and decay-heat in simulated D-T neutron fields, JAERI/USDOE Collaborative Program on Fusion Neutronics, Proc. of 9th Topical Meeting on Technology of Fusion Energy, Oct. 7–11, 1990, Chicago, USA.

[5] A. Kumar, Y. Ikeda, M.A. Abdou and T. Nakamura, Analysis of induced activities measurements related to decayheat in phase-IIC experimental assembly: JAERI/USDOE Collaborative Program, Proc. of 9th Topical Meeting on Technology of Fusion Energy, Oct. 7-11, 1990, Chicago, USA.

[6] A. Kumar, Y. Ikeda, C. Konno and M.Z. Youssef, Experiment and analysis for measurements fo decay heat related induced activities in simulated line source driven D-T neutron fields of Phase IIIA – JAERI/USDOE Collaborative Program on Fusion Neutronics, Proc. of 9th Topical Meeting on Technology of Fusion Energy, Oct. 7-11, 1990, Chicago, USA.

[7] Y. Seki, H. Iida, H. Kawasaki and K. Yamada, THIDA-2: an advanced code system for calculation of transmutation, activation, decay heat and dose rate, JAERI-1301 (1985).

[8] F.M. Mann, REAC2: Status of codes and libraries, Fusion Technol. 15 (1989) 449–452.

[9] D.L. Henderson and O. Yasar, DKR-ICF: a radioactivity and dose rate calculation Code Package, Vol. 1 and 2, UWFDM-714 (1986).

[10] T. Nakamura, H. Maekawa, J. Kusano, Y. Oyama, Y. Ikeda, C. Kutsukake, S. Tanaka and Shu. Tanaka, Present status of the fusion neutron source (FNS), Proc. 4th Symp. on Accelerator Sci. Technol., RIKEN, Saitama, 24-26 November (1982) pp. 155-156.

[11] Y. Oyama, S. Yamaguchi, K. Tsuda, C. Konno, Y. Ikeda, H. Maekawa and T. Nakamura, Measured characteristics of Be multi-layered and coolant channel blankets – Phase-IIC, Experiments of the JAERI/USDOE collaborative on Fusion Neutronics, Proc. of 9th Topical Meeting on Technology of Fusion Energy, Oct. 7-11, 1990, Chicago, USA.

[12] T. Nakamura, Y. Oyama, Y. Ikeda, C. Konno, H. Maekawa and K. Kosako, A line D-T neutron source facility for annular blanket experiment – Phase-III of the JAERI/USDOE Collaborative Program on Fusion Neutronics, Proc. of 9th Topical Meeting on Technology of Fusion Energy, Oct. 7-11, 1990, Chicago, USA.

[13] Y. Seki and H. Iida, Coupled 42-group neutron and 21-group gamma-ray cross section sets for fusion reactor calculations, JAERI-M 8818 (1980).

[14] Y. Ikeda, C. Konno, K. Oishi, T. Nakamura, H. Miyade, K. Kawade, H. Yamamoto and T. Katoh, Activation cross section measurement for fusion reactor structural materials at neutron energy from 13.3 to 15.0 MeV using FNS facility, JAERI-1312 (1988).

[15] M. Nakagawa, T. Mori, K. Kosako, Y. Oyama and T. Nakamura, JAERI/U.S. Collaborative Program on Fusion Blanket Neutronics – Analysis of Phase-IIA and IIB Experiments, JAERI-M 89-154 (1989).